UNIVERSITY OF LIVERPOOL

Study of extracellular vesicles secreted by experimental models of metabolic syndrome, and their effects on adipocytes

Thesis submitted in accordance with the requirements of the University of Liverpool for the degree of Doctor of Philosophy by

Justyna Emilia Mleczko

July 2017

Declaration

This thesis is the result of my own work, unless otherwise stated, and it is based upon the results from experimental work performed as a Ph.D. student between September 2013 and September 2017 on a split-site Ph.D. program between the Department of Cellular and Molecular Physiology at University of Liverpool and the Exosomes laboratory of CICbioGUNE. Neither this thesis nor any part of it has been submitted in support of an application for another degree or qualification at this or any other university or institute of learning.

Justyna Emilia Mleczko

This research was carried out in the Department of Cellular and Molecular Physiology, Institute of Translational Medicine, at the University of Liverpool and at Exosomes laboratory of CICbioGUNE in Derio, Spain.

Acknowledgements

The last four years have been a rocky road but thanks to so many wonderful people, it was without a doubt the most enriching and enjoyable experience.

First and foremost, I would like to thank my primary supervisors, **Dr. Silvia Mora** and **Dr. Juan Manuel Falcón-Pérez** for accepting me on this program and giving me the opportunity to do my Ph.D. thesis in their laboratories, at the University of Liverpool and in CIC_bioGUNE in Bilbao, respectively. Thanks to both for their support throughout my project and their trust in me.

Thank you, Silvia, for teaching me all the basics and preparation for the following stage at CIC_bioGUNE. It was not easy to be supervisor on a distance, so I really appreciate the effort and thanks also for allowing me to stay longer than anticipated in CIC_bioGUNE.

I would like to especially thank **JuanMa** for being a wonderful mentor helping me to grow as a scientist. Thank you for teaching me to think about science and letting me learn from my mistakes. Thank you for being so understanding and having so much patience with me all this time.

Thank you to **Prof Andrea Varro**, my second supervisor at the University of Liverpool for all her help and support throughout these four years.

Thank you to my mentor at the University of Liverpool, **Dr. Lee Hynes** for his understanding and guidance when I really needed it.

Institute of Translational Medicine (**ITM**) Admin at the University of Liverpool, Ms Lisa Crimmins, Ms Helen Davies and Ms Emma Robertson for their splendid administrative work and for always being so efficient and ready to help.

To general director, **Prof Jose María Mato** and to Scientific Director **Jesús Jiménez - Barbero** for successfully running CIC_bioGUNE and for allowing me to stay in CIC_bioGUNE longer than anticipated. Thank you to Alicia for her smile and a good word and for always being on top of everything.

No tengo palabras para describir lo agradecida que estoy a **Félix** por ser un mentor y amigo maravilloso. Gracias por enseñarme todas las técnicas y por estar ahí siempre que necesitaba ayuda. Gracias por soportarme, por mis preguntas molestas, por no escribir los protocolos y por tener que molestarte incontables veces con la misma pregunta. Gracias por ser tan honesto, por nuestras discusiones científicas y por poner la mejor música variada en el laboratorio.

A **Espe** por nuestras charlas sobre ciencia y la vida en general. Por cada uno de tus consejos, gracias por ser tan buena amiga y mentora.

A **Diana** y **Sebastián**, los miembros del Laboratorio de Exosomas y la Plataforma Metabolómica por ser compañeros maravillosos.

A **Laura**, estuvimos muy poco tiempo juntas en el laboratorio antes de que te fueras a escribir tu tesis, pero fue el suficiente para llegar a ser buenas amigas.

A **Pedro**, **Charles** y **Marc,** los otros miembros del Laboratorio de Exosomas. Gracias por todo. Especialmente a Charles por hacer los últimos experimentos.

Vanessa, thank you for coming to CIC_bioGUNE. We have done many Seahorse experiments together, and spent countless hours in the lab. The reward was the chocolate waffles in the morning.

Diana, my wonderful friend, from the moment we met we connected and became best friends. The first ones to arrive and last ones to leave the lab. Thank you for our talks, you were the person that always made me see everything in brighter colours and understood me without words.

Thank you to **Gulizar**, we have discovered the lab together, helped each other with everything. You have been a great friend and support throughout the first year. I don't know what I would have done without you.

To my wonderful friends from Liverpool, **Asia**, **Hania**, **Kasia** i **Bolek**, **Michaela**, **Arnaud**, **Paul**, **Kelly**, **Sumaya**, **Amy**, **Dayani**, the list is long, you have made my first year very enjoyable. You have been a great support. Especially to Kasia i Bolek for letting me stay in their home when I arrived back at Liverpool.

A mis ‘sexy scientists’ **Pauli**, **Marta**, and **Lucía**, compañeras del laboratorio y amigas. Hemos hecho tantas cosas juntas, gracias por acompanarme durante los momentos buenos y malos. ¡Disfruté cada uno de ellos!

A **Lourdes, m**i "compañera en el crimen" y la mejor compañera de piso que podría pedir. Gracias por ayudarme a crecer, haciéndome entender las cosas y ver el lado positivo de todo y por tu apoyo en todo. Por mostrarme un mundo de música y por llevarme a todos los mejores conciertos.

A **Nuria**, mi "hermanita mayor" que nos conocimos en mi primer día de trabajo. Te pedí las indicaciones para el autobús de regreso a Bilbao, así es como comenzó esta hermosa amistad y espero que sea de por vida.

A **Malu**, (nunca te acordaste de mi nombre y en vez de eso, solías llamarme princesa Jasmine), por hacerme sentir muy especial. Gracias por tratarme como una de las tuyas y por interesarte como me iban las cosas.

A los chicos: **Fer**, **Pablo** (Guapito), **Sergio** (Baby Mastodont), **David**, **Jorge**, conocidos como ‘la patrulla monger’. Conseguistéis que el trabajo fuera un sitio divertido! Se nos pasaban las horas de trabajo volando.

A **Teresa** por su constante apoyo y asesoramiento cuando entré en el "Mundo de Seahorse". Por nuestras conversaciones a las 7 de la mañana cuando éramos las primeras en el laboratorio.

A **Vir**, por pensar siempre en todo el mundo, haciendo nuestros días más dulces con bolsas de chuches. Por su ayuda constante con el microscopio, por tus consejos y soluciones.

A **Urra** por su compañía en las tardes en el laboratorio y por nuestras charlas, sobre todo. Lo siento por pisar el piso recién fregado.

A **Nico** por el regalo de las células Raw264.7 macrófagos, indispensable para este proyecto. Gracias por la paciencia conmigo, por enseñarme ELISA y responder a todas mis preguntas molestas.

To those who make reading free scientific research papers possible, which was an indispensable help through the writing of this thesis.

A **David Gil**, el fotógrafo oficial de exosomas. Todas las imágenes de Cryo-EM presentadas aquí fueron tomadas por él. Gracias por estar siempre dispuesto a colaborar y a asumir un reto.

A **Ana Maria Arransay** y su equipo por el análisis del contenido de ARN exosomal. Gracias por sacar el máximo provecho de la minúscula cantidad de material que podía proporcionar.

A **Felix Elortza**, **Mikel Azkargorta** e **Iraide Escobes Corcuera** de la Plataforma Proteómica por el maravilloso trabajo de proteómica de los exosomas, por tener que soportar mi ignorancia en el campo, y por estar siempre dispuestos a contestar mis preguntas.

A mis padres vascos, **Begoña** y **Emilio**, por aceptarme en su familia, por el apoyo constante y fe que depositaron en mi. Gracias Begoña por tener tanta paciencia, siempre pensando en todos, haciendo las galletitas a veces incluso sin dormir, y por tomarte el tiempo para corregir mi español. Muchas gracias a **Sara**, **Iñigo**, **Unai** y **Gorka** por todos los momentos que pasamos juntos, las Navidades, los cumpleaños, nacimiento de Iñigo y muchísimos más. Gracias a amama **Alicia** y aitite **José Luis** por las comidas del domingo y por preguntar que tal van las cosas. Y finalmente a toda la familia. No lo hubiera hecho sin todos vosotros.

Dziękuję Wam **mamo** i **tato**, za wszystko co dla mnie zrobiliście. Dzięki waszemu wychowaniu i wpojeniu mi wartości, jestem kim jestem dziś. Dziękuję Wam za zrozumienie kiedy nie mogłam być z Wami na święta. Moim sistrom i przyjaciółkom za wysychanie moich narzekań i oczywiście mojemu bratu Michałowi, mojej bratowej Kasi i naszej gwiazdce Zuzi, która urodziła się niedługo po tym jak rozpoczęłam doktorat.

Finalmente, a mi mejor amigo y el amor de mi vida, **Imanol**. Siento mucho haberme perdido tu seminario de estudiantes, fue mi primer día en CIC_bioGUNE y tu fuiste la primera persona que me presenataron ese día. Hiciste que viniera a trabajar con una sonrisa todos los días. Gracias por tu apoyo, por entenderme, escucharme y por ser sincero siempre. Por tu paciencia conmigo cuando escribia la tesis y me desesperaba. Gracias por leer mi tesis y tus comentarios. No lo hubiera hecho sin ti. No puedo esperar para empezar nuestra vida juntos sin tener que pensar en la tesis. ¡Nos vemos en NY! ♥

Publications and Congresses

Publications in collaboration

'Hepatocyte-secreted extracellular vesicles modify blood metabolome and endothelial function by an arginase-dependant mechanism', Royo F, Moreno L, **Mleczko J**, Palomo L, Gonzalez E, Cabrera D, Cogolludo A, Perez Vizcaino F, van-Liemp S & Falcon-Perez JM. Scientific Reports. 2017 Feb 17; 7:42798. Doi: 10.1038/srep42798

'Metabolically active extracellular vesicles released from hepatocytes under drug-induced liver-damaging conditions modify serum metabolome and might affect different pathophysiological processes', Royo F, Palomo L, **Mleczko J**, Gonzalez E, Alonso C, Martinez I, Perez-Cormenzana M, Castro A and Falcon-Perez JM. European Journal of Pharmacological Sciences. 2017 Feb 15, 98:51-57. Doi: 10.1016/j.ejps.2016.10.020

'Identification of the metabolic alterations associated with the multidrug resistant phenotype in cancer and their intercellular transfer mediated by extracellular vesicles', Lopes-Rodrigues V, Di Luca A, **Mleczko J**, Meledy P, Henry M, Pesic M, Cabrera D, van Liempd S, Lima RT, O'Connor R, Falcon-Perez JM, Vasconcelos MH. Scientific Reports. 2017 Mar 17; 7:44541. Doi: 10.1038/srep44541

Manuscripts in preparation

'Hepatocyte-secreted extracellular vesicles contain cytochrome activity that is affected by pharmacological compounds associated with drug-induced liver injury', Palomo L, **Mleczko J**, Royo F, Conde-Vancells J, Gonzalez E and Falcon-Perez JM.

Thesis manuscripts in preparation

'Exosomes from Obese individuals and those obtained from in vitro hypoxic adipocytes cause insulin resistance and reduce insulin-stimulated glucose uptake in adipocytes', **Mleczko J***, Ortega F*, Falcon-Perez JM, Wabitsch M, Fernandez-Real JM and Mora S.

'*Zucker Fatty rat hepatocyte derived EVs and their involvement in the development of metabolic syndrome*'

Mleczko J *et al.*

Presentations and congresses

- '*Hepatocytes-derived extracellular vesicles from metabolic syndrome models influence adipocyte metabolism*'. The fifth international meeting of International Society for Extracellular Vesicles (ISEV), Rotterdam, 4-7th of May 2016, **oral presentation**
- *'Molecular and functional characterisation of extracellular vesicles secreted by cellular models of metabolic syndrome'*. Third 'Grupo Espanol de Innovacion e Investigacion en Vesiculas Extracelulares (GEIVEX) Symposium, San Sebastian, 29 -30th of September 2016, **oral presentation**
- First Euskadi Workshop on Exosomes, CICbioGUNE, 23rd of March 2017, Spain, **attendance**
- Ph.D. presentation at University of Liverpool, **oral presentation**
- Ph.D. presentation at CICbioGUNE, 9th March 2016, **oral presentation**

Table of contents

List of Figures

List of Tables

Abbreviations

2-DG	2-Deoxy-D-glucose
4E-BP1	Eukaryotic translation initiation factor 4E-binding protein 1
AB	Apoptotic bodies
ACC	Acetyl-CoA carboxylase
ACC1	Acetyl-CoA carboxylase
ACLY	ATP-citrate synthase
Acrp30	Adipocyte complement-related protein of 30 kDa
ACSI5	Acyl-CoA synthase 5
ACTB	ß-actin
Akt2	Serine/threonine-protein kinase Akt-2
ALB	Albumin
AML12	Alpha mouse liver 12
ANOVA	Analysis of variance
ApoB	Apolipoprotein B
ApoE	Apolipoprotein E
ASCVD	Atherosclerotic cardiovascular disease
ASGR	Asialoglycoprotein receptor
ASP	Acylation stimulating protein
AT	Adipose tissue
ATCC	American Type Culture Collection
ATM	Adipose tissue macrophages
ATP	Adenosine triphosphate
BCA	Bicinchoninic acid
BMI	Body mass index
BODIPY	4,4-Difluoro-1,3,5,7,8-Pentamethyl-4-Bora-3a, 4a-Diaza-*s*-Indacene
BP	Biological process
BSA	Bovine serum albumin
C/EBP	CCAAT-enhancer-binding protein
CC	Cellular compartments
CD9/63/81	Cluster of differentiation 9/63/81

CDAA	Choline-deficient L-amino acid
cDNA	Complementary DNA
CHAPS	3-((3-cholamidopropyl) dimethylammonio)-1-propanesulfonate
ChREBP	Carbohydrate-responsive element-binding protein
CID	Collision-induced dissociation
COMT	Catechol-*O*-methyltransferase
COXIII	*c* oxidase subunit III
COXIV	Cytochrome c oxidase subunit 4
CVD	Cardiovascular disease
CYP2D1	Cytochrome P450
DAPI	4',6-diamidino-2-phenylindole
DASH	Dietary approaches to stop hypertension
DAVID	Database for Annotation, Visualization and Integrated Discovery
DC	Dendritic cell
DEP	Differentially expressed proteins
DEX	Dexamethasone
dH_20	Distilled water
DMEM	Dulbecco modified Eagle's minimal essential medium
DNA	Deoxyribonucleic acid
D-PBS	Dulbecco Phosphate-buffered saline
DTT	Dithiothreitol
ECAR	Extracellular acidification rate
ECL	Enhanced chemiluminescence
ECM	extracellular matrix
EGTA	Ethylene glycol-bis (β-aminoethyl ether)-N,N,N',N'-tetraacetic acid
ELISA	Sandwich Enzyme-Linked Immunosorbent Assay
ER	Endoplasmic reticulum
Erk	Extracellular signal-regulated kinase
ESCRT	Endosomal sorting complexes required for transport
ETC	Electron transport chain
EtOH	Ethanol
EVs	Extracellular vesicles

FA	Fatty acid
FABP4	Fatty acid binding protein 4
FADH	Flavin adenine dinucleotide
FAS	Fatty acid synthase
FBS	Fetal bovine serum
FCCP	Carbonyl cyanide-*4*-(trifluoromethoxy)phenylhydrazone
FDR	False discovery rate
Ferritin-LC	Ferritin-light chain
FFA	Free fatty acids
FITC	Fluorescein isothiocyanate
G6PD	Glucose-6-phosphate dehydrogenase
GLUT1	Glucose transporter 1
GLUT2	Glucose transporter 2
GLUT4	Glucose transporter 4
GRE	Glucocorticoid response element
GRP78	78 kDa glucose-regulated protein homolog
GSV	Glut4 storage vesicles
HCC	Hepatocellular carcinoma
HDL	High-density lipoprotein
HDL-C	High-density lipoprotein cholesterol
HEPES	4-(2-hydroxyethyl)-1-piperazineethanesulfonic acid
HIF	Hypoxia-inducible factor
HIV	human immunodeficiency virus
HNF4α	Hepatocyte nuclear factor 4 α
HPRT	Hypoxanthine-guanine phosphoribosyltransferase
HRP	Horseradish-peroxidase
HSE	Heat shock response elements
HSP70	Heat shock protein 70
HSP90	Heat shock protein 90
H-TGL	Hepatic triacylglycerol lipase
IBMX	3-isobutyl-1-methylxanthine
IDL	Intermediate-density lipoprotein

IGF1	Insulin-like growth factor 1
IGFR	Insulin-like growth factor 1 receptor
IL-1	Interleukin 1
IL-6	Interleukin-6
ILV	Intraluminal vesicles
iNOS	Nitric oxide synthases
IR	Insulin resistance
IRS	Insulin receptor substrate
ISEV	International Society for Extracellular Vesicles
KEGG	Kyoto Encyclopedia of Genes and Genomes
KPO_4	Potassium phosphate
LBPA	Phospholipid lysobisphosphatidic acid
LC-MS	Liquid chromatography coupled to mass spectrometry
LDH-A	Lactate dehydrogenase
LDL	Low density lipoprotein
LDS	Lithium dodecyl sulphate
LIMPII	Lysosomal integral membrane protein II
LIPC	Hepatic triacylglycerol lipase
L-PK	Liver-type pyruvate kinase
LPL	Lipoprotein lipase
LPS	Lipopolysacharide
MAM	Mitochondria-associated ER membrane
MAOX	NADP-dependant malic enzyme
MAPK	Mitogen-activated protein kinase
MB-COMT	Membrane bound Catechol-O-methyl trabsferase
MCE	Mitotic clonal expansion
MCSF1	Macrophage colony stimulating factor 1
MetS	Metabolic syndrome
MF	Molecular function
MHCII	Major histocompatibility complex II
MIF	Microphage migration inhibitory factor
MLP29	Mouse liver progrnitor 29

MØ	Macrophage conditioned medium
MPP	Matrix metalloproteinase
mRNA	Messenger RNA
MSC	Mesenchymal stem cells
mTORC2	Mechanistic target of rapamycin, complex 2
MV	Microvesicles
MVB	Multivesicular body
NAD+	Nicotinamide adenine dinucleotide, oxidized
NADH	Nicotinamide adenine dinucleotide, reduced
NAFLD	Non-alcoholic fatty liver disease
NaOH	Ethanol
NASH	Non-alcoholic steatohepatitis
NCBI	National Center for Biotechnology Information
NEFA	Non-essential fatty acid
NFκB	Nuclear factor kappa-light-chain-enhancer of activated B cells
NIDDM	Non-insulin dependent diabetes mellitus
NO	Nictic oxide
NoNo	Non-POU-domain containing octamer binding protein
nSMase2	Sphingomyelin phosphodiesterase
NTA	Nanoparticle tracking analysis
OA	Oleic acid
OCR	Oxygen consumption rate
OLETF	Otsuka Long-Evans Tokushima fatty
OXPHOS	Oxidative phosphorylation
PA	Palmitic acid
PAI1	Plasminogen activator inhibitor-1
PARP	Poly (ADP-ribose) polymerase
PBMCs	Peripheral blood mononuclear cells
PDC6I	Programmed cell death 6-interacting protein
PGC1α	Peroxisome proliferator-activated receptor gamma coactivator 1-alpha
PGK1	Phosphoglycerate kinase 1

PI	Propidium bromide
PI3K	Phosphatidylinositide 3-kinases
PIP2	Phosphatidylinositol 4,5-bisphosphate
PIP3	Phosphatidylinositol (3,4,5)-trisphosphate
PKB	Protein kinase B
PKC	Protein kinase C
PPAR	Peroxisome proliferator-activated receptor
PPP	Pentose phosphate pathway
PS	Penicillin streptomycin
PS	Phosphatidylserine
PSA	Penicillin streptomycin amphotericin B
PSM	Peptide spectrum matches
PTEN	Tensin homologue deleted on chromosome 10
PTM	Posttranslational modification
PVDF	Polyvinylidene fluoride
Rab10	Ras-related protein10
RAB11	Ras-related protein 11
Rb	Retinoblastoma protein
RI	Refractory index
RNA	Ribonucleic acid
ROS	Reactive oxygen species
RPM	Revelations per minute
RPS6	Ribosomal protein
RTqPCR	Real time quantitative polymerase chain reaction
S1P	Sphingosine-1-phosphate
S6K	Ribosomal s6 kinase
SAM	S-adenosyl methionine
S-COMT	Soluble catecol-O-methyl transferase
SDS-PAGE	Polyacrylamide gel electrophoresis
SEC	Size exclusion chromatography
SGK	Glucocorticoid-induced protein kinase
SH2	Src Homology 2

SOS	Son of Sevenless
SREBP-1c	Sterol regulatory element-binding protein 1c
T2DM	Type 2 Diabetes Mellitus
TCA	Cyctric acid cycle
TfR	Transferrin receptor
TG	Triglyceride
TGFα	Transforming growth factor alpha
TGN	Trans-Golgi network
TLR4	Toll-like receptor-4
TNF	Tumour necrosis factor
T-PBS	Tween-phosphate-buffered saline
TSG101	Tumor susceptibility gene 101
TZD	Thiazolidinedione
UGT1a6	UDP-glucuronosyltransferase 1-6
UV	Ultraviolet
VEGF	Vascular endothelial growth factor
VLDL	Very low-density lipoprotein
VPS4	Vacuolar protein sorting-associated protein 4A
WAT	White adipose tissue
WB	Western blot
ZF	Zucker Fatty
ZL	Zucker Lean

Abstract

Extracellular vesicles (EVs) is a collective name given to nanometer-sized membrane vesicles (30-200 nm) secreted by all cells and found in most body fluids. They originate either from endosomal multivesicular bodies, which by fusion with the plasma membrane are released into the extracellular environment as exosomes, or directly through the budding off the plasma membrane as microvesicles. They were first described to take part in the removal of unwanted plasma membrane proteins during the maturation of reticulocytes to erythrocytes, however, following the decades of research they are now recognized as being important mediators of cell-to-cell communication and vehicles to transfer active biological material. They contain lipids, proteins and different species of nucleic acids. Remarkably, their composition has been shown to be altered in pathological conditions, and although this feature has been widely explored to find low-invasive biomarkers, the physiological effects of such content alteration is greatly unknown.

Obesity is reaching epidemic proportions worldwide mostly due to the growing incidence of metabolic syndrome (MetS), which is a cluster of metabolic abnormalities such as obesity, insulin resistance, dyslipidemia and hypertension that when occurring together increase the risk of cardiovascular complications and type 2 diabetes mellitus.

In the current study, we focused on investigating the nature and the effect of different metabolic alterations observed in MetS development, such as the adipose hypertrophy, hepatic steatosis, inflammation and adipose tissue hypoxia, on the secretion and content of EVs. Furthermore, the work also addressed the effects of these EVs on the biology and metabolism of adipocytes. To achieve our aim, we established *in vitro* cellular models, that resemble the mentioned metabolic conditions and that are suitable for subsequent production and isolation of EVs. We performed detailed biochemical and structural characterization of EVs isolated from conditioned medium of hypertrophic

adipocytes, adipocytes cultured in hypoxia or macrophage- conditioned medium. In addition, we also analyse EVs from chemically-induced steatosis in hepatic cell lines and steatotic primary hepatocytes obtained from Zucker rat hepatocytes that represent a genetic model of obesity.

We used cryo-EM technology to visualize the isolated EVs in their native state, and Nanoparticle Tracking Analysis to measure their concentration and size distribution. Furthermore, by Western blot analysis, we identified the abundance of EV-related and cell type-specific proteins, which could be affected by metabolic perturbation of the parental cell. In the case of Zucker hepatocyte-derived EVs, we performed further analysis of their protein, RNA and lipid content.

Our study demonstrates that the profile of EVs secreted by all our *in vitro* models of metabolic syndrome is highly affected in terms of the concentration and protein abundance. We found that steatotic hepatocytes secrete EVs with significantly reduced exosomal-markers such as Aip1/Alix, CD63, CD81, Tsg101 and Flotillin1, and increased abundane in Hsp70 and 90. Furthermore, a proteomic analysis of EVs released by steatotic Zucker hepatocytes revealed a very specific protein signature, which reflected the metabolic state of the cell. The majority of proteins upregulated were related with the fat metabolism, fatty acid synthesis, glycolysis and pentose phosphate pathway, in turn, the downregulated ones were mainly mitochondrial. Interestingly, the abundance of diverse enzymes involved in xenobiotics metabolism was significantly downregulated in EVs from the steatotic model. Finally, we show that these EVs influence insulin sensitivity in recipient 3T3-L1 adipocytes.

Moreover, we found the proinflammatory cytokine Tnf to be associated with EVs secreted by LPS-stimulated Raw264.7 macrophage-like cells. Interestingly, they were able to significantly reduce the mitochondrial functions in 3T3-L1 adipocytes. In conclusion, our research supports the hypothesis that EVs play an important role in the development of pathologies associated with MetS.

INTRODUCTION

General introduction

1.1 Metabolic syndrome

1.1.1 Overview

The first description of metabolic syndrome (MetS) goes back to 1920 when Kylin, a Swedish physician demonstrated the association of high blood pressure (hypertension), high blood glucose (hyperglycaemia) and gout (Kylin 1923). Later in 1947, Vague described that visceral obesity was commonly associated with metabolic abnormalities found in cardiovascular disease (CVD) and Type 2 Diabetes Mellitus (T2DM) (Emanuela et al. 2012) Finally, in 1988, the term Syndrome X was coined by Reaven describing it as the association of insulin resistance (IR), elevated blood glucose and very low density lipoprotein (VLDL) triglycerides, decreased blood high-density lipoproteins (HDLs) cholesterol, and hypertension (Reaven 1988). A crucial missing factor, not mentioned by Reaven was visceral obesity (Emanuela et al. 2012). It is well known now that the visceral obesity is one of the primary metabolic risk markers of MetS (Dragsbæk et al. 2016). Nowadays, visceral obesity is considered a multifactorial disease and a major risk factor for atherosclerotic cardiovascular disease (ASCVD) and T2DM (Grundy 2016).

1.1.2 Prevalence and Risk Factors

MetS represents one of the major public health challenges worldwide. In 2015, obesity was estimated to occur in 1.4 billion persons worldwide (O'Neill & O'Driscoll 2015). MetS is estimated that occurs in between 10 and 40% of the population around the world (Grundy 2016). It is expected to reach 365 million patients by the year 2030 (Schinner et al. 2005). The syndrome occurs most often in an population characterized by excessive nutrient intake and physical

inactivity with underlying metabolic or genetic susceptibilities (Emanuela et al. 2012). The prevalence has been shown to increase with body mass index (BMI) and age (Ervin 2009).The main risk factors for the development of MetS include heredity, ethnicity, physical inactivity and tobacco exposure (Lee & Sanders 2002).

1.1.3 Clinical characteristics and diagnosis

In 2009, a joint statement from the International Diabetes Federation Task Force on Epidemiology and Prevention, National Heart, Lung and Blood Institute, American Heart Association, World Heart Federation, International Atherosclerosis Society and the International Association for the Study of Obesity, was published regarding a consensus for clinical diagnosis for MetS (Alberti et al. 2009). The parameters include the following points:

- Elevated waist circumference (population and country specific definitions)
- Elevated triglycerides (≥ 150 mg/dL,1.7 mmol/L)
- Reduced high-density lipoprotein-cholesterol (< 40 mg/dL, 1.0 mmol/L) in males; (< 50 mg/dL, 1.3 mmol/L) in females
- Elevated blood pressure (systolic ≥ 130 and/or diastolic ≥ 85 mm Hg
- Elevated fasting glucose (≥ 100 mg/dL)

It was agreed that three abnormal parameters out of five, listed above would diagnose a person with MetS, with none of the parameters being obligatory to make a diagnosis, and waist measurement being a useful preliminary screening (Alberti et al. 2009). Essentially, the syndrome identifies individuals at an elevated risk for CVD and T2DM, according to the pathologies associated, together with other, non-metabolic syndrome risk factors (Grundy et al. 2005) **(Figure 1)**.

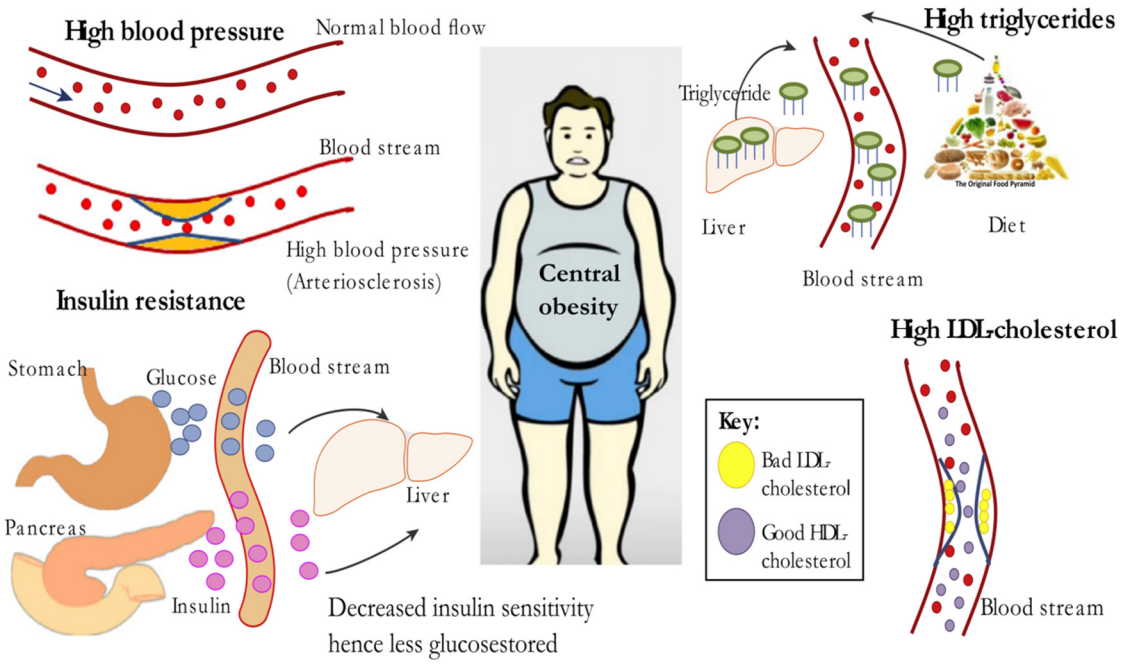

Figure 1 Clinical manifestations of MetS. Hallmarks of MetS include central obesity, insulin resistance, increased blood pressure, and dyslipidemia. Adapted from: (O'Neill et al. 2016).

Most patients suffering from MetS are clinically obese, with a predominant upper body, visceral obesity. The underlying cause is the fat overload in obesity, which feeds free fatty acids to peripheral organs such as the liver and the muscle, which is linked with IR in these organs. Moreover, enlarging fat cells secrete adipose-factors known as adipokines, which additionally contribute to metabolic risk factors of MetS. Among many, adiponectin, interleukin 6 (IL-6), tumour necrosis factor (TNF), resistin, angiotensin, leptin, and the activator inhibitor-1 (PAI1). Importantly, it has been well recognized that obesity is accompanied by macrophages infiltration and low-grade, local adipose tissue (AT) inflammation, triggering increased pro-inflammatory cytokine release leading up the development of low-grade systemic inflammation (Lumeng & Saltiel 2011; Johnson et al. 2012). Moreover, dyslipidemia, characterized by elevated low-

density lipoproteins (LDL) and VLDLs, as well as, triglycerides and reduced HDL-C seen in most MetS cases, is considered a major risk factor for, arterial atherosclerotic plaque formation leading to CV complications. Furthermore, enhanced renal reabsorption of sodium, activation of the sympathetic nervous system and renin-angiotensin-aldosterone system, the release of angiotensinogen from adipose tissue and insulin resistance have been proposed to contribute to the elevated blood pressure in MetS patients (Reaven 1991; Hall 2000; Grundy 2016). Additionally, elevated fasting plasma glucose, known as hyperglycemia is another factor that is directly caused by IR in MetS patients.

1.1.4 Treatment and management

The primary treatment for MetS, which has been proven highly effective for all metabolic risk factors, including raised blood pressure, is a lifestyle change. Dietary modification to favour caloric restriction, increased physical activity and when applicable the cessation of smoking have been proved to be beneficial changes (Grundy 2015). The Dietary Approaches to Stop Hypertension (DASH) trial demonstrated that a diet that emphasizes fruits, vegetables, and low-fat dairy products, that includes whole grains, poultry, fish, and nuts, that contains only small amounts of red meat, sweets, and sugar-containing beverages, and that contains decreased amounts of total and saturated fat and cholesterol significantly lowers blood pressure in hypertensive patients (Sacks et al. 2001). Pharmacological treatment for those persons whose risk factors are not adequately reduced are considered as preventive measures (Kaur 2014). Thus, calcium channel blockers cause slight improvement of IR in MetS patients (Farah et al. 2013), as well as, antihypertensives, insulin sensitizers, thiazolidinediones (TZDs) and cholesterol-lowering agents (Fujioka 2006). Moreover, there are two main classes of agents for targeting obesity, such as appetite suppressants and inhibitors of nutrient absorption such as orlistat, an inhibitor of gastrointestinal lipase (Wilson & Grundy 2003). Apo B-containing lipoproteins (LDL and VLDL)

are a primary target of dyslipidemia therapy (Grundy 2016). Lipid-lowering medications in the form of statin therapy are the first choice for the treatment of dyslipidemia. Moreover, niacin and fibrates have been employed to target elevated triglycerides for primary, as well as, secondary prevention (Daniel 2011). Patients with MetS are in a pre-diabetic state, which implicates increased fasting glucose levels and glucose intolerance, therefore the main goal is to prevent the progression to diabetes. In this case, weight loss and increased physical activity have been shown to be very effective, decreasing the rate of progression from pre-diabetes to diabetes by 50% (Grundy 2016).

1.2 The Introduction to the insulin signalling pathway

The hormone insulin acts on various target tissues, including the liver, skeletal muscle, and fat tissue, and regulates the blood glucose levels by promoting its uptake into target tissues. In the fasted state, glucose homeostasis depends upon the balance between hepatic glucose production and the glucose utilization by the major insulin-dependent tissues such as liver, adipose, and muscle, and by insulin-independent tissues such as brain and kidney. In normal conditions, glucose remains in a narrow range between 4-7 mM (Watson et al. 2004). Thus, in normal conditions, the response to increased plasma glucose is an increase in secretion of insulin from ß-cells of the pancreatic islets. Insulin is the most potent anabolic agent known, promoting the storage and synthesis of lipids, proteins, and carbohydrates and inhibiting their breakdown and release into the circulation (Watson et al. 2004). The increase in circulating insulin levels stimulates glucose transport into peripheral tissues and inhibits hepatic gluconeogenesis. Insulin also plays a role in ion and amino acid transport, lipid metabolism, glycogen synthesis, gene transcription and protein synthesis and degradation, and DNA synthesis.

The existence of the insulin receptor was discovered in 1971, followed by many subsequent studies on its structure and binding. However, a major contribution to understanding the insulin pathway was the observation that the ß-subunit of the insulin receptor possesses Tyr kinase activity, which autophosphorylates upon insulin binding (Kasuga, Masato, Karlsson F. Anders, Kahn 1982).

The IR is expressed in almost all mammalian tissues with a varying number of receptor among different tissues. Two major targets of insulin, the adipose tissue and liver can contain as many as 300,000 receptors per cell (Cheatham & Kahn 1995). The concentration of receptors is higher than the normal plasma insulin levels and ranges from 10^{-10}–10^{-9} M providing rapid binding kinetics (Cheatham & Kahn 1995).

The key action of insulin is to stimulate energy storage or utilization by regulating glucose transport into the cell, mediated by the facilitative glucose transporter 4 (Glut4). This is achieved by increasing the functional units of Glut4 proteins at the plasma membrane, rather than increasing the activity of the transporter (Furtado et al. 2002). In the absence of insulin, Glut4 slowly recycles between the plasma membrane and the vesicular compartment within the cell. Insulin stimulates the translocation of a pool of Glut4 to the plasma membrane via exocytosis. The rate of glucose transport into fat and muscle cells is controlled by the concentration of Glut4 at the cell surface and the duration of which the protein is maintained at the site (Huang & Czech 2007).

1.2.1 The Insulin signalling cascade

The two main insulin transducer pathways starting at the insulin receptor are the phosphatidyl 3-kinase (PI3K)/Akt pathway and the Raf/Ras/MEK/MAPK. The PI3K pathway is responsible for most of the metabolic effects of insulin, whereas the mitogen-activated protein kinase (MAPK) pathway controls the cell growth (“mitogenesis”) and differentiation (De Meyts 2016).

The cascade of phosphorylation events is initiated upon insulin binding to the insulin receptor, which is a tetrameric protein composed of two extracellular α subunits and two transmembrane ß subunits joined together by disulfide bonds.

As graphically explained on **Figure 2**, insulin binding to the α subunits causes a conformational change and activation of kinase activity in the ß subunits, resulting in their transphosphorylation, allowing the recruitment of the insulin receptor substrates (IRS) (Boucher et al. 2014). Moreover, receptor activation leads to the phosphorylation of the tyrosine residues on IRS proteins, which organize and mediate signalling.

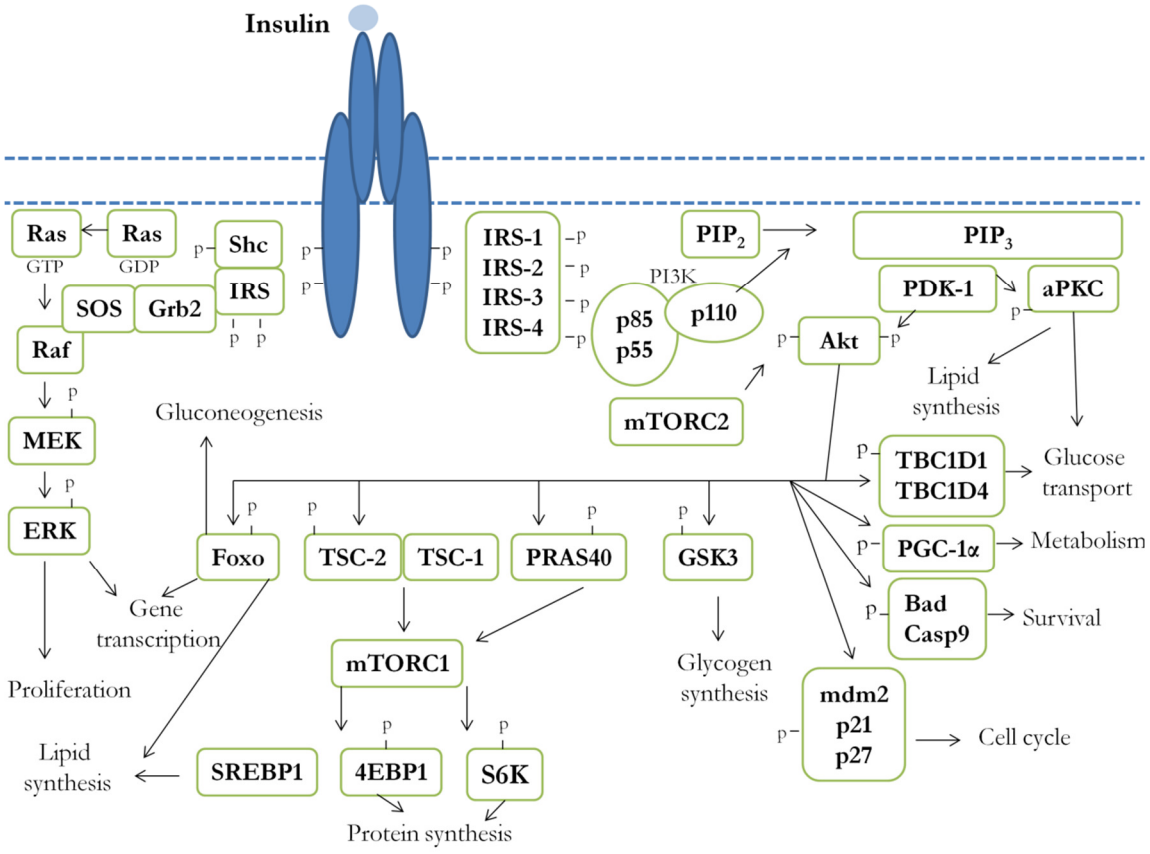

Figure 2 Insulin signalling pathway. Activation of the insulin receptor by their ligand initiates a cascade of phosphorylation events. Upon ligand binding conformational change and autophosphorylation of the receptors occurs, leading to the recruitment and

phosphorylation of receptor substrates such as IRS and Shc proteins Adapted from: (Boucher et al. 2014).

They are recognized by the regulatory subunit of the PI3-kinase (PI3K) (Vadas et al. 2011; Boucher et al. 2014), whose activation depends on the binding of the two Src Homology 2 (SH2) domains in the regulatory subunit of tyrosine-phosphorylated IRS proteins (Myers et al. 1992). This results in activation of the catalytic subunit, which rapidly phosphorylates phosphatidylinositol 4,5-bisphosphate (PIP_2) to generate the lipid second messenger phosphatidylinositol (3,4,5)-triphosphate (PIP_3). PIP3 recruits Akt to the plasma membrane, where it is activated by phosphorylation and induces downstream signalling. Most of the physiological effects of PI3K-generated PIP3 are mediated by a subset of AGC protein kinase family members, which include isoforms of Akt/protein kinase B (PKB), p70 ribosomal S6 kinase (S6K), serum- and glucocorticoid – induced protein kinase (SGK), as well as several isoforms of protein kinase C (PKC). However, Akt phosphorylation at Ser-473 is required for full activation and is accomplished by the mechanistic target of rapamycin complex 2 (mTORC2) (Sarbassov et al. 2005). The Akt/PKB family of proteins is composed of three different isoforms of serine/threonine protein kinases. They all possess a pleckstrin homology (PH) domain, allowing interaction with PIP3 and recruitment to the plasma membrane. Akt2 is most abundant in insulin-sensitive tissues and seems to play a predominant role in mediating insulin action on metabolism. The PI3K-PKB/Akt pathway is highly conserved, and its activation is tightly controlled (Hemmings & Restuccia 2012). Activation of Akt by PDK-1 and mTORC2 allows the phosphorylation and activation of many downstream targets. Akt also phosphorylates and inactivates glycogen synthase kinase 3, resulting in glycogen synthase activation and glycogen accumulation in the liver (Boucher et al. 2014). mTORC1 substrates include the eukaryotic translation initiation factor 4E binding protein 1 (4EBP1), and ribosomal protein S6 kinase, 70 kDa,

polypeptide 1 (S6K1), which, in turn, phosphorylates the ribosomal protein S6 (S6/RPS6), promoting protein synthesis and cellular proliferation (Düvel et al. 2010).

The activation of the serine/threonine kinase Raf/MEK/ Erk1-2 cascade begins with the adapter protein grb2 binding to IRS and Shc. It exists in a complex with the son of sevenless (SOS), a guanyl nucleotide exchange factor that promotes GDP/GTP exchange on the small G protein $p21^{ras}$ (Skolnik et al. 1993). Under sufficient stimulation, phosphorylated Erk1-2 translocates to the nucleus and phosphorylates transcription factors and mitogen- and stress- activated protein kinases

1.3 The energy producing pathways

The metabolic activity of normal cells relies primarily on mitochondrial oxidative phosphorylation (OXPHOS), as it is more efficient than glycolysis in generating ATP for energy (Ramzan et al. 2013). However, glycolysis is an ancient and highly conserved energy producing pathway, and organs in the body still rely on it to function, such as brain, liver, and muscle. As the availability of free oxygen in the atmosphere increased, cells began relying more on OXPHOS for energy (Zheng 2012).

1.3.1 Glycolysis

Glycolysis is carried out in the cytoplasm and leads to the conversion of one molecule of glucose into two molecules of pyruvate with the consequent generation of two molecules of ATP. Pyruvate is a metabolic intermediate with several potential fates including entrance into the TCA cycle within mitochondria to produce nicotinamide adenine dinucleotide (NADH) and flavin adenine

dinucleotide, hydroquinone form ($FADH_2$). The reducing agents subsequently donate electrons to the electron transport chain (ETC), which when fully coupled to complex V (ATP synthase) in the mitochondrial inner membrane generates an additional 34 molecules of ATP per molecule of glucose. Alternatively, pyruvate can be converted to lactate. The glycolytic pathway also supplies biosynthetic intermediates for cell growth and proliferation. The first product of glycolysis, glucose-6-phosphate, can drive the generation of NAPD+ from NADPH in the pentose phosphate pathway, which supplies metabolites for nucleotide biosynthesis that is required for DNA replication and ribonucleic acid (RNA) transcription (Teslaa & Teitell 2014).

1.3.2 Oxidative Phosphorylation

OXPHOS takes place in the mitochondria and consists of the ETC, which comprises NADH-dehydrogenase (complex I), succinate dehydrogenase (complex II), ubiquinone, *bc*1 complex (complex III), cytochrome *c* oxidase (complex IV). Most electrons transferred by the ETC are derived from NADH and enter the chain via complex I. Moreover, complex II pumps in electrons directly. While the electrons are transferred through the ECT, a mitochondrial membrane potential is generated by protons across the inner membrane, which is later used by complex V (ATP synthase) to produce ATP (Hüttemann et al. 2007).

XF Extracellular Flux Analyzer is an instrument that allows studying physiological changes in bioenergetics and metabolic pathways of mitochondrial respiration and glycolysis of live cells. It is achieved by two sensors, one that measures oxygen consumption rate (OCR), as an indicator of mitochondrial respiration and another that measures extracellular acidification rate (ECAR) an indicator of lactic acid production of glycolysis.

During the mitochondrial assay, cells are metabolically challenged by the addition of inhibitors of different complexes of the ETC that essentially shift the

bioenergetic profile of the cell **(Figure 3A)** (Agilent Technologies note 2017). Baseline rates are measured first, and the OCR reported in the unit of picomoles per minute (pmol/min). The first injection is done with a solution containing oligomycin, which is a compound that inhibits ATP synthase **(Figure 3A)**. The response after injection of oligomycin can be used to establish the percentage of oxygen devoted to ATP synthesis and to naturally occurring proton leak. The second injection is a solution containing the ETC accelerator, Carbonyl cyanide-p-trifluoromethoxyphenylhdrazone (FCCP) which disrupts ATP synthesis by transporting hydrogen ions across the mitochondrial membrane instead of the ATP synthase, causing energy usage without ATP production. The use of this compound allows the calculation of the maximal respiratory capacity of cells (Agilent Technologies note 2017).

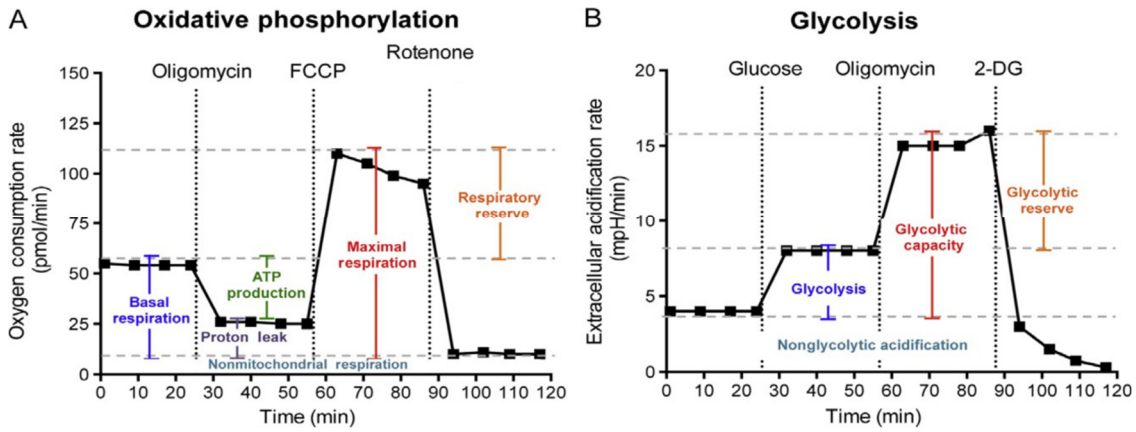

Figure 3 Mitochondrial respiratory and glycolytic profiles. Typical profile obtained with the XF Extracellular Flux Analyzer (Agilent Technologies). **(A)** Mitochondrial stress test graph showing the key parameters of mitochondrial function, following the sequential injection of specific compounds that Oligomycin, FCCP and Rotenone. **(B)** Glycolytic stress test graph with the parameters of cellular glycolysis. Adapted from (Pelletier et al. 2014).

Finally, the third injection is a solution containing rotenone, a complex I inhibitor **(Figure 3A)** that shuts down mitochondrial respiration by disrupting the membrane potential of the mitochondria. This compound allows for the calculation of the nonmitochondrial respiration **(Figure 3A).**

During glycolysis stress test, as glucose is being converted to pyruvate and lactate, resulting in the production and excretion of protons, the acidification of the medium surrounding the cell is detected by the XF sensors as ECAR **(Figure 3B)**. The first injection is a saturating concentration of glucose, which is catabolized via the glycolytic pathway to pyruvate, producing ATP, NADH, water, and protons and allows the estimation of the rate of glycolysis under basal conditions. Second injection is done with a solution containing oligomycin, that, as described previously, inhibits mitochondrial ATP production, shifting the energy production towards glycolysis, revealing the maximal glycolytic capacity of the cell. The final injection is a solution containing 2-deoxy-glucose (2-DG), a glucose analog that inhibits glycolysis through competitive-binding to glucose hexokinase, confirming that the increase in ECAR is associated to glycolysis **(Figure 3B).**

Oxidative phosphorylation and glycolysis are the two major energy-producing pathways in the cell and although seem separate pathways, they are tightly connected and intertwined (Zheng 2012). Most cells pose the ability to adapt to their environment by switching between those two pathways **(Figure 4)**.

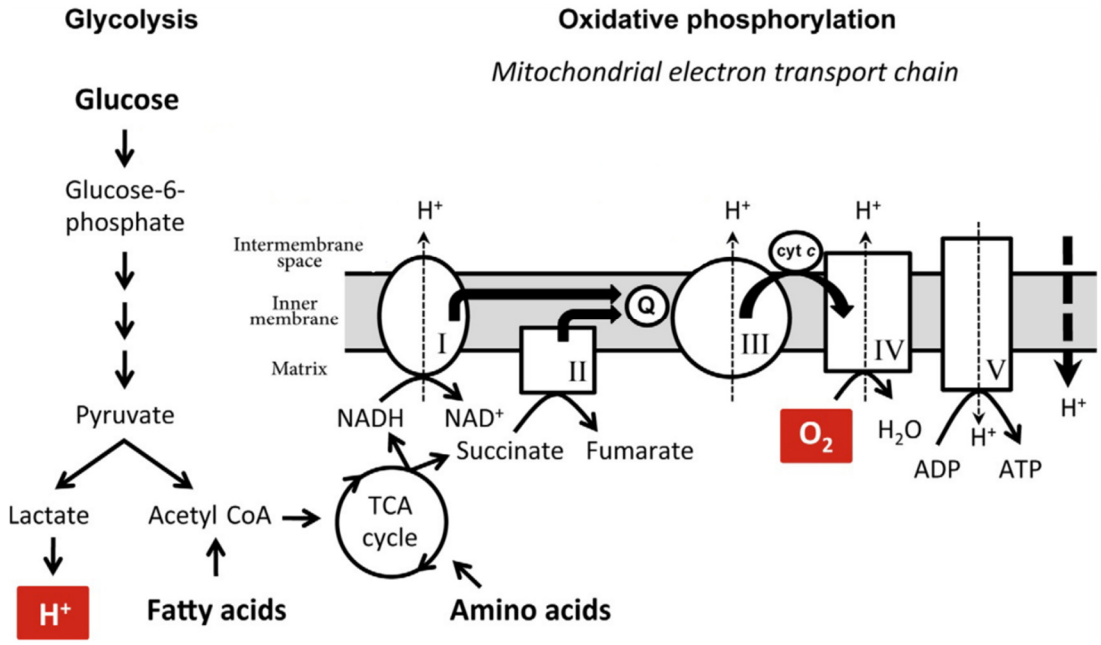

Figure 4. Schematic Representation of Cellular Bioenergetic Pathways. Cells generate energy in the form of ATP by a combination of two main metabolic pathways: glycolysis and oxidative phosphorylation. Glycolysis metabolizes glucose through a series of enzymatic reactions to pyruvate, which can be either reduced to lactate or oxidized via the TCA cycle and the mitochondrial ETC to generate energy. Adapted from (Pelletier et al. 2014).

As already mentioned, adipose tissue is a very active, multifunctional organ maintaining energy homeostasis in check. Adipocytes, from white adipose tissue (WAT), contain a relatively low number of mitochondria compared to the overall size, but they either oxidize incoming fatty acids (FAs) and carbohydrate fuels through the TCA cycle and the ETC **(Figure 4)** or store them in the form of triglycerides until required for release. Glycerol-3-phosphate, a precursor substrate for FA-esterification is produced by mitochondria and is required for the packaging of lipids as triglycerides (TGs) in the lipid droplets (Kusminski & Scherer 2012). Mitochondria play a crucial role in *de novo* lipogenesis, lipolysis and FA-esterification.

1.4 Zucker rats as a genetic model of metabolic syndrome

1.4.1 Discovery and development

Zucker rats (ZRs) arose spontaneously by 'fatty' mutation during crosses between Sherman and Merc 13M rat stock (Zucker & Zucker 1961)(Kava et al. 1990). It was discovered that the '*fa'* mutation was inherited as a Mendelian recessive trait (Zucker & Zucker 1961; Kava et al. 1990) as about 25% incidence of obese pups were regularly found (Zucker & Zucker 1961). The picture presented in the original paper shows Brother and Fatty rats at the age of 10 months with the respective weights of 447 and 1035 grams (Zucker & Zucker 1961). Representative images of Zucker rats used in our experiments shown on **Figure 5**.

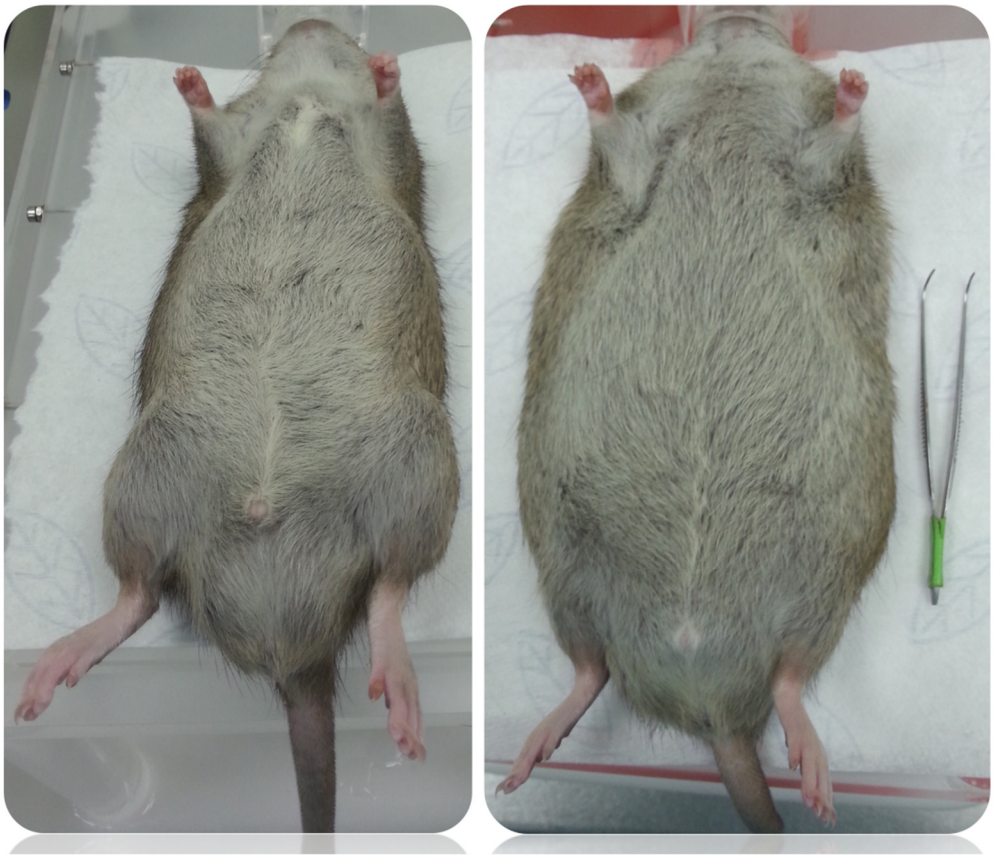

Figure 5. Appearance of heterozygous and homozygous Zucker rats. Clear differences were observed in the size of the animals already at 10 weeks of age. Left, heterozygous (+/*fa*; Zucker lean; ZL) and right, homozygous (*fa*/*fa*; Zucker fatty; ZF).

They observed that morphological manifestations of the obese condition show up at 3 to 5 weeks of age due to overeating and even with a lifelong food restriction, *fa/fa* rats become obese with 50% body fat (Kava et al. 1990). The Zucker fatty rats are significantly hyperphagic compared to lean littermates as early as 17 days of age (Kava et al. 1990). Homozygous animals develop hyperinsulinemia, hyperlipidemia, hypercholesterolemia, adipocyte hypertrophy and hyperplasia and hepatic insulin resistance (Kava et al. 1990)(Aiston et al. 2000). Liver hypertrophy is found as early as 6 weeks of age and persists until one year of age (Goldstein & Johnson 1980). A loss in glucose tolerance occurs in ZR by 10 weeks of age and progressively worsens by 19 weeks of age (Augstein & Salzsieder 2009).

The second important observation was related to the milky appearance of blood serum (lactescence). Biochemical analysis showed a ten-time increase in total fatty acids, raised cholesterol and phospholipids. Fasting lipid levels remained very high even after 18 hours (Zucker & Zucker 1961).

1.4.2 Molecular characteristics of the obese subjects

The Zucker fatty rat (*fa*/*fa*), characterized by a mutation in the leptin receptor gene (Phillips et al. 1996), is considered a model for pre-diabetes. The consequences of this mutation result in hyperphagia, IR, hyperinsulinaemia, hyperlipoproteinaemia, and obesity. Additionally, these animals progressively develop glucose intolerance from 10 to 19 weeks of age, but do not develop T2DM (Apweiler & Freund 1993). Although they maintain their capability to control normoglycaemia, changes to pancreatic islets were also shown, as impaired islets histology, altered ß-cell mass. These abnormalities are related to the very early onset of insulin resistance and glucose intolerance (Augstein & Salzsieder 2009; Weir et al. 2001). In terms of the lean phenotype two genotypes, homozygous lean (+/+) and heterozygous lean (+/fa), exist. The heterozygous lean ZRs have been shown to be susceptible to diet-induced obesity (Morris et al. 2003).

Throughout this thesis, Zucker rats were fed with regular diet and not obese phenotype was found in the heterozygote Zucker lean, and consequenty it was used as control of Zucker obese rats. Throughout the thesis the heterozygote Zucker lean subjects are denoted as **ZL** and the Zucker obese as **ZF**, also when referring to hepatocytes or their secreted EVs.

1.4.3 Worldwide research use of Zucker rats

To detect the early effects of the *fa* mutation and in search for the aetiology of obesity, Goldstain and Jahnson established for the first time a successful primary foetal hepatocyte culture from obese (ZF) and lean (ZL) Zucker rats, in the 1980s. No difference was found in terms of growth or ornithine transcarbamylase activity between both strains. They also concluded that upon a change of media their lipogenic activity decreased in both types of cells (Goldstein & Johnson 1980). A few years later, other groups confirmed this finding by studying the

incorporation of radioactively labelled $U^{14}C$ lactate as a source of carbon for fatty acid and glycerol synthesis. Enhancement in TG production was observed in ZF hepatocytes, reflecting their lipogenic state with augmented TG content as compared to their lean littermates. They concluded that metabolic activities in cells *in vitro* reflect well the phenomenon observed *in vivo* (Porquet et al. 1984).

Yet another group found the increased activity of glucose-6-phosphate dehygrogenase together with the significantly higher rate of $U^{14}C$ glucose and $U^{14}C$ lactate incorporation into C^{14} lipid in ZF hepatocytes. They concluded that a very active phosphate pentose pathway (11-folds) could be responsible for enhanced glucose uptake in these hepatocytes, with no effect of insulin and no enhancement in glucose transport capacity (Carbó et al. 1991).

Additional studies described other metabolic defects in hepatocytes from ZF rats. Aiston, Peak, and Agius discovered increased glucokinase activity and higher rates of glycolysis and lipogenesis in ZF hepatocytes which however had a decreased glycogen synthesis (Aiston et al. 2000).

In summary, several metabolic pathways including insulin signalling and Glut4 translocation with elevated hepatic glycolysis are altered in the Zucker rats.

1.5 Pathology of Metabolic Syndrome

1.5.1 Aetiology

The aetiology of MetS is still matter of continuous debate. An early hypothesis states that insulin resistance is the primary cause of MetS (Reaven 1988). Then, at a closer look, obesity was viewed as the main cause. It is currently thought that the positive energy balance as the causative agent with obesity serving as a clinical indicator of over nutrition (Grundy 2015). Caloric restriction even in the

presence of obesity is able to reverse most metabolic risk factors for the development of MetS (Ikramuddin & Buchwald 2011). Factors that mediate the difference between metabolically healthy and metabolically unhealthy is not obesity *per se*, however fat storage in peripheral organs, which leads to the development of insulin resistance.

As described in the previous section, adipocytes and their secreted components have a profound influence on neighbouring cells and distant organs. Most studies have focused on the adipocyte/macrophage axis in terms of the pathogenesis and progression of MetS. However, another major organ affected in those settings is the liver. As the main synthesizer of many factors in physiological conditions, the possibility cannot be discarded that factors secreted by hepatocytes also play a role in the pathology of MetS. Recently, a study was published, which identified fetuin B, secreted by steatotic hepatocytes, as being a link between steatosis and impaired glucose metabolism. The study concluded that steatosis changes protein secretion in hepatocytes and that they cause insulin resistance and inflammation (Meex et al. 2015).

1.5.2 Adipogenesis

Adipocytes are the major subset of cells in adipose tissue, which is areolar connective tissue forming an insulating layer under the skin and around the internal organs (Ali et al. 2013). Their primary function is insulation and the control of the energy homeostasis, which is storing fat in periods of energy excess and mobilizing it when needed (Cornelius et al. 1994). During long time it was thought that these were their only functions, however, this tissue is now recognized as a highly active metabolic and a very dynamic endocrine organ controlling many physiological processes via secreted factors, collectively called adipokines. One important function of the adipocyte is to deal with the daily influx of dietary fat (Goossens 2008). Importantly, they have a physiological, as well as,

a pathological impact on the metabolism of other tissues, insulin sensitivity, immunological responses and vascular disease.

Adipocytes differentiate and mature from precursor cell to become functional in the process of adipogenesis. First, the undifferentiated mesenchymal stem cells become preadipocytes to later undergo a secondary differentiation featured by lipid accumulation into the cell cytoplasm.

Most of what is known regarding adipogenesis have been studied *in vitro* using the 3T3-L1 pre-adipocyte cell line model, as studying this process *in vivo* is difficult. Differentiation is propagated chemically with an adipogenic cocktail containing a combination of insulin, which acts through the insulin-like growth factor 1 (IGF-1) receptor, a glucocorticoid, an agent that elevates intracellular cAMP levels, and foetal bovine serum. Dexamethasone (DEX), a synthetic glucocorticoid and the cAMP phosphodiesterase inhibitor 3-isobutyl-1-methylxanthine (IBMX) are the most commonly used compounds to drive the differentiation process (Cornelius et al. 1994; Ntambi & Kim 2000). This multistep process is driven by the expression of numerous genes and transcription factors in a highly ordered and well characterized temporal sequence (Rosen et al. 2000). After 48h of the induction of adipocyte differentiation, confluent 3T3-L1 fibroblasts acquire a spherical, adipocyte-like morphology (Fan et al. 1983) due to a change in cytoskeletal components and extracellular matrix (ECM) (Gregoire et al. 1998). On a molecular level, adipogenesis involves the regulation of several genes that is orchestrated by different transcription factors. C/EBP1 and PPARγ transcription factor families are induced at early stages of differentiation, this period is characterized by a prominent period of growth arrest followed by expression of a fully differentiated phenotype (Rosen et al. 2000). Within the first hour after the addition of the of the adipogenic cocktail, a dramatic increases in the expression of CCAAT/enhancer binding proteins (C/EBP) ß and Δ are observed (Cornelius et al. 1994). During the first 24h C/EBP-ß and C/EBP-Δ accumulate. At this point, the cell enters in the cell cycle again and synchronously implements mitotic clonal expansion (MCE) (Tang et al. 2003). At

a G1 to S phase, C/EBP-ß is hyperphosphorylated and sequentially activated by glycogen synthase kinase-3ß and MAPK. Subsequently, both C/EBP-ß and C/EBP-Δ induce the expression of adipogenesis transcriptional regulators, PPAR-γ and C/EBP-α (Tong et al. 2005). They induce the cascade of gene expression that controls adipocyte differentiation. At 48h into the process, C/EBP-α protein accumulates and becomes phosphorylated by the cyclin D3, ceasing proliferation and allowing cells to enter into the terminal differentiation phase (Wang et al. 2006). After just 8 days of induction of differentiation nearly 90% of cells are mature adipocytes (Moreno-Navarrete, Jose Maria and Fernandez-Real 2012). During the terminal differentiation phase, adipocyte *de novo* lipogenesis increases, and they become sensitive to the action of insulin with more insulin receptors as well as glucose transporters, seen as an increase in genes encoding for Glut4 and the insulin receptor. The activity of enzymes involved in triglyceride metabolism such as ATP citrate lyase, malic enzyme, acetyl Co-A carboxylase, fatty acid synthase, glycerol-3-phosphate acetyltransferase, and aP2 among others become up to 100-fold higher with extensive lipid accumulation. During this process, lipid-laden droplets begin to accumulate within the cytoplasm, and over time they become larger.

1.5.3 Obesity

Obesity results from an imbalance between energy intake and energy expenditure (Goossens 2008). Adipose tissue is the main lipid storage depot in the body, which has the capacity to rapidly respond to over nutrition. The excess energy is stored in lipid droplets of adipocytes that can be mobilized during the time of nutrient deprivation. However, if a state of over nutrition persists, to keep up with the nutrient influx adipose tissue expands, recruiting adipocyte progenitor cells to undergo adipocyte differentiation, entering a state of hypertrophy. In this condition, the size of the adipocyte can increase up to 140-180 µm in diameter, but the diffusion limit of oxygen is at most 100 µm resulting in local hypoxia

(Salans et al. 1973). The excess adiposity and adipocyte dysfunction in the state of obesity result in the deregulation of a wide range of adipose tissue-derived secretary factors that conducts to adipose tissue inflammation. Taken together, during the development of obesity, adipose tissue is characterized by adipocyte hypertrophy followed by hypoxia, immune cell infiltration, all leading to the development of insulin resistance, which effectively progresses into the systemic metabolic disease (Chan, Pei-chi and Hsieh 2017). Insulin resistance manifests as hyperinsulinemia in the presence of hyperglycemia and dyslipidemia (Rutkowski et al. 2015). Accumulating evidence suggests that dysfunctional adipose tissue plays a crucial role in the pathogenesis of obesity-related insulin resistance (Goossens 2008).

1.5.4 Adipose tissue in metabolic syndrome

As mentioned in the previous section, during obesity, expanding adipocytes are eventually unable to store excess lipids even with enhanced adipocyte proliferation (hyperplasia). This redirects fatty acids to the liver promoting dyslipidemia, characterized by elevated plasma free fatty acids (FFAs), triglycerides and LDL, and the reduction of high-density lipoproteins. In addition, enlarged adipocytes are characterized by enhanced lipolysis, the breakdown of stored triglycerides (TGs) by lipases releasing FFAs and glycerol, which further increases plasma FFA-level and up regulates TG synthesis in the liver.

The view and understanding on adipose tissue physiology took a turn in 1994 with the discovery of the product of the *Ob* gene that encodes for the hormone leptin (Zhang et al. 1994). With that, WAT was recognized as a major endocrine organ (Trayhurn et al. 2008) and a number of additional adipose products such as adipsin and later, the synthesis of pro-inflammatory TNF was demonstrated and directly linked to obesity-induced IR (Mcardle et al. 2013). Nowadays, it is clear that adipose tissue, through the secretion of adiponectin, resistin, adipsin, leptin, acylation stimulating protein (ASP), PAI-1, and lipoprotein lipase (LPL),

among many more, can signal locally as well as on a systemic level (Hosogai et al. 2007). Adipose tissue of obese insulin resistant subjects is characterized by increased expression and secretion of pro-inflammatory cytokines such as TNF, IL-6, PAI-1 and leptin and down regulation in the insulin-sensitizing adiponectin (Hosogai et al. 2007). The adipocyte 'secretome' also includes lipid moieties, including cholesterol, retinol, steroid hormones and prostaglandins (Trayhurn et al. 2008) that can influence the lipid metabolism.

1.5.5 Hepatocytes

The liver is a multifunctional organ and the metabolic centre of the body (Falcón-Pérez et al. 2010). It plays an important role in many pathways involving nutrient homeostasis such as carbohydrates, lipids, and proteins (Bechmann et al. 2012). It regulates glucose homeostasis by storing excess glucose as glycogen and under hormonal stimulation releasing it into the bloodstream when needed (Klover & Mooney 2004). The liver is also the main detoxifying organ and the unique site for the synthesis of molecules such as bile, clotting factors, and other serum proteins (Medina-Santillán et al. 2013). Although they do constitute nearly 80% of the liver parenchyma, hepatocytes are not the only cells of the liver. Liver macrophages (Kupffer cells), natural killer cells, as well as B and T cells, form a part of the hepatic immune system. Moreover, there are the hepatic stellate cells involved in angiogenesis and the main matrix-producing cells in the process of liver fibrosis (Moreira 2007).

A central metabolic function of the liver is to maintain plasma glucose levels regardless of the nutritional state (Browning & Horton 2004). The liver produces glycogen in response to insulin to clear out and store glucose. However, when the liver is saturated with glycogen there is a shift towards fatty acid synthesis and their subsequent esterification to TG and export to AT as VLDLs (Postic & Girard 2008).

1.5.6 Development of hepatic steatosis

In pathological conditions, hepatic lipid and carbohydrate metabolism is affected, being one of the reasons for the dysfunction of the insulin signalling. Consequently, the inability of metabolic tissues to respond to insulin leads to an increased amount of lipids and retention of TG in the liver causing fatty liver. If this state is maintained, simple steatosis can progress into steatohepatitis with inflammatory response and subsequently into cirrhosis, characterized by the scar tissue formation and leading to the development of hepatocellular carcinoma (HCC).

The accepted hypothesis for the accumulation of triglycerides in the liver is an enhanced hepatic *de novo* lipid synthesis via the lipogenic pathway caused by obesity and insulin resistance of AT, which results in increased release of non-esterified fatty acids (NEFA) from expanding adipose tissue to the liver. Lipid disposal via ß-oxidation and VLDL export are only very slightly affected (Postic & Girard 2008). Adipocyte hypertrophy leads to enhanced activity of hormone-sensitive lipase and consequently an increased hydrolysis of triglycerides. This has a direct effect on hepatic FFA uptake, which are metabolized either to generate ATP via oxidative phosphorylation or esterified to triglycerides, which then can be incorporated into VLDL particles for excretion or stored within the hepatocyte (Browning & Horton 2004; Postic & Girard 2008).

In the presence of excess nutrients, glucose gets converted to fatty acids via the conversion of glucose to pyruvate, which is then fed to the mitochondrial Krebs cycle. Citrate formed in the Krebs cycle is transferred to the cytosol where it is converted to acetyl-coA by ATP citrate lyase. Subsequently, acetyl-CoA is converted to malonyl-CoA by acelty-CoA carboxylase 1 (ACC1), which is used by fatty acid synthase to form fatty acids, such as palmitic, stearic or oleic acids, used for triglyceride synthesis. In steatotic livers, the rates of *de novo* fatty acid synthesis is elevated, as shown in humans and mouse models (Araya et al. 2004). *De novo* fatty acid synthesis is regulated independently by insulin and

glucose (Koo et al. 2001). The insulin-triggered pathway is mediated by the sterol regulatory element-binding protein-1c (SREBP-1c) transcription factor. It activates lipogenesis-related genes in the nucleus and it has been shown to significantly influence the development of hepatic steatosis. Its inactivation in the liver of *ob/ob* mice results in significant reduction in hepatic triglycerides, with unchanged obesity and insulin resistance (Yahagi et al. 2002). On the other hand, over expression of SREBP-1c leads to increased lipogenesis and development of liver steatosis.

The already mentioned, excess glucose also stimulates *de novo* lipid synthesis, via carbohydrate response element binding protein (ChREBP) that transcriptionally regulates the expression of lipogenic genes, such as fatty acid synthase (FAS), and acetyl CoA carboxylase (Medina-Santillán et al. 2013). It does that by binding to the promoter of the key enzyme in glycolysis, liver-type pyruvate kinase (L-PK), which catalyzes the generation of pyruvate used in Krebs cycle for citrate synthesis, the primary source of acetyl-CoA used for fatty acid synthesis. It is important to mention that PPAR-γ is also involved in the development of hepatic steatosis (Gavrilova et al. 2003).

1.5.7 Deregulation of the insulin signalling pathway in metabolic syndrome

Different mechanisms have been proposed to explain the molecular events behind the development of insulin resistance related with MetS. One hypothesis involves an increased serine phosphorylation of IRS-1, which leads to decrease in tyrosine phosphorylation and therefore a decrease in binding of the downstream enzyme PI3K, and essentially a decreased phosphorylation of the Akt kinase (Rask-Madsen & Kahn 2012) and inactivation of the downstream pathway.

Mouse models with a loss of response to insulin have been critical to understanding the mechanism underlying insulin resistance. In particular, the

FIRKO model, with fat-specific deletion of the insulin receptor (Blüher et al. 2002), the LIRKO model with liver-specific *IR* knockout (Escribano et al. 2009), MIRKO representing muscle-specific IR deletion (Brüning et al. 1998), ß cell-specific an ß-IRKO model (Kulkarni et al. 1999) and mice models with adipose-selective reduction of Glut4 ($G4A^{-/-}$) (Abel et al. 2001). Studies on the FIRKO model, show that insulin resistance in adipocytes is crucial for the development of obesity and its metabolic abnormalities (Blüher et al. 2002). Moreover, the adipose-specific deletion of Glut4 in mice leads to impaired glucose tolerance and insulin resistance with no changes in adipose mass and causes the development of insulin resistance in muscle and liver (Abel et al. 2001).

The major cause of fasting hyperglycemia in MetS is insulin resistance in the liver. The LIRKO mice exhibits pure hepatic insulin resistance (Biddinger et al. 2005) with the complete loss of insulin suppressed hepatic glucose output due to increased expression of the gluconeogenic enzymes such as phosphoenolpyruvate carboxylase and glucose 6-phosphate and decreased expression of enzymes that regulate glycogen synthesis and glycolysis, including glucokinase and pyruvate kinase (Escribano et al. 2009; Rask-Madsen & Kahn 2012). Moreover, insulin resistance affects the action of insulin on the regulation of circulating lipids in the liver, leading to hyperinsulinemia and causes increased circulating levels of FFAs and triglyceride as well as decreased clearance of LDLs due to downregulated LDL receptor. In LIRKO mice the secretion of triglycerides is decreased but the secretion of apoB and cholesterol is highly enhanced. LDL receptor expression, and therefore the clearance of apoB-containing particles, is reduced creating pro-atherogenic lesions characterized by decreased HDL cholesterol and an increase in apoB containing particles. Hepatic insulin resistance can alone lead to dyslipidemia and increased risk of atherosclerosis associated with MetS (Biddinger et al. 2005).

1.6 Extracellular vesicles

1.6.1 Overview and classification

It is a commonly accepted fact that cells, both *in vitro* and *in vivo* secrete EVs to the extracellular environment (Simpson et al. 2008). EVs is a collective name suggested by the International Society for Extracellular Vesicles (ISEV) to refer a group of lipid membrane-enclosed vesicles released from prokaryotic and eukaryotic cells (van der Pol et al. 2016). EVs are released during basal conditions and under a stimulus or a cellular stress. Increased release of EVs has been reported to occur under many stress conditions such as hypoxia, oxidative stress, thermal change and many other factors (Iraci et al. 2016). Owing to the plasticity of cellular membranes, the organization of lipid membranes and the content of EVs may vary depending on the stimulus that generates them. Once released, EVs can act as mediators of intracellular communication (Yáñez-Mó et al. 2015). This communication may help to maintain homeostasis or may trigger destructive or degenerating process in a cell or organ. They serve not only as mediators but also effectors of cellular processes (H.-G. Zhang (ed.) n.d.).

The extensive proteomic analysis of EVs in different cellular systems has found some common as well as cell-type-specific protein markers (Kalra et al. 2012; D. K. Kim et al. 2015). Currently, a broad classification of EV subpopulations, based on their size and biogenesis, separates them into exosomes, microvesicles (MVs) and apoptotic bodies **(Figure 6)**. Exosomes are the smallest in this group, which is directly related to their endosomal origin, ranging in size from 30-150 nm. Next are the more heterogeneous population of microvesicles that are formed by budding and shedding directly of the plasma membrane and can be as large as 1 μm in size (Lawson et al. 2016).

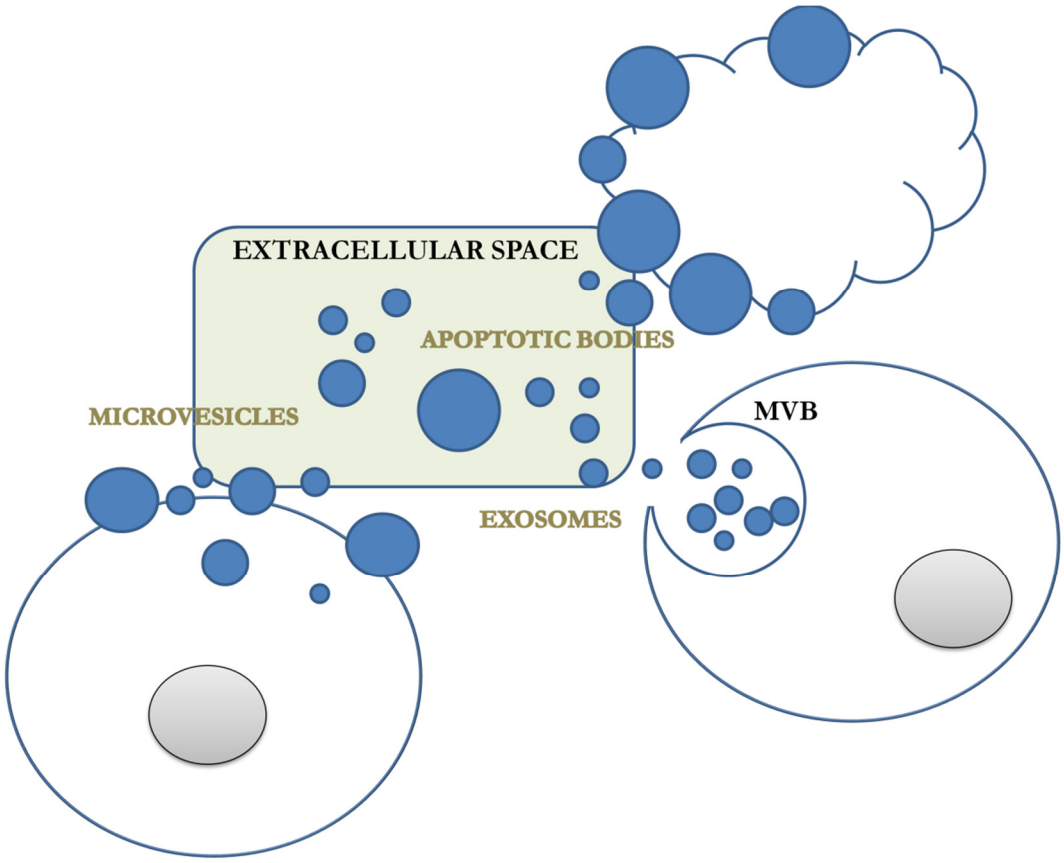

Figure 6 Schematic representation of the different types of EVs based on their intracellular origin. Major populations of EVs include exosomes, microvesicles and apoptotic bodies. Adapted from (György et al. 2011).

Lastly, the apoptotic bodies that are products of cellular death, fall into a wider range of size from 1-5 μm. There are some small discrepancies as to the size range of different populations of EVs in the literature, as it seems to be dependent on cell type.

Furthermore, independently of their biogenesis, EVs can carry proteins, lipids and nucleic acids: both coding and non-coding RNAs and DNA cargo (Abels & Breakefield 2016).

1.6.2 Discovery and brief history of the research in extracellular vesicles

Initially, microparticles, not yet known as vesicles, were described to be the "dust" released by platelets (Wolf 1967). The existence of vesicles released by cells into the extracellular space was first mentioned in 1981 when the term exosomes was also coined (Trams et al. 1981). While studying the ecto-ATPases and ecto-5'-nucleotidases, it was discovered that the culture medium of a variety of cells lines, both normal, as well as neoplastic, contained the ATPase and 5'-nucleotidase, which was shown to be associated with vesicles. The researchers concluded that the vesicle content reflected the ectoenzyme activity phenotype of the parent cells and for the first time the physiological function of those exfoliated membrane vesicles (exosomes) was proposed (Trams et al. 1981). However, most reports attribute the discovery and initial characterization of EVs to the study of the transferrin receptor (TfR) shedding during the maturation of sheep reticulocytes (Pan & Johnstone 1983). The group led by Rose Johnstone followed the fate of the transferring receptor *in vitro* and discovered that it was removed from the plasma membrane and externalized **(Figure 7A)**. Here the composition of the conditioned medium was concentrated by high-speed centrifugation at 100,000 x *g* and analyzed for the TfR-antibody complex. Its release was shown to be associated with released vesicles (Pan & Johnstone 1983).

This system described, for the first time, specific sorting and externalization of a specific material in vesicles, since their protein composition was enriched in TfR which is not characteristic to plasma membranes (Pan & Johnstone 1983). In a later study, more evidence was presented on these vesicles containing enzymatic activity and characteristic components of the reticulocyte plasma membrane (Johnstone et al. 1987). This study has been followed up and validated by electron microscopy. TfR has been identified on the membrane surface of nano sized (50 nm) vesicles localized inside of a larger (1-1.5 μm) multivesicular structure (Pan et al. 1985) **(Figure 7B and 7C)**.

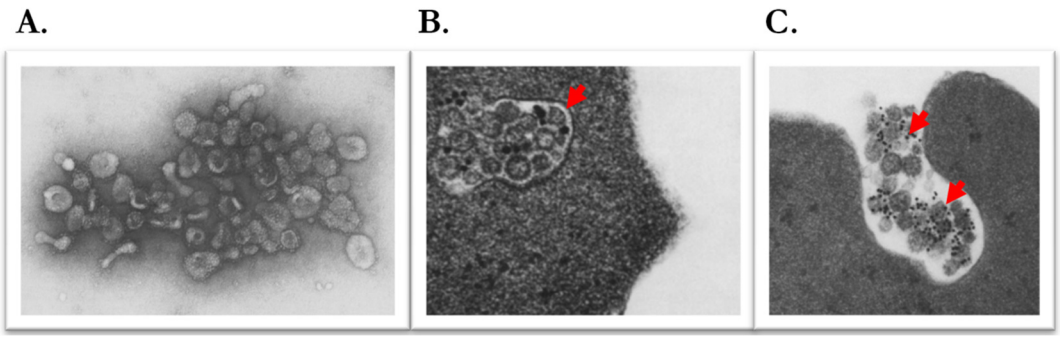

Figure 7 The first report of exosomes existence and biogenesis. Electron micrographs showing **(A)** the evidence of vesicular material secreted from reticulocytes (Adapted from: (Pan & Johnstone 1983). **(B)** The Intracellular localization of multivesicular bodies (MVBs) and their **(C)** fusion with the plasma membrane following the release of gold labelled transferring receptor bearing nanovesicles (Adapted from: (Pan et al. 1985).

These multivesicular structures were formed inside a cell, and upon fusion with the plasma membrane released their vesicular content together with the associated TfR. Authors hypothesized that the exocytosis of these vesicles could represent a mechanism of TfR shedding during reticulocyte maturation (Pan et al. 1985).

Therefore, no major importance was attributed to them and their existence was forgotten for about 10 years until the pioneering studies by Raposo *et al*. which showed that B cells also secrete exosomes, as a result of fusion of multivesicular bodies (MVBs) with the plasma membrane. More importantly, these exosomes were carrying intact major histocompatibility complex class II (MHCII) molecule on their surface capable of triggering an immune response in a target cell (Raposo et al. 1996). A couple of years later, dendritic cells were also shown to release exosomes as a mechanism to modulate immunity (Zitvogel et al. 1998).

1.6.3 Biological Characteristics of EVs

1.6.3.1 Biogenesis

Exosome formation via the endocytic pathway begins with the invagination and endocytosis of the plasma membrane and formation of endocytic vesicles in the cytosol. The ubiquitination of some membrane proteins may serve as one possible internalization signal to trigger endocytosis (Raiborg & Stenmark 2009). These endocytic vesicles are then transported to and fused with early endosomes where they mature and transform to become late endosomes in a process involving changes in size, form, pH, and composition. Depending on their destination, molecules to be recycled are segregated into distinct subdomains of the endosomal membrane (Jovic et al. 2010; Trajkovic et al. 2008). Subsequently, membranes of late endosomes, as they bud inwards and form numerous smaller (30-100nm) vesicles inside to become MVB or intraluminal vesicles (ILV) (Abels & Breakefield 2016). At this point, these vesicles can be addressed to lysosomal degradation or can be fused with the plasma membrane to release exosomes (Colombo et al. 2013).

Microvesicles are formed through direct outward budding and fission of the plasma membrane as a result of dynamic interaction between phospholipid redistribution and cytoskeletal protein contraction (Akers et al. 2013). They are thought to arise from regions of the plasma membrane enriched in lipid rafts, and they expose phosphatidylserine on their membrane (Mittelbrunn & Sánchez-Madrid 2012).

1.6.3.2 Cargo

EVs are formed by a lipid bilayer that encloses distinct biomolecules, such as proteins, lipids, and nucleic acids. Owing to high-throughput proteomic and transcriptomic studies, to date, thousands of vesicular proteins, lipids and RNAs, from many different cells types and body fluids, have been identified and a large

amount of work has been directed at creating databases of proteins and lipids associated to EVs. As a result, three different publically available databases have been created, the Vesiclepedia (Kalra et al. 2012), the EVpedia (D. K. Kim et al. 2015) and Exocarta (Maas et al. 2017). In general, EVs contain a common set of components but also cell specific molecules. They conserve a set of EV-related proteins including ALIX, a member of the ESCRT machinery, and proteins related to membrane transport and fusion including annexins and Rab proteins. EVs also contain cytoskeleton-related proteins like tubulins, actins, moesin, cofilin-1 and profiling-1. Moreover, proteins involved in cell adhesion (integrins, ICAM-1, MFG-E8) that are probably involved in interaction with target cells, as well as, MHCs involved in antigen presentation. Signal trasducing proteins such as insulin growth factor receptor (IGFR) along with heat shock proteins and metabolic enzymes such as elongases, glyceraldehydes 3-phosphate dehydrogenase and pyruvate kinase, that function in distinct cellular pathways. EVs are also known to be highly enriched in tetraspanin molecules such as CD9, CD63 and CD81 and other transmembrane proteins such as Lamp1. HSPs are induced under stress conditions and play many different roles such as directing protein folding, targeting of protein degradation, and binding of antigens for presentation (Tutar & Tutar 2010) and have been repeatedly documented in EVs. All the common proteins identified were found to originate from the cytoskeleton, cytosol, and the plasma membrane. Proteins associated with Golgi, ER or the nucleus were absent in EVs (Thery et al. 2001), however the presence of transcription factors such as Notch and Wnt has been recently reported (Abels & Breakefield 2016).

Most reports regarding the biochemical composition of EVs concentrate on a heterogeneous population of exosomes and microvesicles. Thus, the actual composition of each subtype remains unknown. A group led by Clotilde Théry have characterized exosomal and nonexosomal subpopulations within small EVs and identified protein markers associated with larger EVs, secreted by human primary monocyte-derived dendritic cells (DCs) (Kowal et al. 2016). They confirmed that exosomes were enriched in known protein markers, such as

tetraspanins CD9, 63 and 81, although to a certain degree, they were present in all EV fractions. Moreover, HSPs and flotillin1 were more associated with medium size and larger EVs. Large EVs, in the 2,000 x *g* pellet were abundant in cell markers such as GRP94 and HSP90B1. They also identified proteins either unique or enriched protein markers of small and large EVs. TSG101, syntenin-Annexin XI and ADAM10 as being more specific to small EVs. Actinin-4 and mitofilin were more specific to large- and medium-sized EVs (Kowal et al. 2016).

Lipids are the key components of EVs, with several of them been suggested to have a role in their formation and function. The smaller an EVs is, the larger the proportion of its total mass is contributed by the membrane lipids. ILVs accumulate cholesterol during their biogenesis from the MVB and they are subsequently enriched in cholesterol when compared to the parental cell. EVs are generally enriched in sphingomyelin, cholesterol, phospholipids and glycosphingolipids when compared to the cell of origin, which may be an important factor in their stability (Yáñez-Mó et al. 2015). EVs carry bioactive lipids such as eicosanoids but also transport active lipolytic enzymes such as different phospholipases (Record et al. 2014). They mediate intracellular lipid trafficking of sphingomyelin, leukotrienes, prostaglandins, cholesterol, lysophosphatidylcholine, arachidonic acid and other fatty acids. Moreover, the lipid composition of small EVs points towards sorting of lipidic molecules with enrichment in sphingomyelin, psosphatidylcholine, and phosphatidylethanolamine. On the contrary, the lipid composition of MVs reflects that of the plasma membrane of the secreting cell (Record et al. 2014).

The exchange of RNA between cells by means of EVs was first observed by Valadi *et al.* (Valadi, H. Ekstrom, K. Bossios 2007). They have also demonstrated that vesicular mRNA and miRNA can be functionally transferred and can alter gene expression in neighbouring cells. This was a ground breaking discovery and since then more RNA species enriched in EVs have been identified such as small noncoding RNA species, including RNA transcripts overlapping with protein-coding regions, repeat sequences, structural RNAs,

tRNA fragments, vault RNA, Y RNA, and small interfering RNAs (Bellingham et al. 2012). Moreover, the RNA profile of EVs was found to be enriched relative to one of the originating cells (Valadi, H. Ekstrom, K. Bossios 2007; Ratajczak et al. 2006; Raposo & Stoorvogel 2013).

1.6.3.3 Uptake and Interaction with recipient cells

A body of evidence exists on the physiological and pathological functions mediated by EVs. They are able not only to interact with the recipient cells but also transfer active material to execute the phenotypic change in the target cell. In order for this to be possible, EVs must interact with the cell plasma membrane, directly or indirectly. Different routes have been described such as endocytic pathways clathrin-dependent and independent endocytosis, caveolin-mediated endocytosis, macropinocytosis, phagocytosis, and lipid-rate mediated internalization [Summarized in **Figure 8**; adapted from (Mulcahy et al. 2014)].

Valadi et al, have shown the transfer of functional mRNA and miRNA from mouse to human cells (Valadi, H. Ekstrom, K. Bossios 2007). It has also been demonstrated that EVs secreted by bone marrow BMDCs fused with target DCs, but released their content into the DCs cytosol and the functional miRNA repressed a target mRNA in the target cell (Montecalvo et al. 2012).

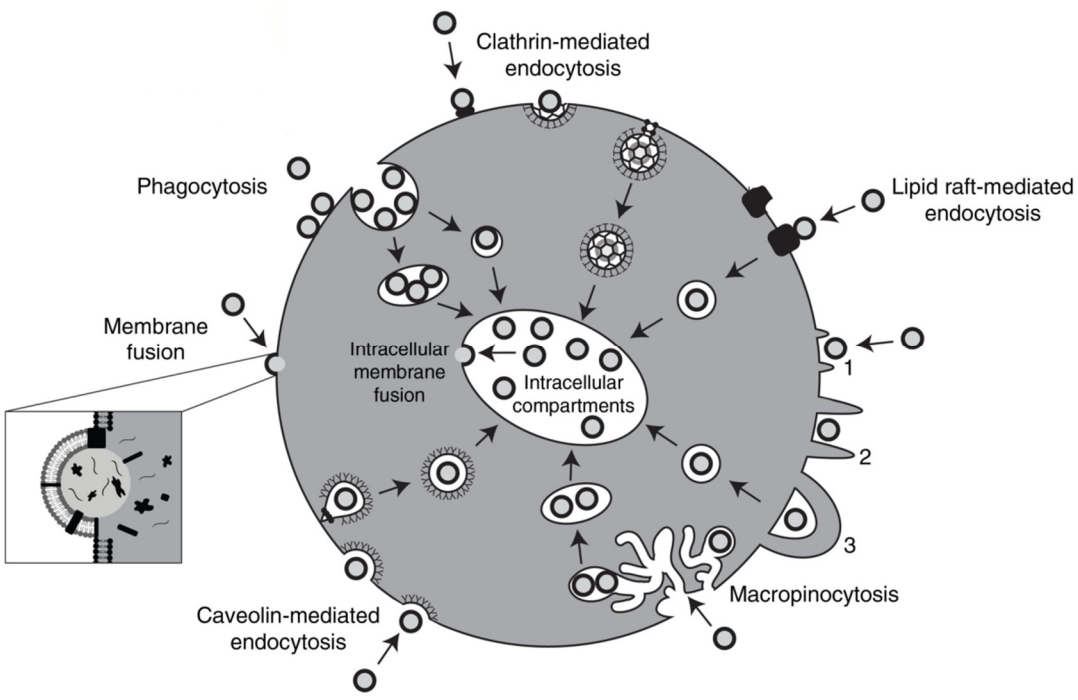

Figure 8 Different routes of EV uptake by the recipient cell. Uptake of EVs has been shown to be mediated through phagocytosis, clathrin- and caveolin-mediated endocytosis. [Image has been adapted from: (Mulcahy et al. 2014)].

The experimental data suggests that endocytosis is the most frequently used process for EVs uptake. It was shown that it is a rapid, energy- and cytoskeleton –requiring process. At 4^0C the uptake was markedly reduced, as well as following actin depolarization with CytochalasinD. Moreover, EVs were not taken up by paraformaldehyde fixed cells (Mulcahy et al. 2014). Under the term of endocytosis there are other independent mechanisms, which have been implicated in EVs uptake such as clathrin-mediated and caveolin-dependent endocytosis and, macropinocytosis. Clathrin-mediated endocytosis, also known as receptor-mediated endocytosis involves internalization through an assembly of clathrin-coated vesicles containing receptors specific to molecules being absorbed and/or their ligand. The process involves membrane deformation and inward clathrin-pit formation. Once mature, it pinches off as a clathrin-coated vesicle. The uncoating and subsequent release of cargo take place at the endosome, where it is sorted and directed. Caveolin-mediated endocytosis,

involves the formation of caveolae-coated pits from domains of plasma membrane glycolipid rafts rich in caveolins, cholesterol, and sphingolipids. Lastly, macropinocytosis, also known as fluid endocytosis, is another endocytic pathway, which involves the formation of membrane invagination ruffles, which once pinched off give rise to macropinosomes absorbing extracellular fluids (Mulcahy et al. 2014). The role of lipid rafts has also been proposed for EVs uptake (Nabi & Le 2003). Clathrin-independent Endocytosis largely requires cholesterol, which is highly enriched in lipid rafts (Mulcahy et al. 2014). In melanoma cancer cells a direct fusion with the plasma membrane has also been shown (Parolini et al. 2009).

1.6.3.4 New Mode of Cellular Communication

Cells are required to communicate with each other for appropriate development and functioning of the whole organism. In addition to classical modes of cell communication, another mechanism, mediated by EVs has emerged. As explored in previous sections, EVs carry bioactive lipids, receptors, proteins, nucleic acids, such as mRNA and microRNA. Moreover, EVs can be taken up by the recipient cell and transfer their cargo to cause either transient or long term phenotypic changes in recipient cells (Tetta et al. 2013). EVs may directly activate the recipient cell by acting as signalling complexes through surface-expressed ligands that directly stimulate the target cell (Camussi et al. 2010). For example, EVs derived from macrophages interact with platelets via the P-selectin glycoprotein ligand-1 expressed on their surface (Tetta et al. 2013). EVs may transfer receptors from LPS activated monocytes, as they were able to induce apoptosis of vascular smooth muscle cells via the caspase-1 contained in their secreted EVs (Sarkar et al. 2009). Moreover, tumour-derived EVs were identified promoting the formation of metastatic niche by priming bone marrow-derived cells towards a pro-angiogenic and pro-metastatic phenotype through upregulation of the tyrosine-protein kinase Met (Peinado et al. 2012).

Furthermore, active Wnt proteins secreted in exosomes activated the Wnt signalling pathway in target cells (Gross et al. 2012). These are just a few examples showing the importance of EVs in physiology and as mediators of pathology.

1.6.3.5 Methods for Isolation and Characterization

The technique chosen for the isolation of EVs has an impact on the amount, type and purity of EVs recovered (Van Deun et al. 2014; Gardiner et al. 2016). Differential-ultracentrifugation still remains the most commonly used technique (Gardiner et al. 2016) and the standard protocol for the isolation of exosomes, or enrichment in exosomes, often in a combination with sucrose density gradients or sucrose cushion (Théry et al. 2006). Differential-ultracentrifugation essentially consists of a series of centrifugation cycles of increasing centrifugal force and duration to isolate particles based on their density. The filtration step, through 0.2 µm filter system, is added to enrich in small EVs. Additionally, as exosomes have been characterized to have densities between 1.1 and 1.19 g/ml, the differential ultracentrifugation is often coupled with the density gradient centrifugation to remove any aggregates and non-vesicular contaminants (Taylor & Shah 2015). However, EV isolation may be achieved by a variety of other methods including polymer-based precipitation, microfluidic separation, affinity capture with antibodies coated on latex beads or size-exclusion chromatography (SEC). Using SEC vesicles are separated based on their size and the interaction with the beads packed in the SEC column. Redistributed bead creates a 'maze', where vesicles, depending on their hydrodynamic diameter, can pass through (Taylor & Shah 2015).

All the above-mentioned techniques are general approaches that isolate all circulating vesicle populations. Since EVs are membrane vesicles with an array of proteins and receptors on the surface, immunoaffinity capture-based techniques were developed to isolate them. Immobilized on different matrices,

beads, plates or filters, antibodies recognize specific antigens on EVs, isolating a very specific sub-population.

Various optical and biochemical methods have been developed or adapted for the assessment of EV quantity, size, morphology and surface markers (Witwer et al. 2013). Single vesicle characterization is now commonly used such as electron microscopy (transmission-electron microscopy (TEM), atomic-force microscopy (AFM), or cryo-electron microscopy (Cryo-EM) for visualization. Size distribution measurements of EVs are done by nanoparticle-tracking analysis (NTA), dynamic light scattering, or resistive pulse scanning. Analytical techniques commonly used for the detection of proteins associated to EVs are WB, flow cytometry (FACS) and global proteomic analysis using mass spectrometry (Gardiner et al. 2016).

1.6.3.6 Potential Application of EVs In the Clinic

Since EVs are present in all body fluids, the emphasis has been placed on their use as non-invasive, early biomarkers for disease detection and assessment of prognosis (Simpson et al. 2009; Royo et al. 2016; Gonzalez & Falcon-Perez 2015). MSCs, present in the stromal fraction of many adult tissues, have a self-renewal potential and ability to differentiate into many tissue types (Di Rocco et al. 2016). MSC-EVs have been proven useful in regenerative medicine with their capacity to restore injured tissue (Quesenberry et al. 2015). MSC-EVs have been shown to suppress hypoxia-induced inflammation and hypertension in mice (Lee et al. 2014). Human umbilical cord-MSC exosomes transplanted into acutely injured and fibrotic livers could restore liver function and improved liver fibrosis (Li et al. 2012). Moreover, MSC-secreted EVs protect against acute kidney damage (Bruno et al. 2009). Furthermore, DC-derived EVs were able to induce antigen-specific naïve T cell activation *in* vivo (Théry, Duban, et al. 2002). EVs from cancer cells carry tumoral antigens and present them to T cells, priming them to induce an anti-tumour response and eventually tumour cell death (Cho et

al. 2005). Using EVs as a cell-free vaccine was proposed by Viaud *et al.*, (Viaud et al. 2010). Cancer-EVs were shown not only to be very promising diagnostic biomarkers but also markers for identification of cancer aggressiveness (Verma et al. 2015). Furthermore, plants also secrete exosome-like nanoparticles, which have been proposed to have potential to influence cell biology through ingested foods as they are highly resistant to gastric juices (Quesenberry et al. 2015).

In terms of the drug delivery, currently preferred systems include liposomes and polymeric nanoparticles, which have been used to deliver anti-cancer drugs, anti-fungal drugs and analgesics (Ha et al. 2016). Recently, accumulating evidence indicate that EVs would be more suitable drug delivery system due to their longer half-life, tissue specificity and minimal toxicity. One study involved the use of EVs to deliver curcumin for treatment of inflammatory disease (Sun et al. 2009). Besides the delivery of small molecules such as drugs, they are used to deliver large molecules such as protens. It has been explored for the delivery of antioxidant catalase for the treatment of Parkinson's desease (Haney et al. 2015). Lastly, there is an increasing interest in using EVs for delivery of therapeutic genetic material for strategy involving gentic therapy (Ha et al. 2016). These are only a few examples of applications of EVs (Quesenberry et al. 2015).

1.6.4 Extracellular Vesicles in Metabolic Syndrome

As already explored, during obesity progression there is an accumulation of immune cells within AT. In that context, the role of adipose-EVs in a crosstalk between adipocytes and macrophages has also been studied and they have been shown to significantly contribute to AT inflammation and insulin resistance development (Zhang et al. 2015). In 2009, a study concluded that EVs released by adipose tissue, cultured *ex vivo* from a genetically obese mouse model (*ob/ob*), were able to activate blood monocytes into M1 pro-inflammatory macrophages (30 µg/mice). Additionally, they enhanced the migration of macrophages into adipose tissue and the liver, where they caused an insulin

resistance (Deng et al. 2009). The presence of immunomodulating factors has been shown in EVs isolated from an *in vitro* model of differentiated human adipocytes and *ex vivo* AT-explants, which were also capable of macrophage activation (Mariette E G Kranendonk et al. 2014).

Another study showed that THP-1 macrophage-derived EVs decreased insulin-stimulated Akt phosphorylation, through nuclear factor kappa-light-chain-enhancer of activated B cells (NFκB) activation, and decreased glucose uptake in human primary adipocytes. Additionally, the amount of insulin-stimulated GLUT4 translocation was reduced in adipocytes pre-treated with M1 macrophages, as compared to M2, anti-inflammatory macrophages (Zhang et al. 2015). Another study showed that MetS patients have increased levels of blood-circulating EVs as compared to healthy patients (O'Neill et al. 2016). Moreover, quantitative differences in microRNA content have been found in exosomes from obese visceral adipose tissue (Ferrante et al. 2015). Together these findings indicate that metabolic stress alters the nature and amount of EVs secreted and that EVs have a potential to alter cellular metabolism.

1.8 Thesis objectives

Extracellular vesicles have been linked with the development of different diseases including MetS. Most studies linking extracellular vesicles to MetS have focused their attention on expanding adipose tissue and associated abnormalities, such as hypoxia and macrophage infiltration.

The aim of this thesis was to perform comparative characterization of extracellular vesicles in the pathophysiology of metabolic syndrome. To address this issue, we first aimed to establish and characterize several *in vitro* models, including hypertrophic (lipid overloaded) adipocytes, adipocytes cultured in hypoxia or in the presence of macrophage conditioned medium and activated M1 macrophages as a model of inflammation. Moreover, two models of hepatoculluler steatosis were used, the chemically-induced in hepatic cells lines and primary hepatocytes from Zucker rats, which represent a genetic model of obesity that accumulates of lipids in hepatocytes.

The goal was to isolate and characterize extracellular vesicles from the conditioned medium of all these cellular models. Lastly, we aimed to shed light on a possible role of hepatic and proinflammatory extracellular vesicles on adipocytes in the context of metabolic syndrome. The experimental design is schematically represented on **Figure 9**.

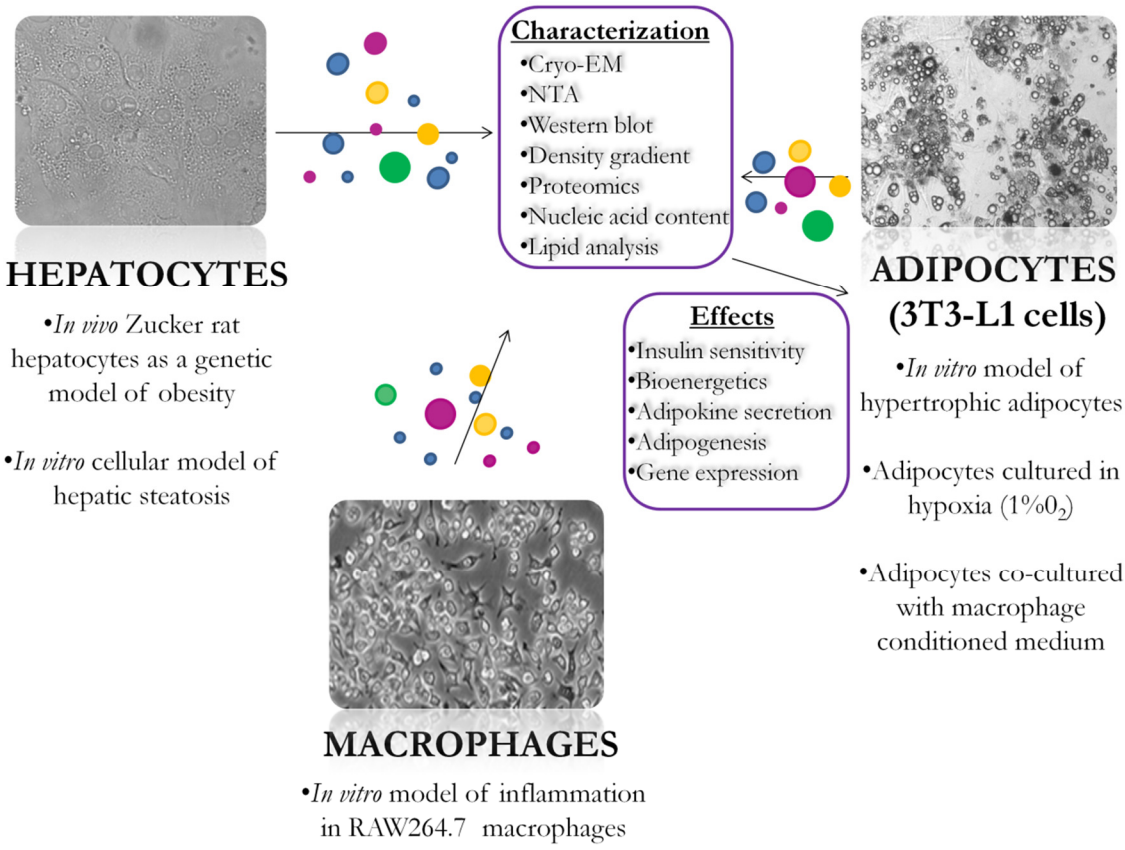

Figure 9 Schematic view of the experimental models and objectives of the thesis. EVs were isolated from the conditioned medium of different cellular models including Hepatocytes, Macrophages, and Adipocytes, and incubated under conditions that resemble some manifestations of metabolic syndrome. Once establishes the models were used to produce and characterized EVs. Next, the objectives were to investigate whether these EVs influenced the insulin sensitivity, adipokine secretion, the progression of adipogenesis and finally bioenergetic balance in 3T3-L1 adipocytes, in the context of MetS.

MATERIALS and METHODS

2. Materials and Methods

2.1 Animal models

Male Zucker rats, Fatty (ZF) and its Lean (ZL) counterpart, (ZUC(Orl)-*Lepr*^{fa} strain) were purchased at 10-12 weeks of age from Charles River Laboratories (France). In CICbioGUNE animal facility, Zucker rats were maintained in an environmentally controlled room at 22^0C on 12 h light/dark cycle and provided with standard, 14% protein diet, (Rodent Maintenance Diet, Harlan Teklad Global Diet 2014) and water *ad libitum*. All experiments were performed following the two weeks adaptation period and in accordance with the guidelines of the CICbioGUNE institutional review committee on animal use.

2.2 Cell culture

2.2.1 Primary cell culture

2.2.1.1 Generation of the primary rat hepatocytes

2.2.1.1.1 Perfusion of the liver to obtain primary hepatocytes

The surgery was performed under anesthetic gas Isoflurane (IsoFLO, Abbott Laboratories), and all efforts were made to minimize the suffering of the animals. Rat hepatocytes were obtained by liver perfusion of Zucker lean (ZL) and Zucker fatty (ZF) rats. Briefly, after the rat was anesthetized with isoflurane, according to our institutions approved animal protocol, a laparotomy was performed to expose the liver and portal vein. The portal vein was cannulated for continuous perfusion with 150 ml Leffert's buffer containing (Leffert's buffer: 4-(2-hydroxyethyl)-1-piperazineethanesulfonic acid (HEPES) 10 mM, KCl 3 mM, NaCl 130 mM, NaH_2PO_4-H_2O mM,glucose 10 mM) with 1 mM ethylene glycol-bis(β-aminoethyl

ether)-N,N,N',N'-tetraacetic acid (EGTA). The infrahepatic inferior vena cava was open to allow the flow through. Then, 150 ml of Leffert buffer was perfused and finally 150 ml of Leffert's buffer containing 30,000 units of collagenase Type I (Worthington Biochemical Corp, Lakewood, NJ). After removing the catheters from the portal vein, the liver was explanted into a Petri dish to be gently minced with tweezers, and finally filtered through a cell strainer into a 50 ml Falcon tube.

2.2.1.1.2 Percoll Density Gradient

Rat hepatocytes suspension was centrifuged at low speed (400 rpm) for 4 min at 4^0C to pellet cells and remove perfusion debris. Resulting cell pellet were resuspensed in 30 ml of cold Dulbecco's modified eagle medium (DMEM) and 15 ml of the 90% Percoll (GE Healthcare, 17-0891-01) in ice cold, sterile 10X Dulbecco's Phosphate-buffered Saline (D-PBS) buffer. The tube was gently inverted and centrifuged at 500 rpm for 10 min for the density separation. Resulting cell pellet was washed with 30 ml of cold DMEM and centrifuged at 500 rpm for 5 min. This step was repeated twice, and the final pellet was resuspended in 50 ml of DMEM for counting and subsequent seeding.

2.2.1.1.3 Cell Counting and Viability

Cell viability was evaluated with a benchtop automated cell counter (Countess™, Life technologies) that performs cell count and viability (live, dead, and total cells) measurements using Trypan blue exclusion method. Briefly, small sample of the hepatocyte cell suspension was diluted 1:10 in DMEM and then mixed 1:1 with Trypan blue. A fraction of 10 µl of the sample/Trypan blue mixture was then loaded onto a Countess™ cell counting chamber slide. The camera of the equipment acquires cell images from the sample on the slide and the image analysis software automatically analyzes acquired cell images, and measures

cell count and viability based on Trypan blue extrusion method. The measurement provides live and dead cell concentration (per ml), total cell concentration (per ml) and viability (% of live cells).

2.2.1.1.4 Collagen coating of cell culture plates

A day prior the perfusion, plates were coated with collagen for the culture of primary hepatocytes. Plates were well covered with 0.05 mg/ml of Collagen type I from Rat Tail (354236, Corning) solution diluted in ultrapure water and 600 µl/500 ml of acetic acid. The solution was left for 1h at room temperature and then washed twice in D-PBS $Cl_2^+Mg_2^+$, and left to dry, wrapped tightly in aluminium foil and stored at 4^0C until needed.

2.2.1.1.5 Cell seeding and cells culture conditions

Primary rat hepatocytes were seeded onto 150 mm collagen-coated dishes at 25-30 million cells per dish. Cells were cultured in complete DMEM [(Gibco, Life technologies, Heidelberg, Germany) containing L-Glutamine and 25 mM (4500 mg/l) glucose and supplemented with 10% (v/v) fetal bovine serum (FBS) (Gibco), penicillin (100 u/ml, Lonza), streptomycin (0.1 mg/L, Lonza, Walkersville, MD, USA), and amphotericin-B (0.25 µg/ml, Lonza) (PSA)] at 37°C and 5% CO_2. Cells were allowed 4 h to attach and were then washed twice with 1X D-PBS and incubated for 36 h in complete DMEM containing 25 mM HEPES (4-(2-hydroxyethyl)-1-piperazineethanesulfonic acid) that previously have been depleted from contaminating vesicles by 16 h ultracentrifugation at 100,000 × *g*, 4°C. The importance of FBS pre-cleaning of contaminating EVs cannot be underestimated as it is known to contain significant quantities of native vesicles. In addition, it has been shown that FBS-EVs overlap in the size and density with exosomes also carrying typical vesilcular protein markers such as TSG101, CD81 and CD63 (Shelke., GV *et* al, 2014). Moreover, when RNA profiles of

cellular and FBS EVs were compared, it was discovered that they were very similar, enriched in small RNAs and undetectable 18S and 28S ribosomal RNA peaks (Shelke., GV *et al*, 2014). Most cells cultured with EV-depleted FBS showed a reduced growth rate, which is enhanced when supplying cells with FBS-EVs (Eitan., E *et al,* 2015). In terms of functionality of the FBS derived EVs, they were shown to be internalized by recipient cells, which could point towards their role as signal carriers (Shelke., GV *et al,* 2014). More importantly, FBS-EVs were able to induce the migratory phenotype in recipient cells and their removal affected proliferation and differentistion of myoblasts *in vitro* (Shelke., GV *et al,* 2014; Aswad., H *et al,* 2016). EV research, the preferred method used for depletion of EVs from FBS is the over night ultracentrifugation based on the knowledge that 95% of RNA containing FBS-EVs were removed by 18h centrifugation at 120,000 x *g* as compared to short time centrifugation (Shelke., GV et al). It is important to come to consensus as to the speed and duration of the EV-FBS depletion, to obtain comparable experimental results. In addition, when studying effect of EVs on recipient cells, it is vital to carry a control incubated with EV-depleted medium only.

2.2.1.1.6 Insulin sensitivity in primary Zucker rat hepatocytes

Primary Zucker rat hepatocytes were cultured on collagen-coated plates for 4 h before being washed with warm 1XD-PBS and stimulated with insulin (100 nM) for 5 min at 37^0C. Primary rat hepatocytes were seeded at a density of 5 x 10^6 cells on collagen-coated cell culture dishes (100 x 20 mm). After 4 h, once attached, hepatocytes were stimulated with insulin (100 nM) for 30 min at 37^0C. After that, cells were immediately lysed on ice with ice-cold lysis buffer (0.5% Triton X-100, 300 mM NaCl, 50 mM Tris-HCl, pH 7.4) in the presence of protease and phosphatase inhibitors cocktail. The untreated controls were carried in parallel. Densitometry analysis was performed on WB bands using ImageJ software. The increase in phosphorylation upon incubation with insulin

was calculated by dividing the value of insulin-stimulated sample by the value of the unstimulated control to obtain a fold increase in phosphorylation upon insulin stimulation.

2.2.1.2 Generation of the bone marrow-derived macrophages

Bone marrow macrophages were differentiated from mice femur bone marrow cells. Mice were euthanized by cervical dislocation with all efforts made to minimize the suffering of the animals, following the guidelines of the Home Office, UK. Bone marrow cells were harvested by gently flushing the bone with pre-warmed DMEM (D5648, Sigma) using a 23-gauge needle attached to a syringe into a sterile Petri dish. The suspension containing bone barrow cells was transferred into 15 ml Falcon tube and centrifuged at 1500 rpm for 4 min. Resulting pellet was re-suspended in 2 ml of 0.83% ammonium chloride (A9434, Sigma) and left for 3min for the erythrocyte lysis. The suspension was centrifuged again at 1500 rpm for 4 min. Cells were plated onto a 6-well cell culture dish ($1.5x10^6$/well) and cultured at 37^{o}C, 5% $C0_2$ in DMEM supplemented with penicillin and streptomycin (100 U/ml and 100 µg/ml respectively, P4333, Sigma), 5% FBS (F7524, Sigma) and 10% (v/v) of media containing macrophage colony stimulating factor 1 (MCSF-1). The fresh media was replaced 24h after seeding to remove debris and unattached cells. After 5 days in culture, macrophage conditioned media was collected, filtered (0.2 µm) and stored at 4^0C if not used immediately.

2.2.2 Cell culture of commercial cell lines

2.2.2.1 Thawing cell stocks

To defrost the cell stocks, the cryo-tube was immediately immersed into the water-bath at 37^0C for 1-2 min. The cell suspension was then gently transferred onto a 100 x 20 mm cell culture plate (83.3902, Sarstedt) with 8 ml of pre-

warmed and pre-calibrated complete culture media at 37^0C incubator, 5% CO_2 and 95% 0_2. Following the cell attachment, media was then replaced with fresh media solution.

2.2.2.2 Culture of AML12, MLP29, HepG2 and Raw264.7 cell lines

All cell lines mentioned in this section were cultured in DMEM containing L-Glutamine and 25 mM (4500 mg/L) glucose supplemented with 10% (v/v) FBS and 1% PSA and incubated at 37°C in humidified atmosphere of 5% CO_2-95% 0_2.

The alpha mouse liver 12 (**AML12**), purchased from American type culture collection [(ATCC (Cat number: CRL-2254)], cell line was established from CD1 mouse strain (line MT42) hepatocytes transgenic for human transforming growth factor alpha (TGFα). Like normal hepatocytes, AML12 cells express high levels of messenger RNA (mRNA) for serum albumin, α_1-antitrypsin and transferrin as well as gap junction proteins, connexins 26 and 32. (Wu et al. 1994). Morphologically, these cells exhibit typical hepatocyte features such as peroxisomes and bile canalicular like structures.

Mouse Liver Progenitor 29 (**MLP29**) were a kind gift of Dr. E. Medico (University of Totino, Italy).

HepG2 cells**,** purchased from ATCC (Cat number: HB-8065) is a human liver cancer cell line, derived from the liver tissue of a 15-year-old Caucasian American male with well-differentiated hepatocellular carcinoma. These cells are epithelial in morphology and tend to grow in multilayer clumps (Costantini et al. 2013). HepG2 cells are highly differentiated and display many of the genotype features of normal liver cells. They exhibit lower metabolic capacity, reduced levels of cytochromes (CYPs) but normal levels of phase II enzymes with the exception of UDP-glucuronosyl transferases (Gerets et al. 2012).

Raw264.7 is a murine macrophage cell line that was established from a tumour induced by Abelson murine leukemia virus (Raschke et al. 1978). For maintenance, cells were kept in suspension in bacterial, non-cell culture treated plates to avoid frequent trypsinization and cell activation. For the experiments, cells were seeded on cell culture treated plates. These cells were a kind gift of Dr Nicolas Navassa (CICbioGune, Spain).

2.2.2.3 Maintenance and differentiation of the 3T3-L1 cells

Table 1 Compounds used for the differentiation of the 3T3-L1 cells.

Compound	[Stock]	[Final]	Vehicle	Supplier
Dexamethasone (DEX)	1mg/mL	0.25µM	100% EtOH	Sigma D4902
Insulin	1mg/mL	1µg/mL	0.1N HCl	Sigma I6634
Isobutylmethylxanthane (IBMX)	55.6mg/mL	500µM	0.35M KOH	Sigma I5879
Rosiglitazone	10mM	1µM	DMSO	Sigma R2408

3T3-L1 cells were purchased from ATCC (CL-173) as a murine embryonic cell line that under a right stimulus can undergo a pre-adipocyte to adipocyte conversion. As fibroblasts cells were cultured in high glucose (4500 mg/L glucose; 25mM) DMEM supplemented with 10% calf serum and 1% penicillin (100 u/ml, Lonza), streptomycin (0.1 mg/L, Lonza, Walkersville, MD, USA) as a monolayer in 100 x 20 mm cell culture plates and were maintained at maximum confluence of 70%. For adipocyte differentiation, cells were used at no more than 10 passages.

For the differentiation to adipocytes, 3T3-L1 fibroblasts were grown to confluence in DMEM supplemented with 10% Calf serum and 1% PS. At 100% of confluence, fresh complete medium was added and incubated for additional 48 h. At 2 days post-confluence, cells were switched to differentiation media containing DMEM supplemented with, 10% FBS, 1 µg/ml insulin, 0.25 µM DEX, 500 µM IBMX and 1 µM Rosiglitazone for 48 h. After 2 days, DEX, IBMX and Rosiglitazone were withdrawn, and cells are maintained in complete medium and 1 µg/ml insulin for another 48 h. At day 4, already differentiated adipocytes were maintained in DMEM with 10% FBS, and 1% PS. The medium was replenished every 2 days until day 12 when adipocytes become fully mature. For experimentation, adipocytes at day 13 were used.

2.2.3 Generation of cellular models

2.*2.3.1 Induction of hepatocellular steatosis*

Steatosis was induced in the following hepatic cell lines, AML12, MLP29 and HepG2 with a mixture of long-chain free fatty acids (FFA), oleic acid (OA, O1008, Sigma) and palmitic acid (PA, P0500, Sigma), at a ratio of 2:1 (1 mM final) for 24 h. For conjugation of FFAs, stock solution of 100 mM was prepared in culture medium containing 1% FFA-free bovine serum albumin (BSA Fraction V, Fatty Acid free, 10775835001, Roche). BSA-conjugated FFA-containing media were used to challenge cells, as previously described (Gómez-Lechón et al. 2007).

2.2.3.2 Induction of adipocyte hypertrophy

The protocol used for induction of heptic steatosis was followed to induce adipocyte hypertrophy in 3T3-L1 cells. Briefly, 3T3-L1 were differentiated to

adipocytes and afterward treated with BSA-conjugated FFA-containing media for 24 h.

2.2.3.3. Activation of Raw264.7 macrophage-like cells

To induce the pro-inflammatory phenotype, Raw264.7 macrophages were treated with 100 nM of lipopolysaccharide [(LPS), from *Salmonella typhimurium,* L 6511, Sigma)] in complete growth medium for 6h at 37^0C. Cells were then washed three times with pre-warmed 1XD-PBS and incubated, in the absence of LPS, with the EV-depleted medium to produce EVs (48-72 h).

2.2.3.4 Hypoxia

For hypoxia experiments, cells were incubated in an Invivo2 400 hypoxia Workstation (Baker Ruskinn, USA) at 1% O_2 for 24 h and lysed/fixed in the hypoxia chamber unless otherwise stated.

Importantly, to avoid contamination by EVs from other sources such as FFAs or the LPS, in the case of all our models, the treatment was removed for the subsequent production of EVs.

2.2.3.5 Generation of the macrophage conditioned medium

The macrophage-conditioned medium was collected from bone marrow differentiated macrophages stimulated with the MCSF-1, as detaled in the **section 2.2.1.2**. The 5-day conditioned medium was collected and centrifuged at 1500 rpm to remove cells and debris to generate the macrophage-conditioned media. After, 3T3-L1 adipocytes were incubated for 24 h with EV-depleted complete media containing 15% of the macrophage-conditioned media.

2.2.4 Experiments to evaluate the effect of EVs on 3T3-L1 adipocytes

2.2.4.1 Adipogenesis

3T3-L1 cells were differentiated as described in **section 2.2.2.3** in a multiwall plate of 12-wells. Alongside the adipogenic agents, cells were treated with 30 µl of ZL or ZF-EVs, in EV-depleted medium, or left untreated. The treatment was repeated every 48 h at each point of medium replenishment and samples collected for subsequent analysis **(Figure 50)**.

2.2.4.2 Insulin sensitivity

3T3-L1 cells were differentiated as described in **section 2.2.2.3** in a multiwall plate of 12-wells. On a 13th day of differentiation, cells were treated with 10 µg of ZL or ZF-EVs per well in EV-depleted medium for 24 h in the case of acute experimental group. For chronic experiments, cells were repeatedly treated (three times) with 10 µg of ZL or ZF-EVs or left untreated in EV-depleted medium for 24 h period each treatment.

Subsequently, cells were incubated with 100 nM insulin for 5 min at 37^{0}C or left untreated, and then directly lysed on ice with ice cold lysis buffer (1% Triton X-100, 300 mM NaCl, 50 mM Tris-HCl, pH 7.4) in the presence of protease and phosphatase inhibitors. Cellular lysates were prepared **(section 2.6.1)** and WB analysis performed **(section 2.6.2)**. Protein bands were quantified by densitometry analysis using ImageJ software. The percentage of phosphorylation was calculated by dividing the density of the phosphorylated protein by the density of the total protein and multiplied by 100. Moreover, the increase in phosphorylation upon incubation with insulin was calculated by dividing the value of insulin-stimulated sample by the value of the unstimulated control to obtain a fold increase in phosphorylation upon insulin stimulation.

2.3 Production and isolation of extracellular vesicles

2.3.1 Preparation of the EV-depleted medium

50 ml of FBS was redistributed into five-70 ml centrifuge polycarbonate tubes (Beckman Coulter Inc, Brea, California) and each diluted with 40 ml of DMEM containing 25 mM HEPES to make up a final volume of 50 ml and subsequently subjected to 16 h ultracentrifugation at 100 000 x g at 4^0C. The remaining of the medium was supplemented with L-Glutamine and PSA if needed, for 3T3-L1 cells PS only, and stored at 4^0C. Following the centrifugation, the supernatant was collected to the bottle of media previously supplemented. EVs-depleted medium was filtrated through a 0.22 µm pore size filter system (Corning, NY USA) and stored at 4^0C until needed.

2.3.2 Isolation of extracellular vesicles by differential ultracentrifugation

The isolation protocol is common to all cell types used in the study and slightly modified from Théry, Amigorena, Raposo, & Clayton, 2006 (Théry et al. 2006). Briefly, to produce EVs, cells were incubated for 36 h in case of Zucker primary hepatocytes and for 48 h for cell lines, at 37^0C and 5% CO_2. The conditioned medium was collected to 50 ml Falcon tube and centrifuged at 2000 × *g* during 10 min at 4^0C and the resultant supernatant was filtrated through a 0.22 µm pore size filter system (Corning, NY USA) to remove large debris while keeping small membranes (under 0.22 µm) for further purification by ultracentrifugation. Filtrated supernatant was transferred to 50 ml centrifuge polycarbonate tubes (Beckman Coulter Inc, Brea, California) and ultracentrifuged 30 min at 14 000 × *g* 4°C to remove large vesicles. The resultant supernatant was transferred to a fresh tube and centrifuged at 100 000 × g 4^0C during 75 min to pellet EVs. To reduce contaminating proteins not associated to the vesicles, the supernatant was completely removed, pellets resuspended in 1 ml of sterile, pre-chilled 1XD-PBS and same samples were pooled in a single centrifuge tube. Tubes were filled up to 50 ml with 1XD-PBS and ultracentrifuged again at 100,000 × *g* 4°C

during 75 min. Supernatants were removed and final pellet resuspended in 150 µl 1XD-PBS. This method favours the enrichment of the preparation in small EVs (mostly exosomes, small microvesicles and small apoptotic blebs). Finally, the sample was split in aliquots of 50 µl to avoid repeated cycles of freezing and thawing. If not used immediately aliquots were frozen at -80ºC. Centrifuge tubes were always pre-chilled on ice for the subsequent centrifugation step and all sample manipulations, such as pellets re-suspension were done on ice to reduce clumping and content degradation.

2.4 Structural and molecular characterization of extracellular vesicles

2.4.1 Protein concentration determination

The concentration of protein present on EVs was quantified by the Bradford protein assay (Bio-Rad Laboratories, Inc) using bovine serum albumin (BSA) as standard and spectrophotometrically determined using a Spectramax M3 spectrophotometer (Molecular Devices, USA). To assure accuracy, the comparison with the bicinchoninic acid (BCA) protein assay (Pierce, USA) was made and as minimal differences were found, the Bradford assay was used in the study.

2.4.2 Cryo Electron Microscopy (Cryo-EM)

The sample of EVs, usually 5 µl, was directly adsorbed onto glow-discharged holey carbon grids (QUANTIFOIL, Germany). Grids were blotted at 95% humidity and rapidly plunged into liquid ethane with the aid of VITROBOT (Maastricht Instruments BV, The Netherlands). Vitrified samples were imaged at liquid

nitrogen temperature using a JEM-2200FS/CR transmission cryo-electron microscope (JEOL, Japan) equipped with a field emission gun and operated at an acceleration voltage of 200 kV. In cryo-EM sessions, digital images were taken using low-dose technique by means of an ULTRASCAN 4000SP (4096 × 4096) cooled slow-scan CCD camera (GATAN). An in-column energy filter (Omega Filter) was used to improve the signal-to-noise ratio of these images by zero-loss filtering.

2.4.3 Nanoparticle Tracking Analysis (NTA)

Particle size distribution and concentration of EVs were analyzed using a NanoSight LM10 system (NanoSight, Amesbury, U.K.), which is equipped with a fast video capture and particle-tracking software. In this system vesicles are visualized by light scattering using a light microscope. NTA software tracks the Brownian motion of individual vesicles and calculates their size and total concentration. NTA post acquisition settings were kept constant for all samples, and each video was analyzed to give the median vesicle size, and the concentration of vesicles in each sample.

2.4.4 OptiPrep™ Density Gradient

5% and 40% OptiPrep™ Density Gradient Medium (D1556, Sigma) was prepared by diluting the 60% original solution in ice-cold 20 mM HEPES pH 7.4 solution. Next, 5.5 ml of the 40% solution was carefully dropped to the bottom of the tube (Beckman centrifuge tube Cat. No. 344059, SW40 Ti rotor) and 5.5 ml of the 5% solution on top. Continuous gradient was made in a Gradient Master (Biocomp) by running the following program: Long Opti 5-40% WV 4 St: Once the gradient was pre-formed, 250 µg of EVs was diluted in 20 mM Hepes pH 7.4 up to 100 µl and it was carefully loaded on top of the gradient. The tube was centrifuged at 100 000 x *g* for 4 h in no break mode for stopping speed. Using

Autodensity-flow 230 V (Cat No 4517200, Labconco), twelve fractions of 1 ml each were collected and mixed by vortex. The refractory index (RI) was measured by means of refractometer (Abbe 2WAJ). RI was translated to density following the correlation built from the data provided by OptiPrep™. The 1 ml fractions were transferred into apolycarbonate thick wall tubes (Cat No 3623.5, Beckman) and diluted with 2 ml of 20 mM Hepes pH 7.4, before being centrifuged at 100 000 x *g* at 4^0C for 1h in a TLA 110 rotor. Supernatant was carefully removed, and pellet resuspended in 30 µl of sterile 1XD-PBS and stored at -80^0C until needed.

2.4.5 Targeted-profiling of EVs-associated RNA

The RNA was isolated from EVs using Rneasy Mini Kit (74104, QIAGEN) according to the manufacturer's instructions. Detection, quality, yield and size of the vesiclular RNA was analyzed using capillary electrophoresis (Qagilent on an Agilent 2100 Bioanalyzer, Agilent Technologies, Santa Clara, CA, USA). 2 µl of the RNA solution was analyzed in the Bioanalyzer.

2.5 Analysis of total RNA in cells

2.5.1 RNA isolation

The isolation of total RNA was carried out using TriReagent (Sigma-Aldrich, USA) or the Rneasy Mini Kit (74104, QIAGEN) according to manufacturer´s instructions. RNA concentration and purity were determined spectrophotometrically in the Nanodrop ND-100 spectrophotometer (ThermoFisher Scientific, USA).

2.5.2 Retrotranscription and Real Time quantitative PCR (RT-qPCR)

1µg of isolated RNA were treated with Dnase I (Invitrogen) according to manufacturer's instructions. Subsequently, complementary DNA (cDNA) was synthesized from 1 µg of eluted RNA using the Quanta cDNA SuperMix (Quanta bioscience, Inc). Resulting cDNA was diluted 1/10 in Nuclease-free water (ThermoFisher Scientific, USA). RT-qPCR was performed using the BioRad iCycler iQ5 Thermalcycler, with 2X SYBR Green Select Master Mix (ThermoFisher Scientific, USA). For the iCycler, 5 µl of cDNA were used and including the specific primers the total reaction volume was 15 µl in a 96-well plate (BioRad). All reactions were performed in duplicate. PCR conditions were as follows, the initial denaturation for 180 secs at 95^0C, 40 cycles of denaturation step for 20 sec each at 95^0C, 20 secs at 60^0C, and 20 secs at 72^0C, annealing and extension.

Primers were designed using the Primer 3 software via the national centre for biotechnology information (NCB)-Nucleotide webpage (Ye et al. 2012) and synthesized by Sigma Aldrich. Primer sequences are detailed in **Table 2 and 3.** After checking the specificity of the PCR products with the melting curve, data was normalized to the expression of a corresponding housekeeping gene.

Table 2 List of mouse primer sequences.

ID	Target	Forward Sequence (5'-3')	Reverse Sequence (5'-3')
11461	*Actb*	CCTGTGCTGCTCACCGAGGC	GACCCCGTCTCTCCGGAGTCCATC
11450	*Adipoq*	AGAATGTGGACCAGGCCTCT	AGTCCATTGTGGTCCCCATC
11770	*Ap2*	GGGAACCTGGAAGCTTGTCT	ACTCTCTGACCGGATGGTGA
11947	*Atp5b*	TGGCTCAGAGGTGTCTGC	TCAGTCAGGTCATCAGCAGG
20296	*Ccl2*	CCACAACCACCTCAAGCACT	AGGCATCACAGTCCGAGTCA
20304	*Ccl5*	TAGTCCTAGCCAGCTTGGGG	GAGCAGCTGAGATGCCCATT
12606	*Cebp1*	GTTAGCCATGTGGTAGGAGACA	CCCAGCCGTTAGTGAAGAGT
59122	*COXIII*	CGTGAAGGAACCTACCAAGG	ATTCCTGTTGGAGGTCAGCA
14104	*Fasn*	GCCACCTCAGTCCTGCTATC	GGTATAGACGACGGGCACAG
14433	*Gapdh*	TGCACCACCAACTGCTTAGC	GGATGCAGGGATGATGTTCT
15452	*Hprt1*	ACATTGTGGCCCTCTGTGTG	TTATGTCCCCCGTTGACTGA
16193	*Il6*	ACCCCAATTTCCAATGCTCTC	AACGCACTAGGTTTGCCGAG
16337	*Insr*	GAGAGGATGTGAGACGACG	CAGGTTGTTCCGGATGTCC
16819	*Lcn2*	GGCCAGTTCACTCTGGGAAA	TGGCGAACTGGTTGTAGTCC
16846	*Lep*	TGACACCAAAACCCTCATCA	AGCCCAGGAATGAAGTCCA
53610	*Nono*	TGCTCCTGTGCCACCTGGTACTC	CCGGAGCTGGACGGTTGAATGC
18126	*Nos2*	CAGCGGGATGACTTTCCAA	AGGCAAGATTTGGACCTGCA
11520	*Plin2*	AAACGTCTGTCTGGACCGAAT	ACACGCCTTGAGAGAAACAGA
66905	*Plin3*	CGCCTATGAACACTCCCTCG	CGAGCACACTTGTTAGCTGC
19016	*Pparg*	ATCATCTACACGATGCTGGCC	CTCCCTGGTCATGAATCCTTG

19288	*Ptx3*	GTGGGGGCTTTGACGAATCA	ATTTCCCCGGATGTGACAGG
57264	*Rent*	CTGCCAGTGTGCAAGGATAG	AGACCCTCAGCTTAGACCTGC
56235	*Rpl*	GGCTGCCGAAGATGGCGGAG	GCCTTCACAGCGTACGACCACC
20525	*Slc2a1*	GCTGTGCTTATGGGCTTCTC	CACATACATGGGCACAAAGC
20528	*Slc2a4*	CTTGGCTCCCTTCAGTTTG	TGCCTTGTGGGATGGAAT
21926	*Tnfa*	CTGTAGCCCACGTCGTAGC	TTGAGATCCATGCCGTTG
21780	*Tfam*	TAGGCACCGTATTGCGTGAG	GTGCTTTTAGCACGCTCCAC
22631	*Ywhaz*	AAAAACAGCTTTCGATGAAGCC	GCCGGTTAATTTTCCCCTCC

Table 3 List of rat primer sequences.

ID	Target	Forward Sequence (5'-3')	Reverse Sequence (5'-3')
24172	*Adh1*	AAGCGGCCGTGCTATGGGAG	CGCGTGATCATCTGAGCGGCA
24177	*Afp*	ACCATCGAGCTCGGCTATTG	CGTTTCAGACTGGGAGCACT
24186	*Alb*	AGCAGCCTGCCTGACACCGA	CAGGTCGCCGTGACAGCACT
24297	*Cyp1a2*	CCCAGGAAGAGCGAGGAGATG	GGGTTGGGCAGGTAGCGCAG
24360	*Fabp1*	CGGCAAGTACCAAGTGCAGAGCC	CTCCAGTTCGCACTCCTCCCCC
50671	*Fasn*	GCCTAACACCTCTGTGCAGT	GGCAATACCCGTTCCCTGAA
25735	*Hnf4a*	TGGACAGATGTGTGAGTGGC	TCTCTGAGGGTGTGAGCCAG
24482	*Igf1*	TTTGCGGGGCTGAGCTGGTG	ATGTCAGTGTGGCGCTGGGC
25664	*Pparg*	GAGATCCTCCTGTTGACCCAG	CCACAGAGCTGATTCCGAAGT
113992	*Ugt1a6*	ACTCGGGGAGCTGGGGTGAC	GCGCCCCCTTGTGCCTCATC

83474	*Tfam*	CCAAAAAGACCTCGGTCAGC	GTGACTCATCCTTAGCCCCC
59086	*Tgfb1*	CTGCTGACCCCCACTGATAC	AGCCCTGTATTCCGTCTCCT

2.6 Protein

2.6.1 Preparation of the whole cell lysates

Extraction of total protein was performed as follows, cell pellets (~$1x10^6$) were lysed on ice with 150 µl of the lysis buffer (1% Triton X-100, 300 mM NaCl, 50 mM Tris-HCl, pH 7.4) supplemented with protease and phosphatase inhibitor cocktails during 15 min, with 3 cycles of vortex every 5 min. Subsequently, the lysates were centrifuged at 10,000 x *g* and the supernatant transferred to a fresh Eppendorf tube. The protein extract was quantified as already described **(Section.2.4.1)**.

2.6.2 Western blotting

Table 4 List of commercial antibodies used for Western blot analysis

Antibody against	Species	Species Reactivity*	Clone	ID	Supplier*	Working Dilution
4E-BP1	Rb	R, M, H, Mk	53H11	9644	CS	1:1000
Actin	M	M, R, Rb, H, C, GP, Hm, Co, Ca, Dg	AC-15	ab6276	Abcam	1:1000
Adiponectin	M	R, M, H, Rb, Ba	19F1	ab22554	Abcam	1:1000
Adipophilin	Rb	H, M, R	-	251533	Abbiotec	1:1000
AIP1	M	R	49/AIP1	611621	BD	1:1000
Akt	Rb	H, M, R, Mk, Pg, C, Hm, B, GP, Dm, Dg	-	9272	CS	1:1000
AnnexinV	Rb	M, R, H	-	ab14196	Abcam	1:1000
Alix	M	M, H, X	3A9	sc:53538	Santa Cruz	1:1000
ApoB	Rb	M, R, H	H-300	sc: 25542	Santa Cruz	1:1000
ApoE	Gt	M, R	R-20	sc: 6385	Santa Cruz	1:1000
Catalase	Rb	M, R, Sh, C, Dg, Cow, H	-	ab1877	Abcam	1:1000
CD63	M	R	AD1	ab108950	Abcam	1:1000
CD81	Hm (Ar)	M, R	Eat2	MCA1846GA	Serotec	1:1000
COMT	Gt	H, R, M, Hr, Pg, Dg	-	ab51984	Abcam	1:1000
COXIV	M	H, M, R, Mk	4D11-B3-E8	11967	CS	1:1000
CytC	M	M, R, H, aquine and avian	7H8	sc: 13560	Santa Cruz	1:1000
Fas	Rb	M, R, H	-	ab: 2759	Abcam	1:1000
Ferritin LC	Rb	H, M, R	H-53	sc: 25617	SC	1:1000
Flotillin-1	M	H, M, C (R)	18	610821	BD	1:1000
GAPDH	M	M, R, Rb, C, Cow, Dg, H, Pg, X, Mk (Cynomolgus), Hm	-	9484	Abcam	1:1000

		(Chinese)				
Glut4	Rb	H, M, R	1F8	2299	CS	1:1000
GRP78	M	D, R, M	40/BiP	610978	BD	1:1000
HSP70	M	R, Rb, M, B, H, Hm, GP, M, Dm	BRM-22	Ab6535	Abcam	1:1000
HSP90	M	M, R, C, Dg	68/Hsp90	610418	BD	1:1000
IR ß	Rb	H, M, R	4B8	3025	CS	1:1000
IRS-1	Rb	H, M, R, Mk	D23G12	3407	CS	1:1000
Lamp1	M	R, H, Mk	H4A3	25630	HB	1:1000
LIMPII	Rb	H, M	-	ab16522	Abcam	1:1000
LIPC	Rb	R, H, M	-	PA5-36962	Invitrogen	1:500
P450 2D1	Rb	R	-	ab22590	Abcam	1:1000
p4E-BP1	Rb	H, M, R, Mk, Dm	236B4	2855	CS	1:1000
p44/42 (Erk1/2)	Rb	H, M, R, Hm, Mk, Mi, Z, B, Pg, Sc	-	9102	CS	1:1000
p-AKT	Rb	H, M, R, Hm, Dm, B, Dg, Pg	Ser473	9271	CS	1:1000
PARP	Rb	H, M, R, Mk	-	9542	CS	1:1000
PGD	M	M, R, H	G-2	sc:398977	SC	1:500
p44/42 (Erk1/2)	Rb	H, M, R, Hm, Mk, Mi, Dm, Z, B, Pg, Ce	Thr202/ Tyr204	9101	CS	1:1000
Prohibitin	Rb	M, R, H, avian	H-80	sc: 28259	SC	1:1000
PTEN	Rb	H, M, R, Mk	138G6	9559	CS	1:1000
p-S6	Rb	H, M, R, Mk, Z (C, X)	Ser240/244	2215	CS	1:1000
Rab8	M	Dg, M, R, Dm	4/Rab4	610844	BD	1:1000
Rab10	Rb	H, M, Mk	D36C4	8127	CS	1:1000
Rab11	M	M, H, R, C	47/Rab11	610656	BD	1:1000
S6	Rb	H, M, R, Mk, Dm	54D2	2317	CS	1:1000
Syndecan4	Rb	M, R, H	-	ab24511	Abcam	1:1000
Syntenin1	Rb	H, M, R	C2C3	GTX108470	GeneTex	1:1000
TSG101	M	M, R, H, Dm	4A10	Ab83	Abcam	1:1000
TGFα	M	M, R, H	134A	sc:36	SC	1:1000
αTubulin	M	M, R, C, GP, Hm, Cow, Dg, H, Pg,	DM1A	ab7291	Abcam	1:1000

		X, Mk (African Green), Gerbil				
VEGF	M	M, R, H, canine	VG-1	sc:53462	SC	1:1000

*Reactivity: H-human, M-mouse, Mk-monkey, R-rat, Rb-rabbit, Ba-baboon, X-*Xenopus laevis,* Dg-dog, C-chicken, Dm-Drosophila melanogaster, B-bovine, Pg-pig, Z-zebrafish, Mi-mink, Ce-C. elegans, GP-guinea pig, Hm-hamster, Hr-horse, Sc-S. cerevisiae, Gt-goat, Sh-sheep

*Supplier: CS-cell signalling, SC- Santa Cruz, HB- Hybridoma Bank

All primary antibodies were diluted in sterile, filtered 5% bovine serum albumin (BSA) in 0.1% sodium azide in Tween PBS (0.1%) solution, kept at 4^0C.

Table 5 List of secondary antibodies used for Western blot analysis.

Antibody against		ID	Supplier	Working Dilution
Mouse	DαMo-HRP	Ab205724	Abcam	1:6000
Rabbit	RbαMo-HRP	315-035-045	Jackson ImmunoResearch	1:6000
Goat	RbαGt-HRP	A5420	Sigma	1:6000
Hamster Armenian	GtαHmAr-HRP	127-035-160	Jackson ImmunoResearch	1:6000
Rat	DαRt-HRP	Ab205723	Abcam	1:6000

All secondary antibody incubations were done in blocking solution of 5% blotting-grade blocker in 1XPBS containing 0.1% Tween-20.

Protein extracts or the sample of EVs were sequentially heated at 37^0C for 5 min, at 65^0C for 10 min and boiled at 95ºC for 15 min in NuPAGE® LDS Sample Buffer [(4X) NP0008, Life Technologies, Inc] to prepare protein samples for denaturing gel electrophoresis. Following the heating cycle, sample was briefly cooled on ice and clarified by centrifugation at 10 000 x *g* for 15 min. An appropriate amount of protein, depending on protein abundance and antibody sensitivity, was separated on 4-12% pre-casted polyacrylamide gel (NuPAGE®

Bis-Tris gel, Life Technologies, Inc) by sodium dodecyl sulphate-polyacrylamide gel electrophoresis (SDS-PAGE) using a Xcell SureLock™ Mini-Cell Electrophoresis System (ThermoFisher Scientific, USA). Gels were transferred onto a Polyvinylidene difluoride (PVDF) membrane using Life Technologies iBlot® 2 Dry Blotting System (program 0: 20V for 1min, 23V for 4 min and 25V for 2 min, default run time being 7 min) or onto nitrocellulose membranes by electroblotting using a Mini Trans-Blot cell (Bio-Rad). Membranes were blocked with 5% blotting-grade blocker (BioRad) in 1XPBS containing 0.1% Tween-20 (Sigma) for 1h at room temperature (RT), washed three times with T-PBS-0.1% and incubated overnight 4^0C with commercial primary antibodies. Primary antibodies and their optimal incubation conditions are detailed in **Table 4**. Membranes were then washed three times with TPBS-0.1% and incubated for 1 hour at RT in blocking solution-containing secondary antibodies conjugated to horseradish-peroxidase (HRP). Chemioluminiscence detection of bands was performed using enhanced chemiluminescence (ECL) Plus chemiluminiscent substrate (GE Healthcare, Buckinghamshire, UK) in a Curix 60 Developer (AGFA, Belgium) under dark room conditions. All proteins were detected under non-reducing conditions, unless otherwise stated. In reducing conditions, 20 mM dithiothreitol (DTT) was added to the sample buffer.

2.7 Proteomics

2.7.1 SDS-PAGE and Sypro Ruby staining

Protein samples were boiled for 5 min and resolved in 12.5% acrylamide gels, using a Mini-Protean II electrophoresis cell (Bio-Rad). A constant voltage of 150 V was applied for 45 min. Gels were fixed in a solution containing 10% acetic acid, 40% ethanol for 30 min, and stained overnight in SYPRO Ruby (Bio-Rad). Gels were then washed in a solution containing 10% ethanol and 7% acetic acid for 30 min, and the image was acquired using a Typhoon Trio scanner (GE

Healthcare). Each lane subjected to tryptic digestion, followed by LC–MS/MS analysis.

2.7.2 Tryptic digestion of gel bands

Gel bands were cut and washed in milli-Q water. Reduction and alkylation were performed using ditiothreitol (10 mM DTT in 50 mM ammonium bicarbonate) at 56 ºC for 20 min, followed by iodoacetamide (50 mM iodoacetamide in 50 mM ammonium bicarbonate) for another 20 min in the dark. Gel pieces were dried and incubated with trypsin (12.5 µg/ml in 50 mM ammonium bicarbonate) for 20 min on ice. After rehydration, the trypsin supernatant was discarded; Gel pieces were hydrated with 50 mM ammonium bicarbonate, and incubated overnight at 37ºC. After digestion, acidic peptides were cleaned with TFA 0.1% and dried out in a RVC2 25 speedvac concentrator (Christ). Peptides were resuspended in 10 µl 0.1% FA and sonicated for 5 min prior to analysis.

2.7.3 Protein extraction

An equivalent volume of a solution containing 7 M Urea, 2 M Thiourea, 4% CHAPS 100 mM DTT was added to the samples for protein extraction, and incubated under agitation for 30 min. The sample was vortexed for 30 secs every 10 min of incubation.

2.7.4 FASP in solution digestion and sample preparation

In solution digestion was carried out following FASP protocol with minor variations (Wisniewski et al. 2009). This protocol relies in the use of standard filtration devices, allowing buffer exchange and acting as a reactor for the digestion. 20 min centrifugations at 13000 rpm are carried out between each digestion step to remove buffer from the filter. Samples were loaded onto Amicon Ultra 0.5 ml 30K centrifugal units (Millipore), washed twice in UA solution (8 M

Urea, 100 mM Tris-HCl pH 8.5) and alkylated by a 20-min incubation in 50mM Chloroacetamide prepared in UA solution. 3 more washes in UA were carried out, followed by additional 3 washes in 50 mM AMBIC. Protein was quantified using Bio-Rad protein assay (Bio-Rad), and trypsin was added to a trypsin: protein ratio of 1:10. The mixture was incubated overnight at 37ºC.

Peptides were recovered from the filter units and subjected to ethyl acetate extraction following the protocol described by Yeung and Stanley (Yeung & Stanley 2010). Briefly, 1ml of water-saturated ethyl acetate was added to the peptide solution and vortexed for 1 min. Then, tubes were centrifuged 15 s at 13000 rpm and the upper ethyl acetate layer was depleted. These steps were repeated 5 times. After the careful removal of the last upper ethyl acetate layer, samples were speed-vacuumed in a RVC2 25 speedvac concentrator (Christ). Samples were further desalted using stage-tip C18 microcolumns (Zip-tip, Millipore) and peptides were resuspended in 0.1% FA prior to MS analysis.

2.7.5 Mass spectrometry analysis

Peptide separation was performed on a nanoACQUITY UPLC System (Waters) connected to an LTQ Orbitrap XL mass spectrometer (Thermo Electron) or a Synapt G2 Si (Waters). An aliquot of each sample was loaded onto a Symmetry 300 C18 UPLC Trap column (180 µm x 20 mm, 5 µm (Waters). The precolumn was connected to a BEH130 C18 column, 75 µm x 200 mm, 1.7 µm (Waters), and equilibrated in 3% acetonitrile and 0.1% FA. Peptides were eluted directly into the nanoelectrospray capillary (Proxeon Biosystems) at 300 nl/min, using a 60-min linear gradient of 3–50% acetonitrile.

The LTQ Orbitrap XL ETD automatically switched between MS and MS/MS acquisition in DDA mode. Full MS scan survey spectra (m/z 400–2000) were acquired in the orbitrap with mass resolution of 30000 at m/z 400. After each survey scan, the six most intense ions above 1000 counts were sequentially subjected to collision-induced dissociation (CID) in the linear ion trap. Precursors

with charge states of 2 and 3 were specifically selected for CID. Peptides were excluded from further analysis during 60 s using the dynamic exclusion feature.

2.7.6 Database searches

Searches were performed using Mascot search engine v2.1 (Matrix Science) through Proteome Discoverer 1.4. (Thermo Electron). Carbamidomethylation of cysteines was set as fixed modification, and oxidation of methionines as variable modification, and 2 missed cleavages were allowed. 10 ppm of peptide mass tolerance and 0.5 Da fragment mass tolerance was used for Orbi acquisitions, whereas 15 ppm peptide mass tolerance and 0.2 Da fragment mass tolerance were used for Synapt G2Si runs. Spectra were searched against *Rattus norvegicus* databases obtained from Uniprot/Swissprot (database version 2016_03). A decoy search was carried out to estimate the false discovery rate (FDR). Only peptides with a false discovery rate of <1% were selected.

2.7.7 Progenesis LC-MS software analysis

Progenesis LC-MS (version 4.0.4265.42984, Nonlinear Dynamics) was used for the label-free differential protein expression analysis. After importing of the Raw files, one of the runs was used as the reference to which the precursor masses in all other samples were aligned to. Only features comprising charges of 2+ and 3+ were selected. The raw abundances of each feature were automatically normalized and logarithmized against the reference run. Samples were grouped in accordance to the comparisons being performed, and an ANOVA analysis was performed. A peak list containing the information of the features was generated and exported to the Mascot search engine (Matrix Science Ltd.) and searched against the database. The list of identified peptides was imported in Progenesis LC-MS and the previously and the three most intense non-conflicting peptides (peptides occurring in only one protein) of each protein were specifically chosen

for quantitative purposes. Proteins with at least two different non-conflicting peptides and a p value<0.05 were selected for further analyses.

2.7.8 Functional analysis

GO enrichment analysis was carried out using the DAVID online tool (http://david.abcc.ncifcrf.gov/summary.jsp) (Huang et al. 2009). DAVID is a GO Term annotation and enrichment analysis tool used to highlight the most relevant GO terms associated with a given gene list. A Fisher Exact test is used to determine whether the proportion of genes considered into certain GO term or categories differ significantly between the dataset and the background. FDR-corrected version of the Fisher's test *p*-value can be obtained and used for more conservative result selection. Biological Process (BP), Molecular Function (MF) and Cellular Component (CC) categories were assessed, and only GO Terms enriched with a FDR<5% were considered for comparison and discussion. Additionally, KEGG Pathways were also analyzed, considering terms with an enrichment p-value<0.01. In addition, DAVID provides a Functional Annotation Clustering report, where similar annotations are displayed together, making the interpretation of the result biology clearer and more focused in interesting enriched processes. The Group Enrichment Score gives the geometric mean (in –log scale) of the cluster member's p-values, and is used to rank their biological significance.

2.8 Immunostaining assays

2.8.1 Immunofluorescence analysis

Table 6 List of commercial antibodies used for Immunofluorescence analysis.

Antibody	ID	Supplier	Working Dilution
DαRb Alexa488	A-21206	Molecular Probes	1:600
DαMo Alexa488	A-21202	Molecular Probes	1:600
DαMo Cy3	715-165-150	Jackson ImmunoResearch	1:600

Cells were seeded at 50–80% confluence over 12 mm glass coverslips and fixed with 2% paraformaldehyde (Santa Cruz Biotechnology) for 10 min then washed with PBS. Coverslips were then blocked and permeabilized with PBS solution containing 0.1% BSA and 0.1% saponin (Sigma) for 30 min at RT. After blocking, the coverslips were washed in PBS and incubated overnight in a humidified chamber with primary antibody in blocking solution. Coverslips were washed to remove unbound antibodies and then incubated with secondary antibody in blocking solution for 30 min at RT protected from light. Following the last PBS wash, the coverslips were mounted onto glass slides in Fluoromont G (Southern Biotechnology Associates, Birmingham, AL) containing 0.7 g/ml 4',6-diamidino-2-phenylindole (DAPI) to stain DNA. The solutions of primary and secondary antibody were clarified by 15 min centrifugation. Images were taken using an Axioimager D1 microscope (Zeiss).

2.8.2 Bodipy Staining

BODIPY^{R}493/503 (4,4-Difluoro-1,3,5,7,8-Pentamethyl-4-Bora-3a,4a-Diaza-*s*-Indacene) was purchased from Molecular Probes (D-3922, Invitrogen). The original stock (10 mg/ml) was diluted in absolute ethanol (EtOH) and stored protected from light at -20^{0}C. The original stock was diluted 100X in sterile 1X D-PBS and clarified by 15 min centrifugation before being used. Cells were fixed as described above **(Section 2.8.1)** and directly stained with Bodipy (10 µg/ml) for 45 min at RT protected from light. Coverslips were then washed twice with D-PBS, 10 min each time and mounted as described above. Protocol modified from (Gocze & Freeman 1994).

2.9 Sandwich Enzyme-Linked Immunosorbent Assay (ELISA)

Table 7 Reagents used for ELISA.

Buffer	Components
Coating buffer	0.2M Na Carbonate, pH= 9.6
Blocking buffer	10% FBS in PBS
Wash buffer	PBS 1X 0.05% Tween
Stop solution	2M Sulfuric acid

The capture antibody was diluted in a coating buffer (Goat Anti-mouse TNFα Cat. No AF-410-NA) at a final concentration of 1:500 and 100 µl of the solution was added to each well of the ELISA microplate before being covered and incubated overnight at 4^{0}C. The following day, the antibody/coating buffer solution was removed, and plate was washed 4 times with 200 µl of the wash buffer using the automated plate washer. Subsequently, 200 µl of the blocking buffer was added per well and incubated for 1 h at RT. In the mean time, samples and standards (KMTNFA, Thermo Scientific) were prepared in a volume of 50 µl per well.

Standard, 100 ng/ml stock solution, was diluted 8 times ½ in blocking buffer starting from 5000 pg/ml. Supernatant samples were centrifuged at 2000 rpm for 5 min to remove cell debris and 50 µl was directly added on a plate, in triplicate. At this point, the blocking buffer was removed and both, standards as well as the samples were added to a plate and incubated for 2 h at 37^0C. Then, the solution was removed, and the wash step repeated 6 times. While the plate was being washed, the Biotinylated detection antibody (Agoat Anti-mouse TNFα, BAF410) was diluted at a final concentration of 1:500. 100 µl of the diluted detection antibody was added to a plate and incubated for 1 hour at RT. The solution was removed, and the plate washed 8 times with 200 µl and dried by tapping the plate on a paper towel. At this point, the enzyme conjugate, streptoavidine HRP (434323, Invitrogen) was diluted 1:1000 in blocking buffer. The volume per well was adjusted to the volume of capture antibody used before. 100 µl of a SA-HRP was added to a plate and incubated for 45 min at RT. The plate was then washed 9 times, as described earlier and towel dried. Additional PBS wash was performed to remove any remaining Tween that could increase the background. The TMB substrate solution (34021, Pierce) was added in a same volume of the capture antibody and incubated for 30 min at RT. The reaction was ceased by adding equal amount of the stop solution and the absorbance was read at 450 nm within 30 min of stopping the reaction.

2.10 Flow cytometry

Flow cytometry analysis was performed using the BD FACSCanto™ II system (BD Biosciences). Data was analyzed using the BD FACSDiva™ software (BD Biosciences) and later processed using FlowJo 7.6 software.

FITC-AnnexinV (556419, BD Biosciences) was used as a sensitive probe to reveal exposure of phosphatidyl serine (PS) on the cell membrane, as an early stages of apoptosis (Gómez-Lechón et al. 2007). AnnexinV-FITC binding was

determined by flow cytometry following manufacturer's instructions. Propidium iodide (PI) was added to detect late apoptotic and necrotic cells.

Flow cytometry analysis of Bodipy staining, cells were lifted with TrypLE ™ (12563, Gibco) and fixed in suspension with 2% formaldehyde solution for 10 min and subsequently washed three times, 10 min each, with D-PBS. Then cells were stained with Bodipy (2 µg/ml) for 30 min at RT, protected from light. Then, cells were washed twice with PBS and finally resuspended with D-PBS (400 µl) for flow cytometry analysis.

2.11 XF Seahorse Extracellualar eflux Analyser

Cellular metabolic profile was determined using a Seahorse XF24 Extracellular Flux Analyzer (Seahorse Biosciences, Billerica, MA), providing real-time measurements of OCR, as a measure of the OXPHOS, and ECAR, as a measure of glycolysis. Primary Zucker rat hepatocytes were seeded at a density of 50 × 10^4 cells per well in collagen-coated (**Section 2.2.1.1.4**; 3h at RT) V7 microplates in complete growth medium (DMEM, 1% L-Glutamine, 1%PSA and 10% FBS). Cells were allowed 4 h to adhere and the culture medium was changed 1 h prior to the assay unbuffered DMEM [D 5030, Sigma, (8.3g/l)], for the mitochondrial stress test supplemented with L-glutamax, glucose and sodium pyruvate, all at the final concentration of 10mM and sodium chloride (NaCl, at 0.18 g/ml) and for glycolysis stress test with NaCl and 0.5 % phenol red (60 µl/100ml) only. The pH was adjusted to 7.4 with sodium hydroxide (NaOH), filtered through 0.22 µm filter system and placed in 37^0C water-bath until needed. Meanwhile, the XF24 Sensor Cartridge, hydrated overnight prior the assay in XF Calibrant pH 7.4 at 37^0C without CO_2 [Seahorse Biosciences, #100840-000 (1 ml/well)], was injected with drugs corresponding to each assay. Mitochondrial stress test requires the sequential injection (per well) of 55 µl assay medium for basal respiration measurement, 60 µl oligomycin (1 µL/ml of 10 mg/ml), 65 µl carbonyl cyanide-*4*-(trifluoromethoxy) phenylhydrazone [(FCCP), 0.3 µl/ml of 10

mM stock] and 70 µl rotenone (20 µl/ml of 1.0 mM stock). The glycolysis stress test requires the sequential injection of glucose (40 µl/ml of 100X), oligomycin (1 µl/ml of 10 mg/ml) and finally 2-Deoxy-D-glucose [(2-DG) 0.18 g/ml, pH 7.4].

For the experiments with the 3T3-L1 adipocytes, 3T3-L1 fibroblasts were differentiated on V7 microplates, according to previously described protocol (**Section 2.2.2.3**). Slight modification to the concentration of drugs used were made for experiments with 3T3-L1 adipocytes, double dose of oligomycin, triple does of FCCP and double dose of rotenone for the mitochondrial stress test. Single dose of glucose, double dose of oligomycin and single dose of 2-DG for the glycolysis stress test. The 3T3-L1 cells were differentiated on V7 microplates coated with 0.1% gelatin solution. Briefly, 2% gelatin (Sigma) solution was prepared in ultrapure H_20 (Sigma) and completely liquefies at 37^0C water-bath. 0.1% working solution was made and 400 µl added/well and incubated for 15 min at 37^0C, allowing gelatin to polymerize. The excess gelatin solution was discarded and plate allowed drying for 2 h under ultraviolet (UV) light.

Following the assay, cells were fixed and stained with 0.1% crystal violet stain in 20% methanol solution for minimum of 1h at RT. Next, the cells were washed twice with distilled H_20 (dH_20) to eliminate the excess crystal violet. The residual H_20 was gently removed by tipping the plate on a paper towel and the plate was left to air dry overnight. Once the wells were completely dry, a 10% acetic acid solution was added to resuspend the crystals (50 µl/well). The absorbance at 595 nm wavelength was determined spectrophotometrically using a Spectramax M3 spectrophotometer, and the data used for normalization (duplicate measurement per well). Normalized data were expressed as pMole of O_2 per minute or milli-pH units (mpH) per minute. The Seahorse XF Analyzer was turned on a day before the assay to allow the instrument to warm to 37^0C before an assay.

2.12 Enzymatic assay to measure lipase activity

Triglyceride content of Zucker rat hepatocytes and secreted EVs was measured using lipase digestion assay. Lipoprotein Lipase (62335 10MG, Sigma) was dissolved in 500 µl of dH_20 (10 mg/ml). Cell pellets were lysed with ice-cold lysis buffer (50 mM Tris pH 7.5, 150 mM NaCl, 1% Triton X-100, 1X protease inhibitor) for 15min on ice following 10min centrifugation at 10 000 x *g*. Resulting cellular extract was transferred to a fresh tube and protein determined by Bradford (**Section.2.4.1**). In case of EVs the same protocol was as follow, and the lysis buffer was 2X concentrated to avoid high sample dilution. All samples in the assay were run in duplicate and taken to the same volume of 30 µl and to equal protein concentration. Samples were incubated at 70^0C for 5 min. Subsequently, 7.5 µl of the Lipoprotein Lipase (10 mg) was added to each tube following the overnight incubation at 37^0C. The next day assay was developed with 200 µl/sample of the Free Glycerol Reagent (FGR). The absorbance was read on 96-well plates at 540 nm wavelength with Spectramax M3 spectrophotometer.

2.13 Glycerol estimation assay

In order to evaluate if the EVs were able to mobilize intracellular TG, cells were exposed to EVs and the amout of glycerol released into the media was estimated by a method modified from (Sagar et al. 2015). Briefly, 3T3-L1 fibroblasts were grown and differentiated into adipocytes (**Section 2.2.2.3**) in the 24-well plate. For the glycerol assay 3T3-L1 adipocytes were serum starved overnight in DMEM supplemented with 2 % FA-free BSA and 1% PS for 24 h. Next, cells were treated with ZL- or ZF-EVs (10 µg), in EV-depleted medium containing 0.5% BSA, for 24 h. Supernatants were assayed for glycerol present with FGR (Sigma) as described in above section.

2.14 P450 activity assay

Luminescent assay that measures the activity of cytochrome P450 2D6 were used to determine the activity of their corresponding rat orthologs P450 2D1 (V8891, Promega), according to manufacturer's instructions. Briefly, luciferin-attached substrate specific of cytochrome P450 2D1 was added to each sample in 1M potassium phosphate (KPO_4) buffer. Samples were incubated for 10min at 37^0C. Next, the nicotinamide adenine dinucleotide phosphate (NADPH) regeneration system was added to each sample following the 30min incubation at 37^0C. NADPH is required for the measurement of oxidase activity catalyzed by P450 cytochromes. After incubation, luciferin detection reagent (LDR) was added to each sample and the luminescence was read in a luminometer.

2.15 Insulin-stimulated glucose uptake

For the glucose uptake experiment, the 3T3-L1 adipocytes were cultured and differentiated in 24-well cell culture plates **(Section 2.2.2.3)**. The cells were serum starved for 12 h before the 24 h treatment with EVs (from 5-10 µg/ml per well). Next, cells were washed with sterile, ice-cold uptake solution (137 mM NaCl, 4.7 mM KCl, 1.2 mM $MgSO_4$, 1.2 mM of $KH2PO_4$, 2.5 mM $CaCl_2$, 20 mM of HEPES and 2 mM of Pyruvate, pH=7.4) and then incubated at 37^0C with the uptake solution for 45 min (255 µl/well). Then, the insulin (100 nM) was directly added to the uptake solution and the plate further incubated for 30 min. The subsequent steps were done over the radioactive work area. Here $^3H2$-deoxyglucose (MP Biomedicals) at 1µCi/ml was added to the uptake solution to a final 0.1 mM concentration and was added in staggered 10 sec intervals to each well. After the solution was added to all the wells the plate was incubated at 37^0C

for a total of 10 min. Subsequently, the reaction was stopped with ice cold stop solution (50 mM glucose in 1XD-PBS) followed by couple of washes. Cells were then lysed with 300 µl of 0.5 N NaOH and suspension transferred to 1.5 ml eppendorf. The protein concentration was measured by Bradford **(Section 2.4.1)** and 150 µl was used for the reading in the scintillation counter. The 5 ml of the scintillation fluid was added to the scintillation vial together with the sample and incubated overnight.

2.16 Adipokine array

Proteome Profiler^{TM} Mouse Adipokine Array Kit (ARY013, R&D) was used for the parallel determination of the relative levels of the 38-selected mouse Adipokines. The assay was performed according to the manufacturer's instructions. Capture and control antibodies spotted in a duplicate, for each adipokine, on nitrocellulose membranes were probed in cell culture supernatant of the 3T3-L1 adipocytes previously treated with ZL- and ZF-EVs. In more detail, 3T3-L1 adipocytes were grown in 12-multiwell plate and differentiated as previously described (**Section 2.4.1**). Mature adipocyts were either left untreated or treated with 30 µg of ZL- or ZF-EVs for 12 h. Subsequently, the EV-depleted medium was replenished and incubated for additional 12 h. The conditioned medium was collected and centrifuged at 1500 rpm to remove cells and large cellular debris. The adipokine assay was performed on the day of the collection to avoid freezing and thawing. Briefly, assay membranes were blocked with the Array Buffer 6 for 1h at RT on a rocking platform. Meanwhile, samples (1 ml) were incubated with Array buffer 4 (0.5 ml) and 15 µl of the Mouse Adipokine Detection Antibody for 1h at RT. After the membranes were blocked, each was incubated with the corresponding sample/antibody cocktail overnight at 4^0C on a rocking platform shaker. Then, membranes were washed three times with the 1X wash buffer (20 ml/membrane each time) to remove any unbound material. Subsequently,

membranes were incubated with Streptavidin-HRP for 30 min at RT, following the three washes. Finally, the chemiluminescence detection reagents were applied, and a signal was produced at each capture spot corresponding to the amount of protein bound. The signal was detected by exposure to X-ray film. Signal was quantified on scanned filmed, using the same exposure time, using ImageJ software.

2.17 Statistical analysis

GraphPad Prism 6 software and Excel were used for all statistical analyses. Unpaired student t-test or ANOVA analyses were carried out with a confidence interval of 95% and statistical significance was considered if $p<0.05$.

RESULTS

RESULTS CHAPTER 1

3. Cells and EVs characterization of the *in vitro* MetS models developed using 3T3-L1 adipocytes

3.1 Chapter 1 Aims:

- Establish a viable working model of *in vitro* adipocytes with high differentiation status.
- Establish and characterize suitable models of lipid overloaded/ hypertrophic adipocytes, adipocytes cultured in hypoxia (1 % 0_2) and cultured in the presence of the macrophage-conditioned medium, for the subsequent isolation of EVs.
- Detailed biochemical characterization of EVs secreted by models established in 3T3-L1 adipocytes.

3.2 Introduction

The exact aetiology for the development of obesity-related complications has not yet been elucidated. However, central obesity, insulin resistance, dyslipidemia and high blood pressure are common characteristics. Obesity causes an expansion of adipose tissue with proinflammatory phenotype and local hypoxia with increased secretion of FFAs. In addition, cells release soluble factors, as well as, membrane vesicles into the extracellular environment. These factors can mediate responses in neighbouring cells or can act at distant locations. There is accumulating evidence supporting the hypothesis that the concentration of EVs are elevated in above mentioned conditions of adipose hypertrophy and may

contribute to some pathophysiology of metabolic syndrome (Lawson et al. 2016; Jayachandran et al. 2011).

With this knowledge, in our study, we used the 3T3-L1 cells as *in vitro* model of adipocytes to find out whether these pathological conditions affect the release and the phenotype of adipocyte-secreted EVs. The work presented in this chapter represents the comprehensive analysis of *in vitro* models established in 3T3-L1 adipocytes and evidence that metabolic syndrome-resembling conditions affect the endocytic pathways that control exosomes secretion, and may activate alternative secretory routes.

3.3 Results

3.3.1 Morphological characterization of the 3T3-L1 adipocytes

The study of adipocyte biology and differentiation has become an area of intense research due to the growing worldwide obesity epidemic. 3T3-L1 cells are a widely used and very well characterized adipocyte model (Ntambi & Kim 2000; Reichert & Eick 1999). 3T3-L1 cells have the capacity to be differentiated into the adipocyte phenotype *in vitro* upon exposure to an adipogenic cocktail of insulin, glucocorticoid agent DEX and IBMX (Green & Kehinde 1975; Green & Kehinde 1974; Mehra et al. 2007). Recently, in more and more studies, a PPARγ agonist, Rosiglitazone, along with above mentioned adipogenic agents, was used for the differentiation of the 3T3-L1 adipocytes and it has been shown to significantly improve the adipocyte phenotype and increase adipose tissue mass (Kallen & Lazar 1996). This compound belongs to the family of thiazolidinediones (TZDs) that are a group of clinically used anti-diabetic drugs, which improve insulin sensitivity (Crossno et al. 2006). They work by stimulating the formation of new

adipocytes from preadipocytes and progenitor cells, by binding to PPAR receptors in fat cells making them more sensitive to the action of insulin.

High level of differentiation of the 3T3-L1 adipocytes depends on many factors such as for example the cell culture dish (Mehra et al. 2007) and the media height above the cell layer (Sheng et al. 2014), maintenance of 3T3-L1 fibroblasts and the passage number. Having that in mind, to assure a high level of differentiation of our cells and to examine to what extent rosiglitazone was improving 3T3-L1 adipocyte differentiation, we tested rosiglitazone, alongside other adipogenic agents. As a readout, we compared the expression of adipocyte differentiation markers, which all play their respective roles in the transcriptional cascade during adipocyte differentiation.

We compared the level of mRNA expression of the Fatty acid-binding protein 4 (*Fabp4*), Adiponectin (*Adipoq*), Glut4 (*Slc2a4*) and CCAAT/enhancer-binding protein alpha (*Cebpa*) in pre-adipocytes and in adipocytes, using confluent fibroblasts stage as a control, differentiated without and with rosiglitazone **(Figure 10).** Results of qPCR indicate that in rosiglitazone-differentiated adipocytes, the expression of all differentiation-related markers is significantly improved at both, the pre-adipocyte and adipocyte stage together with the 20-time increase in C/EBP alpha **(Figure 10D)**, a master regulator of adipocyte differentiation (Reichert & Eick 1999). In consequence, to have the highest rate of adipocyte differentiation we used rosiglitazone for the rest of the study.

The morphological characterization of 3T3-L1 cells was evaluated thought the different stages of differentiation **(Figure 11)**. Using light microscopy images **(Figure 11A)** we could appreciate the morphological changes that 3T3-L1 fibroblasts undergo to become mature adipocytes. The first and most notable alteration is seen in the gain of spherical shape as fibroblasts cells convert to preadipocytes **(Figure 11A, middle panel)**.

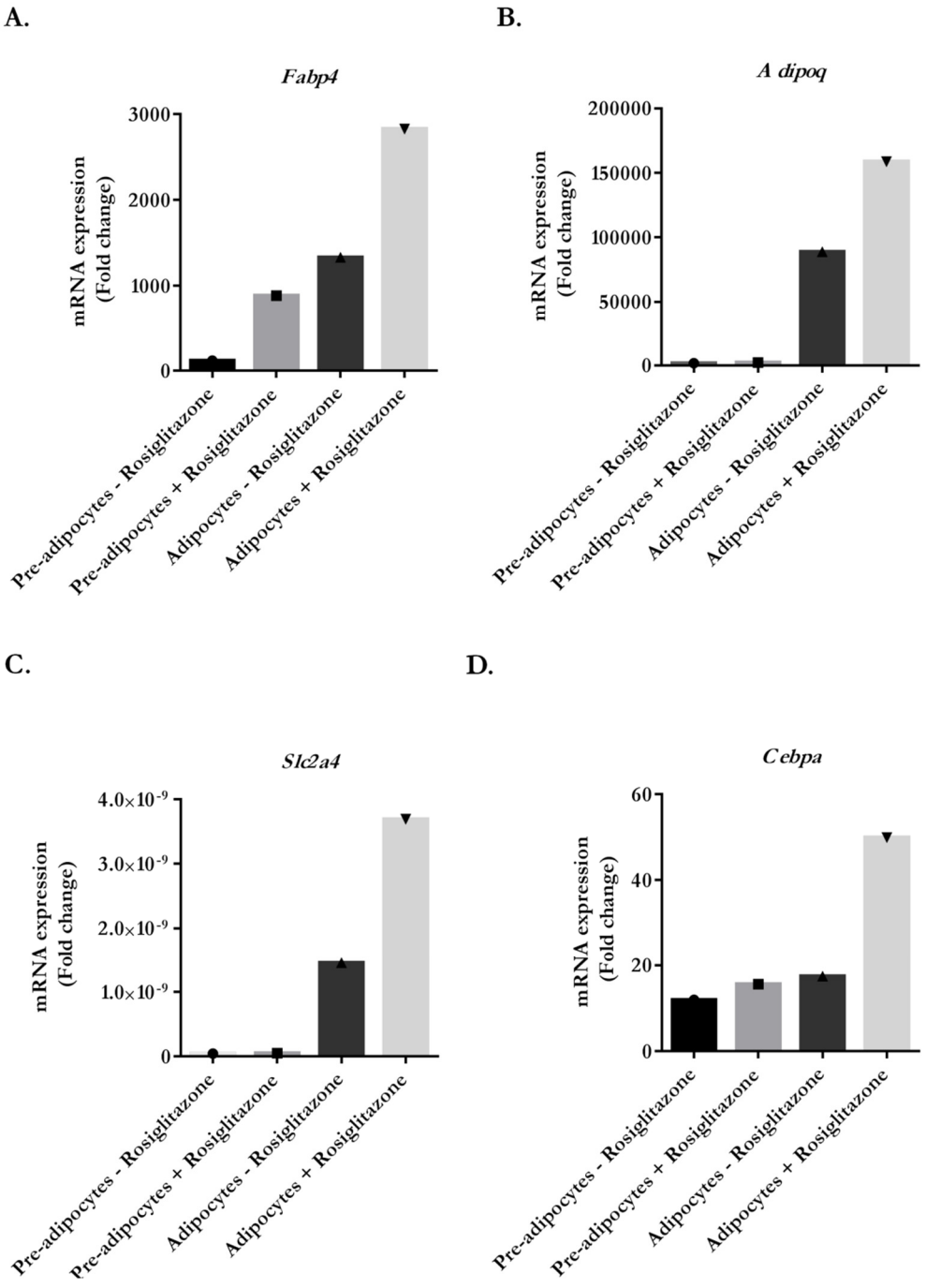

Figure 10 Rosiglitazone improves 3T3-L1 adipocyte differentiation. Differentiation efficiency was compared with and without Rosiglitazone. Quantitative PCR analysis of genes expressed during differentiation, encoding for the **(A)** Fabp4/Ap2 **(B)** Adiponectin, **(C)** Glut4, and **(D)** Cebpα proteins. Expression in fibroblasts was used as a control. Biological replicate = 1, technical replicate = 3

This occurs due to a change in an extracellular matrix (ECM) and cytoskeletal components (Symonds 2012). Moreover, the lipid droplets begin to accumulate as seen by Bodipy staining in **Figure 11B.** The localization of proteins associated with lipid droplets such as adipophilin and adiponectin was assessed by immunostaining **(Figure 11C and 11D)** and their expression confirmed by WB in cellular lysates from 3T3-L1 adipocytes **(Figure 11E)**.

In conclusion, molecular and morphological results confirmed that our method of differentiation is adequate, and consequently, it was used for the rest of the study.

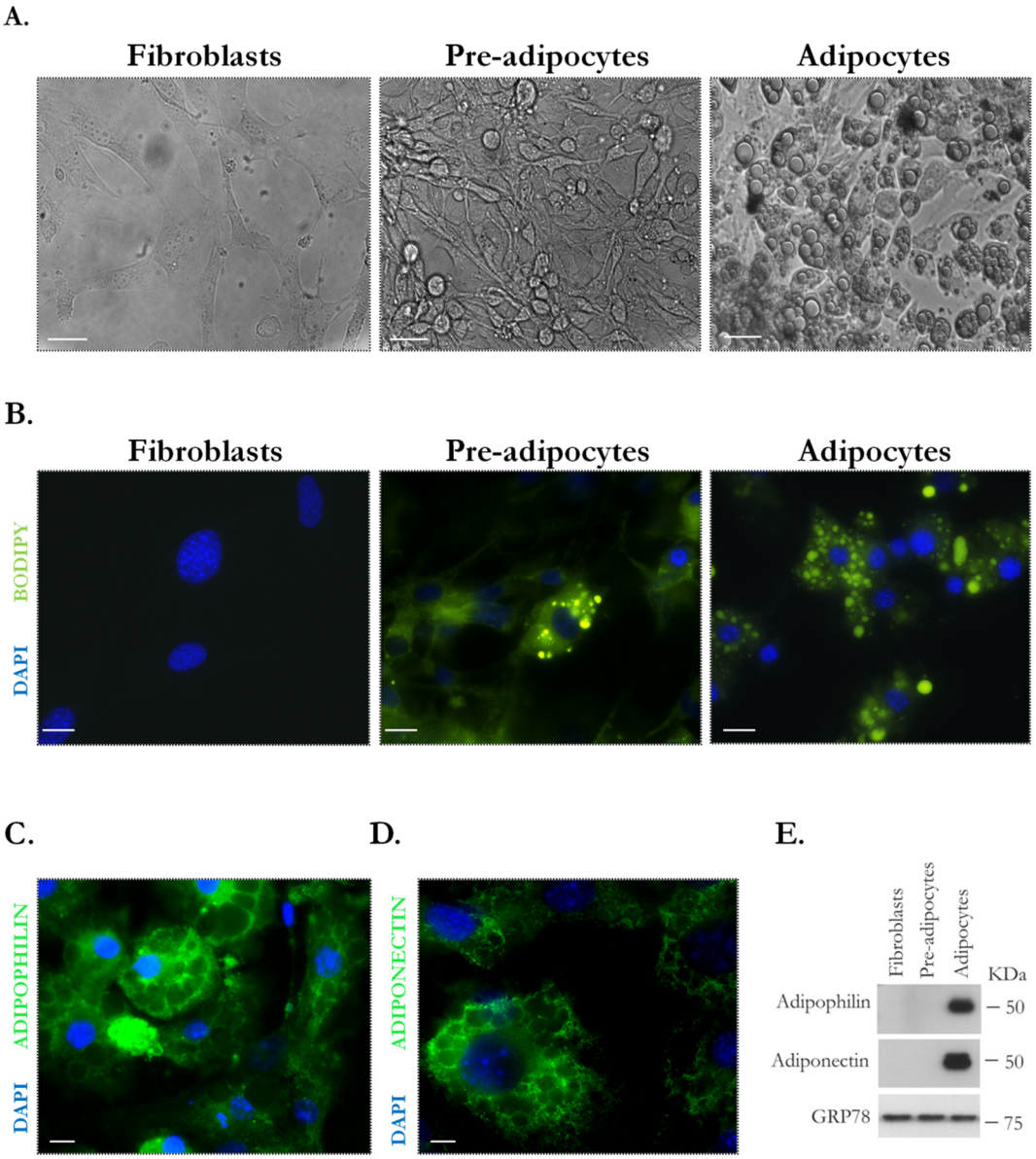

Figure 11 Morphological and molecular changes through 3T3-L1 adipocyte differentiation. (A) Light microscopy images of 3T3-L1 cells throughout the differentiation stages. Live cells were imaged using inverted microscope at 40X magnification. 3T3-L1 fibroblasts were imaged at sub-confluent state, pre-adipocytes at day 6 of the differentiation process and adipocytes at day 13, the final day of differentiation; bar = 50μm. **(B)** 3T3-L1 fibroblasts, pre-adipocytes and adipocytes stained with Bodipy (10 μg/ml) confirming lipid accumulation; bar=20μm. Immunofluorescent staining of 3T3-L1 adipocytes with antibodies against **(C)** adipophilin and **(D)** adiponectin proteins. **(E)** Expression of both markers was confirmed by Western-blotting in 3T3-L1 adipocyte cell lysates (10 μg).

3.3.2 Energetic demands of 3T3-L1 cells during the differentiation process

As cell differentiation progresses, the energetic demand increases significantly to maintain cellular processes. In the terminal differentiation stage, there is an increase in the activity of enzymes responsible for triglyceride synthesis, glucose transport, and synthesis of adipocyte-related products. (Gregoire et al. 1998). Previous studies have also demonstrated an increase in expression levels of essential components of the mitochondrial respiratory chain such as peroxisome proliferator-activated receptor gamma coactivator 1-alpha (PGC1α) and Cytochrome c, concluding that cells increase their mitochondrial content during adipogenesis (Keuper et al. 2014).

Therefore, we decided to monitor the mitochondrial respiratory function throughout the 3T3-L1 differentiation, in fibroblasts, pre-adipocytes, and adipocytes, using a Seahorse XF24 extracellular flux analyzer. During the experiment, by sequential addition of oligomycin, FCCP, and rotenone, mitochondrial ETC can be inhibited at very specific sites, allowing the cellular response to be detected as a change in the rate of oxygen consumed by cells. **Figure 12A** shows the time-lapse measurements of the OCR in values normalized by the number of cells per well. Preadipocytes exhibit higher basal respiration, as compared to fibroblasts and even adipocytes. However, the respiratory capacity increases notably in mature adipocytes **(Figure 12A)**.

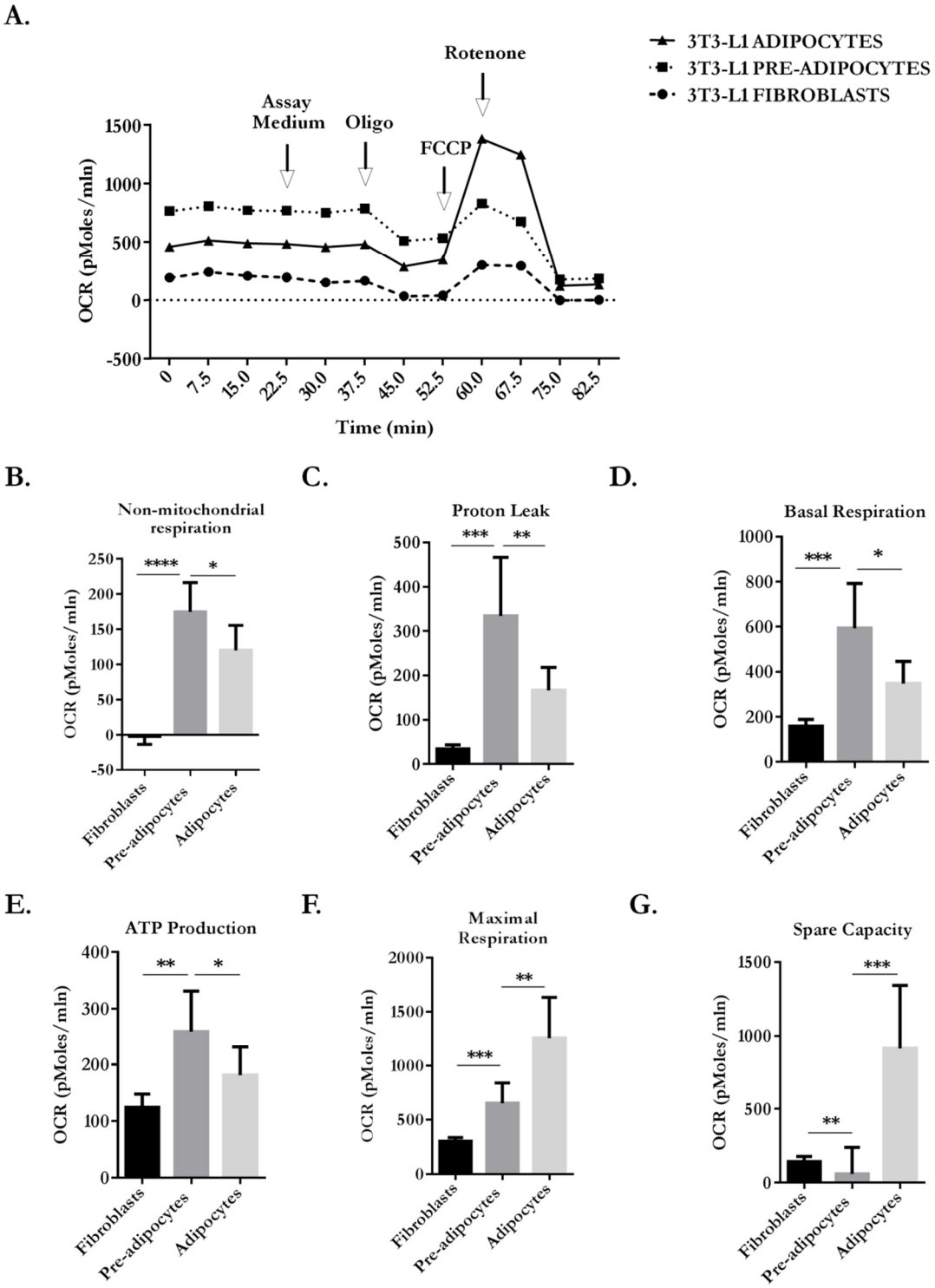
A.
3T3-L1 ADIPOCYTES
3T3-L1 PRE-ADIPOCYTES
3T3-L1 FIBROBLASTS
Rotenone
Assay Medium
Oligo
FCCP
OCR (pMoles/mln)
Time (min)
B.
Non-mitochondrial respiration
C.
Proton Leak
D.
Basal Respiration
E.
ATP Production
F.
Maximal Respiration
G.
Spare Capacity
Fibroblasts
Pre-adipocytes
Adipocytes

Figure 12 The profile of mitochondrial stress test in 3T3-L1 cells throughout the adipocyte differentiation process. **(A)** OCR was measured under basal conditions and following the sequential addition of oligomycin (1 mM) FCCP (300 nM) and rotenone (1 μM) to obtain the response profile of mitochondrial function in 3T3-L1 fibroblasts, preadipocytes and adipocytes. Individual parameters of **(B)** non-mitochondrial respiration, **(C)** proton leak, **(D)** basal respiration, **(E)** ATP production, **(F)** maximal respiration and **(G)** spare capacity were established. 3T3-L1 cells were differentiated directly on specific microplates from the XF24 flux analyzer. Replicate/condition = 6, error bars=SD. The *p* values were denoted as follows: 0.01- 0.05 = *, 0.01-0.001=**, 0.001-0.0001=***. Unpaired student t-test was performed to determine significant differences.

Using XF24 flux analyzer, specific mitochondrial parameters can be studied, such as non-mitochondrial respiration, basal respiration, proton leak, ATP production, maximal respiration and spare capacity, **(Figure 12B-12G)**. Besides the decrease in spare capacity **(Figure 12G)**, all other parameters increase in preadipocytes, upon differentiation. This could be associated with higher energy demand due to preadipocytes conversion. The addition of rotenone, an inhibitor of ETC complex I hindered mitochondrial respiration and therefore allowed us to make a distinction between mitochondrial and non-mitochondrial respiration. In fibroblasts, the non-mitochondrial respiration is barely detectable, indicating that all energy seems to be associated with mitochondria **(Figure 12B)**. There was a significant increase in basal respiration **(Figure 12D)** and the production of ATP by preadipocytes **(Figure 12E)**. Yet surprisingly, the increase in proton leak was also observed upon differentiation **(Figure 12C)**. Maximal respiration **(Figure 12F)** and spare capacity **(Figure 12G)** are the parameters which are significantly higher in mature adipocytes. These processes are related to the maximal ATP output controlled by the cells substrate oxidation capacity (Keuper et al. 2014). They can be measured by the addition of the ion carrier, FCCP, which disrupts ATP synthesis by transporting hydrogen ions across the mitochondrial membrane and dissipating/uncoupling the membrane potential gradient. The energy is rapidly consumed without generation of ATP which allows the estimation of maximal respiration rate that the cell could perform. Spare capacity

is determined by subtracting basal respiration value from the maximal induced by FCCP.

Together these results indicate that adipogenesis is highly energy producing and consuming process as judged by an increase in the main mitochondrial parameters. In addition, the spare capacity was decreased in preadipocytes as compared to fibroblasts which could take place to allow the adipogenic procession, which is later recovered when adipocytes become mature **(Figure 12G)**.

3.3.3 Induction of hypertrophy in 3T3-L1 adipocytes

3.3.3.1 Model characterization

We established an *in vitro* model of hypertrophic adipocytes in differentiated 3T3-L1 adipocytes by challenging them with a mix of oleic and palmitic acids at a ratio of 2:1 and at a final concentration of 1 mM (**section 2.2.3.2**). Bodipy staining of these cells revealed the presence of significantly enlarged fat droplets within adipocytes **(Figure 13A),** as also confirmed by flow cytometry analysis of Bodipy stained FFA-treated adipocytes **(Figure 13B and 13C).**

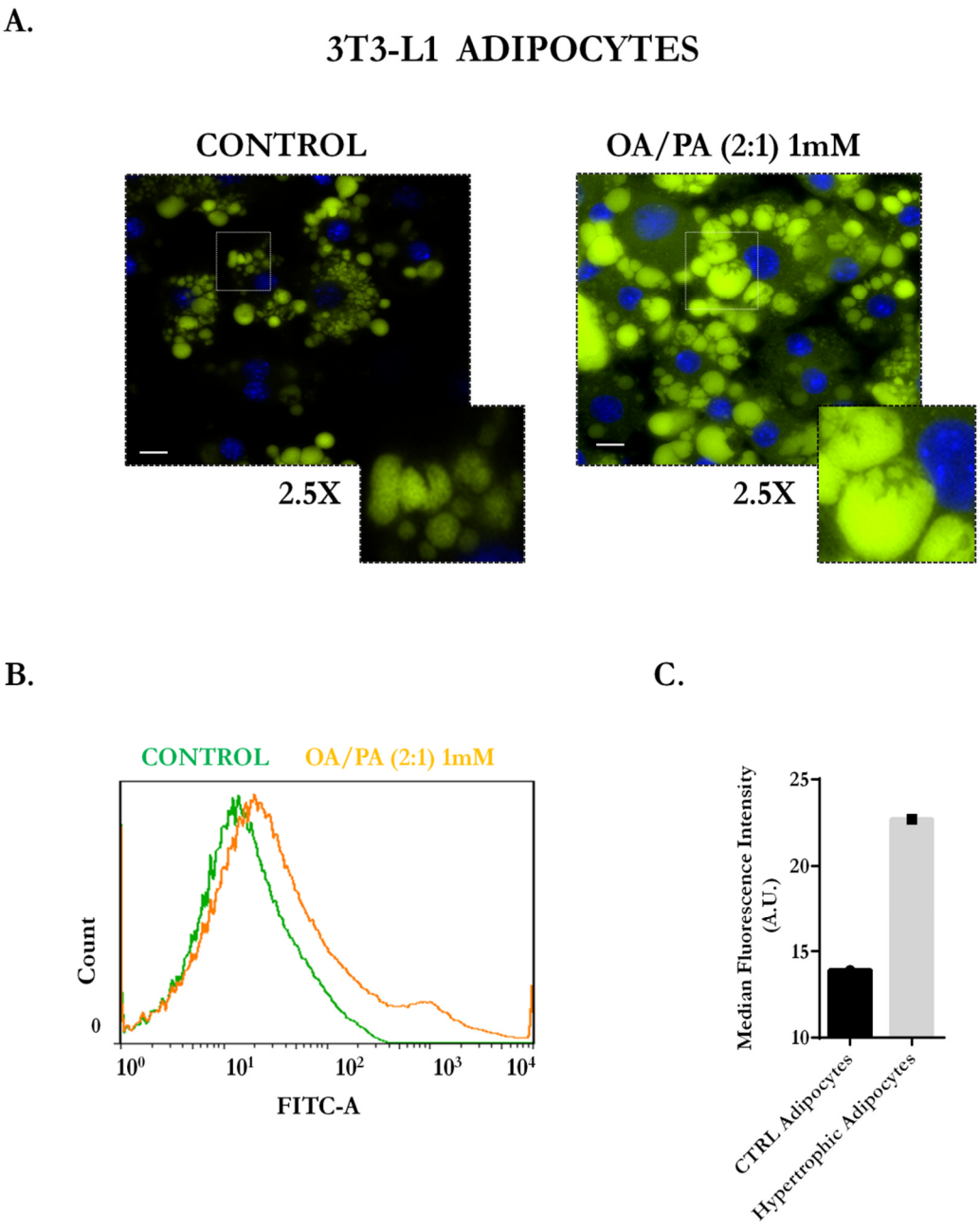

Figure 13 Treatment with FFAs induces fat-overload in 3T3-L1 adipocytes. Mature 3T3-L1 adipocytes were cultured with a combination of oleic and palmitic acid (2:1 ratio), at a final concentration of 1 mM for 24h. **(A)** Images of the Bodipy stained, control and lipid-overloaded 3T3-L1 adipocytes, inserts were magnified 2.5X, bar=20 μm. **(B)** Representative flow cytometry histogram of Bodipy stained control and FFA-treated cells. **(C)** Quantification of FITC-A fluorescence in control and hypertrophic 3T3-L1 adipocytes.

3.3.3.2 Characterization of isolated EVs

Adipose tissue inflammation is a hallmarks of obesity, characterized by hypertrophic adipocytes, increased influx of immune cells and AT inflammasome activation (Mariëtte E G Kranendonk et al. 2014; Weisberg et al. 2003; Zhang et al. 2015). Soluble factors and adipokines, secreted by adipose tissue are involved in the recruitment and activation of macrophages (Keophiphath et al. 2010). Through secreted adipokines, adipose tissue actively communicates with other organs such as liver, skeletal muscle and the brain (Ailhaud 2006; Zhang et al. 2016). EVs from *in vitro* differentiated adipocytes were previously characterized (Mariëtte E G Kranendonk et al. 2014). They were visualized by TEM and on a density gradient, they were detected at known exosomal density range, between 1.12-1.14 g/ml. Subjected to the WB analysis, they were found to contain EV specific markers such as CD9 and CD63 and adipocyte specific proteins like adiponectin and fatty acid binding protein. The increase in EVs secreted by omental adipose tissue in obese patients, has also been reported (Mariëtte E G Kranendonk et al. 2014).

We performed the characterization of EVs derived from chemically-induced hypertrophic 3T3-L1 adipocytes. Importantly, to avoid the contamination coming from FFAs, medium was removed after 24 h and cells were cultured for an additional 48 h for the isolation of EVs **(section.2.3.2)**. Detailed characterization, including visualization by cryo-EM, size distribution profile and particle concentration by NTA and protein expression profile of common EV markers by WB was performed **(Figure 14)**.

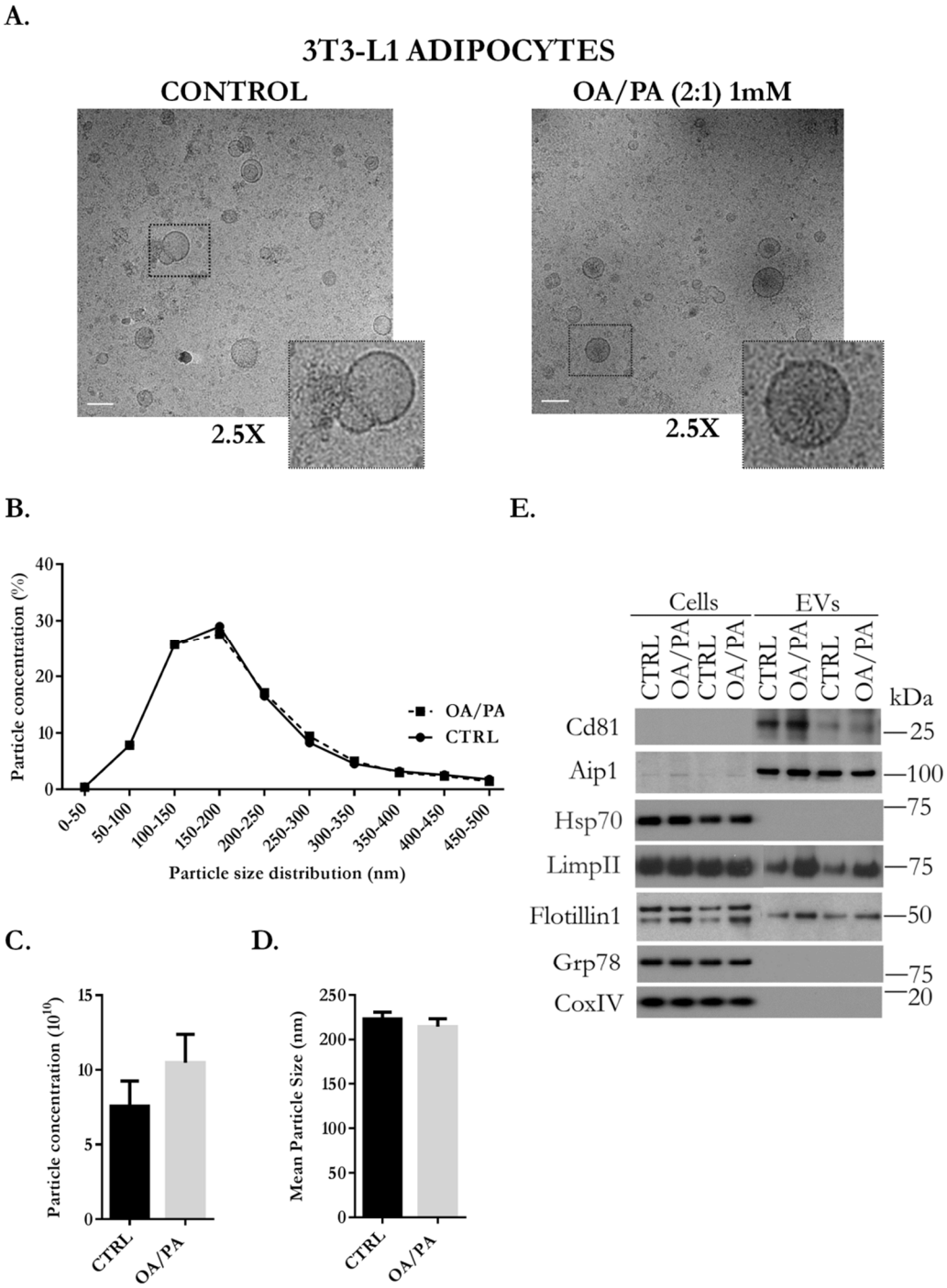

Figure 14 Characterization of EVs secreted by hypertrophic 3T3-L1 adipocytes. Ultrastructural and biochemical characterization of EVs isolated from conditioned medium of hypertrophic 3T3-L1 adipocytes. **(A)** Cryo-EM analysis; bar=100 nm, inserts are magnified 2.5X **(B) Particle** size range distribution profile measured by NTA. **(C)** Particle concentration (10^{10}) **(D)** Particle mean size was measured by NTA, n=4 **(E)** Protein extracts from two independent preparations of EVs (5 μg) together with their corresponding cell lysates (10 μg) were analyzed by WB with antibodies for EV specific as well as cellular markers. Error bars = SD

Cryo-EM analysis revealed the presence of a heterogeneous population of membrane vesicles limited by a lipid bilayer. Representative electron micrographs are shown in **Figure 14A**. Concerning the size of secreted vesicles, previous studies have shown that, the peak size distribution of EVs secreted by human adipose tissue derived mesenchymal stem cells was found to be between 150 and 200 nm (Katsuda et al. 2013; Zhang et al. 2016). Our analysis of four independent preparation of EVs from control and hypertrophic adipocytes reinforced this result, as the peak size of our EV preparations ranged between 150-200 nm for both groups, with no difference in the overall size distribution of vesicle population **(Figure 14B)**. On the other hand, there was a slight increase in the concentration of particles released by hypertrophic adipocytes **(Figure 14C)** with no change in the mean particle size between both groups **(Figure 14D)**.

Protein analysis of EV-related markers was performed by WB in control and hypertrophic adipocytes, two independent preparations are shown on **Figure 14E**.

Importantly, organelle marker proteins, such as, Grp78 and CoxIV, endoplasmic reticulum and mitochondrial markers, respectively, were absent in the EV preparations (**Figure 14E**). These results indicate that under our lipid overload conditions no significant cell toxicity was produced and consequently no contamination by intracellular material. Interestingly, Hsp70 is a protein frequently found in EVs preparation obtained from different cell-types (Kalra et al. 2012). However, although we could detect this protein in the cell extracts, it was not present in the adipocyte-EV preparations (**Figure 14E**). Comparison of the abundance of Cd81 and Aip1 proteins, in 3T3-L1 adipocytes and their corresponding EVs, reveals that these EVs were highly enriched in these two exosomal markers **(Figure 14E)**. No significant changes were observed in the abundance of these proteins depending on the FFA treatment **(Figure 14E)**. Moreover, significantly increased expression of the lysosomal protein, LimpII, as well as, Flotillin1 were observed in EVs isolated from hypertrophic adipocytes.

Interestingly, while the higher expression of Flotillin1 was also observed in hypertrophic adipocyte-cell lysates, the intracellular expression of LimpII was not altered by the treatment. This result could indicate that there are different mechanisms for sorting these proteins into EVs.

Therefore, these results indicate that lipid-overload of adipocytes increases EV secretion and alter their composition.

3.3.4 3T3-L1 Adipocytes cultured under hypoxia and in the presence of the macrophage conditioned medium

3.3.4.1 Model characterization

Adipocyte hypertrophy that occurs during obesity is associated with macrophage infiltration and local hypoxia due to limiting blood supply resulting from lipid overload in adipocytes. To mimic these conditions *in vitro*, 3T3-L1 adipocytes were incubated in a hypoxic chamber with 1%0_2 or were cultured in the presence of macrophage conditioned medium (MØ) (v/v) (15%), previously obtained from differentiated primary mouse bone marrow cells, for 24 h **(Section.2.2.1.2)**. Induction of a cellular response to counter the lack of oxygen was confirmed in lysates of 3T3-L1 adipocytes **(Figure 15A)**. Elevated expression levels of various oxygen sensitive proteins such as Catalase, Ferritin-LC, Vegf and Rab11 were observed by WB **(Figure 15A)**. Rab11 is important in vesicular transport in the cell and it has been described to be implicated in hypoxia-induced invasion of breast cancer cells (Yoon et al. 2005) Cellular hypoxia has been reported to correlate with increased glucose uptake, and accordingly, we have also observed elevated expression of the S*lc2a1* gene encoding for the glucose transporter 1 (Glut1) in hypoxic adipocytes **(Figure 15B)**.

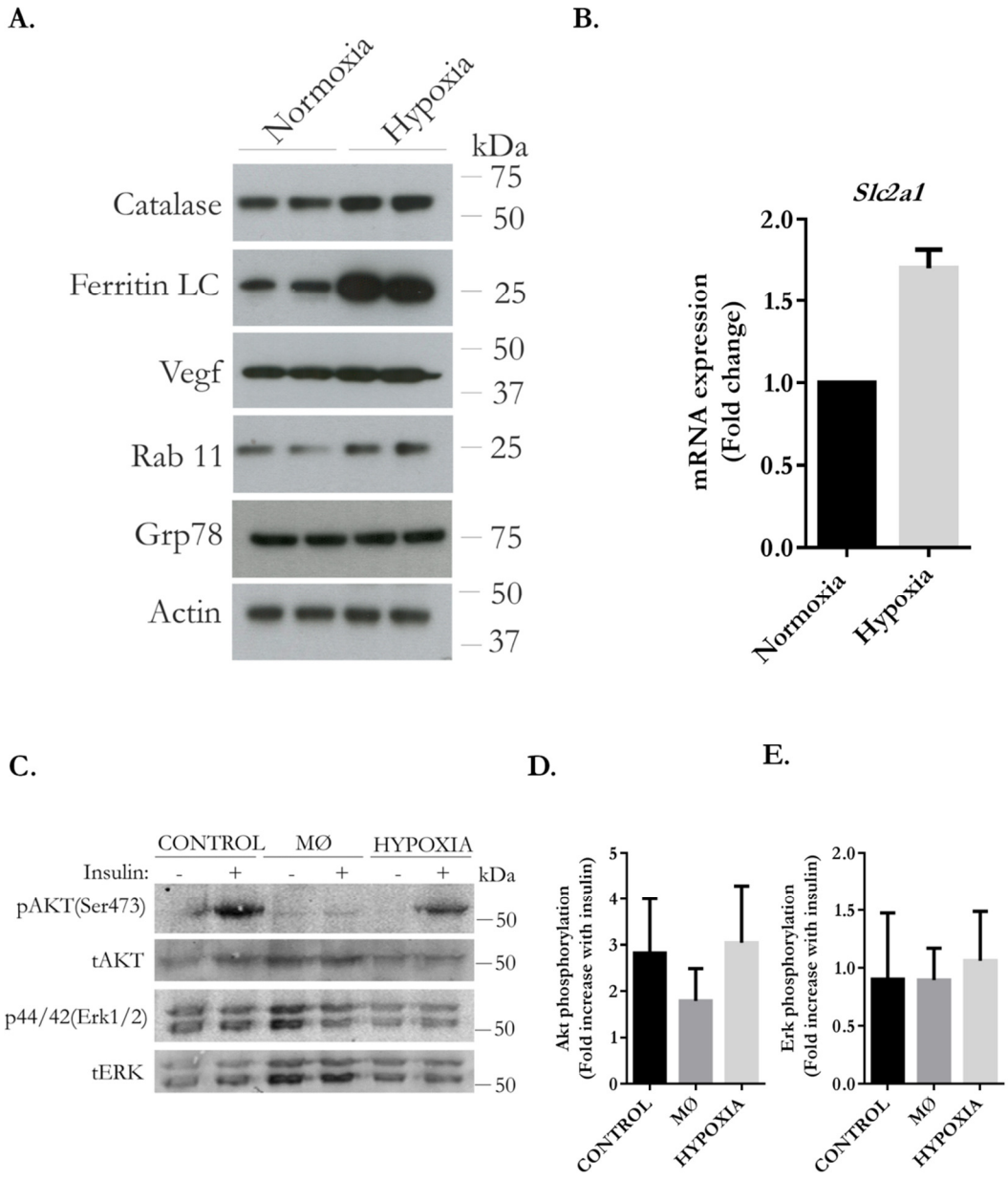

Figure 15 Characterization of 3T3-L1 adipocytes cultured in hypoxia and in macrophage-conditioned medium. Differentiated 3T3-L1 adipocytes were exposed to hypoxia (1%0_2) and to the macrophage-conditioned medium (MØ) for 24h. **(A)** 3T3-L1 cell lysates (10µg) from normoxic and hypoxic adipocytes were characterized by WB for the induction of hypoxia, n=2 **(B)** Hypoxia induced Glut1 (*slc2a1*) mRNA expression in normoxic and hypoxic adipocytes, n=2 **(C)** Representative WB of insulin stimulated Akt on Ser473 and Erk1/2 phosphorylation in 3T3-L1 adipocytes exposed to hypoxia and the macrophage-conditioned medium. Quantification of phosphorylation, represented as the fold increase in phosphorylation with insulin **(D)** Akt(Ser473) **(E)** Erk1/2. Quantification

was done using ImageJ software. Representative figure and quantification of 4 independent experiments. Error bars = SD.

We then sought to investigate the insulin sensitivity in our cellular models by evaluating the phosphorylation of the serine/threonine-protein kinase akt-1 (Akt) and extracellular signal-regulated kinase (Erk1/2) following insulin stimulation. We studied the insulin response in two models: the 3T3-L1 adipocytes under hypoxic conditions, and the 3T3-adypocytes exposed to medium conditioned by macrophages to resemble inflammatory conditions **(Figure 15C)**. Results of WB analysis, although not statistically significant, indicate that insulin sensitivity is slightly inhibited in 3T3-L1 adipocytes cultured in proinflammatory conditions **(Figure 15D)** with no the change in hypoxic adipocytes. Although a higher level of Erk1/2 total and phosphorylated was found in inflammatory conditions, no differences in the response to insulin were observed **(Figure 15E)**.

3.3.4.2 Characterization of isolated EVs

It has been demonstrated that cellular stress such as hypoxia induces increased release of EVs (Belting & Christianson 2015). It is also true for adipocytes cultured in hypoxic conditions (Syn et al. 2016). Interestingly, the hypoxia-inducible factor-1α (HIF-1α) was found to be excreted in hypoxic adipocytes-derived EVs (Syn et al. 2016). Moreover, results of quantitative proteomic analysis showed that hypoxic EVs contain increased amount of lipogenic enzymes such as fatty acid synthase (FASN), glucose-6-phosphate dehydrogenase (G6PD), and acetyl-CoA carboxylase (ACC). These *in vitro* results have been validated in serum of obese mice (*ob/ob*) (Sano et al. 2014). Furthermore, hypoxic EVs were able to transfer their proteomic phenotype on neighbouring cells as seen by elevated expression of *Fasn* and higher lipid accumulation in normoxic 3T3-L1 adipocytes exposed to hypoxic-EVs (Sano et al. 2014)

In our model we characterized EVs secreted by 3T3-L1 adipocytes exposed to hypoxia **(Figure 16)** and to the macrophage conditioned medium (MØ) **(Figure 17)** for 24h, as two independent models.

Cryo-EM analysis confirmed the presence of a heterogeneous size population of lipid membrane-enclosed vesicles, as can be appreciated on the electron micrographs in **Figure 16A**. Fused vesicles can also be found as well as vesicles slightly larger than defined exosomes. NTA analysis of the size distribution confirms the presence of larger particles **(Figure 16B)**. However, it also verifies that taking the whole population into account, most vesicles present were found to be within the size range of 100-150 nm and that more vesicles were secreted in hypoxic conditions in that size range **(Figure 16B)**. It can also be seen that the concentration of EVs secreted in hypoxia was increased as compared to control 3T3-L1 **(Figure 16C).** Together with the increased release of EVs by adipocytes in hypoxia the mean particle size decreases **(Figure 16D)**.

Western blot analysis revealed that the tetraspanin Cd81 was present in the EV fractions as well as in the parent whole cell lysates **(Figure 16E)** with an enrichement in EVs. Moreover, the expression of Cd81 in donor cells correlated negatively with the expression in corresponding EVs, as more Cd81 was secreted with control EVs **(Figure 16E)**. Reverse situation was observed in hypoxia **(Figure 16E)**. Interestingly, as compared to the control EVs, the expression decreased in EVs secreted by hypoxic adipocytes. The organelle markers, prohibitin (mitochondria) and Grp78 (endoplasmic reticulum) were detected exclusively in the whole cell lysates, indicating the presence of very low or none contamination in our preparations by cellular lysis.

To address the hypothesis of whether possible changes in insulin stimulated glucose uptake in adipocytes could be related with the amount of glucose transporter, we evaluated the protein level of Glut4, one of the prominent glucose transporter isoforms expressed in adipocytes. Although we could not detect the protein in the cell extracts, Glut4 was in fact present in EV fractions secreted by

adipocytes, and remarkably, the transporter was more abundant in EVs from hypoxic adipocytes **(Figure 16E)**.

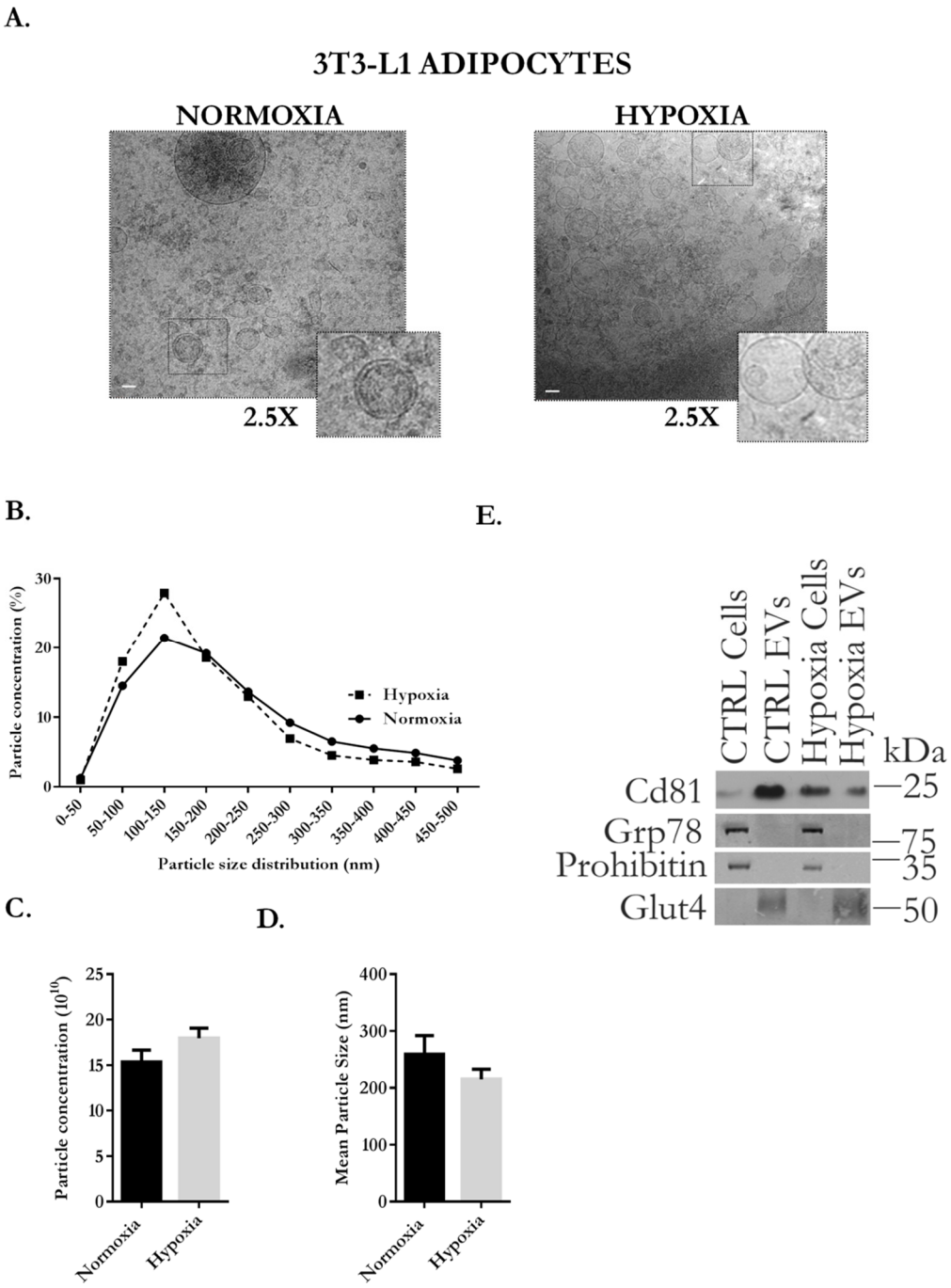

Figure 16 Characterization of EVs released by hypoxic 3T3-L1 adipocytes. Ultrastructural and biochemical characterization of EVs, isolated from conditioned medium of 3T3-L1 adipocytes in normoxia and hypoxia ($1\%0_2$). **(A)** Cryo-EM analysis, size bar=100nm, inserts magnified 2.5X **(B)** Size range distribution **(C)** Particle concentration (10^{10}) **(D)** Particle mean size was measure by NTA, n=3 **(E)** Protein extracts from two

independent preparations of EVs (5 μg) together with their corresponding cell lysate (10 μg) controls were analyzed by WB, with antibodies against protein markers of EVs as well as protein markers of intracellular compartments. Representative figure. Error bars = SD.

EVs obtained from control as well as from 3T3-L1 adipocytes cultured in the presence of the MØ. Isolated EVs were visualized in their native state by cryo-EM, again revealing some important structural details such as the presence and thickness of phospholipid bilayer or the electron density of vesicles. **Figure 17A** shows representative electron micrographs where it can be noted the presence of mostly electron lucent vesicles can be appreciated. It also seems that smaller vesicles have a more densely packed lipid bilayer **(Figure 17A, Control, 2.5X insert)** than larger vesicles. NTA confirmed this heterogeneity of isolated vesicle populations **(Figure 17B)**. A filtration step in the isolation protocol to some degree discards the presence of larger particles, however due to clumping or formation of fused vesicles, frequently observed by cryo-EM, they are present in the sample and detected by NTA. Their presence was abundant in the control EV sample, as can be observed on the size distribution curve **(Figure 17B)**. Furthermore, the MØ EV sample shows a 10 % increase in the amount of 100-150 nm EVs with a significant decrease in the overall mean particle size **(Figure 17C)**. The total concentration remains unchanged **(Figure 17C)** between both groups. Western blotting confirmed the presence and enrichment of Cd81 in the EV preparations, with a slight reduction in the expression in EVs produced by adipocytes exposed to the macrophage-conditioned medium **(Figure 17D).** Mitochondrial (prohibitin) and ER (Grp78) markers were solely associated to whole cell lysates, discarding contamination by cell lysis. Moreover, as already observed, Glut4 was found to be secreted into the extracellular space by means of EVs, and importantly, slightly more in EVs from adipocytes exposed to the macrophage-conditioned medium than the control ones.

The results obtained from these experiments indicate that the secretion of EVs by adipocytes is sensitive to stress conditions such as hypoxia and presence of proinflammatory cytokines.

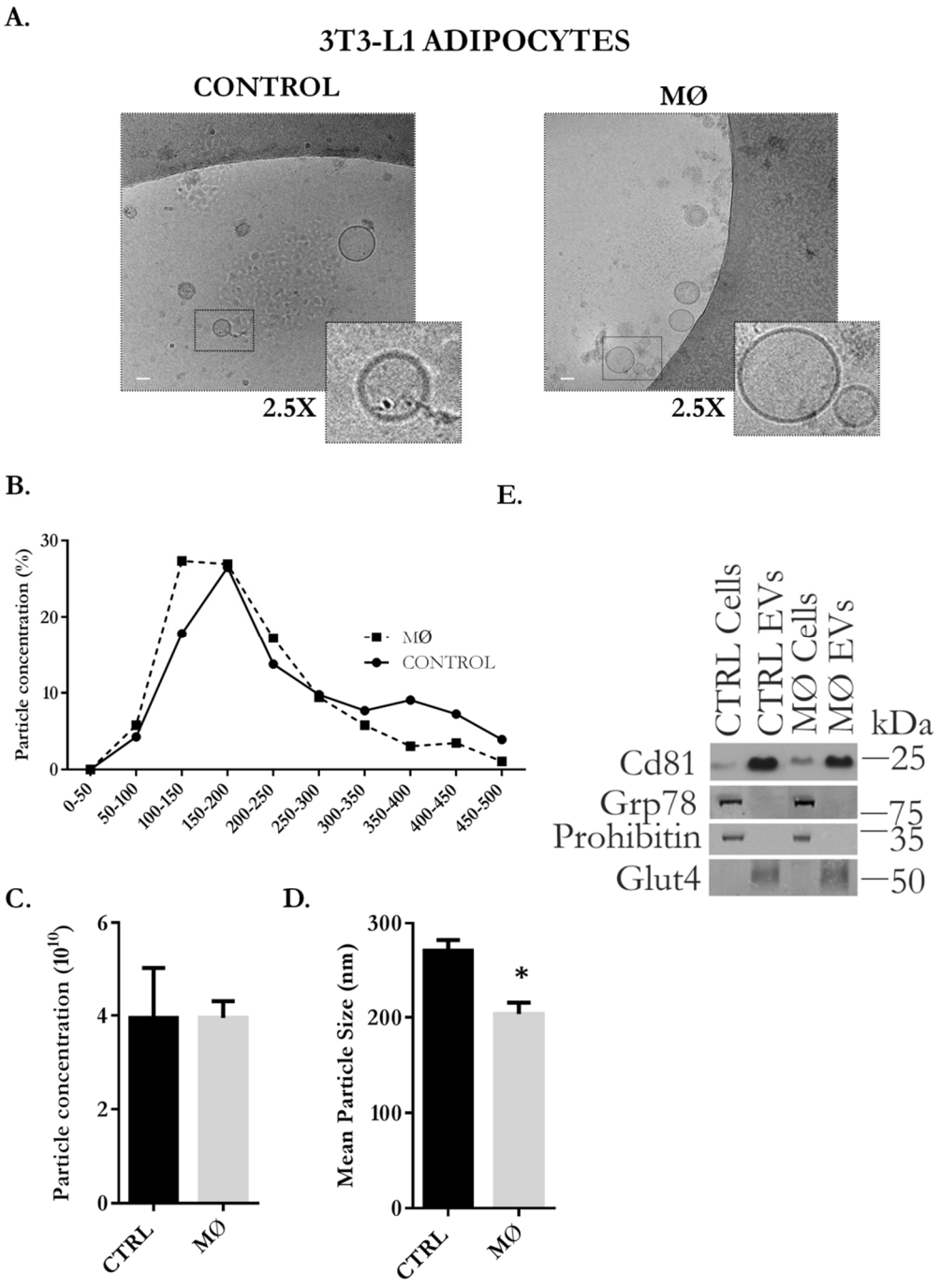

Figure 17 Characterization of EVs released by 3T3-L1 adipocytes cultured with macrophage-conditioned medium. Ultrastructural and biochemical characterization of EVs, isolated from the conditioned medium of the 3T3-L1 adipocytes cultured in the presence of the macrophage-conditioned medium. **(A)** Cryo-EM analysis; bar=100nm; inserts magnified 2.5X. **(B) S**ize range distribution **(C)** Particle concentration (10^{10}). **(D)** Particle mean size, n=2. **(E)** Protein extracts from two independent preparations of EVs (5 µg) together with their corresponding cell lysate (10 µg) controls were analyzed by WB, with antibodies for EV as well as cellular markers. Replicate/condition = 3, error bars=SD. The *p*

value = 0.001-0.05=*. Unpaired student t-test was performed to determine significant differences.

3.3.4.3 Investigating the insulin sensitivity in 3T3-L1 adipocytes upon exposure to hypoxic- and MØ-EVs

As previously mentioned, in obesity, adipose tissue expansion results in local tissue hypoxia and macrophage infiltration causing local inflammation. We have demonstrated that our *in vitro* models of 3T3-L1 adipocytes cultured in hypoxia or co-cultured with macrophage-conditioned medium exhibit altered insulin sensitivity **(Figure 15C)** reflecting the metabolic state adipose tissue in obesity and MetS.

These two mechanisms cause cellular stress and as shown by our results, contribute to the increased generation of EVs with altered expression of EV-related markers **(Figure 16 and Figure 17)**. With that knowledge we next aimed to determine whether these EVs could have en influence the metabolic phenotype of the 3T3-L1 adipocytes. We determine the activation of the insulin signalling pathway by monitoring phosphorylation of Ser473 of Akt and of Thr201/Tyr204 on Erk1/2 in response to insulin stimulation upon treatment with EVs. For these experiments, differentiated 3T3-L1 adipocytes were either left untreated or treated with EVs isolated from either control adipocytes, adipocytes cultured in hypoxia or adipocytes cultured in the presence of the macrophage-conditioned medium for 24 h. In dose dependant manner, we detected a small but significant decline in Ser473 Akt phosphorylation in cells treated with EVs secreted by 3T3-L1 adipocytes cultured in hypoxia as compared to untreated cells or control 3T3-L1 adipocytes **(Figure 18A and 18B)**. On the contrary, we did not detect any difference in the activation of Erk1/2 proteins in any of the experimental groups **(Figure 18C).**

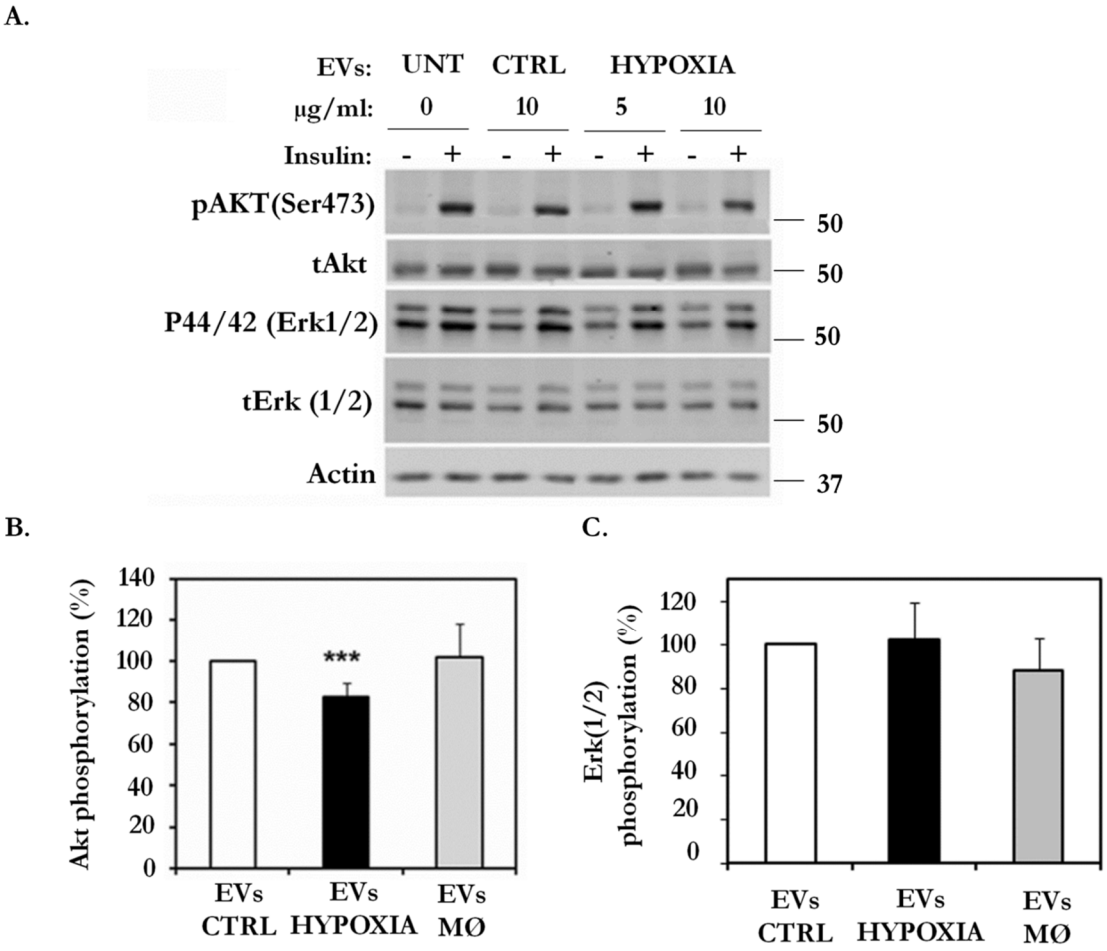

Figure 18 EVs from hypoxic 3T3-L1 adipocytes inhibit insulin signalling in recipient 3T3-L1 adipocytes. (A) Cellular lysates from 3T3-L1 adipocytes treated for 24 h with EVs from CTRL 3T3-L1 adipocytes (EVs CTRL), cultured in 1% oxygen (EVs hypoxia) and cultured in macrophage conditioned medium (EVs MØ), at concentration between 5-10 µg. Cells were then stimulated with 100 nm insulin for 30 min. Equal amounts of lysates were immunoblotted with antibodies as indicated. **(B)** Quantification of Akt phosphorylation (%) compared to the phosphorylation in cells treated with EVs CTRL. **(C)** Quantification of Erk1/2 phosphorylation (%) compared to the phosphorylation in cells treated with EVs CTRL. Graphs show ± STDEV; n=4 for Akt and n=2 for Erk1/2. *p* value *** <0.01. One Way ANOVA.

3.3.4.4 Investigating the insulin stimulated glucose uptake in 3T3-L1 adipocytes upon exposure to hypoxic- and MØ-EVs

To confirm our results, we performed the insulin stimulated glucose uptake in 3T3-L1 adipocytes upon exposure to EVs. Following 24 h treatment with EVs, the insulin-stimulated glucose uptake was measured.

In untreated control cells insulin increased 2-DG uptake levels by 3-fold over basal uptake **(Figure 19A and 19B)**. Cells treated with EVs from control adipocytes exhibited a similar response to untreated cells and no statistical significance were detected in basal or insulin-stimulate uptake values compared to untreated cells **(Figure 19A)**. However, cells treated with EVs from hypoxic adipocytes displayed a 25% decrease in the insulin-stimulated response, while no statistical significances were observed in the basal glucose transport rates **(Figure 19A)**. Moreover, the insulin-stimulated glucose uptake achieved treated with EVs obtained from hypoxic cells was restored upon heating hypoxic EVs at 40^0C for 30 min prior treatment of cells **(Figure 19C)**. This result suggests that heat-mediated denaturation of proteins associated to EVs either has an effect over the uptake of EVs by recipient 3T3-L1 adipocytes or other mediator of the action over the insulin sensitivity. Furthermore, cells treated with EVs released by adipocytes cultured with macrophage conditioned medium did not display any significant differences in either basal or insulin-stimulated glucose uptake compared to cells untreated or cells treated with EVs derived from control cells **(Figure 19B)**.

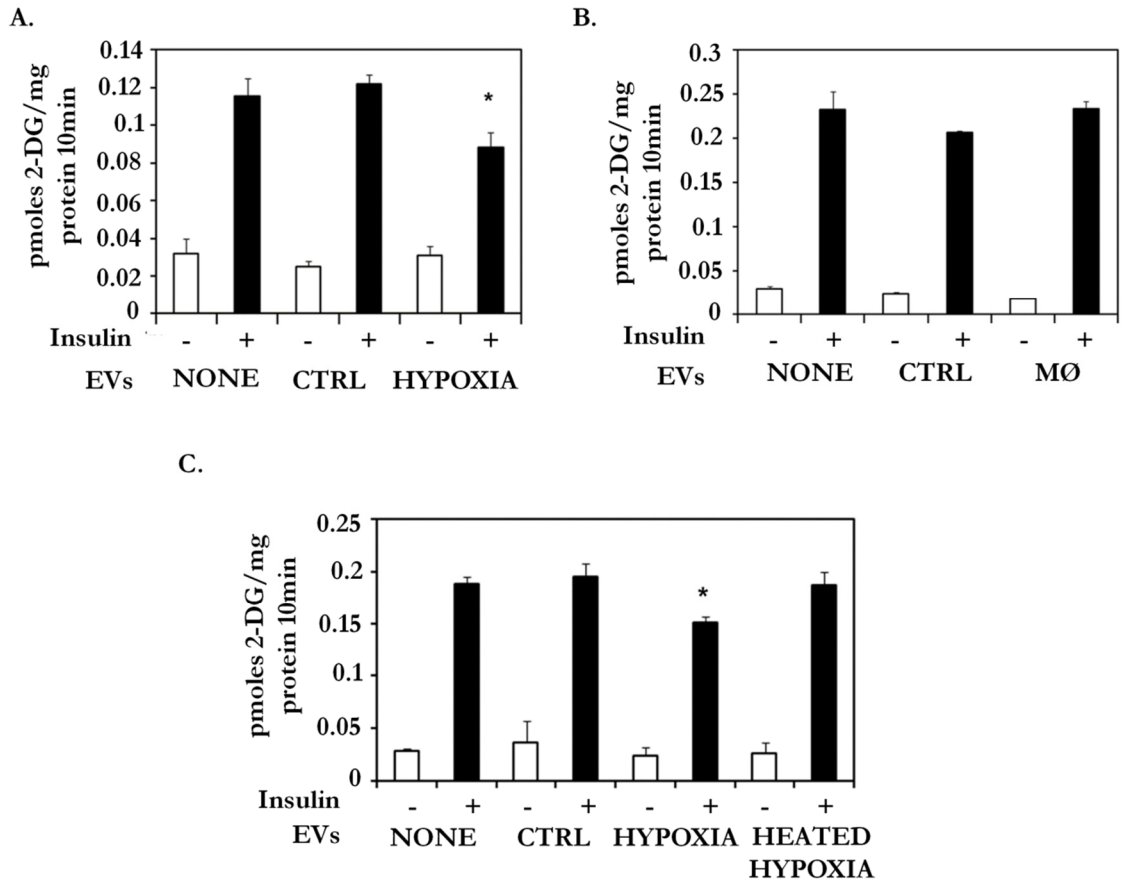

Figure 19 EVs from hypoxic 3T3-L1 adipocytes inhibit insulin-stimulated glucose uptake in recipient 3T3-L1 adipocytes. (A)(B)(C) Differentiated 3T3-L1 adipocytes were left untreated or treated for 24 h with EVs from CTRL 3T3-L1 adipocytes (EVs CTRL), cultured in 1% oxygen (EVs hypoxia), cultured in macrophage conditioned medium (EVs MØ) or with heat inactivated EVs hypoxia (40^0C for 30 min). In all three independent experiments, basal or stimulated with insulin (100 nM) 2-DG uptake was measured. Uptake was normalized to protein content in cellular lysates. The (A)(B)(C) represent three independant experiments. The graph show mean ± SEM; biological replicates n=3; *p* value * indicates <0.05; One Way ANOVA.

3.4 Summary

In summary, adipocytes under cellular stress conditions such as hypertrophy, hypoxia or cultured in the presence of the macrophage-conditioned medium alter the number and the composition of secreted EVs. Hypertrophic adipocytes have shown to secrete more EVs and displayed higher expression of Flotillin1 and Cd81 in cells and secreted EVs.

We identified the presence of Glut4 protein and increased expression level of it in EVs coming from adipocytes cultured in hypoxia and with macrophage-conditioned medium. Moreover, in both cases, the expression of Cd81 protein in EVs was downregulated.

Finally, we have also shown that EVs released by 3T3-L1 adipocytes cultured in hypoxia caused a significant reduction in insulin-stimulated phosphorylation of Akt on Ser473 and in addition, these EVs significantly affected the insulin-stimulated glucose uptake in 3T3-L1 adipocytes (Graphically represented in **Figure 20**).

3.5 Discussion

For studies in biomedical research different methods are employed, from experimental animals, to tissues, primary cell culture and immortalized cell lines (Kanuri & Bergheim 2013). Establishing a valid cellular *in vitro* model for subsequent isolation of EVs from the conditioned medium is very challenging, with many factors to consider, such as the contamination with EVs from other sources, minimal toxicity to avoid the contamination by cellular debris or the release of apoptotic bodies.

The characteristic of obesity is an enlargement of adipose tissue due to increase storage of the excess energy. There are two possible growth mechanisms, a pathological enlargement of adipocytes known as hypertrophy and hyperplasia, an increase in adipocyte cell number (Jo et al. 2009). Currently, there is not any well-established *in vitro* model of hypertrophic transition of adipocytes. In a recent study, researchers maintained already mature 3T3-L1 adipocytes in culture supplemented with 10% FBS and 0.1% insulin. The hypertrophic phenotype was already seen on day 24, approximately two weeks post-differentiation, manifested as en enlargement of lipid droplets, accompanied by elevated levels of pro-inflammatory factors, with conditioned medium displaying macrophage-attracting activity in cell migration assays. Additionally, they showed that the activity of cytochrome c oxidase was reduced in hypertrophy (Xinxu et al. 2016). Yet another group, challenged the 3T3-L1 adipocytes with saturated (palmitic and stearic) and monosaturated (oleic) FFAs, which resulted in adipocyte hypertrophy in time and dose dependant manner. Moreover, they found that oleic acid did not cause the induction of the inflammatory responses in adipocytes as the saturated palmitic acid. Regardless the treatment, hypertrophic adipocytes exhibit attenuation in insulin-dependent glucose uptake, with Akt and Irs-1 phosphorylation being unchanged between the treatment and the control groups. Insulin dependent Glut4 translocation to the plasma membrane was decreased in hypertrophic adipocytes (J. I. Kim et al. 2015).

In addition, a study from 2012 provided evidence that adipose hypertrophy results in lysosomal destabilization and the activation of the lysosomal cysteine protease, cathepsin B (Ctsb) in the cytosol (Gornicka et al. 2012). Similarly, to a previous group, they used the 3T3-L1 adipocyte model and only saturated FAs (palmitic and stearic) for up to 18 h for the induction of hypertrophy. It has been reported that individual FFAs have a distinct toxic potential, with palmitate alone being highly toxic to hepatocytes, when compared to oleic and that the combination of both FFAs, with a low proportion of palmitic acid, result in maximal fat accumulation and minimal cytotoxic effect (Gómez-Lechón et al. 2007). Having that in mind, we tested different concentration of oleic and palmitic acids alone, as well as the combination of both, and we found that the ratio of 2:1 of oleic and palmitic acid at a final concentration of 1 mM was most appropriate for our study (data not shown). To avoid contamination from FFAs in our EV preparations, mature 3T3-L1 adipocytes were exposed to FFA mix for 24 h for the induction of hypertrophy, following the replenishment of fresh, EV-depleted medium for the production of EVs.

The visualization of EVs by EM-techniques and the size and concentration analysis are often the first steps into a more detailed characterization of isolated EVs from different sources. We found that under hypertrophic conditions, adipocytes released more particles as compared to basal conditions. This phenomenon is widely accepted in EVs research field that under stressed conditions, cells secrete overall more EVs. It is clear, from the WB analysis, that hypertrophy in adipocytes induce the release of a distinct population of EVs, exhibiting striking differences in protein abundance of EV-specific markers. One possible explanation of this result could be obtained from the existence of a heterogeneous population of MVBs (Simons & Raposo 2009). The authors reasoned that there must be at least two classes of MVBs, one that fuses with the lysosome and another, which fuses with the plasma membrane to release exosomes (Simons & Raposo 2009). Moreover, it seems obvious to think that that there is a transfer or exchange of material between the different cellular compartments involved in vesicular transport, which would explain the presence

of late endosomal/lysosomal markers in our preparations. Our results could suggest alteration of the composition of MVBs and in the intracellular vesicular trafficking.

Unexpectedly, minor changes were observed in NTA distribution analysis and clear difference in abundance of EV markers by WB, such as an increase in Cd81 in EVs secreted by hypertrophic cells. It is important to highlight that we focused on the characterization of small vesicles, thus under our conditions we cannot study the possible difference caused in larger vesicles. In addition, it is important to have into account that NTA has some limitations in terms of determining purity of the samples, considering, for example, protein aggregates and lipoproteins (Boing et al. 2014) which may contribute to the final EV concentration.

Regulation by EVs has been widely implicated in adipose tissue development and homeostasis (Lakhter & Sims 2015). Adipocyte-EVs have been well studied, during pre- and post-adipogenesis (Connolly et al. 2015), in hypoxia (Sano et al. 2014), identified as mediators of macrophage-induced insulin resistance (Deng et al. 2009). Moreover, exosomes from visceral adipose tissue of obese individuals induced deregulation of the transforming growth factor ß (TGF-ß) pathway in HepG2 and hepatic stellate cell line (Koeck et al. 2014).

Flotillins are highly conserved proteins involved in many cellular processed such as signal transduction, cell adhesion, and cellular trafficking. They are post-translationally modified by fatty acid acylation (a single palmitate in flotillin-1) and form hetero-oligomers constitutively associated with cholesterol- and sphingolipids-enriched microdomains (Meister & Tikkanen 2014). Reversible palmitoylation on Cys residues was suggested as a means of recruitment or exclusion of proteins from lipid microdomains, with a single palmitoylation not being sufficient for protein recruitment to rafts (Levental et al. 2010). Upon differentiation of 3T3-L1 adipocytes, flotillin-1 from a cytoplasmic compartment to the plasma membrane (Liu et al. 2005). It is important to mention this fact, as we detected Flotillin1 protein, as a double band in our adipocytes and one in their

corresponding EVs. Interestingly, Flotillin-1 was more abundant in hypertrophic adipocytes and their secreted EVs, as compared to control adipocytes. Lipid rafts have been strongly implicated in the endocytic process, endosomal trafficking and cargo sorting (Meister & Tikkanen 2014). Glebov *et al.* found increased amounts of flotillin-1 in early endocytic vesicles with no co- localization with clathrin, and proposed the existence of the flotillin-1 mediated clathrin-independent endocytic pathway (Glebov et al. 2006). We observed not only higher Flotillin-1 accumulation in hypertrophic adipocytes but also in their secreted-EVs, which could indicate the possible enrichment of vesicles, which production is mediated by Flotillin1-mediated endocytic pathway.

Interestingly, increased abundance of lysosomal protein, LimpII in hypertrophic-EVs is very clear, however, in cells, LimpII does not seem to be affected. The enrichment in LimpII in secreted-EVs could be related with lysosomal permeability was seen in adipose hypertrophy, which could contribute to the lysosomal-marker enrichment in hypertrophic-EVs.

Genes involved in all aspects of lysosome biogenesis and function are upregulated with insulin resistance and obesity (Xu et al. 2013) translated as increased expression of lysosomal proteins. Excess lipid supply largely impair lysosomal function as observed in diet-induced obesity and metabolic disorders (Jaishy & Abel 2016).

The absence of Hsp70 in EVs secreted by adipocytes was somewhat a surprise, as it is considered one of the principal makers of EVs. One possibility for not detecting its expression is that as the 24 h media containing FFAs for the induction of hypertrophy is removed, a population of EVs could be lost there and not replenished in the following 48 h. In one study it has been concluded that Hsp70 release from peripheral blood mononuclear cells (PBMCs) does not occur via raft-dependant pathway (Lancaster & Febbraio 2005), which could be the predominant secretory pathway in hypertrophic adipocytes.

The understanding of molecular events occurring in hypertrophic adipocytes is important to understand changes seen in their secreted-EVs. The use of primary adipocytes would be ideal, however, there are various technical drawbacks such as their fragility, purity, due to possible contamination from stromal vascular cells and macrophages, and therefore separating pure population would not be feasible (J. I. Kim et al. 2015).

Whole-animal studies have been very useful in deciphering the metabolic abnormalities associated with insulin resistance, however when studying molecular mechanisms, cell culture conditions have been extensively used, mostly in assessing insulin-receptor-coupled processes (Knutson & Balba 2012). Insulin resistance can be induced in cultured adipocytes by a variety of treatments, however, it remains unknown what aspects of the *in vivo* responses are covered by these models and how closely they resemble the situation *in vivo* (Lo et al. 2014). The 3T3-L1 cell line has been widely used to study insulin resistance in adipocytes, following an induction with Tnf, IL-6, IL-1, FFAs, high insulin, hypoxia, DEX, among others. It was found that different *in vitro* models capture distinct features of adipose insulin resistance. Researchers concluded that the combination treatment with Tnf and hypoxia caused the downregulation of many glucose, lipid and amino acid metabolic pathways observed *in vivo*, more than any individual treatment (Lo et al. 2014). The existence of hypoxic areas within adipose tissue was assessed in *ob/ob* obese mice and in dietary-induced obese mice, by immunihistochemistry, use of 0_2 sensors and lactate detection (Regazzetti et al. 2009).

In our study, we also used the 3T3-L1 adipocytes and cultured them in hypoxia (1% 0_2) or with macrophage conditioned medium (MØ) for the induction of insulin resistance phenotype. We observed marked decrease in insulin stimulated-Akt phosphorylation in MØ-adipocytes with no change in Erk1/2 phosphorylation, and surprisingly a slight increase in adipocytes cultured in hypoxia. One study has investigated the impact of transient (2-4 h) hypoxia on differentiated 3T3-L1 adipocytes and they found an increase in insulin-dependant and independent

glucose uptake and on differentiating adipocytes what caused the enhanced insulin sensitivity (Brown et al. 2016).

Our findings do not agree completely with published data. In 2009 it was reported that hypoxia creates a state of insulin resistance in adipocytes by inhibiting phosphorylation of the insulin receptor tyrosine, leading to a decrease in glucose transport. Moreover, it was found to be dependent upon hypoxia-inducible factor 1 and 2 (HIF) transcription factor expression (Regazzetti et al. 2009). Studies on hypoxic cancer cells have shown enhanced exosome secretion accompanied by an increase in typical protein markers associated with exosomes, CD81 and CD63 (L. Li et al. 2016; Rong et al. 2016). Our results indicate that the pathological state of hypoxia or co-culture with macrophage-conditioned medium inhibit the secretion of certain subpopulations of EVs or other secretory pathways are activated. A recent paper demonstrated the existence at least two distinct populations of EVs secreted by 3T3-L1 adipocytes, termed the small and the large EVs. They carry a very distinct protein and lipid profile (Durcin et al. 2017a). They found that the typical proteins associated with exosomes such as ALIX, TSG101, and tetraspanins CD9, CD63 and CD81, were significantly less abundant in larger EVs, with CD9 and CD81 being barely detectable (Durcin et al. 2017a). This could mean that in our experimental conditions of adipocytes cultured in hypoxia as well as in the presence of macrophage-conditioned medium, we are enriching in larger EVs as opposed to exosomes, indicated by a decrease in expression of Cd81 protein. Interestingly, by means of proteomic analysis, they were able to identify proteins specifically associated to larger EVs such as aP2/Fabp4, AnnexinA2, and Endoplasmin, and with smaller EVs Adiponectin and Fas (Durcin et al. 2017b). Moreover, they saw an enhanced secretion of both populations induced by stimuli related to the chronic low-grade inflammation state of obesity such as FFAs and TNF. The difference in results is most probably related to modifications in experimental settings such as the purification of EVs, which might have profound effect on the population of EVs isolated.

Lastly, in this part we investigated the biological impact of EVs secreted by stressed adipocytes on the insulin sensitivity and specifically tested the hypothesis that these EVs could contribute to the development of the insulin resistance, a hallmark of adipose dysfunction seen in pathological states such as obesity and T2DM. We found that hypoxic-EVs negatively impact on insulin-stimulated glucose uptake in 3T3-L1 adipocytes and our results indicate that it could be in part by inhibiting their Ser473 Akt phosphorylation. The uptake was restored upon heating up the hypoxic-EVs before treatment, with the intact EV structure. This could be an indication that the effect on glucose uptake is mediated by membrane associated proteins that are denatured by heat, or by heating we inhibited the actual EV upake in recipient cell and thus suppressing the negative effect over insulin signalling in 3T3-L1 adipocytes. In addition, several other molecular mechanisms could contribute to the inhibition of insulin signalling in recipient adipocytes such as the altered secretion of adipokines, which act in both autocrine and paracrine fashion. Thus, it cannot be discarded that adipose-EVs affect insulin signalling indirectly through an adipokine mediated mechanism. Moreover, a tumour suppressor protein, normally localized in the cytoplasm and nucleus is also a natural inhibitor of the PI3K/Akt pathway was described to be associated with exosomes (Putz et al. 2012). In addition, it was shown that PTEN was internalised by recipient cells and exerted functional activity over the Akt phosphorylation. We have seen that our EVs secreted by 3T3-L1 adipocytes carry associated PTEN and interestingly more PTEN was secreted in hypoxic-EVs as compared to the control, with the simultaneous reduction in protein abundance in parental cells (data not shown). Thus, it is plausible that PTEN may be in an active form in our EVs and as significantly more is being excreted by hypoxic cells, those EVs will exert more profound inhibitory effects on the Akt(Ser473) phosphorylation in recipient 3T3-L1 adipocytes. However, further studies are needed to reveal the exact mechanism behind the inhibition in our system.

Most of studies, which used the macrophage-conditioned medium co-culture with adipocytes, focused on its antiadipogenic effect. Medium conditioned by

macrophages inhibits adipogenesis of murine 3T3-L1 cells and primary human preadipocytes in dose-dependent fashion (Constant et al. 2006) and that the anti-adipogenic effect was associated with inhibition of cyclin-dependant kinase 2 activation, one of the key upstream kinases that phosphorylates retinoblastoma protein (Rb) binding transcription factors driving adipogenesis (Ide et al. 2011). Moreover, yet another study concluded that macrophage-secreted factors induced a major inflammatory response in human adipocytes with strong upregulation of inflammation-related genes, matrix metalloproteinase (MPP) family members. Additionally, they showed that the effect was mediated by the proinflammatory cytokine TNFα (O'Hara et al. 2009)

Likely, there are other subgroups of EVs based on the mechanism of secretion and on their content, as it has already been shown that cellular activation can alter the dynamics of exosomes release by increasing the release of specific populations of vesicles (Willms et al. 2016). Still, a generally accepted fact is that three distinct populations of EVs exist such as, exosomes, microvesicles and apoptotic bodies. However, it has recently been identified that as thought homogenous population of exosomes, there are at least two distinct subpopulations based on the difference in densities (Willms et al. 2016). Interestingly, typical exosomal markers were identified in both, low (fractions 3-5) and high (fractions 8-9) -density exosomes such as ALIX and TSG101, but with significantly lower relative abundance in low-density exosomes. Both populations were formed through a ceramide-dependant pathway, as assessed by nSMase inhibition. The mean size difference is probably responsible for the difference in density with HD-Exo (66 nm) and LD-Exo (117 nm). Our results indicate that hypoxia has an influence on the secretion of EVs by 3T3-L1 adipocytes as observed by the expression of Cd81 marker in EVs but also in parent cells.

It has been shown that cargo of EVs is actively sorted, as the level of a given molecule can be very different in EVs and in the parent cell, which indicates their specific physiological roles (Yáñez-Mó et al. 2015). EVs can serve to remove unwanted material from a parent cell such as missfolded soluble proteins, which

were found to be released in EVs (Bellingham et al. 2015). The first example being the process of maturation of the transferrin receptor (Johnstone et al. 1991).

Evidence are beginning to accumulate in support of the hypothesis that the release of EVs often serves as an alternative disposal pathway, with an active role of the lysosome in the secretion of EVs and sorting of their cargo. The exact mechanism remains unknown as to how MVBs are directed to the plasma membrane or to the lysosome, however, it has been shown that the inhibition of the lysosome increases EV secretion (Eitan et al. 2016).

Theories that could be explored as to the differences in EV-related proteins in stress conditions could be the activation of an alternative disposal pathway under conditions of oxidative stress when endosomal machinery is overloaded. On the other hand, the unspecific expulsion of EVs in increased concentration, which is specifically modified under these stress-inducing conditions. The evidence of alternative usage of endosomal-lysosomal pathway came from studies of neurodegenerative diseases where researches have shown that causative agents such as self-aggregated proteins are secreted in EVs (Bellingham et al. 2015).

Interestingly, we found Glut4 to be associated with adipocyte-EVs, secreted by adipocytes not previously stimulated with insulin. Moreover, the protein abundance was slightly higher in EVs secreted by adipocytes cultured in hypoxia as well as when cultured with the macrophage conditioned medium. Glut4 is an insulin-regulated glucose transporter in fat and muscle cells. In the absence of insulin, the majority of Glut4 is stored in small (50-70 nm) intracellular vesicles, Glut4 storage vesicles (GSVs) as well as in larger structures derived from endosomes or sub-compartments of the trans-Golgi network (TGN) (Stöckli et al. 2011). The possible existence of the separate Glut4 storage compartment was proposed previously (Hashiramoto & James 2000). The group has proposed that in the insulin-sensitive cells, there may be a unique Glut4-containing vesicular population derived of the endosomes which exhibit little insulin responsiveness

(Hashiramoto & James 2000). Our results would indicate that in the population of EVs isolated from conditioned medium of adipocytes, there is an enrichment of Glut4 containing-EVs and their secretion increases in pathological conditions.

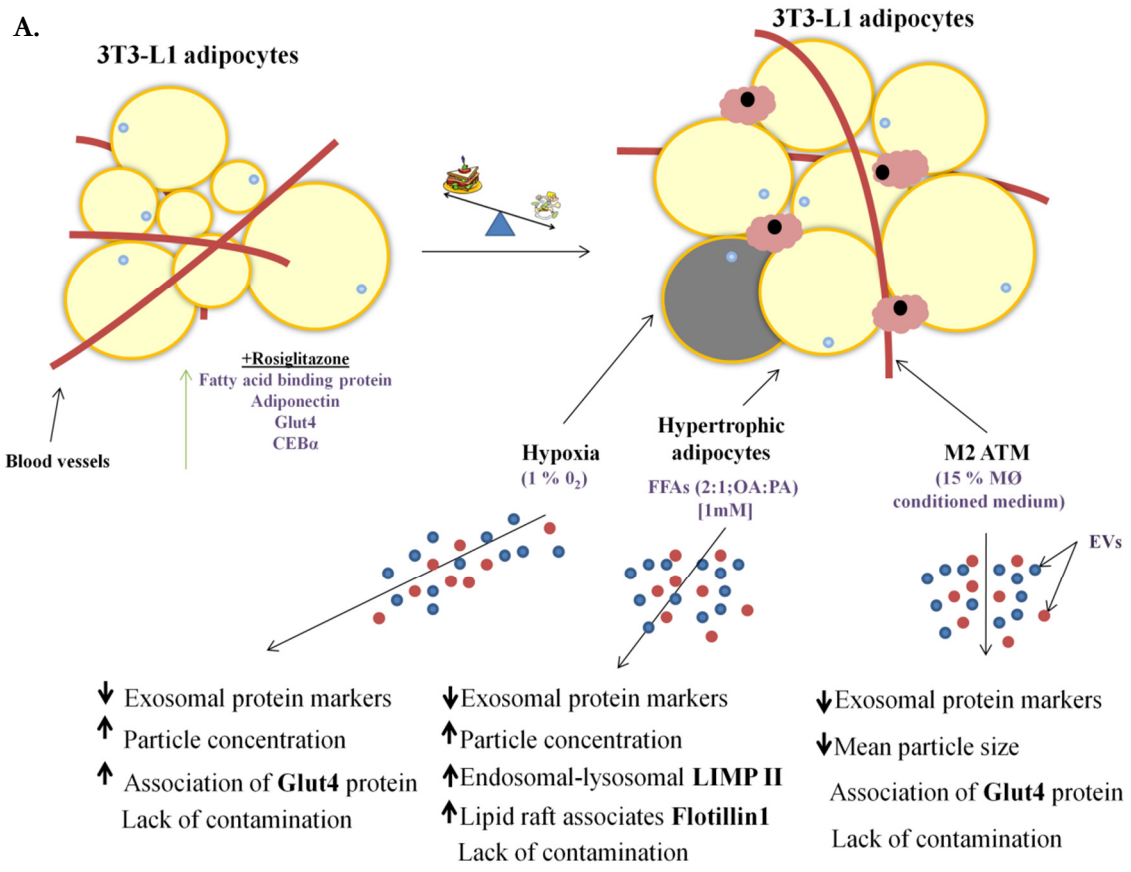

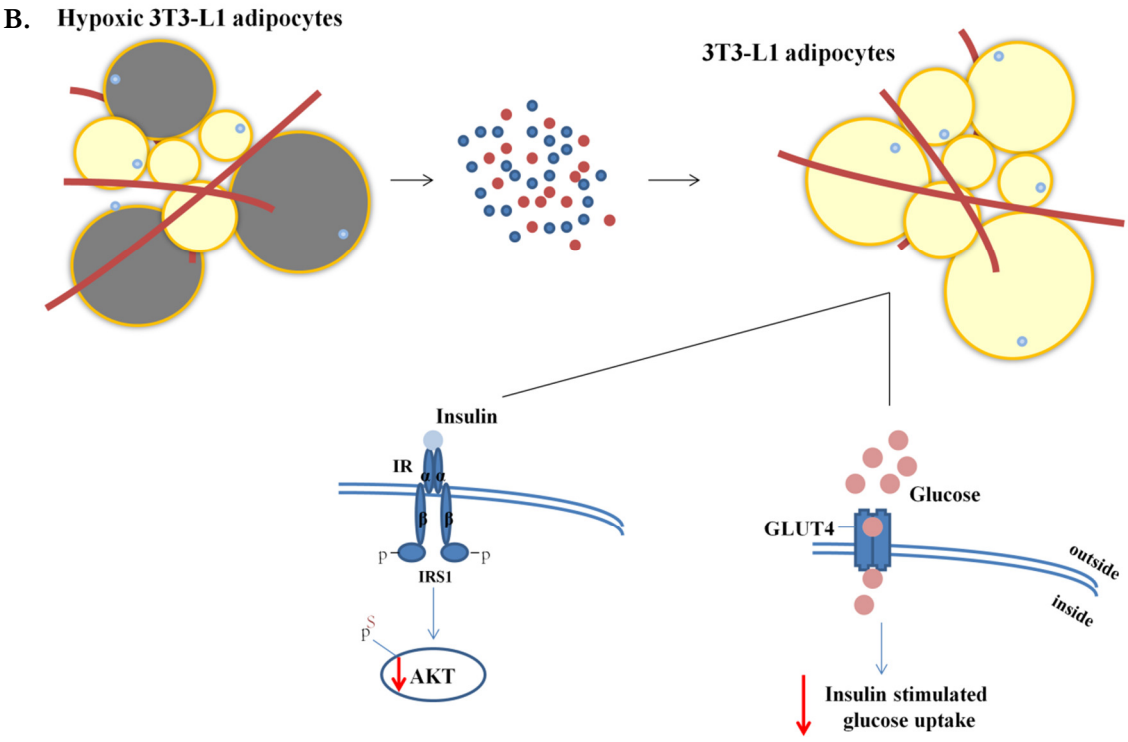

Figure 20 Summary diagram of results described in chapter 1. Graphical representation of results regarding **(A)** the characterization of EVs obtained from *in vitro* models induced in 3T3-L1 adipocytes and **(B)** the effect of hypoxic adipose-EVs on recipient 3T3-L1 adipocytes in terms of insulin sensitivity.

RESULTS CHAPTER 2

4. Characterization of the *In Vitro* model of inflammation in Raw264.7 macrophage-like cells and the EVs secreted by them.

4.1 Chapter 2 Aims:

- Characterize the Raw264.7 macrophage-like cells following LPS activation.
- Morphological and biochemical characterization of EVs secreted by Raw264.7 macrophage-like cell under basal (EVs CTRL) and proinflammatory conditions (EVs LPS).
- Investigate a possible influence of the macrophage-EVs on bioenergetics and insulin sensitivity of the 3T3-L1 adipocytes.

4.2 Introduction

Inflammation is a feature of many pathologies, including MetS, which is manifested as an infiltration of AT by macrophages that causes an enhancement in the secretion of proinflammatory cytokines from AT. In addition, EVs from adipose tissue have been shown to contribute to the development of inflammation and insulin resistance associated with obesity and MetS via interaction with healthy adipocytes and peripheral organs (Lakhter & Sims 2015).

Our aim was to isolate EVs secreted by proinflammatory macrophages activated with LPS, as an *in vitro* model of AT-infiltrating macrophages. That could allow the distinction between the population of EVs secreted by affected adipocytes

from the population of EVs secreted by infiltrating macrophages and their contribution to the effect that AT-EVs produce peripherally in the context of MetS.

The results presented in this chapter include a characterization of Raw264.7 macrophage-like cells following the activation with LPS followed by detailed biochemical characterization of EVs secreted by macrophages in basal state as well as following LPS activation, and lastly effects of macrophage-EVs on mitochondrial functions and insulin sensitivity of 3T3-L1 adipocytes.

4.3 Results

4.3.1 Induction of the Proinflammatory Phenotype in Raw264.7 Macrophages

Bacterial lipopolysaccharide (LPS), the major structural component of the outer wall of Gram-negative bacteria (Fujihara et al. 2003) was used for the induction of the proinflammatory phenotype in Raw264.7 macrophage-like cells. Upon stimulation with LPS, macrophages secrete cytokines, including TNF, IL-6 and IL-1ß, among others, that activate the inflammatory responses (Rutledge et al. 2012; Soromou et al. 2012).

The ultimate objective was to isolate EVs from the conditioned medium of macrophages at a basal state as well as upon LPS activation. Therefore, when setting up the experimental conditions the contamination with LPS-derived EVs as well as secondary effects for downstream experiments had to be considered. Briefly, the proinflammatory phenotype in Raw264.7 cells were induced with LPS (100 nM) in complete DMEM for 6 h, followed by three washes with 1X D-PBS, and the addition of fresh, EV-depleted medium to produce EVs, for another 48-72h.

First, the activation in Raw264.7 macrophage-like cells was confirmed by morphological analysis using Phalloidin that selectively binds to F-actin filaments and allows observing actin cytoskeleton remodeling. Reorganization of the actin cytoskeleton can be appreciated in Raw264.7 cells stimulated with LPS **(Figure 21A).** On a biochemical level, the secretion of Tnf, following LPS stimulation, was measured by ELISA that reveals a significant increase in the concentration of Tnf secreted by LPS-stimulated macrophages at 6 h **(Figure 21B)**. Although, slightly decreased, the levels of secreted Tnf stays elevated at 72 h, meaning that the pro-inflammatory phenotype is maintained even without constant LPS stimulation **(Figure 21B).**

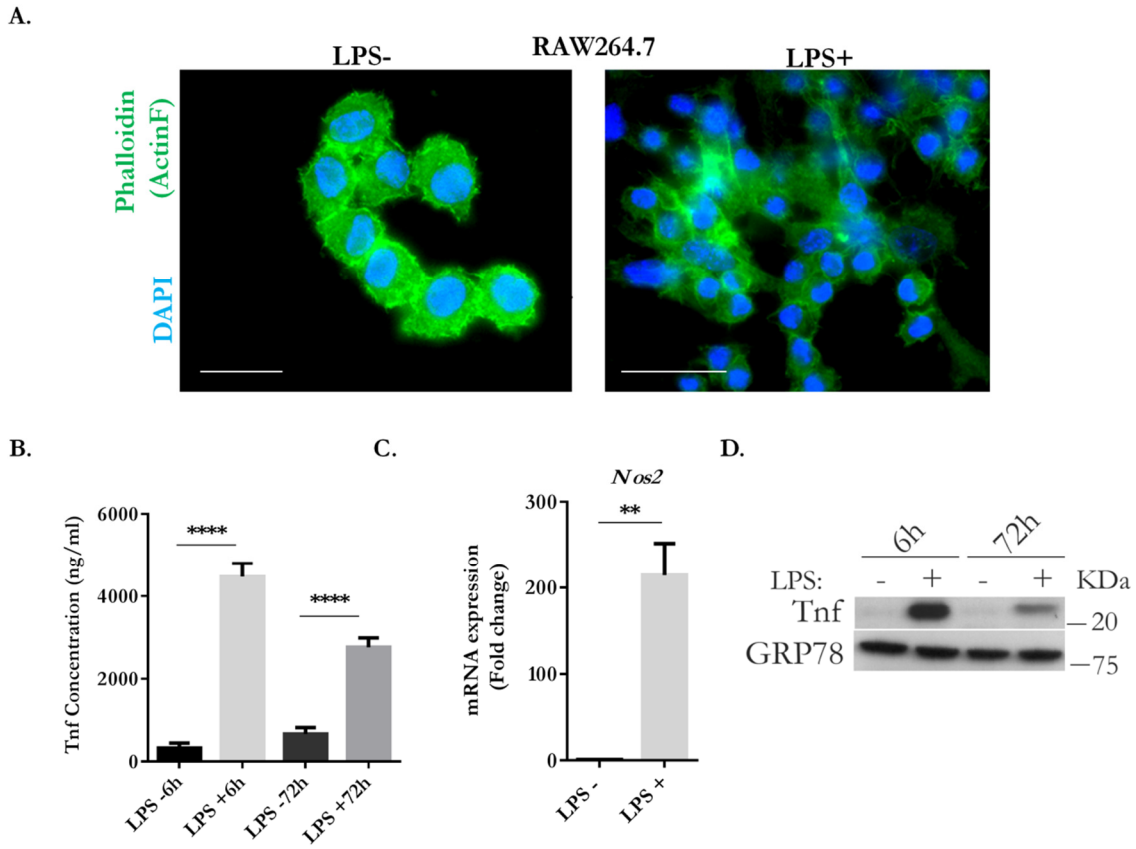

<u>Figure 21</u> LPS induces proinflammatory phenotype in Raw264.7 macrophages. 6h of exposure to LPS induces a proinflammatory phenotype in Raw264.7 macrophages **(A)** Phalloidin immunostained Raw264.7 macrophages with and without LPS, bar=20μm **(B)**

LPS stimulated cells had increased Tnf secretion as measured by ELISA; biological replicates=3, technical replicates=3. **(C)** LPS induced *Nos2* mRNA expression in Raw264.7 macrophages; n=3; error bars=SD *p* values were denoted as follows: 0.01- 0.05=*, 0.01-0.001=**, 0.001-0.0001=*** and p value< 0.0001=**** **(D)** Western immunoblot for Tnf expression in Raw264.7 macrophages at 6 and 72h. Unpaired student t-test was performed to determine significant differences.

Similar results can be observed by WB analysis **(Figure 21D)**. Together with the induction of Tnf, macrophages also secrete nitric oxide (NO) (Reis et al. 2011). Inducible nitric oxide synthase encoded by *Nos2 gene* is one of the main enzymes catalyzing the generation of NO (Lirk et al. 2002). We therefore measured the mRNA expression level of *Nos2* in stimulated macrophages and found a 200-fold increase in expression at 6 h as compared to untreated cells **(Figure 21C)**. The results indicate that the proinflammatory phenotype is maintained even without the constant exposure to LPS. Thus, this culture and activation conditions are valid for producing EVs of activated macrophages without being contaminating with LPS.

4.3.2 Characterization of isolated EVs

First, in order to justify our experimental design, we isolated EVs from the cell culture medium (EV depleted) containing LPS (100 nM) only, that we incubated for 48h at 37^0C in the absence of cells. The isolated EVs were analysed by Cryo-EM **(Figure 22A)** and size distribution profile was established by NTA **(Figure 22B)**. The analysis has revealed the presence of membrane-bound vesicles of a mean particle size of 208nm (SD=17.0) and concentration $3.5x10^8$/mL (SD=0.16). It can be observed that structurally LPS isolated EVs resemble EVs secreted by cells, therefore we concluded that in fact, LPS could greatly influence the accuracy of EVs characterization if not removed.

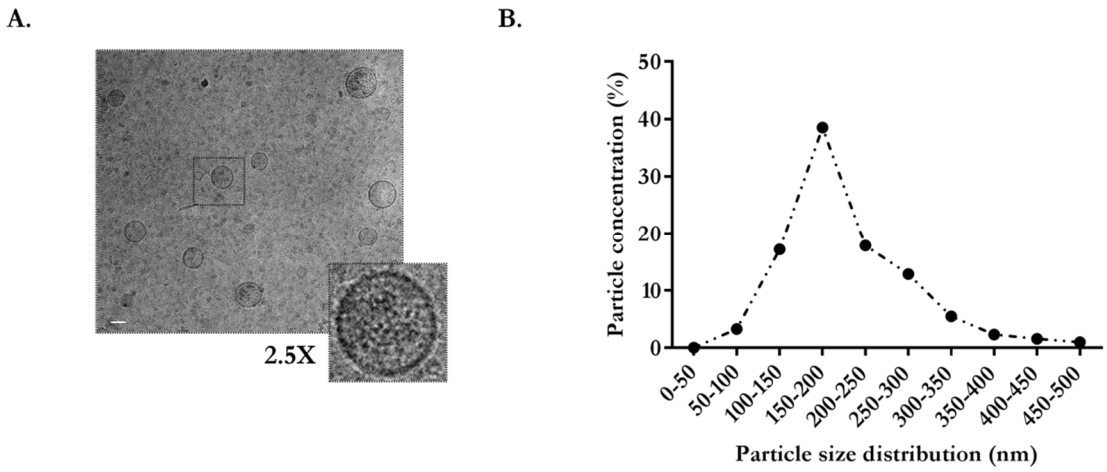

Figure 22 Vesicles isolated from EV-depleted LPS-containing medium. Analysis of the material isolated by using the conventional EV isolation produce from EV-depleted LPS-containing medium incubated in the absence of cells during 48h at 37^0C. Note the presence of vesicles resembling EVs. **(A)** Cryo-EM analysis, bar = 100nm, inset magnified 2.5X. **(B)** Size range distribution by NTA; n=3. Error bar s= SD.

Cryo-EM analysis of EVs isolated from Raw264.7 macrophages at basal conditions **(EVs CTRL)** and following the stimulated with LPS **(EVs LPS)**, revealed the presence of a heterogeneous population of membrane-bound vesicles of different sizes. Representative electron micrographs are shown in **Figure 23A**. Raw264.7 macrophage-like cells were found to release a significant amount of EVs in both conditions. The size distribution of the distinct population of vesicles did not change significantly with the LPS treatment as revealed by NTA **(Figure 23B).** In the LPS treated group, there was an enrichment in larger vesicles as judged by the tiny shift of the curve towards the right. Moreover, a 5% decrease was observed in concentration size of the sub-population between 50-100 nm **(Figure 23B)**.

However, considering the total concentration of particles there was a significant decrease in the amount secreted by LPS-treated cells **(Figure 23C)** with no change in mean particle size **(Figure 23D)**. WB was performed to compare the abundance of some well-known EV markers as well as cell specific proteins selectively packaged in EVs and excreted into the extracellular space. **Figure 23E** shows results from two independent preparations of EVs isolated from LPS stimulated Raw264.7 macrophages with their corresponding untreated controls. We found that potent proinflammatory cytokine, Tnf was shuttled out in EVs secreted by LPS-activated macrophages. In terms of specific EV-related markers, the endosomal machinery specific, Aip1/Alix and Tsg101 was barely detectable in EVs LPS as opposed to EVs CTRL. In cells, on the other hand, Aip1/Alix was equally abundant in both conditions as well as the tetraspanin Cd63. The decrease in Tsg101 expression in proimflammatory macrophages, with respect to the control macrophages, was mirrored in their corresponding EVs. Along the same line, expression of the adapter protein Syntenin1, which forms a complex with Syntaxin and Alix, necessary for exosome secretion, was abundant in EVs CTRL and has not been detected in EVs isolated from LPS-treated cells **(Figure 23E)**.

On the contrary, macrophage-EVs were found to be rich in lysosomal glycoprotein, LimpII, which is naturally located in both, late endosomes (often restricted to the limiting membranes) and lysosomes. The expression profile of the LimpII protein in cells **(Figure 23E)** indicates that the proinflammatory macrophages contain slightly more LimpII, which is not reflected in their secreted-EVs, as EVs LPS contain reduced LimpII protein. In the support of this result, the expression of another late endosome and lysosomal marker, Lamp1 protein was also significantly decreased in EVs LPS. Moreover, cellular abundance of one of the major cytosolic chaperons, Hsp70 was variable in cellular lysates, whereas in their corresponding EVs there was a clear reduction in EVs LPS. In addition, Hsp70 associated to EVs LPS, was post-translationally modified, as seen by the appearance of the double band **(Figure 23E)**.

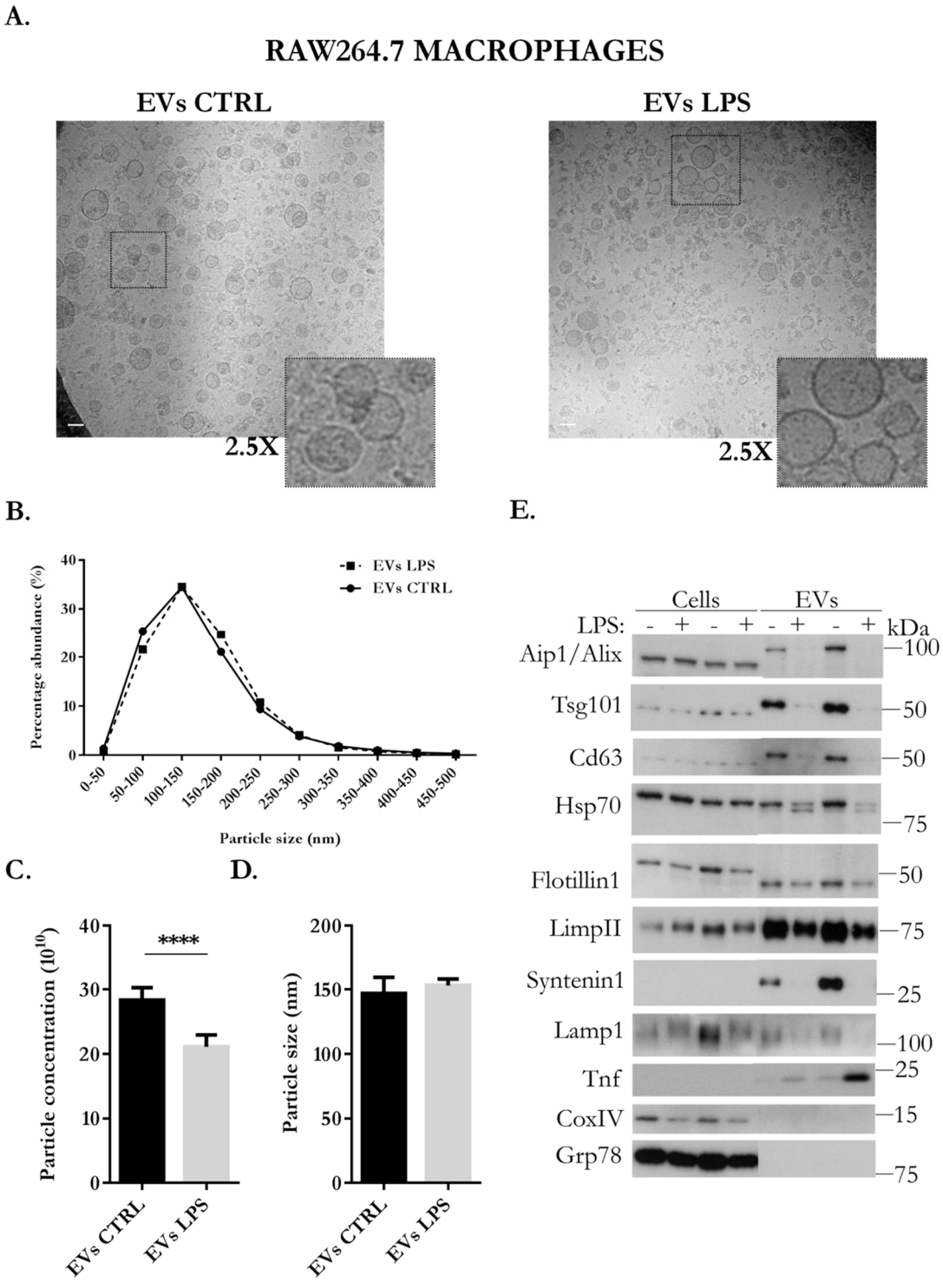

Figure 23 Characterization of EVs released by proinflammatory Raw264.7 macrophages. Ultrastructural and biochemical characterization of EVs isolated from conditioned medium of Raw264.7 macrophages at a basal state and following the exposure

to LPS. **(A)** Cryo-EM analysis, bar=100nm, inserts magnified 2.5X **(B)** Size range distribution. **(C)** Particle concentration (10^{10}). **(D)** Particle mean size; n=3. **(E)** Protein extracts from two independent preparations of EVs (5 μg) together with their corresponding cell lysate (10 μg) were analyzed by WB, with antibodies for EV as well as cellular markers; n=4; representative figure. Unpaired student t-test was performed to determine significant differences. Error bars = SD.

Furthermore, EVs LPS exhibit reduction in amount of Flotillin1 protein. Flotillin1 appears at a different molecular weight as compared to their corresponding cellular lysates, as it was the case of the Aip1, Cd63 and Tsg101 proteins. Lastly, immunoblotting of mitochondrial and ER proteins, CoxIV and Grp78 respectively was performed for quality control. As can be observed, both, CoxIV and Grp78 were readily detectable in the whole cell lysates and were completely absent in the EV samples indicating that the EV preparations were not contaminated with cellular compartments.

Moreover, the mitochondrial functions in proinflammatory macrophage cells could have been affected, as seen by decreased expression of CoxIV. Additionally, ER was affected by LPS polarization, reflected in the decrease in Grp78 expression in proinflammatory macrophages. Our results indicate that under our conditions, activated, proinflammatory macrophages release not only significantly fewer vesicles when compared to the control, but also with the abundance of protein markers specific to EVs being significantly affected.

Once having done the characterization of the macrophage derived-EVs, we progressed to the subsequent aim, which was to shed a light onto a possible effect of these EVs on the 3T3-L1 adipocytes. For that purpose, we isolated and characterized the protein content of another set of macrophages derived-EVs **(Figure 24)**. The association of Tnf protein was confirmed in EVs LPS. Moreover, a significant decrease in markers of exosome biogenesis such as Tsg101 and Syntenin1 was confirmed in EVs LPS. Interestingly, we found a member of a family of small GTPases, Rab8, one of the key regulators of membrane trafficking, to be highly associated to macrophage-EVs. Interestingly, the abundance of Rab8 in LPS-activated Raw264.7 macrophages was reduced.

On the contrary, no difference in EVs was found in the abundance of Rab8 protein when comparing both groups. Finally, the lack of organelle contamination can be deduced from the association of Grp78 solely to macrophage lysates and not to their secreted-EVs.

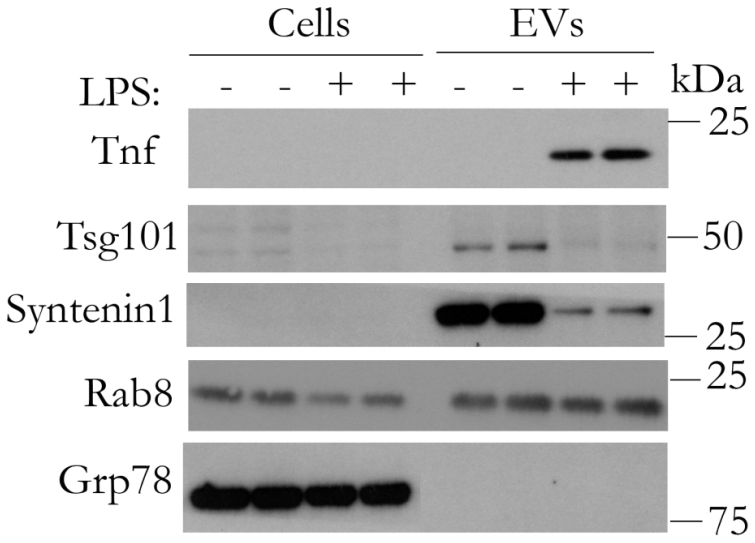

Figure 24 Raw264.7 macrophage-like cells activated with LPS secrete EVs with the proinflammatory phenotype. Protein extracts from two independent preparation of EVs (5 μg) together with their corresponding cell lysates (5 μg) were analyzed by WB, with antibodies for EV as well as cellular markers; n=2.

4.3.3 The effect of the macrophage-secreted EVs on mitochondrial and glycolytic function of the 3T3-L1 adipocytes

The inflammatory effect of macrophage-secreted EVs on adipose tissue has already been shown (Zhang et al. 2015). The reciprocal relationship of adipose-tissue EVs on the activation of blood monocytes has also been reported (Deng et al. 2009). However, we sought to find out whether EVs LPS had any effect on the bioenergetics of the 3T3-L1 adipocytes. A Seahorse FX analyzer was employed to analyze the mitochondrial and glycolysis function on 3T3-L1 adipocytes upon exposure to EVs LPS **(Section.2.2.3.3)**. For that, cells were treated with 10 µg of EVs per well, in EV-depleted medium, for 24 h. The general scheme of mitochondrial stress test is shown in **Figure 25A**. For this experiment, 3T3-L1 fibroblast cells were differentiated into mature adipocytes on Seahorse V7 microplates and were treated on the day 13 of the differentiation. As previously mentioned, during the experiment, serial injection of oligomycin, FCCP and rotenone allow establishing the profile of mitochondrial function of assayed cells. For the mitochondrial stress test, various parameters were measured such as non-mitochondrial respiration, proton leak, basal respiration, ATP production, maximal respiration and spare capacity in receiving adipocytes **(Figure 25B-25G)**.

Our results indicate that upon exposure to macrophage-secreted EVs, at the basal level there was no difference in mitochondrial respiration between the treated cells and the control group **(Figure 25C)**. A slight increase in non-mitochondrial respiration was observed in adipocytes treated with macrophage-derived EVs **(Figure 25B)**. Moreover, a significant reduction was seen in ATP production, maximal respiration and spare capacity in cells treated with EVs LPS **(Figure 25E-25G)**. This difference was specific to the subset of EVs secreted by proinflammatory macrophages, as the EVs CTRL did not have any effect on mitochondrial functions of the 3T3-L1 adipocytes.These results could indicate that the limited OXPHOS capacity reported in white adipocytes of the high fat

diet murine obesity models (Schöttl et al. 2015), might be mediated via pro-inflammatory EVs.

In terms of glycolysis, a figure representative of three independent experiments and normalized to the untreated sample is shown in **Figure 25H**. Individual parameters, non-glycolytic acidification, glycolysis, glycolytic capacity and glycolytic reserve are plotted. Slight increasing trend can be seen in glycolysis and glycolytic capacity in adipocytes treated with EVs secreted by the pro-inflammatory adipocytes. No changes were observed in other glycolytic parameters **(Figure 25H)**. Our results indicate that adipocytes exposed to EVs LPS reduce the capacity to maximal respiratory response, additionally reflected in the decrease in spare capacity. Moreover, it could be that due to slightly increased proton leak, there is a significant decrease in ATP production of the cell exposed to EVs LPS, possibly due to uncoupling of the membrane gradient potential.

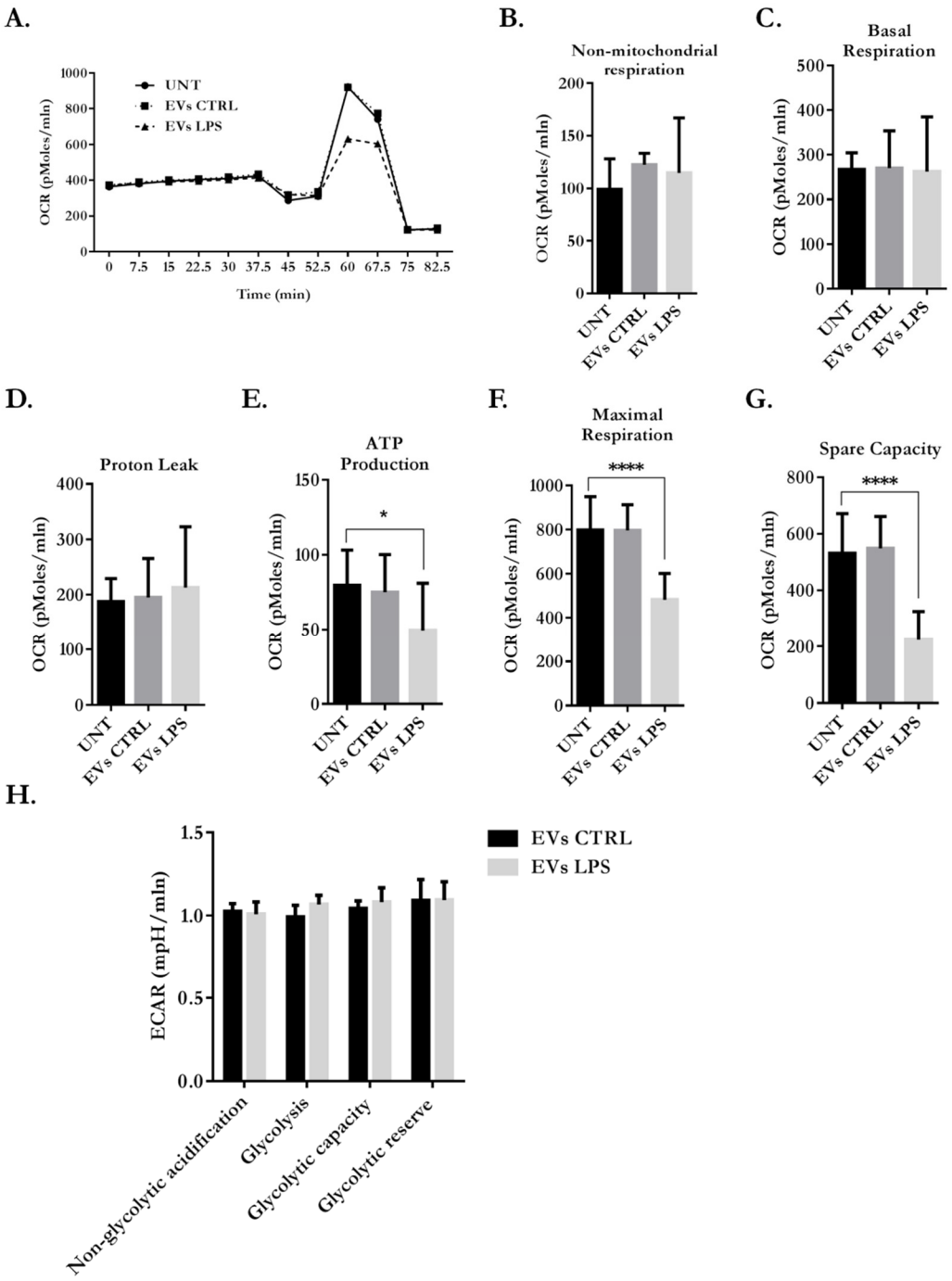

Figure 25 Bioenergetic changes in 3T3-L1 adipocytes treated with Raw264.7 macrophage-derived EVs. A Seahorse XF analyzer was used to measure mitochondrial and glycolytic functions in 3T3-L1 adipocytes treated with 10 μg of EVs CTRL and EVs LPS **(A)** A representative figure of the mitochondrial stress test with the experimental groups indicated on the graph by arrows. Individual parameters of the mitochondrial functions such as **(B)** non-mitochondrial respiration **(C)** basal respiration **(D)** proton leak **(E)** ATP production **(F)** maximal respiration **(G)** spare capacity, were plotted; biological

replicates=3, technical replicates=9 **(H)** Parameters of glycolysis function; biological replicates= 3; technical replicates=18 (per experimental group); error bars=SD *p* values were denoted as follows: 0.01- 0.05=*, 0.01-0.001=**, 0.001-0.0001=*** and p value< 0.0001=****. Unpaired student t-test was performed to determine significant differences.

4.3.4 Investigating the insulin sensitivity in 3T3-L1 adipocytes upon exposure to proinflammatory-EVs

Disturbance in insulin signalling is a hallmark of MetS and diabetes. The involvement of adipose tissue macrophages (ATMs) in altering adipocyte function, including firing inflammatory responses and decreasing insulin sensitivity has long been described as a factor sufficient for the development of adipose tissue inflammation. Recently, however, the notion that EVs could mediate the phenotypic tranfer is being explored. It has been shown that treatment with M1 macrophage-derived EVs significantly reduce insulin-stimulated Akt phosphorylation in human primary mature adipocytes and in 3T3-L1 adipocytes as compared to the M2 macrophages. This result was coupled with decreased GLUT4 translocation (Zhang et al. 2015).

To study insulin sensitivity in 3T3-L1 adipocytes upon exposure to macrophage-derived EVs two experimental groups were created: acute and chronic. In the acute group, cells were treated with 10 µg of EVs for 24 h and the chronic group that was expose to three doses of 10 µg separating each dose by 24 h. Following the treatment, adipocytes were stimulated with insulin (100 nM) and directly lysed. **Figure 26A** and **Figure 26D** show representative WB figures of acutely and chronically treated cells, respectively. We showed the phosphorylation of Akt(Ser473) and Erk1/2, with and without insulin stimulation. The percentage of phosphorylated Ser473 on Akt was quantified with relation to the total protein present, in basal and insulin-treated cells **(Figure 26B)**. Then, the fold increase

following the insulin treatment was plotted **(Figure 26C)**. The same was done for Erk1/2 phosphorylation in chronic group **(Figure 26G** and **Figure 26H).**

Our results show that 3T3-L1 adipocytes, following acute exposure to EVs CTRL, exhibit an increase in Akt(Ser473) phosphorylation when compared to untreated cells **(Figure 26B)**. Moreover, EVs LPS did not cause the same effect, they only induce a very slight increase in the percentage of Akt(Ser473) phosphorylation with the decrease in the basal level of phosphorylation. The increase in the percentage of the Akt(Ser473) phosphorylation was maintained when EVs were administered chronically **(Figure 26E)**. A small decrease in Akt phosphorylation after insulin was seen in adipocytes treated with both EVs CTRL and EVs LPS when compared to untreated **(Figure 26F)**.

Currently, research is being conducted on targeting the ERK signalling pathway as a potential treatment for insulin resistance, as it has been implicated in the development of IR associated with obesity and type 2 diabetes mellitus. Erk1/2 activity increases during the development of 3T3-L1 adipocyte hypertrophy and is elevated in adipose tissue of leptin receptor-deficient (*db/db*) mice. We therefore investigated whether Erk1/2 phosphorylation in 3T3-L1 adipocytes was affected by chronic exposure to the proinflammatory EVs. Quantification of WB bands indicates the increase in basal Erk1/2 phosphorylation in EV-treated adipocytes **(Figure 26G)**. After stimulation with insulin, Erk1/2 activity was seen and was higher in treated cells **(Figure 26H)**. Furthermore, when analyzing the fold change in Erk1/2 phosphorylation after insulin, there is a decline in Erk1/2 phosphorylation in EVs from LPS-treated adipocytes.

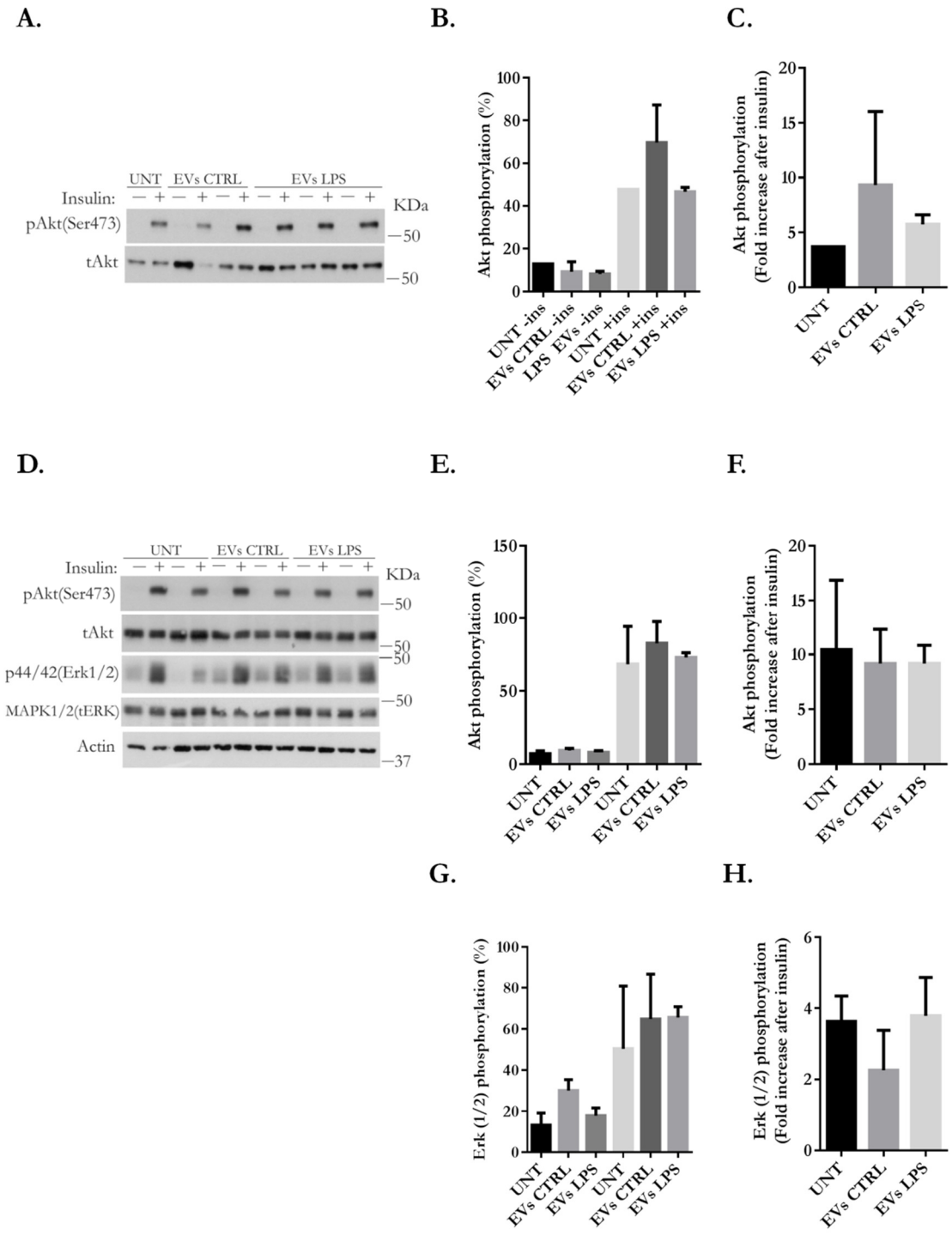

Figure 26 Insulin Sensitivity Studies in 3T3-L1 Adipocytes Upon Exposure to Raw264.7 macrophage-derived EVs (A) Representative WB for of 3T3-L1 adipocytes **acutely** exposed to macrophage-EVs (30 μg) for 24 h **(B)** Quantification of the Akt(Ser473) phosphorylation (%). **(C)** Fold increase in Akt(Ser473) phosphorylation upon insulin

stimulation. **(D)** Representative WB figure of 3T3-L1 adipocytes chronically exposed to macrophage EVs (10μgx3) 24h each dose; UNT n=1, EVs CTRL n=2, EVs LPS n=3. **(E)** Quantification of the Akt(Ser473) phosphorylation (%). **(F)** Fold increase in Akt(Ser473) phosphorylation upon insulin stimulation. **(G)** Quantification of the Erk1/2 phosphorylation (%). **(H)** Fold increase in Erk1/2 phosphorylation upon insulin stimulation; n=3. ImageJ was used for densitometry. Error bars = SD.

To summarize, EVs secreted by macrophages, both at basal and following LPS stimulation caused changes in Akt(Ser473) and Erk1/2 phosphorylation in 3T3-L1 adipocytes. It seems that acute exposure to EVs cause increase in Akt phosphorylation (higher effect is caused by CTRL-EVs). Moreover, following a chronic exposure to EVs, insulin stimulated Akt phosphorylation was decreased in 3T3-L1 adipocytes by both, CTRL and LPS-EVs. Moreover, CTRL-EVs caused marked decrease in insulin-stimulated Erk1/2 phosphorylation.

4.4 Summary

We conclude that Raw264.7 macrophage-like cells stimulated with LPS are a viable model to study cellular inflammation, as seen by the secretion of the Tnf and the expression of *Nos2*. Moreover, our protocol is appropriate for the subsequent isolation of EVs from the conditioned medium of macrophages, with minimal contamination of cellular organelles and LPS.

The overall concentration of EVs secreted by activated Raw264.7 macrophages is significantly reduced. In addition, Raw264.7 macrophage-like cells at a basal state and previously activated with LPS, secrete a very distinct population of EVs, as seen by the abundance of EV-related proteins. All of them, including Aip1/Alia and Syntenin1, related with exosome biogenesis, as well as lysosomal

protein LimpII, are significantly downregulated in EVs LPS. Hsp70 protein was found to be post-translationally modified in EVs LPS as compared to EVs CTRL.

Interestingly, macrophages previously activated with LPS, were found to have markers of mitochondrial and ER decreased.

In terms of the functional effects mediated by macrophage derived-EVs, we observed that they cause a significant reduction in mitochondrial functions as well as modification of insulin sensitivity in 3T3-L1 adipocytes.

Finally, we identified the presence of the proinflammatory, Tnf protein, in EVs LPS, which was absent in EVs CTRL. The association of the potent mediator of pro-inflammatory responses could be a possible mediator of the effects observed in 3T3-L1 adipocytes Graphically represented in **Figure 27**.

4.5 Discussion

Raw264.7 cell line has been widely used in the study of macrophage cellular physiology due to its resemblance to primary macrophages (Maurya et al. 2013). Considering that FFAs are elevated in obesity and activate macrophages via Toll-like receptor-4 (TLR4), in our model we used LPS, the TLR4 ligand to obtain M1, proinflammatory phenotype in Raw264.7 macrophages.

Macrophage derived-exosomes were previously described in the context of the complex regional pain syndrome (CRPS) (McDonald et al. 2014). Mouse macrophage cells stimulated with LPS secreted EVs that contained elevated levels of cytokines and miRNAs, and were able to mediate inflammation by activating the NF-κB pathway in naïve macrophages. Furthermore, their results suggested that activated macrophages secrete exosomes that are primed to signal an immune response to recipient cells (McDonald et al. 2014). Another study using EVs secreted by THP-1 as an *in vitro* polarized M1 proinflammatory

macrophages, show reduced abundance of the exosomal marker TSG101, as compared to their M2 counterpart (Zhang et al. 2015), which is in agreement with our results, that exosomal markers are all markedly decreased in EVs LPS.

We isolated and characterized EVs from the conditioned medium of the Raw264.7 cells at basal, naive state and activated with LPS. A difference with most of the published work, in our study, LPS was removed after 6 h to avoid contamination during the production of EVs, thus, reducing the carryover of LPS-derived particles in our EV preparations. In these conditions, we observed a significant decrease in the concentration of EVs secreted by the proinflammatory cells in the 48 h production time, which goes against the generally accepted notion that LPS exposure enhances the secretion of EVs (Kalra et al. 2016). Our unexpected results as to the concentration of EVs secreted by proinflammatory macrophages, could be an indication that stressed cells release higher concentration of EVs in an initial response to cellular stress such as LPS the population of EVs we are removing. The initial phase may follow by a decline in secretion of EVs by stressed cells, on a contrary to a cell at a basal state, which might be releasing EVs at steady constant rate. The contamination with particles from other sources are especially important to consider when EVs are used for downstream experiments, as they may carry active components, other than EVs. This hypothesis is supported by evidence, as we isolated particles, overlapping in size with EVs, as estimated by NTA, from the medium containing LPS only that has not been incubated with the cells **(Figure 22)**.

In addition to the significant decrease in the overall concentration of EVs secreted by proinflammatory macrophages, the abundance of protein markers related with EVs were also markedly decreased. To explain our findings, we hypothesize that either we are dealing with an enrichment in completely distinct population of EVs or in part, the subset of EVs carrying these markers was removed together with LPS after the 6 h, with low level of replenishment in the next 48 h. Another possible explanation is that the endosomal pathway may be inhibited or affected in these cells. Additionally, the mechanisms that control

exosome composition and content are not very well understood yet (Villarroya-Beltri et al. 2016). Lastly, it cannot be discarded that because of cellular stress, the cell uses EVs to discards the unwanted or damaged cellular components.

Interesting finding regards the possible post-translational modifications of proteins associated to EVs secreted by Raw264.7 macrophage-like cells, regardless the condition. We observed that some proteins, associated to EVs, such as Tsg101, Cd63, Aip1/Alix, and Flotillin1 seem to be modified in EVs secreted by macrophages. Aip1, Cd63, Tsg101, and Hsp70 proteins are of a higher molecular weight as compared to their corresponding cellular lysates from their parent cells. Flotillin1 on the other hand was found to be of a lower molecular weight and additionally as a single band as opposed to a double band in cell lysate controls. Interestingly, the modification of the Hsp70 protein was found to be solely associated to EVs LPS, which may be triggered by the conditions of cellular stress.

A protein can undergo many posttranslational modifications (PTMs), changing its properties and broadening its capacity to adapt to cellular needs. Specific pattern of PTMs is seen in EVs (Moreno-Gonzalo et al. 2014) which are involved in the sorting of specific proteins into exosomes (Villarroya-Beltri et al. 2016). Several examples have already been described such as the CD63 was previously described to be post-translationally modified by poly *N*-acetyl lactosamine addition during dendritic cell maduration (Engering et al. 2003). Interesting, the HSP70 was found to be sorted into exosomes independently of its ubiquitination, meaning that the knockdown of the deubiquitin domain increases the enrichement of both, modified and non-modified HSP70 in EVs (Moreno-Gonzalo et al. 2014). It could be that depending on a state that the cell, distinct subset of the Hsp70 protein is being selectively secreted, as we observe in our macrophage derived-EVs.

The markers of ER (Grp78) and mitochondria (CoxIV) were markedly decreased in our M1 macrophages. ER stress is often associated with inflammation, it modulates inflammatory responses during chemical stress or microbial infection

(Bronner et al. 2015). They have discovered that ER stress factors mediate the activation of mitochondrial damage pathway, which in turn activate the inflammasome and IL-1ß production (Bronner et al. 2015). Subsequently, mitochondrial ROS leads to lysosomal membrane permeabilization (Heid et al. 2013). Under these conditions the cell might be switching to the survival mode, which may have a profound influence on the secretion of EVs as well as on their content. EVs released by inflamed macrophages have been proposed to represent a class of inflammatory factors involved in inflammatory processes associated with metabolic diseases by their ability to upregulate proinflammatory mediators such as NFkB.

One of the first, most striking findings on EVs biology, was the fact that they harbour molecules involved in the function of the cell from which they are derived. In our study, we found the Tnf protein, potent proinflammatory mediator, to be associated with EVs isolated from the conditioned medium of LPS activated, M1 Raw264.7 macrophages. TNF naturally occurs in two forms: a 26-kDa type II membrane protein (mTNF) and a soluble form (sTNF) that is derived from the membrane form by proteolytic cleavage (Zhang et al. 2006). The association of the membrane form of TNF with EVs secreted by immune cells, such as DCs has been demonstrated (Zhang et al. 2006; Munich et al. 2012; Gao et al. 2016). Employing protein array and ELISA and using intact as well as lysed EVs, it was demonstrated, that the TNF was associated to the membrane of EVs as opposed to being carried in their lumen. In addition to that, they were shown to contribute to the inflammation of endothelial cells, through an activation of the NF-κB pathway in a manner similar to that of LPS, and induce atherosclerotic lesions *in vivo* (Gao et al. 2016). Furthermore, another study has revealed that DC-EVs activated natural killer cells and mediated apoptosis in tumour cells, via associated TNF superfamily ligands, such as TNF, FasL and TRAIL (Munich et al. 2012).

In the context of obesity accompanying MetS, expanding adipose tissue and the infiltration of macrophages, generate inflammatory responses in adipose tissue.

Underlying insulin resistance has lead to many studies on the adipocyte/macrophage axis and the involvement of EVs as mediators and possible causative agent for the development of MetS associated metabolic perturbations. Mitochondrial dysfunction, which has been implicated in the development of insulin resistance, seen as a decrease in the mitochondrial OXPHOS (Montgomery & Turner 2014).

Having that in mind, we have investigated the possible role of EVs LPS on bioenergetics of the 3T3-L1 adipocytes. We observed a significant reduction in mitochondrial functions, as measured using Seahorse XF extracellular flux analyzer. Mitochondrial dysfunction can result from a number of factors such as decrease in mitochondrial biogenesis, reduced mitochondrial protein content and the oxidative activity of the ETC (Montgomery & Turner 2014). The Tnf, associated to the membrane of EVs LPS, could be a possible mediator, however additional experiments would have to be performed to reveal the exact mechanism involved in producing these effects.

On the other hand, we also were interested to study the influence of EVs LPS, secreted by proinflammatory Raw264.7 macrophages, on insulin sensitivity in 3T3-L1 adipocytes.

One study has examined the effect of M1 THP-1 macrophages on insulin sensitivity in adipocytes by measuring the phosphorylation of the Akt kinase (Zhang et al. 2015). Treatment of primary adipocytes with 100 µg of M1 THP-1 derived-EVs caused a significant reduction in the abundance of phosphorylated Akt protein and decreased translocation of Glut4, effectively reduce glucose uptake activity and enhanced activation of the NF-kB. In contrast, the anti-inflammatory M2-derived EVs significantly increased the insulin sensitivity in adipocytes and mibilize Glut4 protein toward at the plasma membrane (Zhang et al. 2015). In our experiments we treated the 3T3-L1 adipocytes with one dose of 10 µg of macrophage derived-EVs, at a basal as well as the pro-inflammatory state. In agreement with previous results, but with 10-times less EVs concentration they caused increased phosphorylation of Akt and Erk1/2 protein.

The pro-inflammatory EVs were not able to cause the same effect over the insulin stimulated Akt phosphorylation with only a slight decrease in basal Akt phosphorylation upon exposure with Raw-EVs. These differences could be an indication that a higher dose of EVs would have to be needed to produce similar results. Three consecutive doses of macrophage-EVs (10 µg/each for 24h), the Akt phosphorylation was slightly reduced as seen in Akt protein abundance. It is important to consider that the induction of insulin resistance is not an instant process, therefore additional experiments would be needed to establish the dose curve response.

Interestingly, it has been demonstrated that macrophage-secreted factors block the insulin action in adipocytes via downregulation of Glut4 and IRS-1, leading to a decrease in Akt phosphorylation and impaired insulin-stimulated Glut4 translocation to the plasma membrane (Lumeng, Deyoung, et al. 2007). It was discovered by culturing adipocytes with conditioned medium of activated M1 macrophages, as well as co-culture of both cell types. Moreover, TNF-neutralizing antibodies partially reversed the insulin resistance produced by macrophage-conditioned media. This is another supporting evidence for the involvement of TNF in the development of insulin resistance in context of MetS, that may be mediated in association with M1 macrophage-EVs.

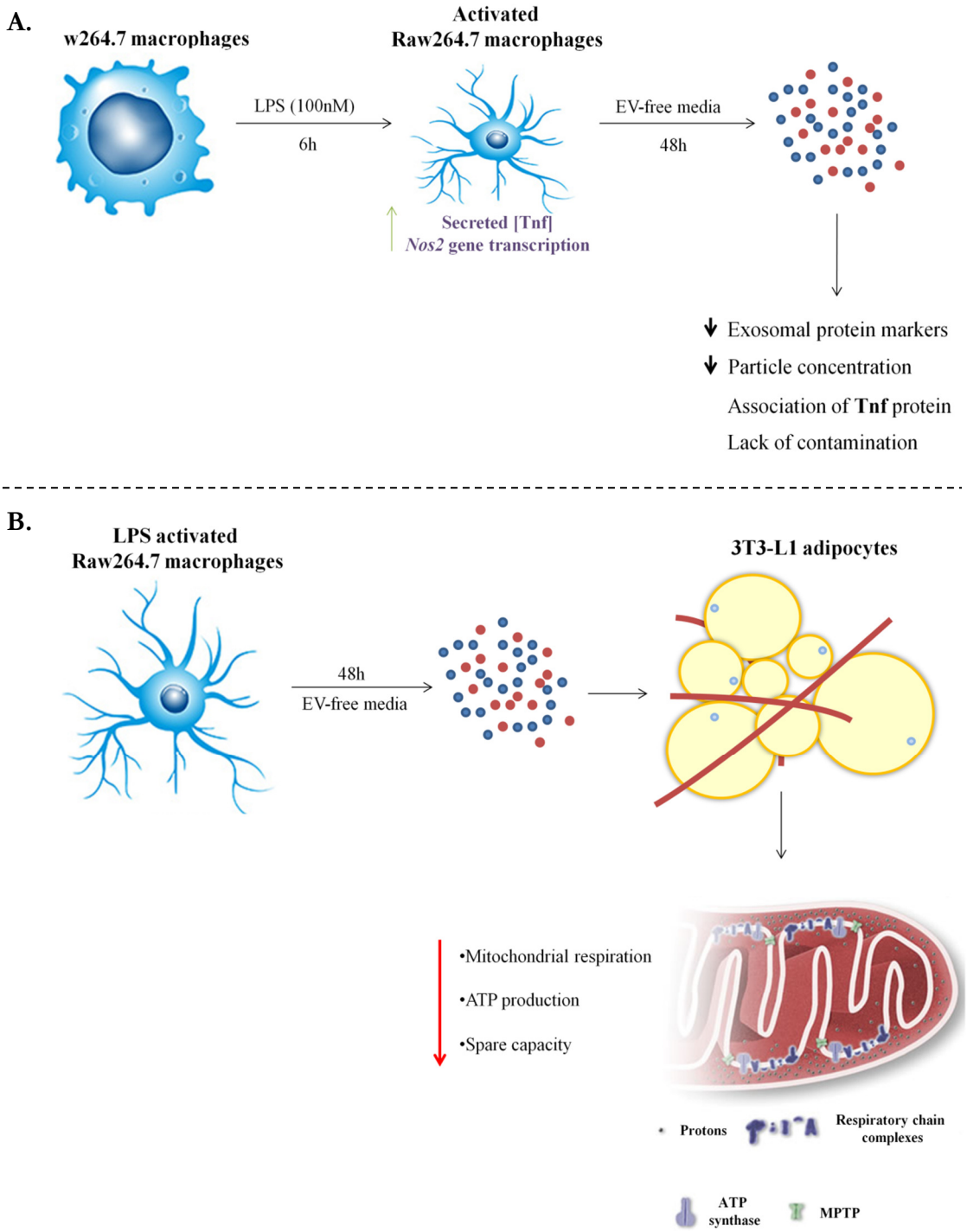

Figure 27 Summary diagram of results described in chapter 2. Graphical representation of results regarding **(A)** the characterization og EVs obtained from LPS induced Raw264.7 cells and **(B)** their effect on mitochondrial respiration of the 3T3-L1 adipocytes.

RESULTS CHAPTER 3

5. Characterization of the *in vitro* models of hepatocellular steatosis and their secreted-EVs

Chapter 3 Aims:

- Establish and characterize the *in vitro* models of hepatocellular steatosis in hepatic cell lines.
- Characterize the genetic model of steatotic Zucker rat hepatocytes in a primary *in vitro* culture.
- Characterize EVs secreted by models of hepatocellular steatosis
- Comprehensive characterization of EVs secreted by the primary Zucker rat hepatocytes, in terms of morphology, concentration, protein, lipid and nucleic acid content.

5.2 Introduction

The liver is a complex environment comprised of several different cell types (Imani Fooladi & Hosseini 2014) **(Figure 28)**. Hepatocytes and cholangiocytes, both types of liver epithelia, natural killer T cells, hepatic stellate cells, adult liver stem cell, and hepatic sinusoidal endothelial cells, were all shown not only to release EVs but also be the direct target of EVs (Masyuk et al. 2013; Conde-Vancells et al. 2008; Witek et al. 2009; Fonsato et al. 2012; Royo & Falcon-Perez 2012).

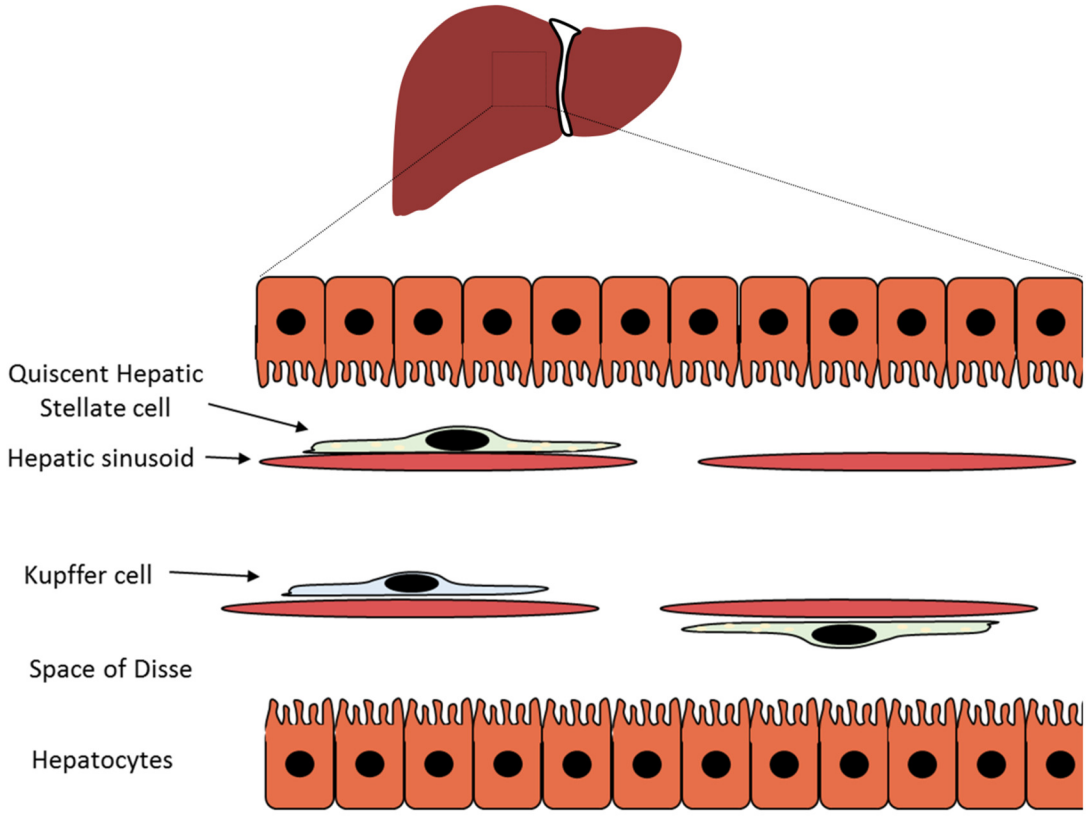

Figure 28 Cells of the liver. Healthy liver lobules are formed from hepatocytes on a loose basal membrane (space of Disse) surrounding sinusoid. The space of Disse is alsowhere quiescent hepatic stellate cells are found, while Kupffer cells can be found in the hepatic sinusoid.

In addition, EVs have been implicated in a spectrum of liver diseases such as NAFDL, NASH, cirrhosis, fibrosis, and HCC (Shen et al. 2016; Borges et al. 2013; Guo & Guo 2015; Ban et al. 2016). The level of circulating vesicles has been shown to be increased in liver disease, particularly associated with the alcohol consumption (Momen-Heravi et al. 2015), viral infection and features of MetS including diabetes, obesity, and dyslipidemia, as a result of increased secretion and/or decreased clearance of EVs. Moreover, EVs released by injured

hepatocytes include certain antigens, specific hepatic enzymes, miRNAs, and mRNAs (Imani Fooladi & Hosseini 2014).

Simple steatosis, known as the fatty liver is a common, and reversible condition when employing behavioural changes. However, little attention has been attributed to EVs secreted by hepatocytes in conditions of simple steatosis.

In our study, we used two different models of hepatic steatosis to isolate and characterize EVs from their conditioned medium. On one hand, we used three different hepatic cell lines and induced hepatocellular steatosis with the mix of FFAs, oleic and palmitic (2:1, 1 mM for 24 h). Then, we isolated hepatocytes from Zucker lean and fatty livers, as a genetic model of obesity induced liver steatosis.

In this part of the thesis, *in vitro* models were characterized in terms of lipid accumulation profile and in the case of primary rat hepatocytes, their bioenergetic profile, the expression of markers related to hepatic functions and insulin sensitivity. Subsequently, we performed the comprehensive characterization of their secreted EVs in terms of morphology, overall concentration, specific cargo and association of active compounds.

5.3 Results

5.3.1 Induction of steatosis in hepatic cell lines

As already mentioned, we used three different hepatic cell lines for the induction of hepatocellular steatosis. The AML12 cell line was created in 1994 as a differentiated, nontransformed hepatic cell line derived from mice transgenic for transforming growth factor α (TGFα) (Wu et al. 1994), the human HepG2 cells, derived from differentiated hepatocellular carcinoma of the liver tissue of a fifteen-year-old Caucasian American male (Costantini et al. 2013) and MLP29 a

liver progenitor cell line. All three cell lines were widely used in a variety of *in vitro* studies (Conde-Vancells et al. 2008; Cui et al. 2010; Kohli et al. 2007).

We tested different conditions of steatosis induction, to achieve a fat accumulation profile with a minimal cytotoxic and apoptotic effect. In our work and as previous studies have revealed, individual fatty acids have a distinct toxic potential (Gómez-Lechón et al. 2007) with saturated, palmitic acid being the most toxic one. Having that in mind, several concentrations of the oleic and palmitic acid were tested ranging from 0.1 to 1 mM (data not shown). However, the most effective approach, with optimal cytosolic fat accumulation and minimal toxicity, as measured by AnnexinV/PI assay, resulted to be the combination of both FFAs. After testing the different combination of concentrations, a 2:1 ratio of oleic to palmitic acid at a final concentration of 1 mM (BSA-conjugated) was selected for further experiments.

AML12, MLP29 and HepG2 cell viability, following 24 h treatment with the FFA mixture was determined with AnnexinV-FITC/PI assay. Representative FACS plots, for the three tested cell lines, are shown in **Figure 29A-29C**. A slight displacement of the treated population can be seen with respect to the untreated control. AML12 cells seem to be more sensitive exhibiting overall lower viability (>75%), as compared to the MLP29 (<80%) and HepG2 cells (>80%). However, considering that the same drop in viable cell count can be seen in the control sample, it could be the result of the handling and the assay sensitivity. Importantly, in all three experimental groups, the treatment did not seem to significantly affect cell viability as compared to their respective controls **(Figure 29)**.

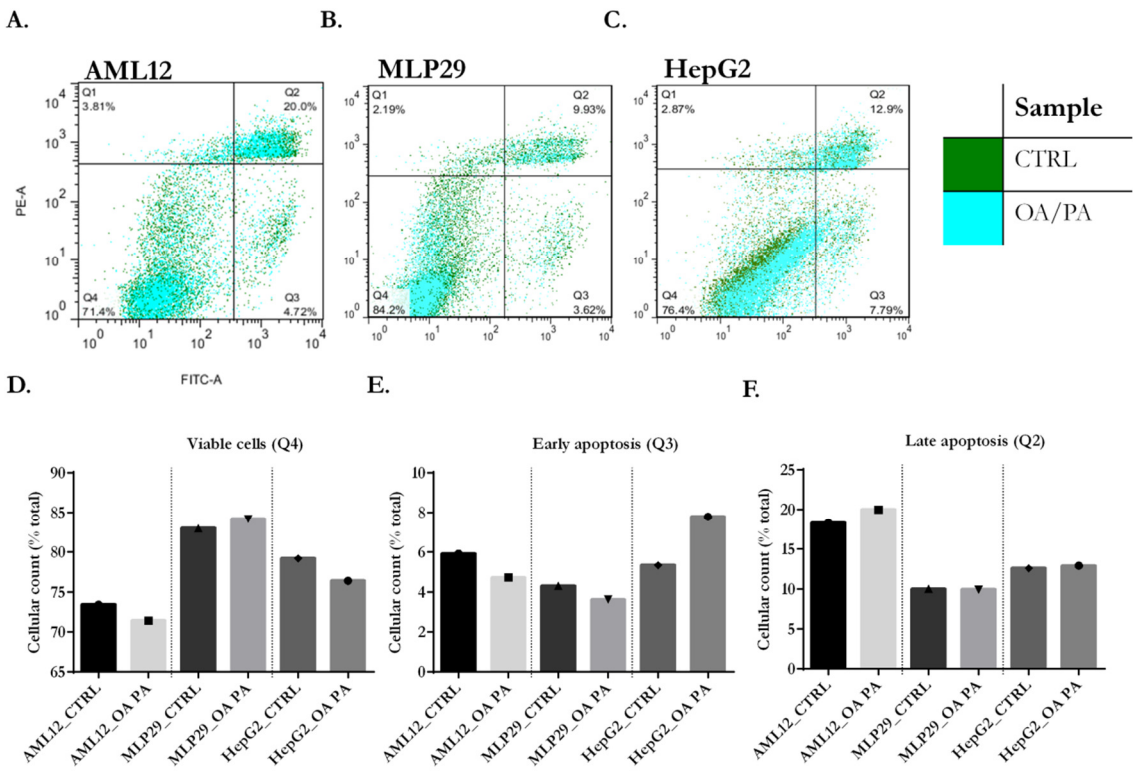

Figure 29 Treatment with FFAs does not affect viability of hepatocyte-like cells. Flow cytometry analysis of AnnexinV-FITC/Propidium iodide staining in **(A)** AML12 **(B)** MLP29 and **(C)** HepG2 hepatocyte-like cells, following the treatment with FFA mix (OA/PA; 2:1; 1 mM). Graphs represent: **(D)** viable cells, **(E)** cells entering in early apoptosis and **(F)** late apoptotic cells, for all three cell lines; n=1.

5.3.1.1 AML12

FFA (OA/PA; 2:1;1 mM;24 h) challenged AML12 cells were stained with Bodipy (10 µg/ml) for the estimation of fat accumulation. Upon exposure to OA/PA mixture, AML12 cells accumulated large number of fat droplets, when compared to untreated control **(Figure 30A)**. This result was confirmed and quantified by flow cytometry. Representative histogram is shown on **Figure 30B** with the quantification of the fluorescent signal **(Figure 30C)**.

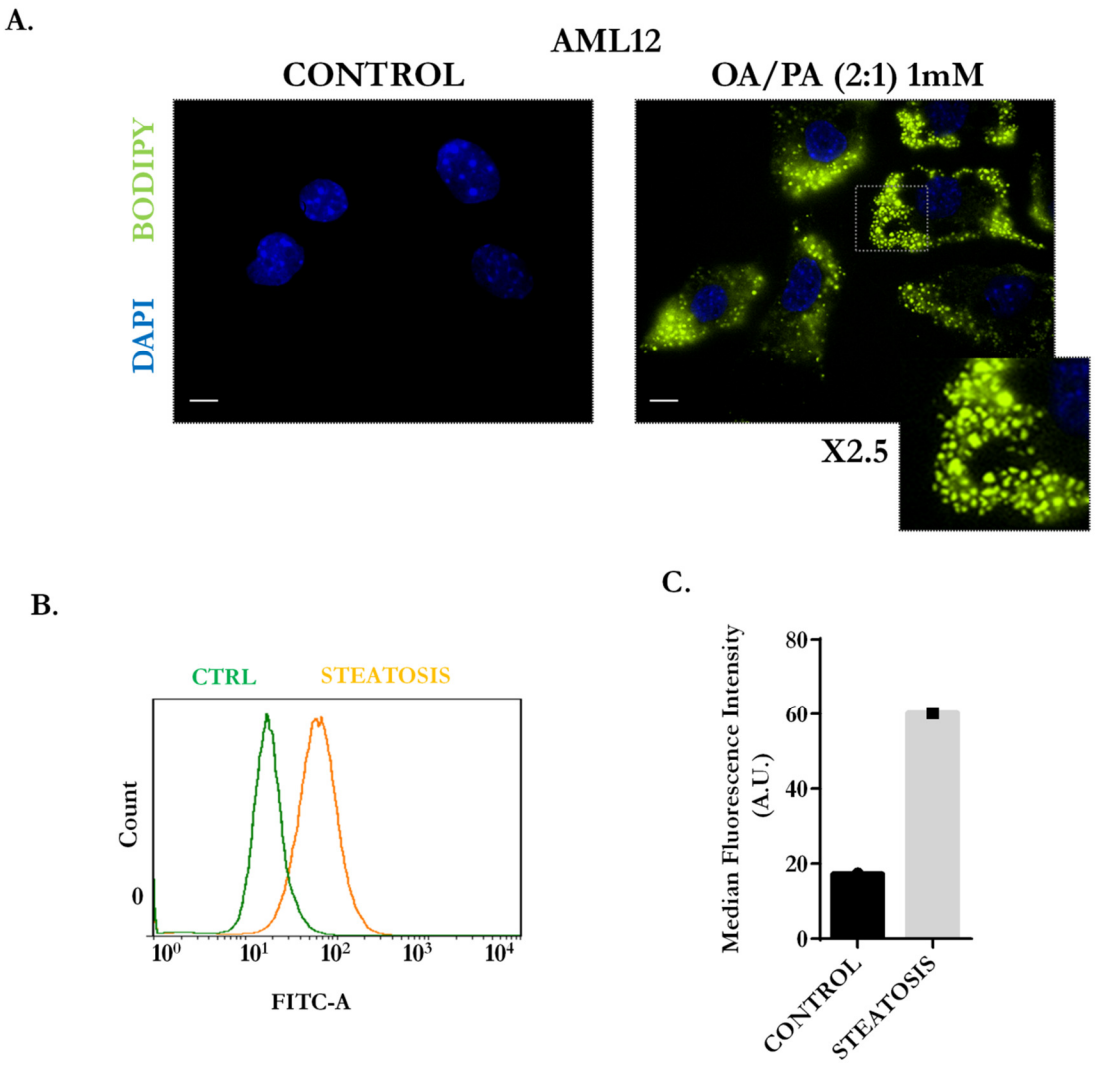

Figure 30 Treatment with FFAs causes triglyceride accumulation in AML12 hepatocyte-like cells. Steatosis was induced in AML12 hepatic cell line with FFA mixture: OA/PA, at 2:1 ratio, final concentration at 1 mM for 24 h. **(A)** Representative images of Bodipy staining showing accumulation of lipids in AML12 cells. Following the treatment, cells were fixed with 2% paraformaldehyde and stained. Lipid content was additionally quantified by flow cytometry. **(B)** Flow cytometry histogram of control and steatotic population of cells stained with Bopdipy. **(C)** FITC-A median fluorescent intensity quantification of Bodipy (30,000 events/P1); bar = 20 μm; n=1.

5.3.1.1.1 Characterization of EVs secreted by steatotic AML12 cells

We characterized AML12-EVs, following the same schema as in previous sections. Evaluation of the purity of EV preparations as well as their initial structural characterization was done using cryo-EM without fixation or staining. In the case of AML12 hepatocyte secreted EVs, control as well as steatotic, cryo-EM demonstrated the presence of membrane-enclosed vesicles of different sizes **(Figure 31A)**. The majority however, fell into the exosomal size range, around 100 nm. Among them smaller electron dense round structures could be identified. Larger vesicles were also present, as well as fusions of two or more vesicles **(Figure 31A, right panel, 2.5X)**.

NTA was carried out to measure the range size distribution of particles **(Figure 31B)** and their concentration **(Figure 31C)** in the AML12-derived EV samples. The results show two peaks that represent the largest size groups in terms of the amount of EVs, at 100-150 nm and at 150-200 nm in both samples, constituting 25 and 28% for the control and steatotic within 100-150 nm size range respectively and 27 and 29% in 150-200 nm range. 80% of the whole population is confined to 50-250 nm. Moreover, there was a slight increase in the overall concentration of vesicles released from AML12 cells **(Figure 31C)**. No change was observed in terms of mean size distribution between the samples **(Figure 31D).**

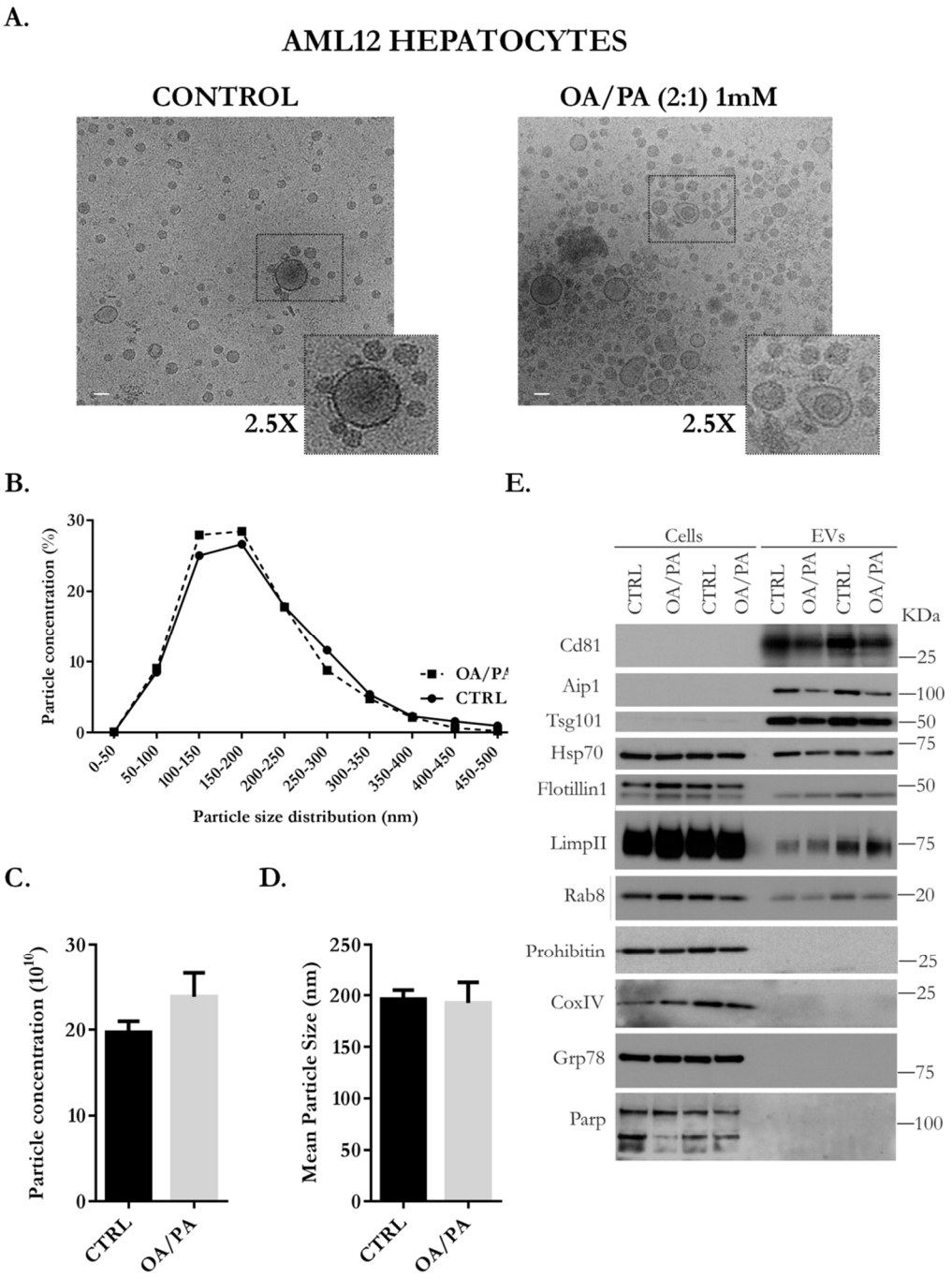

Figure 31 Characterization of EVs secreted by steatotic AML12 hepatocyte-like cells. Ultrastructural and biochemical characterization of EVs isolated from conditioned medium of steatotic AML12 cells. **(A)** Cryo-EM analysis; bar=100 nm, inserts are magnified 2.5X. **(B)** Size range distribution. **(C)** Particle concentration (10^{10}). **(D)** Particle mean size; parameters measured by NTA; n=4 **(E)** Protein extracts from two independent preparations of EVs (5 µg) together with their corresponding cell lysates (10 µg) were analyzed by WB with antibodies for EV specific as well as cellular markers. Error bars =SD

AML12-derived EVs were shown to be highly enriched in markers such as membrane tetraspanin Cd81, endocytic marker proteins such as Aip1/Alix, and Tsg101 as compared to the cellular extracts of their parent cells. Interestingly, their expression was notably decreased in steatotic EVs. Flotillin1 was detected in both cells and EVs. However, there was no enrichment of this marker in EVs. Flotillin1 expression seems to be post-translationally regulated at the level of EVs as in cells it is expressed as a double band, with the upper band being more pronounced compared to the single band in EVs. Moreover, glycoprotein, LimpII was found to be abundant in AML12 cells. Comparing the control cells of steatotic hepatocytes, there is an enhancement in LimpII expression in steatotic hepatocytes with the expression mirrored in EVs. Similar expression pattern was observed for the Ras-related protein, Rab8. Hsp70 is a chaperon protein involved in maintaining cellular protein homeostasis and cell survival in response to stressful cellular conditions (Lancaster & Febbraio 2005). Exosomes were shown to contribute to the release of Hsp70 in both basal and stress induced conditions (Lancaster & Febbraio 2005). AML12 cells secreted Hsp70 into the extracellular environment in association with EVs. However, the amount secreted in EVs did not correlate with that remaining in cells. Its level of expression remain unchanged in the parent cell regardless the condition, however, there was a clear decrease in Hsp70 shuttled in steatotic EVs as compared to the control ones. In addition, to discard the presence of contamination from cellular compartments in our preparations, the expression of protein markers of endoplasmic reticulum (Grp78) and mitochondria (CoxIV and Prohibitin), was assessed. They were readily detectable in whole cellular lysates and absent in our EV preparations, ruling out possible contamination by these intracellular organelles. Importantly, expression of the apoptosis related protein Parp, although detected in all samples there was no significant difference between them. Together, the lack of intracellular organelles in EVs and the lack of the alteration in the cellular Parp pattern indicate that under our culture conditions there was not cell death induction by the FFA treatment.

Overall, the AML12 cells with fat accumulation phenotype secreted increased number of vesicles when compared to the control cells. Moreover, the expression of exosomal markers was markedly decreased in these EVs.

5.3.1.2 MLP29

Lipid accumulation was evaluated in MLP29 cells treated with FFAs mixture for the induction of hepatocellular steatosis, using the same scheme as for the AML12 cells. Bodipy staining confirmed lipid accumulation in the MLP29 cells **(Figure 32A)**. Moreover, the signal of Bodipy, lipid staining was quantified by flow cytometry **(Figure 32B and Figure 32C)**.

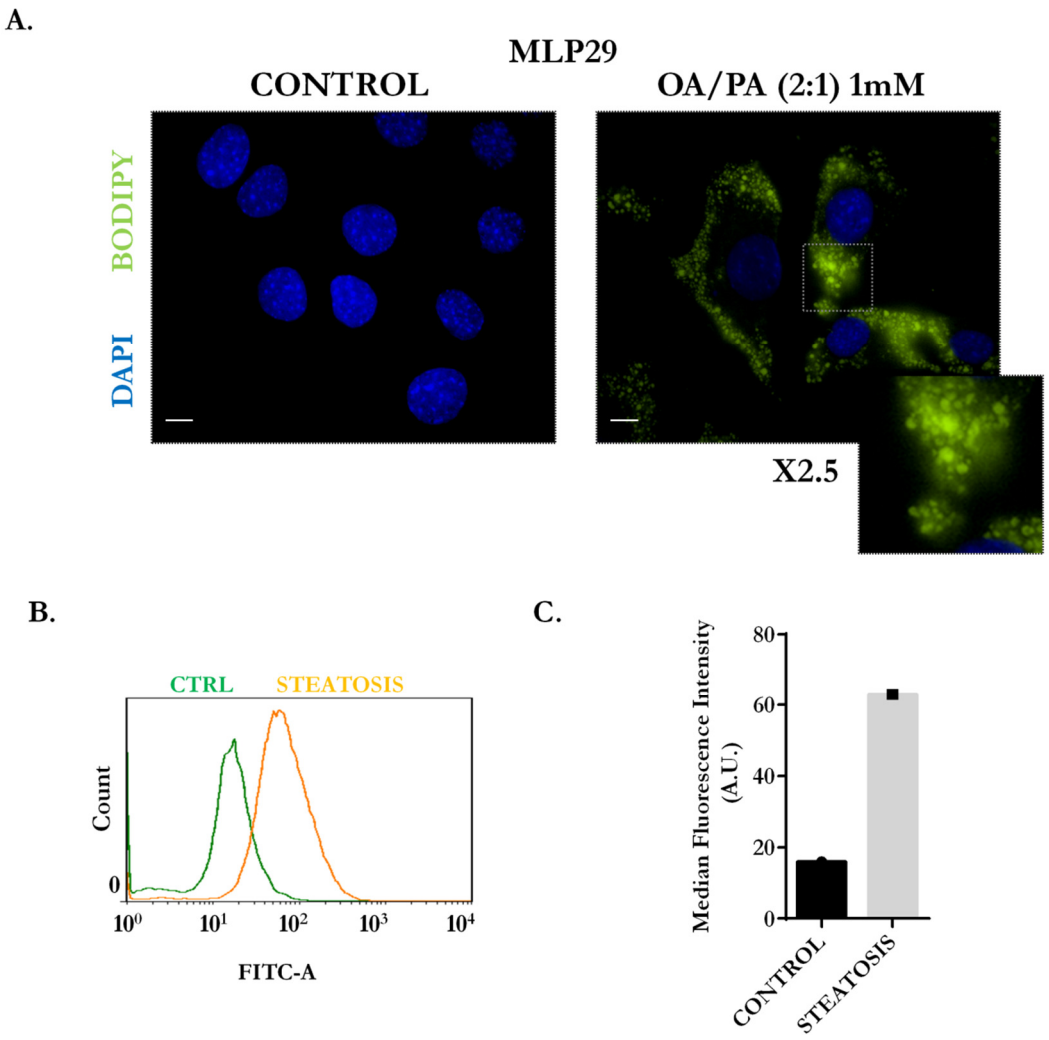

Figure 32 Treatment with FFAs causes triglyceride accumulation in MLP29 hepatocyte-like cells. Steatosis was induced in MLP29 hepatic cell line with FFA mixture: OA/PA, at 2:1 ratio, final concentration at 1 mM for 24 h. **(A)** Representative images of Bodipy staining showing accumulation of lipids in AML12 cells. Following the treatment, cells were fixed with 2% paraformaldehyde and stained. lipid content was additionally quantified by flow cytometry. **(B)** Flow cytometry histogram of control and steatotic population of cells stained with Bopdipy. **(C)** FITC-A median fluorescent intensity quantification of Bodipy (30,000 events); bar = 20μm; n=1.

5.3.1.2.1 Characterization of EVs secreted by steatotic MLP29 cells

We characterized the EVs secreted by MLP29 cells, at basal state and during hepatocellular steatosis **(Figure 33).** Ultrastructurally, MLP29 EVs present a heterogeneous population of typical, bilayered-membrane vesicles **(Figure 33A)**. The NTA profile of MLP29-derived EVs is slightly different than the AML12 cells, a peak at the 100-150nm size **(Figure 33B)** and with a slight shift in the size distribution curve towards larger vesicles. Moreover, there is a slight increase in the total concentration of particles in EVs isolated from steatotic MLP29 cells **(Figure 33C).** There was no difference observed in mean size distribution **(Figure 33D).** Furthermore, results obtained from WB **(Figure 33E)** show that MLP29 cells secrete a slightly different population of EVs than AML12 cells. The expression pattern for many proteins was different when comparing EVs coming from control and treated cells. It should be considered that both cell lines, although both of hepatic origin, they are very distinct. MLP29 cells are a hepatic progenitor cell line and AML12 overexpress a potent hepatocyte mitogen, TGFα, of human origin (Wu et al. 1994).

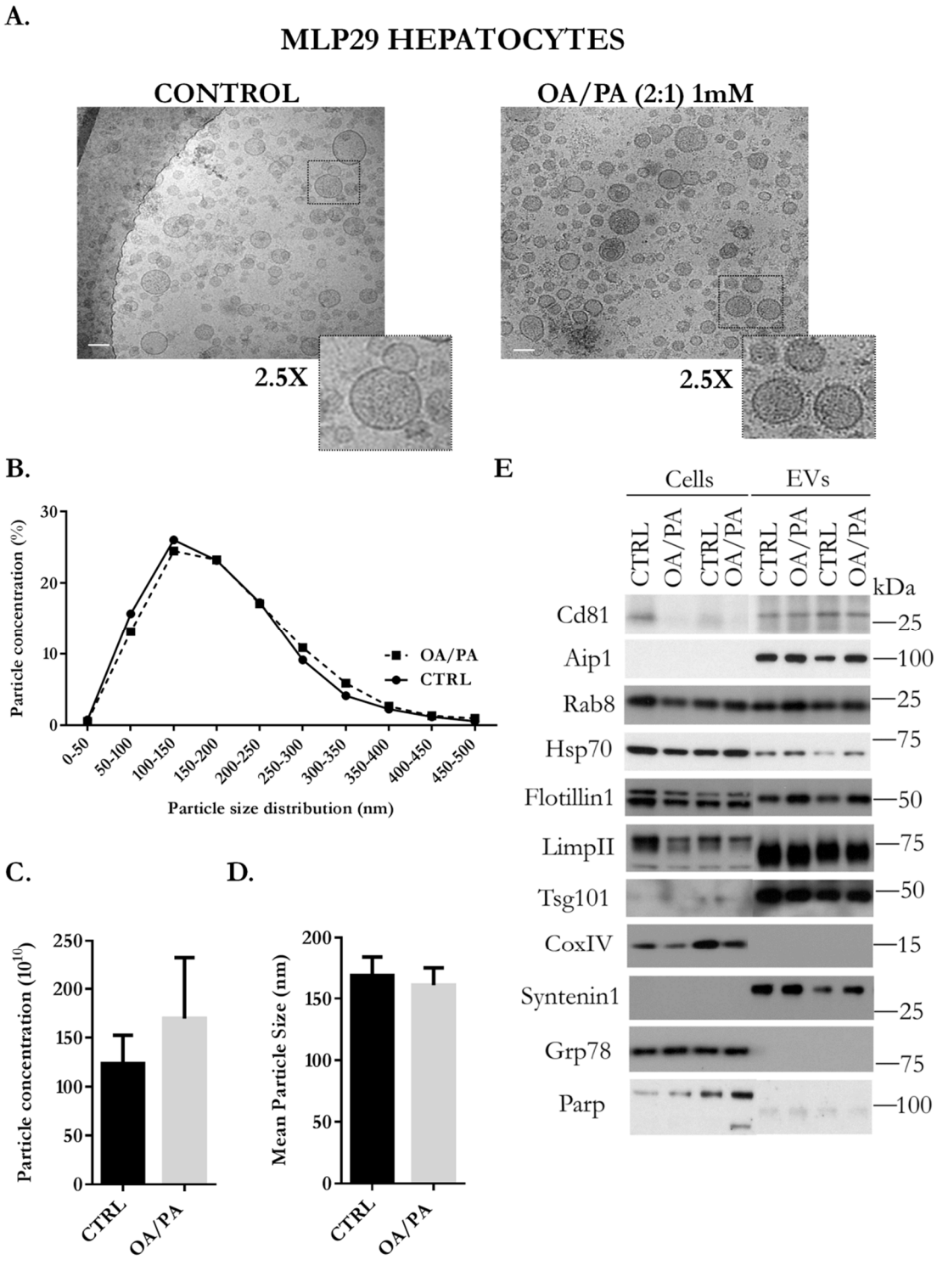
A.
MLP29 HEPATOCYTES
CONTROL
OA/PA (2:1) 1mM
2.5X
2.5X
B.
Particle concentration (%)
30
20
10
0
OA/PA
CTRL
0-50
50-100
100-150
150-200
200-250
250-300
300-350
350-400
400-450
450-500
Particle size distribution (nm)
C.
Particle concentration (10^{10})
250
200
150
100
50
0
CTRL
OA/PA
D.
Mean Particle Size (nm)
200
150
100
50
0
CTRL
OA/PA
E
Cells
EVs
CTRL
OA/PA
CTRL
OA/PA
CTRL
OA/PA
CTRL
OA/PA
kDa
Cd81
25
Aip1
100
Rab8
25
Hsp70
75
Flotillin1
50
LimpII
75
Tsg101
50
CoxIV
15
Syntenin1
25
Grp78
75
Parp
100

Figure 33 Characterization of EVs secreted by steatotic MLP29 hepatocyte-like cells. Ultrastructural and biochemical characterization of EVs isolated from conditioned medium of steatotic MLP29 cells. **(A)** Cryo-EM analysis; bar=100 nm, inserts are magnified 2.5X. **(B)** Size range distribution. **(C)** Particle concentration (10^{10}). **(D)** Particle mean size was measured by NTA; n=4. **(E)** Protein extracts from two independent preparations of EVs (5 μg) together with their corresponding cell lysates (10 μg) were analyzed by WB with antibodies for EV specific as well as cellular markers. Error bars = SD.

There was a clear enrichment in protein markers of EVs in our MLP29 preparations, Cd81, Aip1/Alix and Tsg101 are highly expressed in EVs compared to whole cellular lysates of parent cells. Interestingly, Cd81 and Aip1/Alix were detected in cells. The abundance of Cd81 was decreased significantly in steatotic hepatocytes, which was mirrored in their secreted EVs. Positive correlation can be observed in the expression of Hsp70 and Rab8 between the amount of protein retained in the cell and the amount excreted in EVs. There was a decrease in Hsp70 in steatotic cells with more protein being shuttled out of the cell in association with steatotic EVs. Also, in this model, Flotillin1 was modified for secretion of EVs and significantly more was packaged into steatotic EVs as compared to control EVs. Interestingly, as opposed to AML12 cells, in the MLP29 model, the bottom band was more highly expressed. MLP29-EVs exhibit significant enrichment in LimpII protein with no major differences between the control and steatotic vesicles. Interestingly, as seen by the expression in cellular lysates, fat overload in cells affected its abundance. Syntenin1, an important adaptor protein for the formation of exosomes was found to be more associated to steatotic EVs, as compared to the control. Steatosis also caused a decrease in the expression of mitochondrial CoxIV. Importantly, CoxIV as well as Grp78 expression was absent in EV preparations, discarding the presence of contamination. Finally, although more amout of Parp protein was found in one of the preparation, as judged by the abundance of the unprocessed 100 kDa Parp band, it could be concluded that cells were not significantly affected by the treatment with FFAs **(Figure 33E)**. This result together with the already

mentioned lack of traces of intracellular organelles in EVs indicate that under our culture conditions there was not cell death induction by the FFA treatment.

5.3.1.3 HepG2

Finally, we assessed the lipid accumulation profile upon treatment with the FFAs mixture in the human HepG2 cell line. Bodipy staining confirmed the presence of lipid droplets in the cytoplasm of the HepG2 cells **(Figure 34A)**. Flow cytometry quantification of Bodipy confirmed significant lipid accumulation, as seen by immunostaining of fixed cells **(Figure 34B)**. Moreover, as can be deducted from the FITC-A channel of the FACS analysis, HepG2 cells, under similar conditions, accumulated significantly more lipids than the previously characterized AML12 and MLP29 cells **(Figure 34C)**.

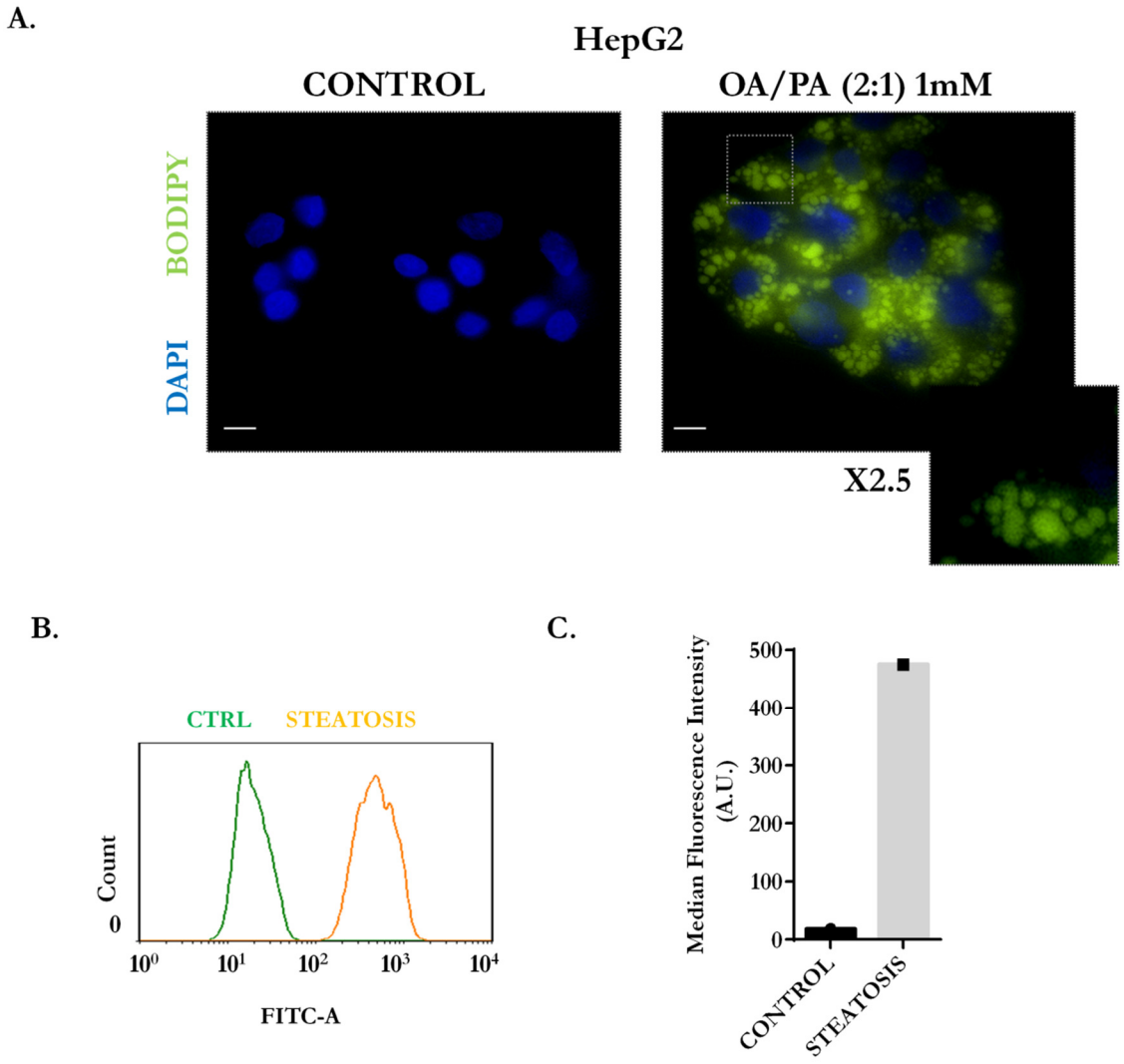

Figure 34 Treatment with FFAs causes triglyceride accumulation in HepG2 hepatocyte-like cells. Steatosis was induced in HepG2 hepatic cell line with FFA mixture: OA/PA, at 2:1 ratio, final concentration at 1 mM for 24 h. **(A)** Representative images of Bodipy staining showing accumulation of lipids in HepG2 cells; bar = 20µm. Following the treatment, cells were fixed with 2% paraformaldehyde and stained. Lipid content was additionally quantified by flow cytometry. **(B)** Flow cytometry histogram of control and steatotic population of cells stained with Bopdipy. **(C)** FITC-A median fluorescent intensity quantification of Bodipy (30,000 events); n =1.

5.3.1.3.1 Characterization of EVs secreted by steatotic HepG2 cells

EVs isolated from HepG2 cells at basal state and in steatosis, were observed in their native state by Cryo-EM analysis revealing some important structural details such as the presence of a phospholipid bilayer or electron density. **Figure 35A** shows representative electron micrographs of EVs obtained from control, as well as, steatotic HepG2 cells. Vesicles of a varying sizes and electron density can be appreciated. The size of the EV population, as determined by NTA, peaked around 150-200 nm for both, control and steatotic hepatocytes **(Figure 35B)**. An 8% decrease in the number of smaller vesicles, 50-100 nm secreted by steatotic hepatocytes was observed. On the contrary, the number of vesicles between 100-200nm increased by 10%, with the total concentration (10^{10}) remaining unchanged (**Figure 35C).** There seem to be a drop in the mean particle size of the overall population of steatotic EVs **(Figure 35D). Figure 35E** shows a representative immunoblotting of two HepG2-EV preparations together with their corresponding whole cell lysates. WB analysis revealed that EV fractions were highly enriched in tetraspanin Cd63, which was undetectable in whole cell lysates **(Figure 35E)**. The amount of Cd63 was unchanged between control and steatotic EVs. Tsg101, the ESCRT machinery protein was found abundant in HepG2-EVs, and was increased in steatotic-EVs, mirroring the expression in cells.

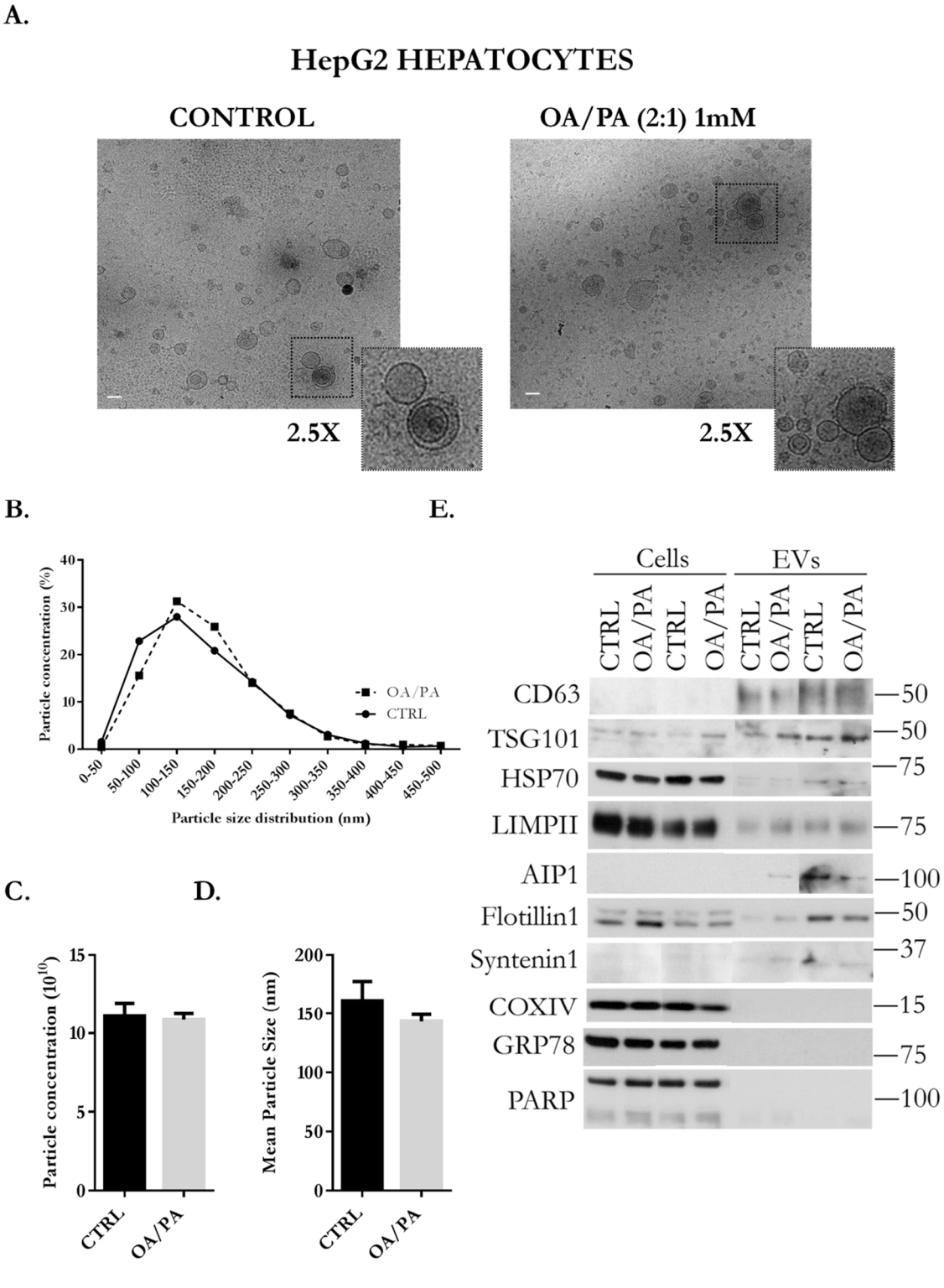
A.
HepG2 HEPATOCYTES
CONTROL
OA/PA (2:1) 1mM
2.5X
2.5X
B.
Particle concentration (%)
40
30
20
10
0
OA/PA
CTRL
0-50
50-100
100-150
150-200
200-250
250-300
300-350
350-400
400-450
450-500
Particle size distribution (nm)
C.
Particle concentration (10^10)
15
10
5
0
CTRL
OA/PA
D.
Mean Particle Size (nm)
200
150
100
50
0
CTRL
OA/PA
E.
Cells
EVs
CTRL
OA/PA
CTRL
OA/PA
CTRL
OA/PA
CTRL
OA/PA
CD63
—50
TSG101
—50
HSP70
—75
LIMPII
—75
AIP1
—100
Flotillin1
—50
Syntenin1
—37
COXIV
—15
GRP78
—75
PARP
—100

Figure 35 Characterization of EVs secreted by steatotic HepG2 hepatocyte-like cells. Ultrastructural and biochemical characterization of EVs isolated from conditioned medium of steatotic HepG2 cells. **(A)** Cryo-EM analysis; bar=100 nm, inserts are magnified 2.5X. **(B)** Size range distribution. **(C)** Particle concentration (10^{10}). **(D)** Particle mean size was measured by NTA, n=4. **(E)** Protein extracts from two independent preparations of EVs (5 μg) together with their corresponding cell lysates (10 μg) were analyzed by WB with antibodies for EV specific as well as cellular markers. Error bars = SD.

HepG2 cells were found to highly express the lysosomal protein LimpII as well as the chaperone Hsp70. The amount of Hsp70 protein was reduced in steatotic HepG2 cells. In comparison, the quantity in EVs was significantly less with no clear differences seen between the control and steatosis. Flotillin1 expression in EVs was variable between the two independent preparations, although in cells it seems that there was a slight increase in steatotic HepG2 cells. Syntenin1 was barely detected in EV fractions. Cellular markers, CoxIV and Grp78 were exclusively present in cells with decreasing amount of CoxIV in steatotic EVs. The expression of apoptosis marker Parp, was unaffected by the treatment.

Important to remark at this point is that when comparing the abundance of proteins in EVs isolated from AML12, MLP29 and HepG2 cell lines, we discovered some remarkable differences. The one that called most attention was the expression of the lysosomal LimpII protein. It was highly enriched in MLP29-derived EVs as compared to the secreting cells. Moreover, its expression was affected upon induction of steatosis **(Figure 33E)**. The opposite effect was seen in AML12 and HepG2 cells were LIMPII was mostly associated to cells (**Figure 31E** and **Figure 35E**). Moreover, the expression of Hsp70, Rab8 and Flotillin1 were clearly augmented in steatotic MLP29-derived EVs, which cannot be observed for the AML12 and HepG2-derived EVs. There was a very little of Hsp70 in HepG2-derived EVs. Furthermore, Flotillin1 in cellular lysates was detected as a double band, which was modified in EVs and expressed as a single band. Interestingly in MLP29 lysates there was an enrichment in the lower

band of flotillin1 and in AML12 cell lysates in the upper band. Syntenin1 was readily detected in MLP29-derived EVs and barely in HepG2. Lastly, Cd81 protein was detected in cell lysates from MLP29 and it was undetectable in AML12 or HepG2. The MLP29 cells release EVs with distinct protein profile and most probably it is related with the fact that the MLP29 is a liver progenitor cell line **(Figure 33E)**.

5.4 Primary Zucker rat hepatocytes as a genetic model of obesity

5.4.1 Characterization of primary hepatocytes from Zucker rats

5.4.1.1 Morphological characterization of steatotic primary hepatocytes isolated from Zucker lean and fatty livers

Zucker fatty (*fa/fa*) rats (strain Crl: ZUC-Lepr^{fa}) are widely used as a research model in the study of obesity and its metabolic complications such as hyperinsulinaemia and insulin resistance. They have a homozygous mutation in the leptin receptor gene resulting in severe obesity due to hyperphagia. Although the phenotype of these genetically obese rats is well characterized *in vivo*, little research has been conducted on isolated hepatocytes from Zucker rat livers. We aimed to culture these hepatocytes *in vitro* and isolate secreted EVs from their conditioned medium.

Zucker rat hepatocytes were obtained by two-step collagenase perfusion and subject to Percoll density gradient centrifugation **(Section 2.2.1.1.1 and 2.2.1.1.1.2)** before seeding. Cell viability after perfusion was determined by trypan blue exclusion method and the results from 12 independent isolations were presented **(Figure 36A)**. Overall viability ranged from 86-98%. ZF-

hepatocytes were found to be slightly more sensitive, as noted in the drop of viability when compared to their lean control hepatocytes. The cultured cells were then examined for the lipid content by immunostaining with Bodipy at 4 h and 36 h of culture **(Figure 36B).** Representative images, with quantitative data obtained by flow cytometry analysis of Bodipy stained hepatocytes are presented on **Figure 36C-36D.**

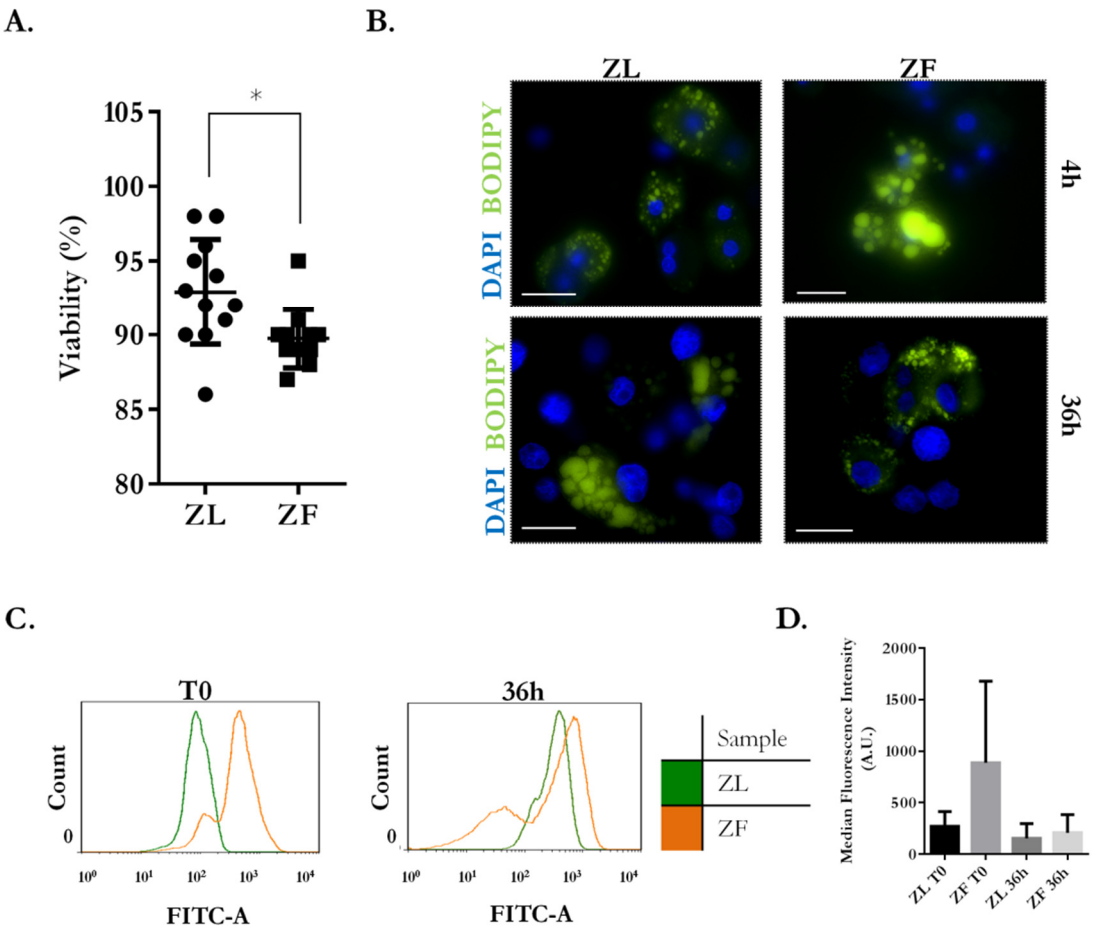

Figure 36 Characterization of Primary Zucker Rat Hepatocytes In Culture. Zucker rat hepatocytes, from ZL *(Fa/+)* and ZF *(fa/fa)* livers were isolated by two step collagenase perfusion technique. **(A)** Cell viability was assessed by trypan-blue exclusion method; n=12. **(B)** Bodipy lipid staining of ZL- and ZF- hepatocytes, previously fixed with paraformaldehyde (2%), at 4 h and 36 h in culture; size bar=20 µm. **(C)** Flow cytometry

histogram of Bopdipy stained ZL- and ZF-hepatocytes at T0 and after 36 h in culture. **(D)** Flow cytometric quantification of lipids in ZL- and ZF-hepatocytes at T0 and after 36h in culture; (30,000 events); n=4. Error bars represent SD. The *p* values were denoted as follows: 0.01-0.05=*, 0.01-0.001=**, 0.001-0.0001=***.

As expected, ZF-hepatocytes were found to have higher lipid content before plating (T0) as compared to their lean counterpart. This difference can be well appreciated on the flow cytometry histograms **(Figure 36C).** The fat content of ZF-hepatocytes did not seem to be affected by the culture conditions, between T0 and 36h. Moreover, ZL-hepatocytes in culture seem to accumulate lipids in the cytoplasm, as seen by the shift in the stained population, reflected in flow cytometry histograms **(Figure 36C)**.

5.4.1.2 Gene Expression changes in cultured Zucker rat hepatocytes

To further characterize the phenotype of Zucker rat hepatocytes in cell culture conditions, we analyzed the expression of a panel of genes related to hepatic functions, lipid management and metabolism **(Figure 37)**. The analysis was done by normalizing the level of expression in ZF hepatocytes to their lean control hepatocytes (value=1) at T0 (just after perfusion of the liver, before seeding the primary culture) and after 36h in culture. The expression of key genes involved in lipid metabolism including fatty acid synthase (*Fasn*), the enzyme catalyzing the formation of long-chain fatty acids and the fatty acid binding protein (*Fabp1*) mRNAs were 1.5 and 1-fold increased with respect to the control hepatocytes at T0 (**Figure 37B** and **Figure 37A** respectively). Insulin growth factor 1(*Igf1*), primarily produced by the hepatocytes in the liver (Mallea-Gil et al. 2012), was significantly augmented in ZF hepatocytes at T0 and this difference was reduced after 36h of culture **(Figure 37C)**. Albumin (*Alb*), hepatocyte nuclear factor 4 α (*Hnf4α*), and transforming growth factor ß (*Tgfß*), are important markers of

hepatic function, and were found to be over 1-fold increased in ZF over ZL hepatocytes at T0 and the differences were reduced after 36h in culture (**Figure 37D**, **Figure 37E** and **Figure 37F** respectively). UDP-glucuronosyltransferase 1-6, encoded by the *Ugt1a6* gene, important for the conjugation and elimination of toxic compounds, was nearly 2-fold increased in ZF hepatocytes at T0 and significantly decreased after 36h, as compared to the lean, control hepatocytes **(Figure 37I)**.

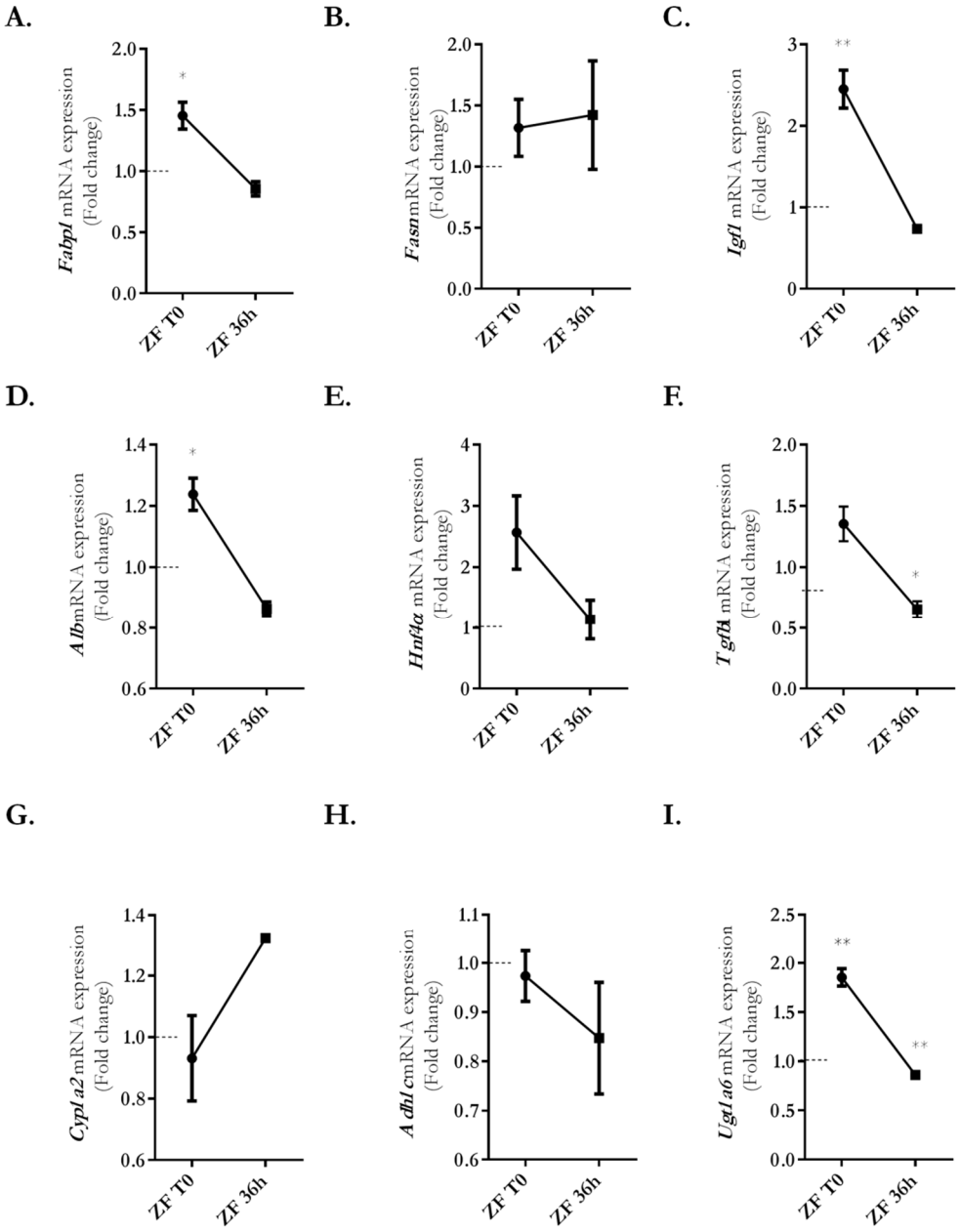

Figure 307 Gene expression changes in Zucker hepatocytes. qPCR analysis of RNA transcripts in ZL- and ZF-hepatocytes, encoding for: **(A)** fatty acid binding protein 4, **(B)** fatty acid synthase, **(C)** insulin-like growth factor 1, **(D)** albumin, **(E)** hepatocyte nuclear factor 4 α, **(F)** transforming growth factor ß, **(G)** cytochrome 1a2, **(H)** alcohol dehydrogenase 1, and **(I)** glucuronosyltransferase 1a6, at T0 and following 36h in culture. Represented are changes in ZF- hepatocytes, normalized to the control, ZL hepatocytes (set as a value of 1). Biological replicate = 1, technical replicate=3. Unpaired student t-test was performed to determine significant differences. Error bars = SD.

The expression of nearly all genes analyzed, except for cytochrome P450 1a2 **(Figure 37G)** and aldehyde dehydrogenase 1 **(Figure 37H),** was upregulated in ZF-hepatocytes at T0 as compared to their control cells. Interestingly, the expression of *Cyp1a2*, encoding for an important enzyme involved in an NADPH-dependant electron transport pathway, increased over time, between T0 and 36 h when compared to ZL hepatocytes **(Figure 37G)**.

5.4.1.3 Insulin Sensitivity of Cultured Zucker Rat Hepatocytes

Insulin regulates the transcription of genes for hepatic glucose and lipid metabolism (Zhang et al. 2011). The insulin sensitivity of ZL- and ZF-hepatocytes in culture upon stimulation with insulin was tested by WB analysis for the expression of the Akt(Ser473), and its major negative inhibitor, the phosphatase and tensin homologue deleted on chromosome 10 (PTEN), both components of the insulin signalling pathway **(Figure 38A)**.

In the case of ZF-hepatocytes, the fold increase in phosphorylation of Akt, although not significant, is higher when compared to the ZL hepatocytes **(Figure 38B)**. It is worth noting however that the total amount of Akt protein in ZF hepatocytes was notably decreased when compared to ZL-hepatocytes **(Figure 38A)**. The increase in the Pten phosphorylation upon insulin was unchanged between ZL- and ZF- hepatocytes **(Figure 38C)**.

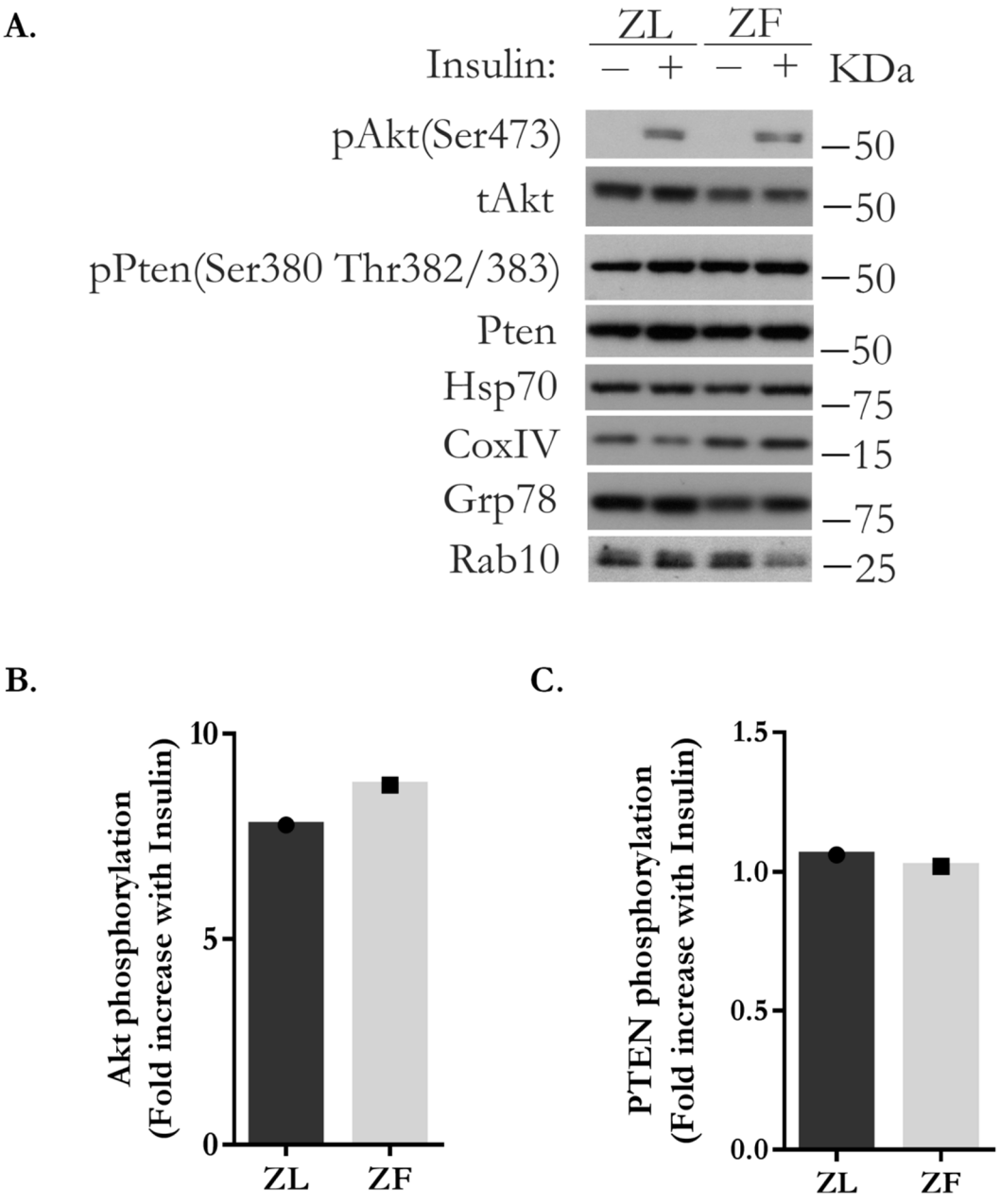

Figure 38 Insulin sensitivity in ZL and ZF hepatocytes. (A) Protein extracts (30 μg) from untreated and insulin treated ZL- and ZF-hepatocytes, were analyzed by WB for the abundance of phosphorylated Akt(Ser473) and phosphorylated Pten, together with their corresponding total proteins, and other control proteins. The percentage of phosphorylation was quantified with respect to the total protein for the **(B)** Akt(Ser473) and **(C)** Pten protein.

Moreover, WB analysis also showed an increase in CoxIV levels in ZF-hepatocytes. Interestingly, upon stimulation with insulin, the expression of Rab10, an important regulator of insulin that controls Glut4 trafficking to the plasma membrane (Karunanithi et al. 2014) was significantly decreased in ZF-hepatocytes after insulin induction.

5.4.1.4 Metabolic differences between Zucker lean and fatty hepatocytes in culture

To further characterize the Zucker primary culture hepatocytes in culture, we sought to measure cellular metabolism and gain insights into the possible metabolic alternations in ZF-hepatocytes. For that, a Seahorse XF analyzer was used to measure the mitochondrial and glycolytic functions of ZL-and ZF-hepatocytes, at 4 h and 24 h of cell culture.

Representative figures of the general scheme for the mitochondrial stress test at 4 h and at 24 h are shown on **Figure 39A** and **Figure 39C** respectively. As indicated by arrows, during the experiment, cells were metabolically challenged with sequential injections of ETC inhibitors, oligomycin, FCCP, and rotenone. We obtained several respiratory parameters including basal respiration, ATP production, proton leak, maximal respiration and spare respiratory capacity of the cell **(Figure 39B)**. It can be clearly seen that ZF- hepatocytes have significantly decreased mitochondrial function as compared to ZL-hepatocytes **(Figure 39A)**. Beyond the basal level changes, ZF-hepatocytes did not respond in the same way when subjected to the mitochondrial stress test. Following the injection of inhibitors, the response of ZF- hepatocytes was reduced, however, the action was delayed as compared with the ZL- hepatocytes, indicating perhaps that cells were more resistant to the action of inhibitors. Highly significant differences were found in most parameters measured **(Figure 39B).**

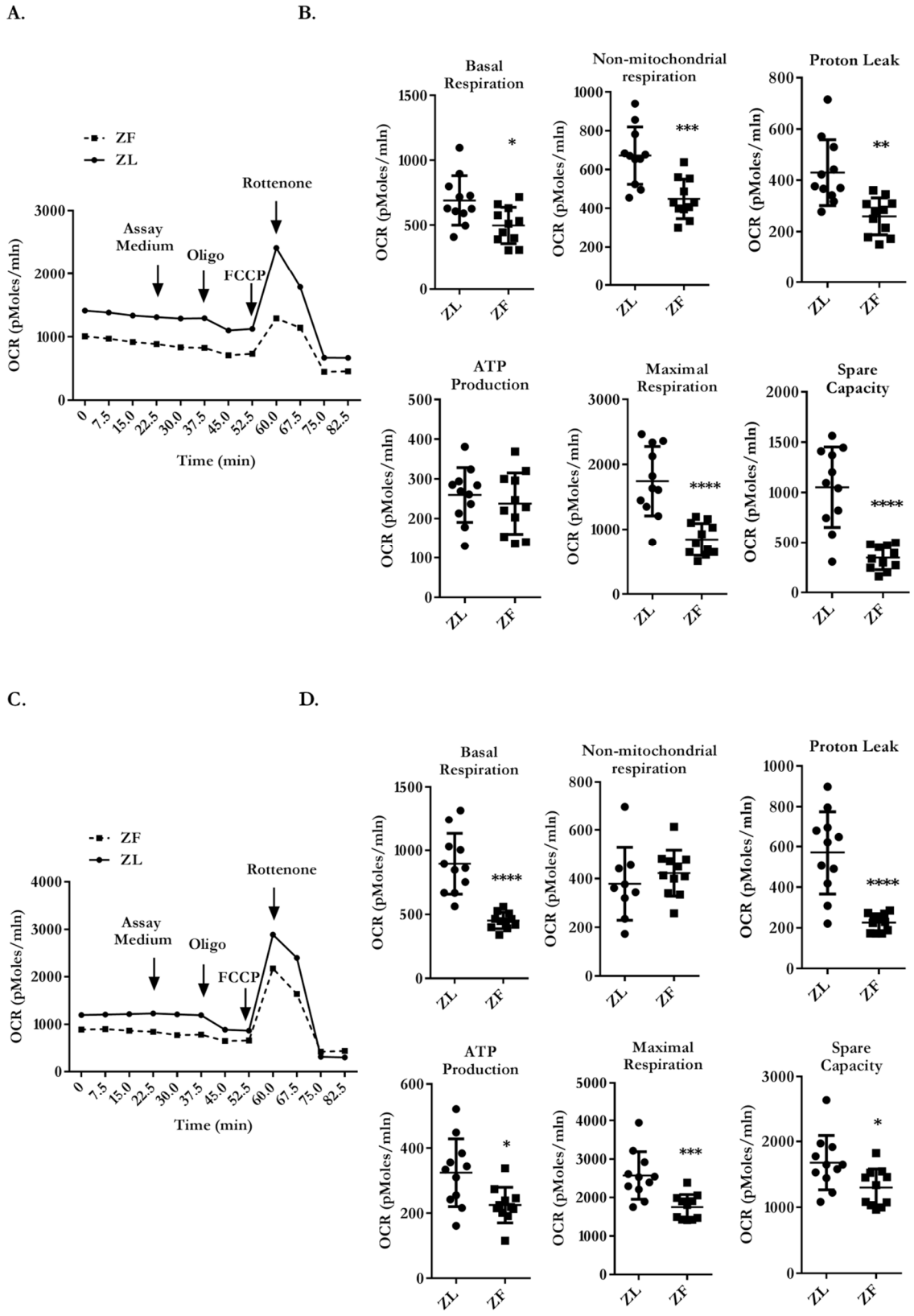
A.
B.
ZF
ZL
Rottenone
Assay Medium
Oligo
FCCP
OCR (pMoles/mln)
Time (min)
Basal Respiration
Non-mitochondrial respiration
Proton Leak
ATP Production
Maximal Respiration
Spare Capacity
C.
D.

Figure 39 Zucker fatty hepatocytes show decreased mitochondrial functions. ZL and ZF-hepatocytes were metabolically profiled using Seahorse XF 24 Analyzer at 4 h and 24 h in culture. **(A)** Representative response curve of the mitochondrial stress test at 4 h. **(B)** Individual parameters of the mitochondrial functions at 4 h. **(C)** Representative response curve of the mitochondrial stress test at 24 h. **(D)** Individual parameters of the mitochondrial stress test at 24 h. Values of individual parameters are represented as OCR following additions of ETC inhibitors such as oligomycin (1 mM), FCCP (300 nM) and rottenone (1 μM). Replicate/condition=11; error bars=SD. The *p* values were denoted as follows: 0.01-0.05=*, 0.01-0.001=**, 0.001-0.0001=***. Unpaired student t-test was performed to determine significant differences.

Maximal respiratory rate, that occurs under conditions of uncoupled respiration following the FCCP injection, and spare capacity were significantly decreased in ZF-hepatocytes **(Figure 39B)**. The ATP production was not significantly different between ZF- and ZL-hepatocytes **(Figure 39B)**. Following 24 h in culture, the mitochondrial response of the ZF-hepatocytes shifts slightly towards the lean counterpart, exhibiting higher response as compared to the 4 h time point **(Figure 39C).** Most notably there was a slight recovery in mitochondrial respiration and spare capacity in ZF-hepatocytes **(Figure 39D)**. The differences however remained pronounced and ZF-hepatocytes maintain decreased mitochondrial function as compared to ZL-hepatocytes. The ATP production dropped slightly in ZF hepatocytes over the time in culture **(Figure 39D)**.

Cells also generate energy in the form of ATP through the conversion of glucose to lactate via glycolytic pathway (Nicholls et al. 2010). Using the Seahorse XF analyzer was used to alongside the mitochondrial functions, also to perform the glycolysis stress test. During the experiment, the first injection of saturating glucose concentration (10 mM) causes the switch towards glycolysis as the main energy-producing pathway **(Figure 40A** and **Figure 40C)**. Released protons cause acidification of the surrounding medium detected as ECAR and reflects the glycolytic response of our Zucker rat hepatocytes.

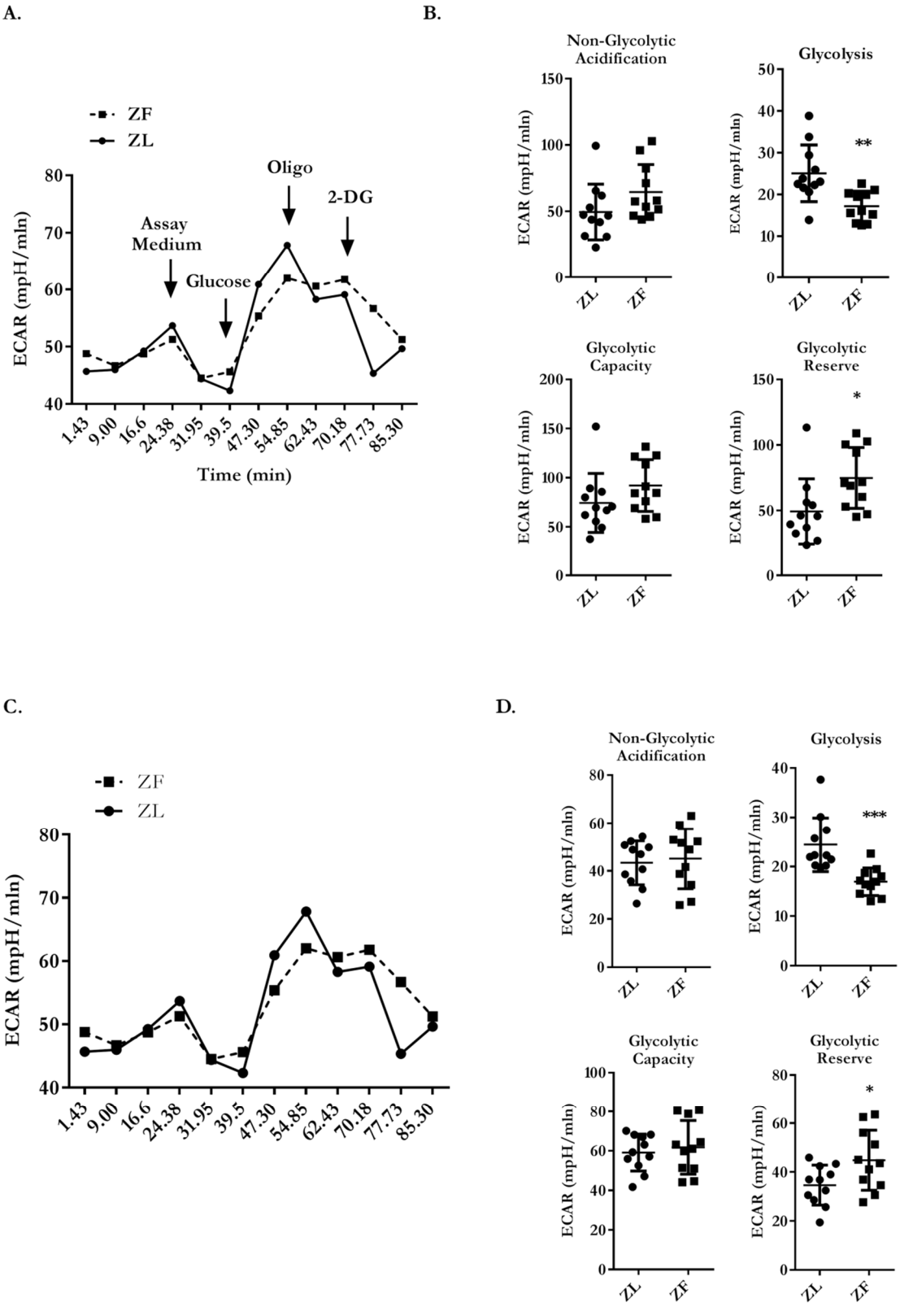
A.
B.
C.
D.
ZF
ZL
Oligo
2-DG
Assay Medium
Glucose
ECAR (mpH/mln)
Time (min)
1.43
9.00
16.6
24.38
31.95
39.5
47.30
54.85
62.43
70.18
77.73
85.30
Non-Glycolytic Acidification
Glycolysis
Glycolytic Capacity
Glycolytic Reserve
**
*
***
ZL
ZF

Figure 40 Zucker Fatty hepatocytes show increased glycolytic capacity. ZL- and ZF-hepatocytes were metabolically profiled using Seahorse XF 24 Analyzer at 4 h and 24 h in culture. **(A)** Representative response curve of the glycolytic stress test at 4 h. **(B)** Individual parameters of the glycolytic functions at 4 h. **(C)** Representative response curve of the mitochondrial stress test at 24 h. **(D)** Individual parameters of the mitochondrial stress test at 24 h. Values of individual parameters are represented as ECAR following additions of ETC inhibitors such as glucose (10mM), oligomycin (1μM) and 2-DG (100mM). Replicate/condition=11; error bars=SD. The *p* values were denoted as follows: 0.01-0.05=*, 0.01-0.001=**, 0.001-0.0001=***. Unpaired student t-test was performed to determine significant differences.

Briefly, following the injection of oligomycin, by shutting down the ATP synthase of the ETC, and with it the ATP production, the cell is forced to generate energy entirely via a less efficient route of glycolysis. Finally, the glucose analog, 2-DG, which competitively occupies the binding sites of the first enzyme in the glycolytic pathway, glucose hexokinase is added. This causes the inhibition of glycolysis and confirms that the ECAR previously measured was in fact due to glycolysis. We found that ZF-hepatocytes had an increased glycolytic reserve and an increasing trend was seen in their glycolytic capacity, when compared to the ZL control cells **(Figure 40B)**.

The general scheme of glycolysis stress test at 4h is shown in **Figure 40A** and at 24h in **Figure 40C**, with sequential injections indicated by arrows. At a basal level, the non-glycolytic acidification was not significantly different between ZL and ZF hepatocytes **(Figure 40B)**. Although, for both cell types, the addition of assay medium cause a slight decrease in ECAR. From the graph in **Figure 40A** glycolysis is also highly increased in ZF-hepatocytes. However, after the injection of glucose, the response of ZL is higher, resulting in an increased glycolysis value following oligomycin injection. Moreover, it is worth noting that, after the first measurement, following the injection of oligomycin, although the response of the ZL-hepatocytes is higher, it plateaus immediately. ZF hepatocytes, did not only not reach the plateau but after two measurements the trend was still

ascending. This is reflected in a higher glycolytic reserve and glycolytic capacity values **(Figure 40B)**. At 24h the graph slightly changed **(Figure 40A)** Non-glycolytic acidification levels out and the decrease in glycolysis in ZF-hepatocytes is greater **(Figure 40B)**. The augmented glycolytic reserve remains.

Lastly, to sum up all independent experiments, comparing ZL and ZF-hepatocyte mitochondrial function and glycolysis, the fold change difference observed in ZF-hepatocytes with respect to its control in the time between 4 and 24 h was plotted **(Figure 41)**. In terms of mitochondrial functions, besides ATP production, which remains unchanged, there is a recovery tendency in all other parameters measured in ZF-hepatocytes between 4 and 24 h in culture **(Figure 41A)**. Substantial recovery of the maximal respiratory and spare capacity by ZF-hepatocytes is observed. The opposite effect can be seen for the measure of glycolytic functions.

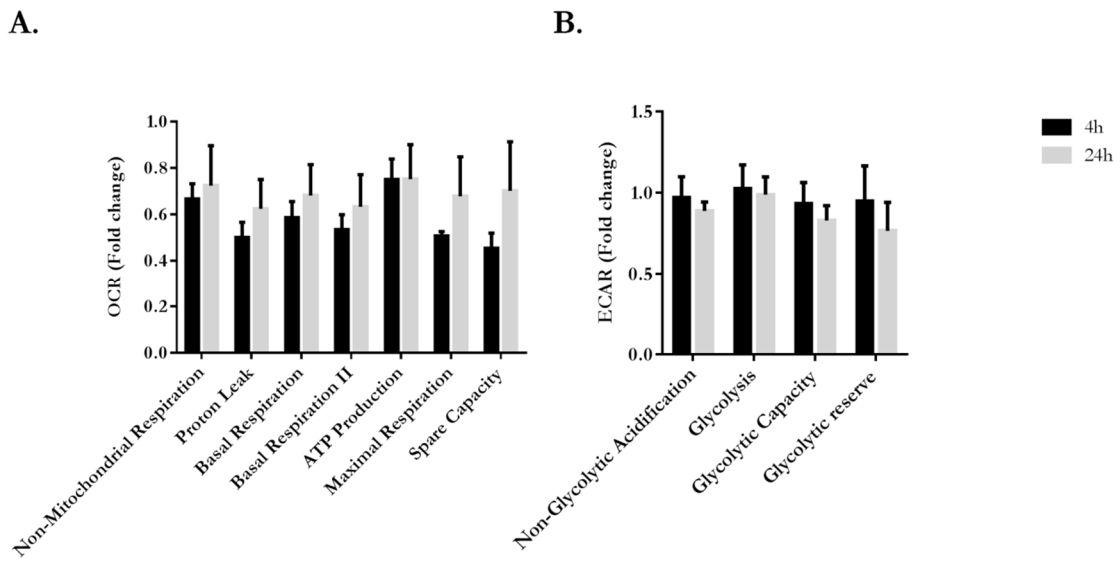

Figure 41 Fold change in OCR and ECAR in ZF hepatocytes. Fold change difference in ZF-hepatocytes compared to the ZL control hepatocytes in individual parameters of the **(A)** Mitochondrial stress test (OCR), and the **(B)** Glycolysis stress test (ECAR). Error bars represented as SD; n=4.

There was a decrease in fold change difference in all parameters related to cellular glycolytic functions at 24 h **(Figure 41B)**. Our results indicate that metabolically, ZL and ZF-hepatocytes are significantly different. ZF-hepatocytes exhibited a significant decrease in all mitochondrial functions, most notably in maximal respiration and spare capacity. Interestingly, following 20 h of additional cell culture, there was some recovery in these parameters, mostly in spare capacity. Moreover, at 20 h there was a significant decrease in ATP production by ZF-hepatocytes.

5.4.2 Characterization of Zucker Rat Hepatocyte-derived EVs

5.4.2.1 Zucker fatty hepatocytes secrete distinct population of EVs in terms of protein concentration as well as composition

Having performed the initial characterization of the primary Zucker rat hepatocytes, we proceeded into the isolation and analysis of their secreted-EVs. The first report on hepatocyte-derived EVs was published in 2008 by Conde-Vancells *et al.* (Conde-Vancells et al. 2008) with detailed ultrastructural and proteomic characterization of EVs isolated from the conditioned medium of the cultured primary rat hepatocytes as well as hepatic cell lines. In the current study, for the first time, Zucker rat hepatocytes, obtained by hepatic perfusion of fatty (*fa/fa*) and lean (*Fa/+*) matched Zucker rat livers, were cultured for subsequent isolation of EVs from the conditioned medium.

A plethora of different methods is currently available for the quantification of EVs in a liquid sample, based on diverse structural parameters, or the presence of a specific protein marker. Choosing the appropriate quantification technique is vital for further downstream applications. Here, the protein concentration of the EV-samples was determined by Bradford assay and the result of the quantification

from 12 independent preparations is shown in **Figure 42A**. Values obtained (µg/µl) were normalized by the total number of cells plated in each preparation. Results indicate that the mean concentration (µg/µl) was 3.9 (SD=1.4) and 6.8 (SD=3.3) in ZL and ZF respectively, across 12 independent EV preparations. Nearly a two-fold increase in total protein concentration in ZF-EV sample was observed as compared to their lean counterparts. Following normalization, this result was maintained with 8.3×10^{-09} ($SD=3.4^{-09}$) and 1.90×10^{-08} ($SD=1.2^{-08}$) protein (µg/number of cells) in ZL and ZF-EV samples respectively per number of cells plated. A statistically significant increase in total protein concentration was found in the ZF-EVs sample, despite a degree of variability **(Figure 42A)**.

To assure the accuracy of the Bradford measurements, the total protein concentration in 6 independent preparations was determined simultaneously by Bradford and BCA protein assay **(Figure 42B)**. Results obtained by Bradford and BCA were comparable between the 6 independent samples assayed. Slight differences were seen in highly concentrated samples, however remained within the same range **(Figure 42A)**. Relying on this result, Bradford assay was used to determine protein-loading amounts for the rest of the study.

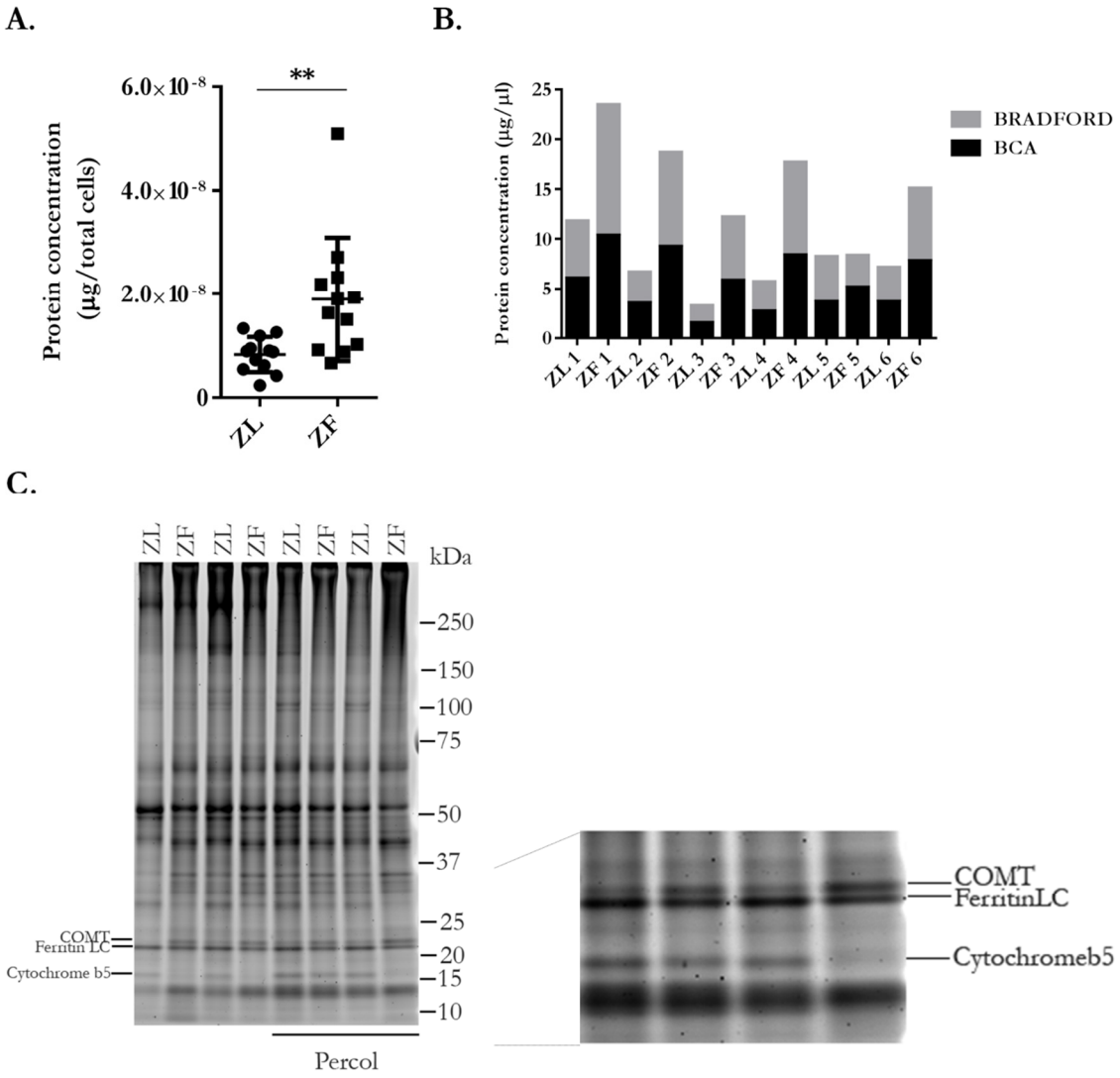

Description	Peptides	Unique peptides	MW [kDa]	Score
Catechol O-methyltransferase (COMT)	15	15	29.57827	1279.85
Ferritin Light Chain	11	11	20.73569	875.19
Cytochrome b5	3	3	15.3456	537.26

Figure 42 Determination of protein concentration in Zucker rat hepatocyte-derived EVs. (A) The protein concentration in the EV samples was measured by Bradford. Represented are normalized values to the total amount of cells plated/preparation; n=12. **(B)** Comparison of protein concentration measurement by Bradford and BCA; n=6. **(C)** Sypro Rubi staining of the gel loaded with 2 µl of Zucker rat hepatocyte-secreted EVs; n=4.

Differentially expressed bands are indicated. **(D)** Identity of differentially expressed bands; n=3. Error bars = SD. Unpaired student t-test was performed to determine significant differences.

Additionally, in order to validate the accuracy of Bradford protein quantification, 2 µg of ZL and ZF-EVs were subjected to SDS-PAGE, followed by a SYPRO Ruby protein gel staining of separated proteins **(Figure 42C)**. EV samples, from 4 independent preparations, two of which were isolated from hepatocytes treated with Percoll density gradient centrifugation, as indicated on **Figure 42C** were assayed. The analysis revealed no significant differences in protein loading between samples as judged by the intensity of the staining. Interestingly, some differentially expressed band pattern between ZL- and ZF-EVs could be identified, notably in the low size range. Indicated bands were cut and analyzed by MALDI-MS with the pool of three selected samples for each band was used for proteomic analysis. Resulting proteins were identified according to the highest protein score, which is the sum of the ion scores of all peptides identified, and the highest number of peptide spectrum matches (PSM) for that protein. Selected proteins, were identified as Catechol-*O*-methyltransferase (COMT), Ferritin light chain (Ferritin-LC) and Cytochrome b5 (**Figure 42D)**.

Interestingly, Comt was more abundant in ZF-EVs. COMT is an enzyme involved in the degradation of catecholamine transmitters such as dopamine, epinephrine and norepinephrine as well as the metabolism of endogenous substances and catechol drugs with the liver being the main metabolic site. The expression of the other two proteins, Ferritin-LC and cytochrome b5, was decreased in ZF EVs. Interestingly, very early studies have associated cytochrome b5 to liver microsomes and that it acts as an intermediary electron carrier, and takes part in hepatic microsomal fatty acid desaturation (Oshino et al. 1971).

Our results show that ZF-EVs have higher protein content when compared to ZL-EVs. Moreover, we identified some important differences in the protein composion between ZL- and ZF-EVs.

5.4.2.2 Ultrastructural comparison of ZL and ZF secreted EVs

Isolated EVs were identified and purity verified by cryo-EM analysis. Representative electron micrographs show that in general, most particles visualized in culture supernatant of Zucker rat hepatocytes were round, typically translucent and enclosed in a visible, electron dense lipid bilayer **(Figure 43A)**. Most vesicles isolated by differential ultracentrifugation were consistent with exosomal size vesicles. However, cryo-EM also revealed more structural details and considerable morphological heterogeneity. Apart from round vesicles, complex triple vesicles with smaller vesicles inside a larger one, all translucent and carrying a lipid membrane as well as incompletely closed vesicle were observed. Varying thickness of the lipid bilayer was also noted, with smaller vesicles having a slightly thicker membrane. Moreover, some vesicles were electron dense indicative of a lumen filled with cargo.

Electron dense round structures lacking the membrane were not considered true EVs. The presence of some impurities in the EV samples that could correspond to protein aggregates, were also observed. The majority (>90%) of particles were below 300 nm in diameter, with the main population at around 100-200 nm **(Figure 43B)**. The vesicle count was 166×10^{10} per millilitre in ZL sample and 630×10^{10} in ZF-EV sample. These significant differences in concentration of vesicles were seen across specific size groups with 50% increase in the number of smaller vesicles up to 50nm. 11% of the total population in both samples occupy a size between 50-100 nm. Moreover, a 4% decrease, from 28%-24% was seen in 100-150 nm population. Statistically significant decrease was seen in the subsequent 150-200 size range. On the other hand, a statistically significant increase in larger vesicles between 300-350 nm was seen in ZF-EV samples. Furthermore, only about 1% of the total population was composed of larger vesicles up to 500 nm. NTA indicates a very slight decrease in the total mean size, however the size difference was not significant **(Figure 43D)**. In terms of particle concentration there was a significant 3.5-time increase in ZF derived EVs **(Figure 43C)**.

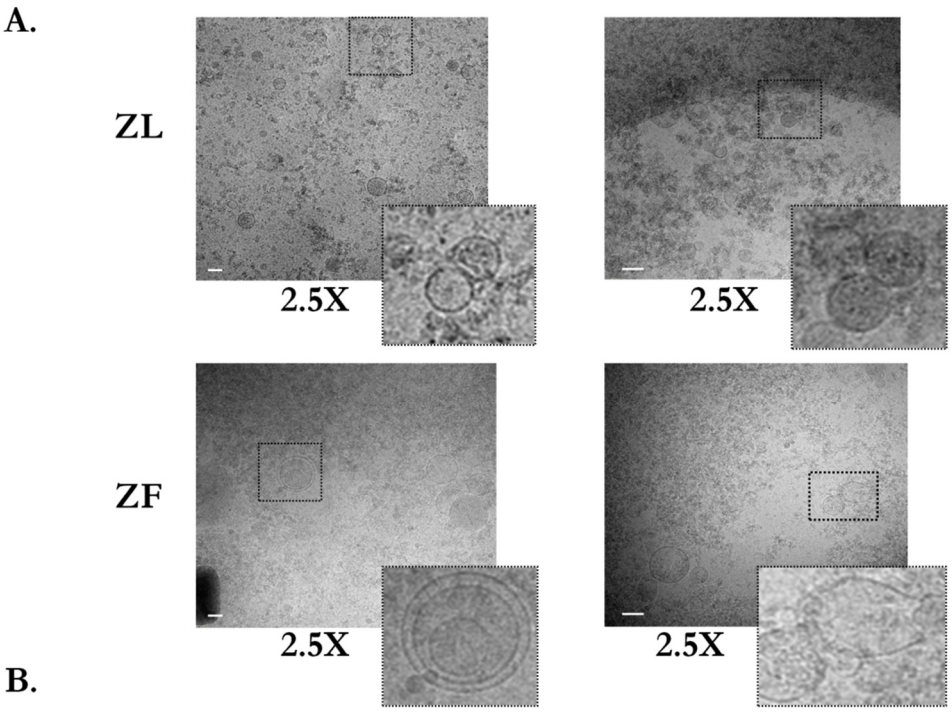
A.
ZL
2.5X
2.5X
ZF
2.5X
2.5X

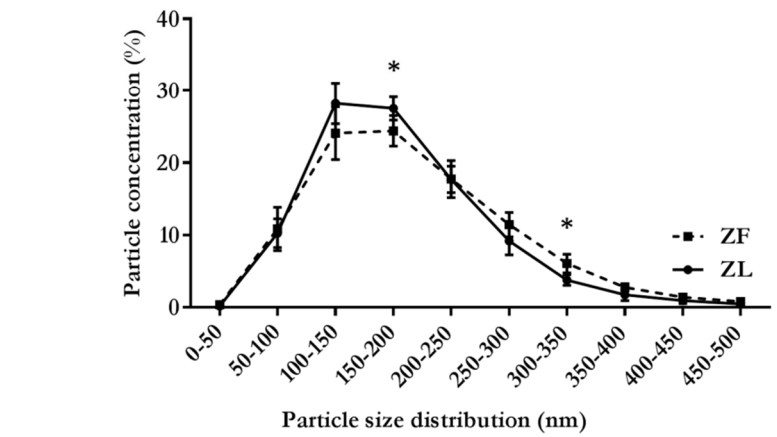
B.
Particle concentration (%)
40
30
20
10
0
*
*
ZF
ZL
0-50
50-100
100-150
150-200
200-250
250-300
300-350
350-400
400-450
450-500
Particle size distribution (nm)

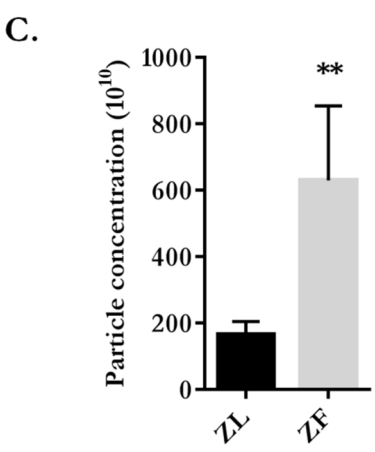
C.
Particle concentration (10^10)
1000
800
600
400
200
0
**
ZL
ZF

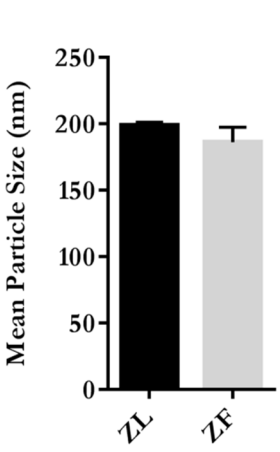
D.
Mean Particle Size (nm)
250
200
150
100
50
0
ZL
ZF

Figure 43 Ultrastructural characterization of EVs secreted by Zucker rat hepatocytes. Ultrastructural and biochemical characterization of EVs isolated from conditioned medium of ZL and ZF hepatocytes. **(A)** Cryo-EM analysis, two electron micrographs are shown/condition, size bar=100nm, inserts magnified 2.5X. **(B)** Size range distribution. **(C)** Particle concentration (10^{10}). **(D)** Particle mean size; n=4. Error bars=SD. The *p* values were denoted as follows: 0.01-0.05=*, 0.01-0.001=**, 0.001-0.0001=***. Unpaired student t-test was performed to determine significant differences.

5.4.2.3 Protein composition analysis

Protein expression analysis of ZL and ZF-derived EVs was carried out to determine whether vesicles identified by cryo-EM and NTA, carried exosome-associated markers. Three independent preparations of EVs along with their corresponding cell extracts was separated by SDS-PAGE and immunoblotted with antibodies for specific EV markers **(Figure 44)**. Results show that vesicles isolated from conditioned medium of Zucker rat hepatocytes highly resembled exosomes in their protein composition since they were enriched in several exosomal markers such as Cd81, Cd63, Tsg101, and Aip1/Alix. However, the amount of protein expressed varied significantly between the ZL and ZF samples. The tetraspanins Cd63 and Cd81 were very abundant in ZL-EVs and barely detectable in ZF-EVs. The same trend of expression was seen in whole cell lysates, however with detectable expression of both markers in ZF whole cell lysates. ESCRT machinery associated proteins, Tsg101 and Alix were both found in Zucker rat hepatocyte derived- EVs. A comparable amount of AIP1 was found in whole cell lysates as in EVs. The expression of both markers was down regulated in ZF whole cell lysates as well as in EVs. Moreover, Flotillin1, a common lipid raft marker widely considered to be an exosomal marker was again highly decreased in ZF-EVs.

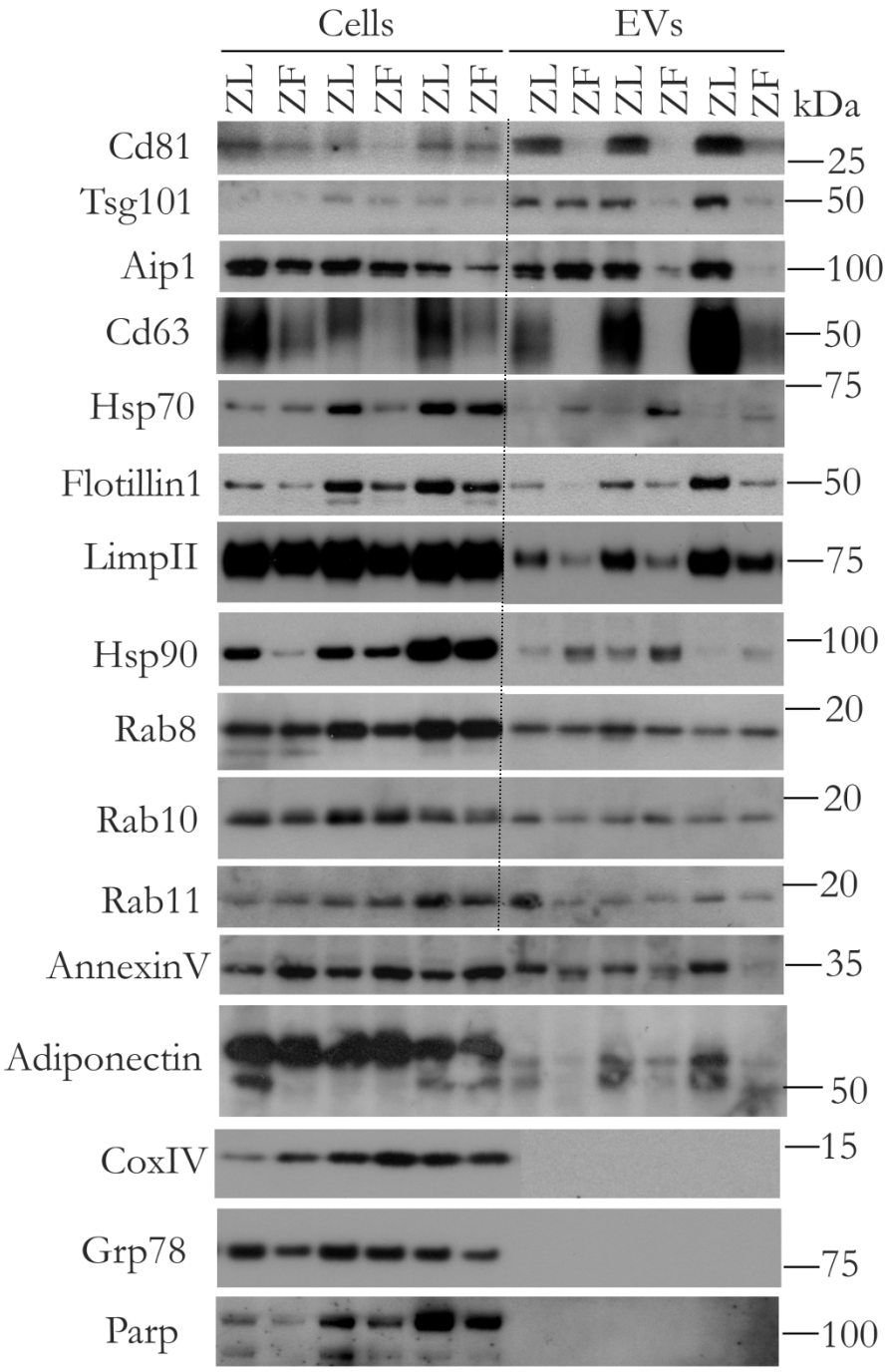

Figure 44 Protein profiling of EVs secreted by primary hepatocytes from Zucker rats. Whole cell lysates (10 μg) of Zucker rat hepatocytes, ZL and ZF, with their corresponding EVs (5 μg) were analyzed by WB, using antibodies against several markers of exosomes (Cd81, Tsg101, Aip1, Cd63, Hsp70, Hsp90, Flotillin1) microvesicles (AnnexinV), and markers of other cellular components such as ER (Grp78), mitochondria (CoxIV), lysosomes (LimpII) and G-proteins (Rab8, 10 and 11) and adiponectin. Representative figure; n=4.

Along with the typical exosome-related markers, we detected few members of small GTPases proteins. Rab8 was highly expressed in cells and clearly less protein was found in ZF hepatocytes as compared to the lean control, across all three preparations. The same situation was found for Rab11.

The only proteins in the above panel, which were found to be more abundant in ZF-EVs as compared to ZL-EVs, were heat shock family member proteins, Hsp70 and Hsp90. Interestingly, when comparing their expression in cell lysates and in secreted EVs, the pattern was reversed. As more protein was being secreted out via EVs, the cellular abundance was effectively decreasing, which could be an indication of the regulated cargo sorting. Moreover, LimpII was found abundant in Zucker rat hepatocytes, with decrease expression in ZF-hepatocytes. In addition, LimpII was associated to vesicles secreted by Zucker hepatocytes, with a significant reduction in ZF-EVs.

Protein expression analysis has revealed very significant differences in the composition of EVs secreted by ZL- and ZF-hepatocytes. While investigating the lipid content of Zucker hepatocyte-EVs, we were also interested in the expression of adipocyte-related proteins, more importantly, adiponectin, a hormone affected by obesity. The adipocyte complement-related protein of 30 kDa (Acrp30) was discovered to be produced by adipocytes during identification of adipocyte differentiation genes (Combs & Marliss 2014). The expression of adiponectin was reported to be decreased in adipose tissue of obese (*ob/ob*) mice as well as in fat samples from obese human individuals, with no other adipose-specific genes being unaffected by obesity (Hu et al. 1996). In the liver, adiponectin acts through the activation of 5-AMP-activated protein kinase and peroxisome proliferator-activated receptor-α pathways (Polyzos et al. 2010). Adiponectin has been shown to suppress hepatic glucose production, therefore the reduction in circulating adiponectin in T2DM contributes to the increased glucose production leading to fed and fasted hyperglycemia (Combs & Marliss 2014). The effect of high insulin and low adiponectin signalling in humans is

characteristic of fatty livers (Combs & Marliss 2014). Furthermore, adiponectin levels can serve as a guide in predicting grade of hepatic steatosis (Polyzos et al. 2010).

Adiponectin was highly abundant in Zucker hepatocytes as shown by WB analysis **(Figure 44)**, with no clear differences between ZL- and ZF- hepatocytes. However, surprisingly adiponectin was also found to be associated to Zucker-EVs with significantly reduced expression in ZF-EVs. Representing the metabolic phenotype of fatty liver and adiponectin reduction described in obesity

Annexins are a family of cytosolic proteins that have phospholipid-binding domains, and associate with intracellular membranes in a calcium dependant manner. Several annexins were found to be involved in membrane-fusion events between intracellular compartments (Théry, Zitvogel, et al. 2002), and have been recognized markers of microvesicles due to their membrane origin. The expression of AnnexinV was confirmed in Zucker rat hepatocyte secreted EVs. The abundance in whole cell lysates was clearly increased in ZF-hepatocytes as compared to the control **(Figure 44)**. Reverse expression pattern was seen in EVs, with decreased amount of AnnexinV being secreted in EVs. Finally, the protein markers for other subcellular compartments such as mitochondrial CoxIV and ER-associated Grp78 were absent in EV preparations discarding the possibility of contamination with cellular organelles in our preparations. Interestingly, both proteins were differentially expressed in ZL and ZF-hepatocytes. The amount of CoxIV was higher in ZF hepatocytes however Grp78 was decreased as well as Parp protein when compared to lean. Lastly, some degree of cleaved Parp was detected, more in ZL hepatocytes, however it was not significant. This result indicates a low degree of apoptosis and that existing apoptosis was not significantly different between both groups.

Our results show that ZF-EVs have significantly higher concentration of proteins. Moreover, there is a significant increase in the concentration of particles in ZF-EV samples together with a decrease in all exosomal markers, except Hsp's. These changes could be the reflection of the metabolic state of the cell.

5.4.2.4 Distribution of protein markers on a density gradient

The differential expression of most markers as seen in the previous section suggest that ZF-hepatocytes could secrete a different population of EVs or the secretion of a specific type of EVs is enriched in ZF- in comparison to ZL-samples.

To shed some light on this idea, we explored one of the hallmarks of exosomes as vesicular carriers, which is, their floatation in a sucrose gradient. Specifically, exosomes have been determined to float at a density that ranges from 1.13 to 1.21 g/ml. A study by Conde-Vancells and co-workers determined that purified exosomes released by primary hepatocyte float at a density of approximately 1.21 g/mL in a continuous sucrose gradient, which remain in the exosome density range as described for other cell types (Conde-Vancells et al. 2008). We analysed the buoyant density of vesicles to verify whether EVs purified from primary Zucker rat hepatocytes also float at similar density, using iodoxanol, OptiPrep^{TM} in the velocity gradient. 250 µg of EVs were separated on a 5-40% density gradient into 12, 1 ml fractions. Subsequent WB analysis indicated that Zucker rat hepatocyte secreted EVs, ZL and ZF, were enriched at a buoyant density of 1.16 g/ml, based on the presence of markers such as Cd63, Rab8 and ApoE **(Figure 45)**. The presence of Cd63 and Rab8 was detected in two distinct fractions at a density of 1.16 and 1.19 g/ml. In ZF-EVs, Rab8 enriched fractions were at 1.19 g/ml, however for ZL EVs it was at 1.16 g/mL indicating the existence of a distinct population of EVs between ZL and ZF secreted EVs.

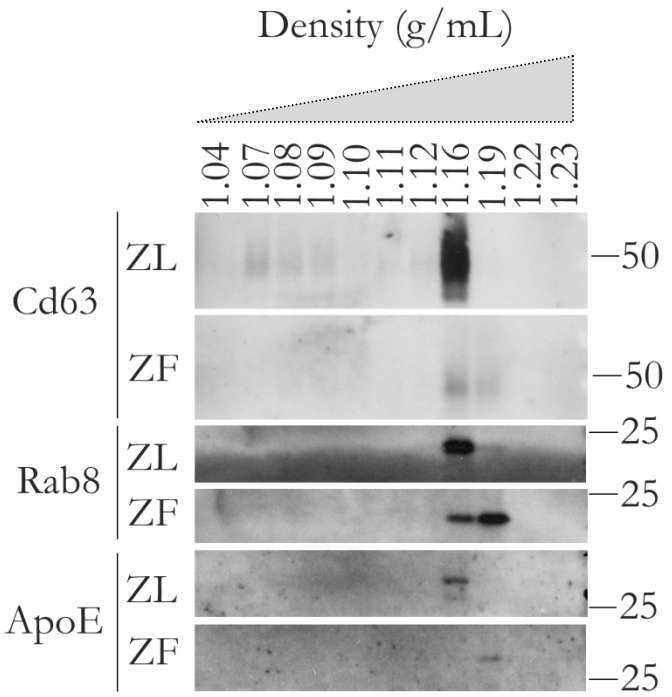

Figure 45 Zucker rat hepatocytes-derived EVs float at a density characteristic of exosomes. The density of EVs secreted by Zucker rat hepatocytes, ZL and ZF, was determined by floatation on an OptiPrep™ density gradient. Samples were collected from 12, 1 ml, fractions following 16 h ultracentrifugation at 32,000 rpm. Fractions were analyzed by WB using antibodies against the indicated proteins, Cd63, Rab8 and ApoE. Starting material of 250 μg of EVs.

The same enrichment pattern was seen for the ApoE protein; however, it was associated with a single fraction. In terms of the expression of the tetraspanin Cd63, the abundance in ZF-EVs was markedly decreased, as previously shown **(Figure 45)**. Moreover, the pattern of separation across the different fractions was different for both samples. In ZF-EVs, Cd63 and Rab8 were present in two fractions the 1.16 and 1.19 g/ml, while Cd63 was enriched in the lower density fraction, Rab8 was enriched in the higher density fraction. In addition, the presence of Cd63-positive vesicles, floating at lower densities, between 1.07 and 1.12 g/ml was detected in ZL-EVs.

5.4.2.5 LC-MS/MS analysis

We wanted to obtain further insight into the nature of EVs secreted by steatotic Zucker hepatocytes and for that we performed a mass spectrometry proteomic analysis. Mass spectrometry is a powerful technique for the identification, quantitation, and characterization of proteins. The sample to be analyzed is subjected to enzymatic digestion with a protease such as trypsin to generate a heterogenous mixture of peptides. The peptides obtained are subsequently separated by liquid chromatography coupled to mass spectrometry (LC-MS) (Schmidt et al. 2014). Tandem MS/MS provide information about the sequence of the peptide, which is key to their identification.

Proteomic analysis of EVs from many different sources had shown the presence of vesicle-specific as well as cell-type specific proteins. As already mentioned, the very first report with a comprehensive proteomic analysis of EVs secreted by primary hepatocytes as well as hepatic cell lines, was published in 2008 by Conde-Vancells and co-workers (Conde-Vancells et al. 2008). The analysis resulted in the identification of 251 proteins including EV-specific markers such as tetraspanins, Cd81 and Cd63, endosomal pathway related proteins, annexin and GTPases. Moreover, hepatocyte specific proteins were also detected, asialoglycoprotein receptor and members of P450 family of enzymes.

The aim of the current study was to profile EVs isolated from conditioned medium of Zucker rat hepatocytes. The method chosen for our analysis was shotgun approach where no prior knowledge of the peptides present in the sample is required to define peptide selection criteria during the LC-MS analysis. Liquid Chromatography-MS/MS of protein quantification analysis of four replicates for each group (ZF vs ZL) yielded a total of 438 proteins, 137 being upregulated in ZF-EVs and 301 were downregulated in ZF-EVs **(Figure 46A)**.

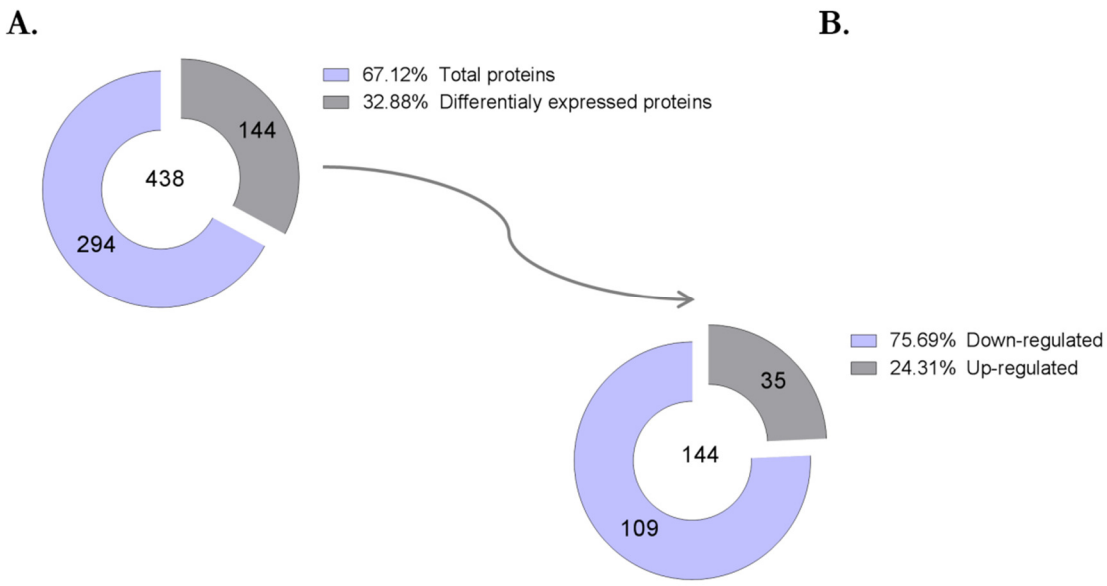

Figure 46 Proteomic analysis of Zucker rat hepatocyte-secreted EVs. (A) Comparison of proteins identified in LC-MS/MS analysis. A total of 438 proteins were identified, among which 144 were differentially expressed proteins (DEPs), between ZL- and ZF-EVs. **(B)** Up- and down-regulated DEPs in ZF-EVs. Analysis was carried out on 4 independent biological replicates.

Among these 438 proteins, 144 (33% of the total) were categorized as statistically significant ($p < 0.05$), differentially expressed proteins (DEPs) **(Figure 46B)**. In turn, among DEPs, 35 proteins (24.3%) occupy the category of significantly up-regulated in ZF EVs and the remaining 109 were down-regulated. A full list of DEPs identified for ZL- and ZF-EVs are available in the supplementary information **(Table 16 and 17)**.

Table 8 Gene ontology cellular component classification of all proteins detected in Zucker rat hepatocyte derived-EVs

PANTHER GO-Slim Cellular Component			
Rattus norvegicus-REFLIST			
Analysis Type:	PANTHER Overexpression Test		
Analysed List:	Upload_1 (Rattus norvigcus)	Fold change	*p* value
Bonferroni correction:	True		
Bonferroni count:	61		
Cytosol (GO:0005829)		4.59	5.67E-21
Cytoplasm (GO:0005737)		2.4	8.81E-19
Intracellular (GO:0005622)		1.83	6.65E-15
Ribosome (GO:0005840)		4.76	2.62E-14
Ribonucleoprotein complex (GO:0030529)		3.23	5.93E-10
Integral to membrane (GO:0016021)		<0.2	1.27E-09
Membrane (GO:0016020)		0.22	2.45E-08
Macromolecular complex (GO:0032991)		2.04	5.76E-08
Organelle (GO:0043226)		1.72	9.84E-07
Cell part (GO:0044464)		1.44	2.25E-06
Plasma membrane (GO:0005886)		0.31	4.42E-05
Tubulin complex (GO:0045298)		16.65	1.32E-04
Actin cytoskeleton (GO:0015629)		3.41	1.73E-02
Microtubule (GO:0005874)		4.05	2.93E-02
Vesicle coat (GO:0030120)		6.4	7.62E-02
Nucleoplasm (GO:0005654)		<0.2	5.61E-01
Extracellular space (GO:0005615)		0.35	5.90E-0.1
Cytoskeleton (GO:0005856)		1.87	8.30E-0.1
Endosome (GO:0005768)		0.55	1.00E+00
Extracellular region (GO:0005576)		0.65	1.00E+00

We were then interested whether there was a specific enrichement in proteins related with extracellular environment, considering all proteins identified in Zucker rat hepatocyte-derived EVs. We therefore performed the PANTHER Gene Ontology (GO) Cellular component analysis. The identified cell components are listed in **Table 8**. The analysis revealed that most of the proteins identified have cytoplasmic and plasma membrane localization.

Further, we began interpreting the differentially expressed proteins, again using GO classification. The total 137 up-regulated proteins and 301 down-regulated proteins in ZF-EVs were categorized according to the molecular function (**Figure 47A)**, the biological processes **(Figure 47B)** and the cellular compartment **(Figure 47C)**.

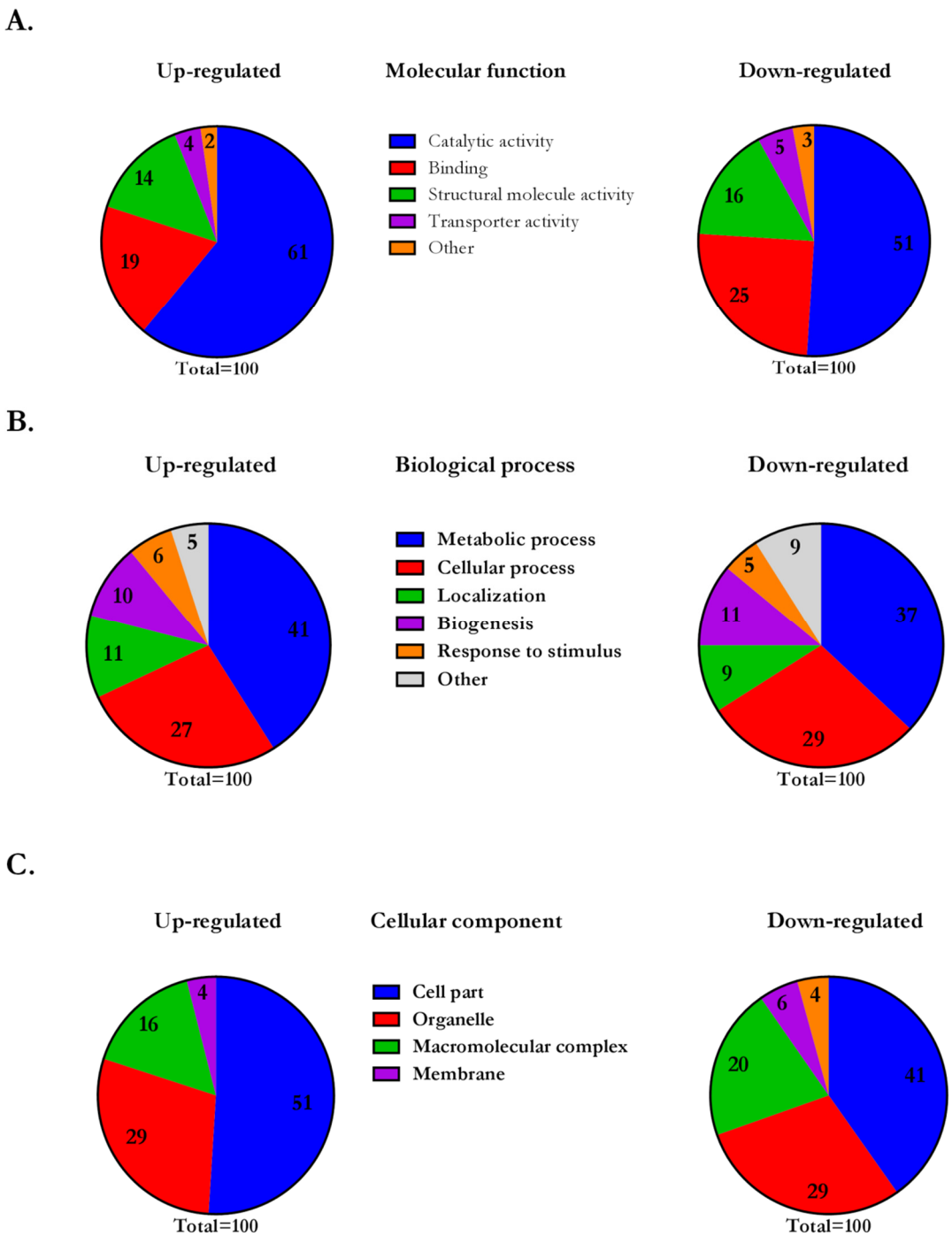

Figure 47 Gene ontology classification of up- and down-regulated proteins identidied in ZF-EVs. Up (137) and down-regulated (301) proteins found ZF-EVs were classified according to the **(A)** molecular function, **(B)** biological process, and **(C)** cellular compartment categories. Data is expressed in percentages.

Results were presented as pie diagrams and percentage distribution was annotated for each individual process. Although, twice as many proteins were found to be down-regulated, as much as 10% of up-regulated proteins were categorized as having catalytic activity. Moreover, in terms of biological processes, an increase in proteins associated with metabolic processes was seen **(Figure 47B)**. More importantly, the analysis revealed, that the major differences between the content of up and down-regulated proteins identified in ZF-EVs lies in enrichment of DEPs related to metabolic processes. Nearly 60% of all DEPs up-regulated in ZF-EVs were implicated in general metabolic processes, which was a very significant difference in biological processes, when considering that 2.5-times less total DEPs were detected **(Figure 48)**.

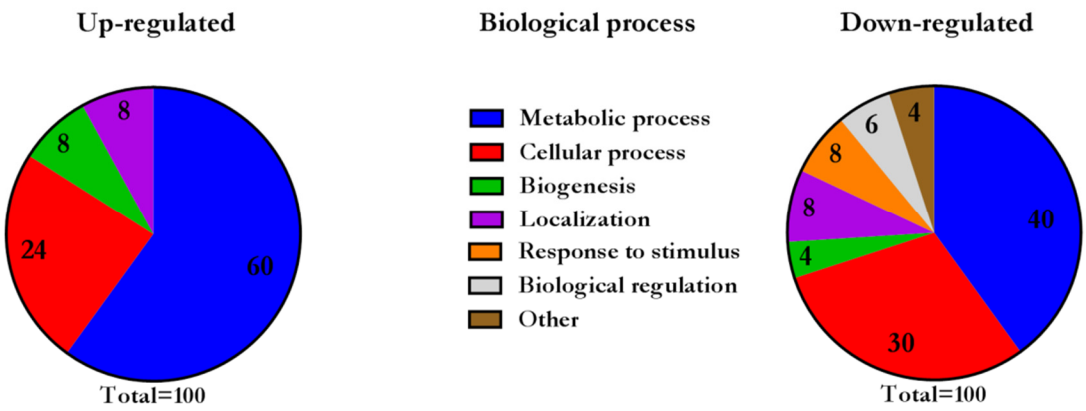

Figure 48 Proteins related with metabolic processes are enriched in ZF-EVs. GO gene ontology classification of up (35) and down regulated (109) DEPs in ZF EVs in category of biological processes.

5.2.2.5.1 Classification of proteins up-regulated in ZF-EVs

Functional annotation of identified proteins was done with GO enrichment analyses using the Database for Annotation, Visualization and Integrated Discovery (DAVID) online tool to highlight the most relevant GO terms associated with up- and down-regulated DEPs in ZF-EVs.

In terms of ZF-EVs, a specific set of proteins was identified. The majority, 75% of all upregulated DEPs in ZF-EVs were found to be enzymes involved in variety of metabolic processes **(Table 9)**. Moreover, our results indicate that the most significant active pathways enriched in ZF-EVs were the energy producing pathways, namely pentose phosphate pathway and glycolysis **(Table 10).** The two most differentially expressed proteins in ZF-EVs were 6-phosphogluconate dehydrogenase (6PGD) and glucose-6-phosphate 1-dehydrogenase (G6PD), both enzymes having their role in oxidative phase of the pentose phosphate pathway (PPP). G6PD is responsible for the first step in the conversion of glucose to ribose-5-phosphate, a nucleotide component, making NADPH. However, 6PGD, an oxidative carboxylase that catalyses the decarboxylating reduction of 6-phosphogluconate into ribulose 5-phosphate in the presence of NADP. The second most highly represented pathways were glycolysis with NADP-dependant malic enzyme (MAOX) and ATP-citrate synthase (ACLY) being highly represented in ZF-EVs. MAOX generates NADPH for fatty acid and cholesterol biosynthesis (Al-Dwairi et al. 2014). Moreover, rat liver malic enzyme plays an important role in lipogenesis (Morioka et al. 1988). It is a major lipogenic enzyme that catalyzes the oxidative decarboxylation of malate to pyruvate and reduces NADP+ to NADPH, which is used in fatty acid and cholesterol biosynthesis, especially in the rate limiting steps catalyzed by fatty acid synthase (Al-Dwairi et al. 2014). ATP-citrate synthase is the primary enzyme responsible for the synthesis of cytosolic acetyl-CoA. A central role in several important biosynthetic pathways of *de novo* lipid synthesis and cholesterogenesis. Lastly, phosphoglycerate kinase 1 (Pgk1), the first ATP-generating enzyme in the glycolytic pathway that catalyzes the transfer of the high-energy phosphate from

the 1 position of 1,3-diphosphogly- cerate (1,3-BPG) to ADP, which leads to the generation of 3-phosphoglycerate (3-PG) and ATP of 1,3 diphosphoglycerate to 3-phosphoglycerate (X. Li et al. 2016). In tumours it has been shown mitochondria-translocated PGK1 functions as a protein kinase to coordinate glycolysis.

Hepatocytes play an essential role in carbohydrate and lipid metabolism. Most processes of lipid metabolism are predominantly performed in the liver, including synthesis of lipoproteins, fatty acids, and triglycerides. As identified by proteomic analysis, the second most enriched group of up-regulated proteins found in ZF EVs were associated with lipid metabolism **(Table 11)**. In that group, the most highly enriched protein was the proinflammatory cytokine, the microphage migration inhibitory factor (MIF), which has been implicated in obesity, insulin resistance, T2DM and associated hepatic pathologies. Its role in the development of hepatic steatosis was indicated (Morrison & Kleemann 2015). Moreover, hepatic lipogenic gene expression was significantly lower in the absence of microphage migration inhibitory factor (Finucane et al. 2014). Furthermore, enzymes crucial for the catalysis of long-chain fatty acid formation such as fatty acid synthase (Fas) and acetyl-CoA carboxylase 1 (Acaca) were also highly up-regulated in ZF-EVs. Moreover, the acyl-CoA synthase 5 (Acsl5), which activates long-chain fatty acids for the synthesis of cellular lipids as well as degradation via beta-oxidation and retinaldehyde dehydrogenase 1 has been shown to coordinate hepatic gluconeogenesis and lipid metabolism (Kiefer et al. 2012).

Table 9 Majority of up-regulated proteins in ZF-EVs are enzymes.

Mapped ID	Catalytic activity	Fold change	ANOVA (*p*value)
6PGD_RAT	6-phosphogluconate dehydrogenase, decarboxylating	3.5	0.00000356
MIF_RAT	Macrophage migration inhibitory factor	1.9	0.000123
MAOX_RAT	NADP-dependent malic enzyme	7.2	0.000209
G6PD_RAT	Glucose-6-phosphate 1- dehydrogenase	15.5	0.000605
ACYL_RAT	ATP-citrate synthase	3.9	0.000618
AL1A1_RAT	Retinal dehydrogenase 1	3.6	0.001163
FAS_RAT	Fatty acid synthase	2.5	0.002199
ST2A2_RAT	Alcohol sulfotransferase A	5.1	0.003782
EF1A1_RAT	Elongation factor 1-alpha 1	1.7	0.006062
AL1L1_RAT	Cytosolic 10-formyltetrahydrofolate dehydrogenase	3.6	0.006914
VAT1_RAT	Synaptic vesicle membrane protein VAT-1 homolog	2.3	0.008198
ACSL5_RAT	Long chain fatty acid CoA ligase 5	2.5	0.00896
PGK1_RAT	Phosphoglycerate kinase 1	1.7	0.009191
TBA1C_RAT	Tubulin alpha-1C chain	2.3	0.009453
CMBL_RAT	Carboxymethylenebutenolidase homolog	2.4	0.011306
PUR9_RAT	Bifunctional purine biosynthetic protein PURH	1.9	0.011392
GSTK1_RAT	Glutathione S-transferase kappa 1	3.0	0.012802
SYDC_RAT	Aspartate-tRNA ligase, cytoplasmic	1.8	0.013114
CP2A1_RAT	Cytochrome P450 2A1	2.5	0.013636
AL1A7_RAT	Aldehyde dehydrogenase, cytosolic 1	3.4	0.018937
TERA_RAT	Transitional endoplasmic reticulum ATPase	1.9	0.019298

ACACA_RAT	Acetyl-CoA carboxylase 1	1.5	0.021909
GSTT1_RAT	Glutathione S-transferase theta 1	1.6	0.038933
DHPR_RAT	Dihydropteridine reductase	1.9	0.040027
LPP60_RAT	60 kDa lysophospholipase	1.7	0.045716
PH4H_RAT	Phenylalanine-4-hydroxylase	1.5	0.049157

Table 10 Pathways significantly enriched in ZF-EVs.

Mapped ID	Pentose biosynthetic process	Fold change	ANOVA (*p*value)
6PGD_RAT	6-phosphogluconate dehydrogenase, decarboxylating	3.5	0.000003
G6PD_RAT	Glucose-6-phosphate 1-dehydrogenase	15.5	0.000605
	Pyruvate Metabolism		
MAOX_RAT	NADP-dependent malic enzyme	7.2	0.000209
ACLY_RAT	ATP-citrate synthase	3.9	0.000618
PGK1_RAT	Phosphoglycerate kinase 1	1.7	0.009191

Table 11 Group I: proteins overexpressed in ZF-EVs.

Mapped ID	Fat Metabolism	Fold change	ANOVA (*p*value)
MIF_RAT	Macrophage migration inhibitory factor	1.9	0.000123
MAOX_RAT	NADP-dependant malic enzyme	7.2	0.000209
G6PD_RAT	Glucose-6-phosphate 1-dehydrogenase	15.5	0.000605
ACLY_RAT	ATP-citrate synthase	3.9	0.000618
AL1A1_RAT	Retinal dehydrogenase 1	3.6	0.001163
FAS_RAT	Fatty acid synthase	2.5	0.002199
ACSL5_RAT	Long Chain Fatty Acid CoA Ligase 5	2.5	0.00896
CP2A1_RAT	Cytochrome P450 2A1	2.5	0.013636
ACACA_RAT	Acetyl-CoA carboxylase 1	1.5	0.021909
LPP60_RAT	60 kDA Lysophospholipase	1.7	0.045716

The remaining proteins were manually grouped into ones involved in the synthesis and post-translational modifications of proteins and cytoskeleton related proteins **(Table 12)**.

Table 12 Group II: proteins overexpressed in ZF-EVs.

Mapped ID	Protein synthesis and post translation modifications	Fold change	ANOVA (*p*value)
RS4X_RAT	40S ribosomal protein S4	1.5	0.003988
EF1A1_RAT	Elongation factor 1-alpha	1.7	0.006062
RL9_RAT	60S ribosomal protein L9	2.0	0.037221
EF1D_RAT	Elongation factor 1-delta	1.6	0.040249
	Cytoskeleton-related proteins		
TBA1C_RAT	Tubulin alpha-1C chain	2.3	0.009453
MARE2_RAT	Microtubule-associated protein RP/EB family member 2	3.0	0.018809

5.2.2.5.2 Classification of proteins down-regulated in ZF-EVs

In the category of proteins identified as down-regulated in ZF-EVs, 40% were of mitochondrial origin **(Table 13)**. Surprisingly in that group, one of the proteins identified was the molecular ER chaperone, Grp78, which is generally localized in the ER (Sun et al. 2006) and assist in folding of cytoplasmic proteins (Prasad et al. 2017). We have already shown the expression of Grp78 by WB in Zucker rat hepatocytes **(Figure 44)**. Its abundance was reduced in lysates from ZF-hepatocytes, as compared to the control, and by WB it was not detected in EVs. The presence of Grp78 protein among the mitochondrial proteins associated to hepatocyte-EVs coud be due to the fact that GRP78 was shown to be present at the mitochondria-associated ER membrane (MAM), which physiologically connects the ER to mitochondria (Prasad et al. 2017) and this apposition of the outer mitochondrial membrane and the ER was first shown in rat liver and cultured rat hepatocytes (Lebiedzinska et al. 2009). Another protein in this

category, which presence was previously validated by MALDI-MS from SYPRO Ruby protein gel staining was the **Cytochrome b5 (Figure 42).** Here we confirm that the reduction of the Cytochrome b5 protein was statistically significantly (*p* value = 0.003195) in ZF-EVs.

Table 13 Group III: proteins down-regulated in ZF-EVs.

Mapped ID	Mitochondria	Fold change	ANOVA (*p*value)
PDIA3_RAT	Protein disulfide isomerase family A, member 3	2.5	5.38E-05
BSG_RAT	Basigin	4.5	0.000395
DHE3_RAT	Glutamate dehydrogenase 1	6.1	0.000455308
CATA_RAT	Catalase	2.7	0.000515
RHOA_RAT	Ras homolog family member A	2.0	0.000621
CYP2D4_RAT	Cytochrome P450, family 2, subfamily d, polypeptide 4	4.0	0.000995789
HMGCL_RAT	3-hydroxymethyl-3-methylglutaryl-CoA lyase	3.4	0.001006814
HSD17B4_RAT	hydroxysteroid (17-beta) dehydrogenase 4(Hsd17b4)	3.1	0.001532433
PYC_RAT	Pyruvate carboxylase	3.5	0.001833
PCCA_RAT	Propionyl-CoA carboxylase alpha subunit	3.4	0.001952956
CYP2D1_RAT	Cytochrome P450, family 2, subfamily d, polypeptide 1	3.2	0.001968706
ACOX3_RAT	Peroxisomal acyl-coenzyme A oxidase 3	1.9	0.002165
IVD_RAT	Isovaleryl-CoA dehydrogenase	2.9	0.002316491
CYB5A_RAT	Cytochrome b5 type A	3.9	0.003195191
MGST1_RAT	Microsomal glutathione S-transferase 1	2.5	0.003286481
CH60_RAT	60 kDa heat shock protein, mitochondrial	1.9	0.005119052
ALDH2_RAT	Aldehyde dehydrogenase, mitochondrial	4.1	0.006310028
GRP78_RAT	78 kDa glucose-regulated protein	2.0	0.007384784

IDHP_RAT	Isocitrate dehydrogenase [NADP], mitochondrial	3.7	0.009461225
AGT2_RAT	Alanine-glyoxylate aminotransferase 2, mitochondrial	2.9	0.009529205
PCCB_RAT	Propionyl-CoA carboxylase beta subunit	4.5	0.010487016
PECR_RAT	Peroxisomal trans-2-enoyl-CoA reductase	2.1	0.011373881
MDHM_RAT	Malate dehydrogenase, mitochondrial	2.2	0.012192884
S22A7_RAT	Solute carrier family 16 member 1	2.6	0.012442
MCCA_RAT	Methylcrotonoyl-CoA carboxylase 1	3.2	0.012851807
ACADM_RAT	Medium-chain specific acyl-CoA dehydrogenase, mitochondrial	3.0	0.013927
SDHA_RAT	Succinate dehydrogenase complex flavoprotein subunit A	2.3	0.017234
AL3A2_RAT	Fatty aldehyde dehydrogenase	1.9	0.018048282
ETFDH_RAT	Electron transfer flavoprotein dehydrogenase	2.2	0.020696775
THIM_RAT	3-ketoacyl-CoA thiolase, mitochondrial	2.6	0.021379907
MMSA_RAT	Methylmalonate-semialdehyde dehydrogenase, mitochondrial	2.2	0.02176398
CPS1_RAT	Carbamoyl-phosphate synthase 1	2.7	0.022820558
CLU_RAT	Clusterin	2.3	0.023728152
HMCS2_RAT	Hydroxymethylglutaryl-CoA synthase, mitochondrial	3.4	0.026934354
BDH_RAT	D-beta-hydroxybutyrate dehydrogenase, mitochondrial	2.5	0.029277
SARDH_RAT	Sarcosine dehydrogenase	2.7	0.029758
AL4A1_RAT	Delta-1-pyrroline-5-carboxylate dehydrogenase, mitochondrial	2.8	0.03048617
ACOX2_RAT	Peroxisomal acyl-coenzyme A oxidase 2	3.6	0.03222387
HSPA1A_RAT	Heat shock 70 kDa protein 1A	1.6	0.033711025
ACON_RAT	Aconitate hydratase, mitochondrial	2.8	0.036747316
ANXA6_RAT	Annexin A6	1.8	0.037249
CHDH_RAT	Choline dehydrogenase		0.038216395
NADK2_RAT	NAD kinase 2, mitochondrial	1.7	0.040638811

Table 14 Group IV: proteins down-regulated in ZF-EVs.

Mapped ID	The citric acid (TCA) cycle and electron transport	Fold change	ANOVA (*p*value)
BASI_RAT	Basigin	4.5	0.000395
MOT1_RAT	Monocarboxylate transporter 1	3.9	0.000853
IDHP_RAT	Isocitrate dehydrogenase [NADP], mitochondrial	3.7	0.009461
MDHM_RAT	Malate dehydrogenase, mitochondrial	2.2	0.012193
SDHA_RAT	Succinate dehydrogenase flavoprotein subunit, mitochondrial	2.3	0.017234
ETFD_RAT	Electron transfer flavoprotein-ubiquinone-oxidoreductase, mitochondrial	2.2	0.020697
ACON_RAT	Aconitate hydratase, mitochondrial	2.8	0.036747
NDUAA_RAT	NADH dehydrogenase 1 alpha subcomplex subunit 10, mitochondrial	2.2	0.045338

Only a few exosomal markers were identified in the proteomic analysis of Zucker rat hepatocyte-derived EVs, namely Cd81 (*p* value = 0.010499), Aip1/Alix (*p* value = 0.002796), Ras-related protein Rab1A (*p* value = 0.014829) and Rab11A (*p* value = 0.04518) They were all down-regulated in ZF-EVs, which was previously shown by WB analysis carried out to characterize the content of Zucker rat hepatocyte-secreted EVs **(Figure 44)**. AnnexinVI, a member of a group of calcium dependant membrane and phospholipid binding proteins, which have been implicated in endocytic pathways, specifically in membrane organization and cell surface receptor activity through interactions with the actin cytoskeleton (Cornely et al. 2011). Another annexin, AnnexinV was validated by WB, confirming its down-regulation in ZF-EVs **(Figure 44)**. Another differentially expressed protein was PDC6I which is involved in sorting cargo proteins of the MVB for incorporation into ILVs. Proteomic analysis has also revealed the presence of the tetraspanin Cd81 was also identified in EVs secreted by Zucker rat hepatocytes and, as previously shown, significantly less abundant in ZF-EVs. In agreement with the proteomic analysis there were also increased shuttling of

Hsp70 in ZF-EVs. Various GTPases, the key regulators in intracellular membrane trafficking were also found in ZL DEPs, such as Rab1A and Rab1B. On the other hand, GTP-binding protein SAR1b is a curvature-sensing component of the COPII coat complex and has been showing to be crucial in membrane bending, recruitment of coat components and vesicle formation. Additionally, the intrinsic GTPase activity of Sar1 is necessary for remodelling lipid bilayers (Hanna et al. 2016). The lysosomal protein, Lamp1 was also associated to ZF-EVs (*p* value = 0.00216).

The list of proteins rendered by the proteomic analysis was also searched for proteins which were characteristic to hepatocytes. Thus, we found that the facilitated glucose transprter 2 (Glut2) was significantly down-regulated in ZF-EVs (*p* value=0.000316). This transporter is specific to the liver and it is responsible for the transfer of glucose across the plasma membrane of hepatocytes. On the other hand, classification according to functions revealed the presence of proteins involved in detoxification processes and xenobiotic metabolism **(Table 15)**. Several members of the P450 superfamily were included, with specific enrichment of those belonging to the 2D family. However, other proteins functioning in metabolism of endogenous and exogenous compounds such as UDP, UGTs and glutathione S-transferases were detected as well. UGTs are, after P450s, the major contributors to drug metabolism. At least three distinct members of the 2B family of UGT proteins were present in Zucker rat hepatocyte secreted EVs and their expression reduced in ZF-EVs. UGT enzymes are membrane bound and are found primarily in ER (Conde-Vancells et al. 2010).

Table 15 Group V: proteins down-regulated in ZF-EVs.

Mapped ID	Xenobiotic metabolism	Fold change	ANOVA (*p*value)
MGST1_RAT	Microsomal glutathione S-transferase 1	2.5	0.003286481
CP2C7_RAT	Cytochrome P450 2C38	2.3	0.03454715
CP2DQ_RAT	Cytochrome P450 2D26	3.5	0.001033149
CP2D1_RAT	Cytochrome P450 2D1	3.3	0.000933666
CP2D4_RAT	Cytochrome P450 2D6	4.0	0.001033149
UGDH_RAT	UDP-glucose 6-dehydrogenase, mitochondrial	1.7	0.024328271
ALDH2_RAT	Aldehyde dehydrogenase, mitochondrial	4.1	0.006310028
CP2DA_RAT	Cytochrome P450 2D10	3.7	0.001968706
HYEP_RAT	Epoxide hydrolase 1	3.7	0.005862539

Some of the proteins specifically produced by the liver such as serum albumin, fibrinogen, angiopoietin, plasminogen, serotransferrin, alpha-1-macroglobulin and, prothrombin, were all identified in EVs isolated from conditioned medium of Zucker primary rat hepatocytes and were all reduced in ZF-EVs, which again may reflect the condition of steatotic hepatocytes.

5.2.2.5.3 Validation by Western blot

To confirm the quantitative proteomics data, the differential abundance of a set of proteins was investigated using WB analysis **(Figure 49)**. In agreement with the proteomics data, an increased expression in Fas, Comt and Pgd6 proteins was seen in ZF-EVs. Moreover, Catalase, Cyp2d1, Syndecan4 as well as FerritinLC, among others were found to be highly down-regulated in ZF-EVs. WB has revealed that Fas and Ferritin LC were solely detected in EVs. ZF-EVs were highly enriched in Comt protein, interestingly, we detected a lower mobility, protein band for Comt in association with Zucker rat hepatocyte-derived EVs, probably corresponding to post-translationally modified forms of the protein. Modified Catalase protein was also secreted in EVs, and visualized as a double

band. Pgd6 protein expression in cells was mirrored in their secreted EVs, and confirmed our previous proteomics results of its increased abundance in ZF-EVs. Syndecan4, one of four members of transmembrane proteoglycan family of proteins that functions as a receptor in intracellular signalling (Ju et al. 2014). Additionally, together with Syntenin and Alix regulate exosomes formation (Baietti et al. 2012) was not detected in neither ZF-hepatocytes nor in their secreted EVs. Additionally, as already mentioned, other proteins, previously validated by WB **(Figure 44)** were identified in our proteomic analysis.

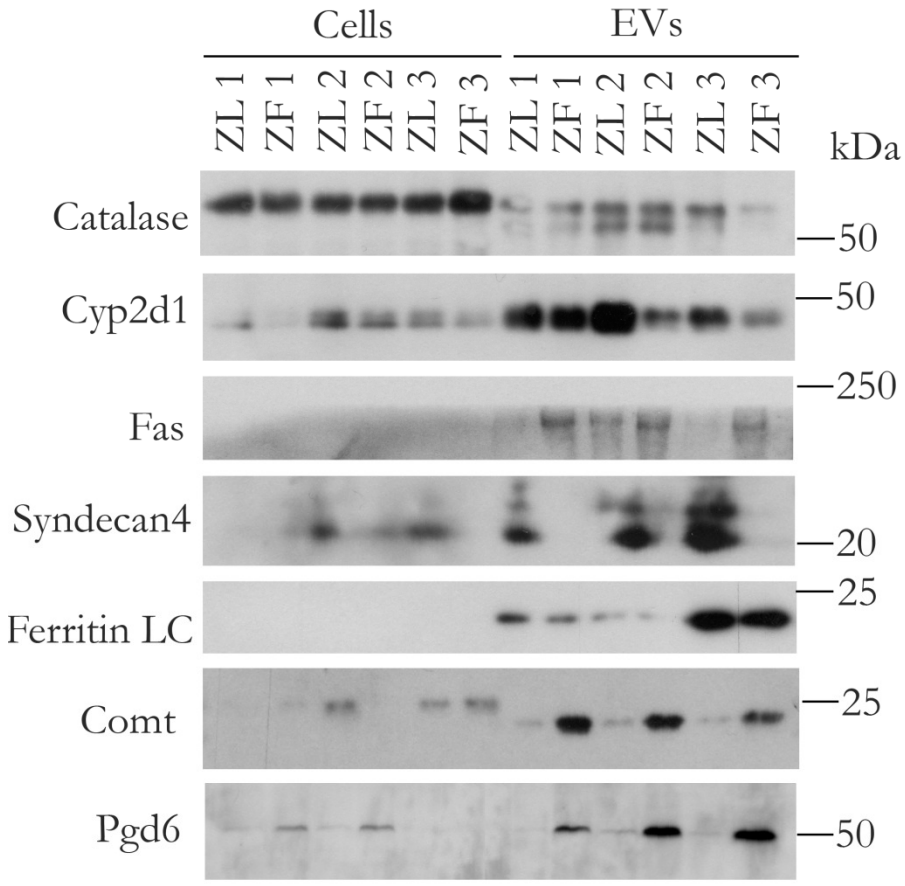

Figure 49 Western-blot analysis of DEPs identified by quantitative label free proteomic analysis, by WB. Representative WB of three independent preparations of EVs. Whole cell lysates of Zucker rat hepatocytes (10 µg) and their corresponding EVs (10 µg) were immunoblotted using antibodies against proteins such as fatty acid synthase (Fas), 6-phosphogluconate dehydrogenase, decarboxylating (Pgd6) and Catechol O-methyltransferase (Comt), which were up-regulated in ZF-EVs and Catalase, Cyp2d1, Syndecan4 and FerritinLC, which were found down-regulated in ZF-EVs.

5.4.2.6 Nucleic acid content

Afterwards, we have analyzed the nucleic acid material that was contained in 250 µg of ZL- and ZF-EVs. Briefly, following EV lysis and nucleic acid purification, a small amount of the exosomal RNA (exoRNA) fraction was stored for analysis and the remaining part was treated with DNaseI. The RNA concentration before and after the treatment with DNaseI was measured by NanoDrop **(Figure 50A)**. Most of the nucleic acid disappeared with the DNaseI treatment, indicating that these EVs contained a significant amout of DNA **(Figure 50C)**. Our results show that although the overall amount of isolated RNA was low in both, ZF-EVs contained nearly 3-times more RNA as compared to the ZL-EVs **(Figure 50A, bottom table)**. However, the nucleic acid concentration before DNA treatment was 12 times lower in ZF-EVs **(Figure 50A, top table)**. Together these results could indicate that different proportion of DNA and RNA are found in ZL versus ZF, with ZF containing more RNA and less DNA than ZL. It seems that, before the treatment with DNaseI, the measurement of RNA concentration was inaccurate **(Figure 50A)**.

A.

DNAse -	ZL	ZF
[RNA] ng/µL	0.76	0.06
Total RNA	30.4	2.4

DNAse +	ZL	ZF
[RNA] ng/µL	1.45	4.27
Total RNA	43.5	128.1

B.

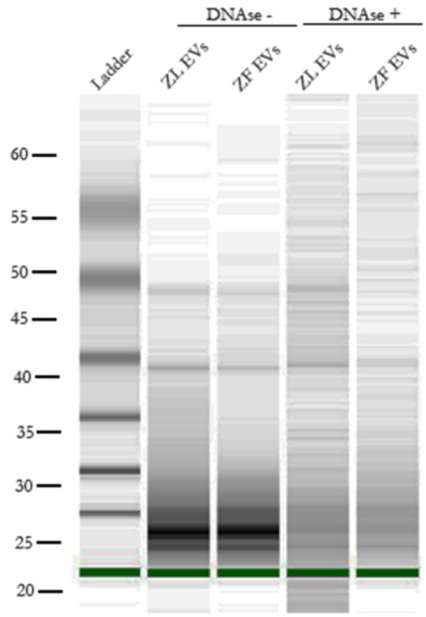

C.

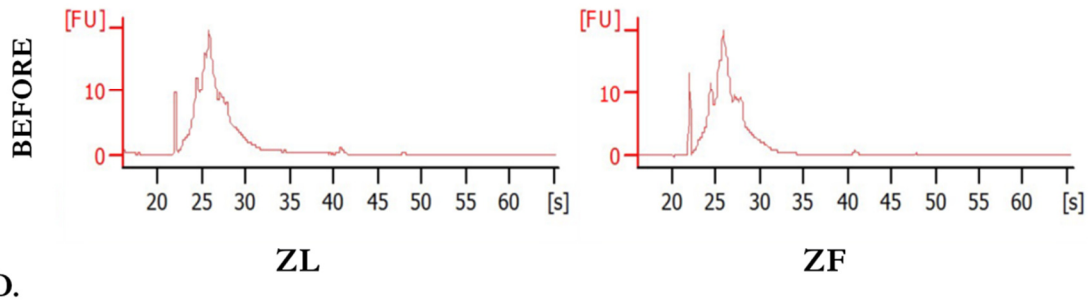

D.

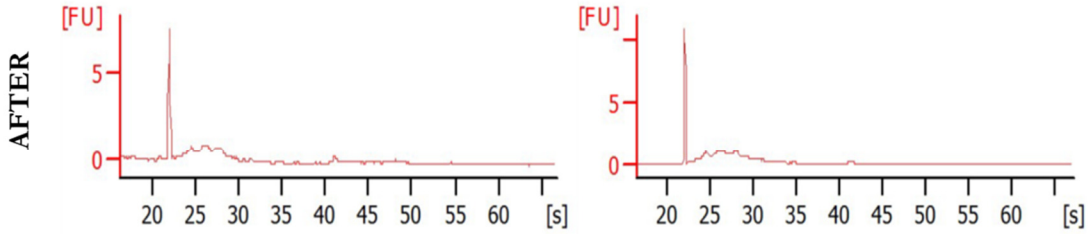

E.

DNAse +	ZL	ZF
RNA Area	13.4	29.9
[RNA] pg/µL	107	238

Figure 50 Nucleic acid content of Zucker rat hepatocyte-derived EVs. RNA was isolated from 250 µg of ZL-EVs and ZF-EVs using RNeasy Mini Kit. **(A)** Quantification of isolated RNA with NanoDrop, before (top) and after (bottom) the DNase treatment. **(B)** 2 µl of each RNA sample was resolved by SDS-PAGE electrophoresis. **(C)** The

electropherograms showing the size distribution in nucleotides (nt) and fluorescent intensity of the total RNA in EVs before the DNase treatment **(D)** The electropherograms showing the size distribution in nucleotides (nt) and fluorescent intensity of the total RNA in EVs after the DNase treatment **(E)** RNA quantification (pg/µl), as analyzed by Bioanalyzer. n=1.

Subsequently, the RNA profiles of both fractions were analyzed using Agilent 2100 Bioanalyzer **(Figure 50)**. Individual electropherograms corresponding to untreated samples **(Figure 50C)** and DNaseI-treated samples **(Figure 50D)** are shown. We did not observe significant amount of ribosomal RNAs, and the major peak detected indicated the presence of nucleic acids of small size. Furthermore, this major peak was significantly reduced after the DNaseI treatment what was indicative as already mentioned that these EVs contains DNA **(Figure 50E)**.

In summary, our results show that EVs secreted by Zucker hepatocytes contain DNA and RNA, and the proportion of these two nucleic acids are different in EVs secreted by lean (ZL) and fatty (ZF) hepatocytes.

5.4.2.7 Lipid content

Once having explored proteins and nucleic acids that are present in Zucker hepatocyte secreted-EVs, we studied their lipid content. The presence of sphingomyelin, cholesterol, lysophosphatidylcholine, arachidonic acid and other fatty acids, prostaglandins and leukotrienes among other, has been shown in EVs (Record et al. 2014). As a starting point in this section, we decided to evaluate the possible contamination of our preparations with lipoproteins, giving that they are major carriers of lipids.

To address this issue, we analysed the presence of some Apolipoproteins by WB, in particular ApoB, a protein forming part of the core of lipoproteins, and ApoE, a protein involved in the renewal of lipoproteins (Getz & Reardon 2009). We performed WB analysis of three independent preparations of lysates obtained from Zucker rat hepatocytes and their secreted EVs and confirmed the presence of both, ApoB and ApoE **(Figure 51A)**. As can be observed, ApoB was highly enriched in cells, as compared to ApoE, with no differences between the two sample groups (ZL *vs.* ZF). However, ApoE clearly was more abundant in ZF-hepatocytes as compared to the control (ZL). Moreover, Zucker-EVs were enriched in ApoE protein, with no obvious difference between the two sample groups. Importantly, although we could detect some ApoB in the EVs preparations that could indicate certain degree of contamination by lipoproteins, there was no difference in enrichment between ZL- and ZF-EVs. The elevated levels of ApoE associated to hepatic EVs, rise the possibility of EVs having a role in lipoprotein metabolism or serving to transport out recycled lipoprotein-associated proteins has already been proposed (Conde-Vancells et al. 2008). In agreement with this possible role of ApoE-associated to EVs in metabolism of lipoproteins, although in other cellular systems came from a recent article published by van Niel and co-workers (van Niel et al. 2015). This work highlight the role of ApoE in sorting molecules to ILV in MVB (van Niel et al. 2015). In summary, the low presence of ApoB and taking also into account, the cryo-EM analysis that has been performed for a significant number of independant preparatios of Zucker-EVs **(Figure 51A)** in which was not observed the presence of lipoproteins, it is possible to conclude that the lipoprotein contamination of the hepatic-EV preparation was low.

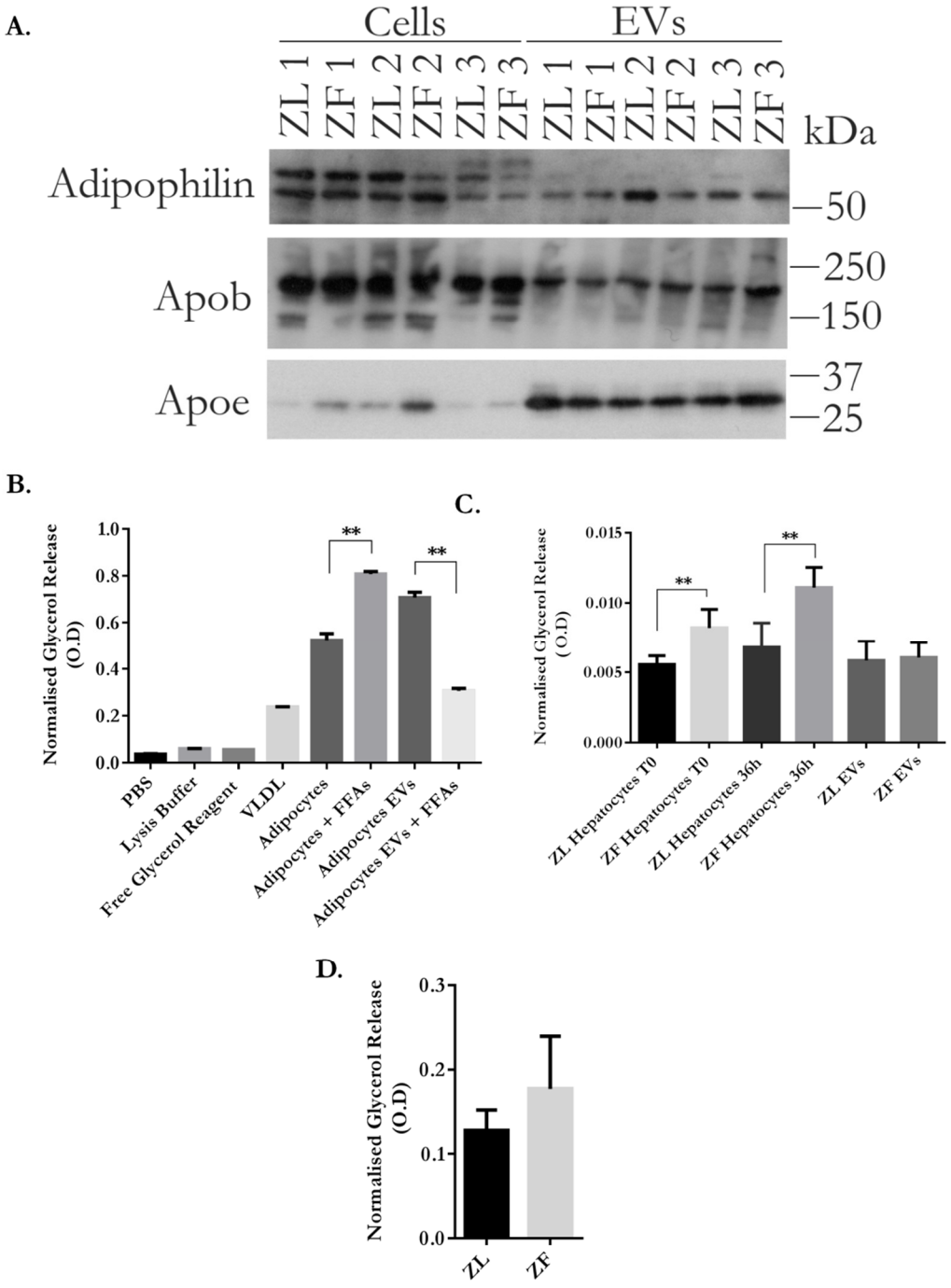

Figure 51 Triglyceride content in Zucker rat hepatocyte-derived EVs. Triglyceride content of primary Zucker rat hepatocytes and their secreted-EVs was measured using lipase activity assay. **(A)** Lipid-related proteins were analyzed by WB in lysates from Zucker rat hepatocytes (10 μg) and their secreted-EVs (5 μg). **(B)** Lipase assay of lysates from the 3T3-L1 adipocytes and hypertrophic 3T3-L1 adipocytes with their secreted-EVs, to establish the sensitivity of the assay. 50 μg of the whole cell lysates of Zucker rat hepatocytes and 2μg of lysed EVs were used in the assay **(C)** Lysed samples; n=4. **(D)** Intact EV samples; n=4. Error bars=SD. The p values were denoted as follows: 0.01-0.05=*,0.01-0.001=**, 0.001-0.0001=***. Unpaired student t-test was performed to determine significant differences.

Adipophilin, another adipocyte-associated protein was also secreted in Zucker hepatocyte EVs as seen by WB **(Figure 51A)**. We found adipophilin/perilipin2 associated with our vesicles and, although it varied between preparations, it was slightly reduced in ZF-EVs, as compared to the lean control. The trend was mirrored in the parent cells, although it was also variable. These results could indicate the presence of some lipid droplets in our preparations although alternatively, it could be as ApoE, in which the protein plays a role in their metabolism.

Subsequently, using the lipase activity assay **(section 2.12)**, we investigated the triglyceride content in Zucker hepatocytes and their secreted EVs. In order to determine the triglyceride concentration, the amount of free glycerol, enzymatically hydrolyzed from triglycerides by lipoprotein lipase, can be accurately measured (Demel & Jackson 1985). The optimization of the assay was performed first, with negative controls of PBS, lysis buffer and the FGR, producing minimal background **(Figure 51B)**, and VLDLs as positive controls confirming the functionality of the assay. Biological samples of lysates obtained from 3T3-L1 adipocytes as well as as hypertrophic 3T3-L1 adipocytes and their corresponding, secreted-EVs were also assayed in parallel as positive controls **(Figure 51B).** Hypertrophic adipocytes were found to have significantly higher triglyceride content as expected. Interestingly, their secreted EVs present exactly the opposite trend, with more triglycerides being retained in the cell as to what is being secreted in EVs **(Figure 51B)**. Subsequently, Zucker rat hepatocytes at T0 and after 36 h in culture, and their secreted EV were lysed and subjected to the lipase activity assay to measure their triglyceride content. OD values were normalized by the protein concentration and presented in **Figure 51C**. As expected, significantly increased levels of triglyceride content were observed in ZF-hepatocytes at T0 as well as at 36 h, with a slight increase at 36 hours, indicating possible accumulation of TG in culture. Moreover, no differences were found between the triglyceride content of ZL- and ZF-EVs.

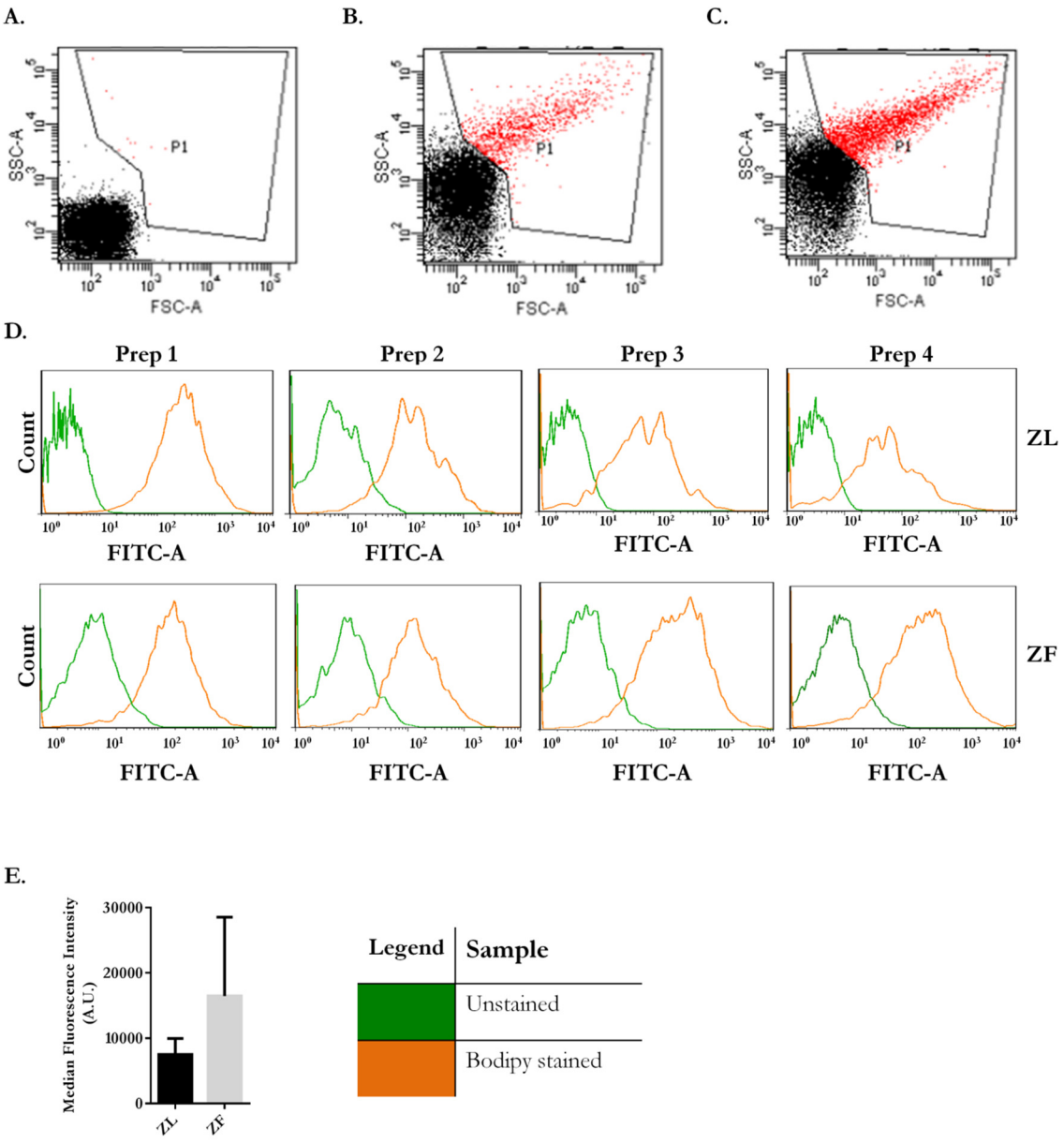

<u>Figure 52</u> Validation of the lipid content in intact Zucker rat hepatocyte-derived EVs. The content of lipids in EV samples was evaluated directly by flow cytometry of Bodipy-stained EV samples. A representative SSC *vs.* FSC density plots of Bodipy stained samples: **(A)** PBS control **(B)** ZL-EVs **(C)** ZF-EVs. **(D)** Flow cytometry histograms of P1 gated unstained (green line) and Bodipy-stained (orange line) EVs in 4 independent preparations of ZL- and ZF-EVs. **(E)** Median FITC-A fluorescent intensity, in 30,000 events; n=4. Error bars = SD.

However, when intact EV samples were subjected to the lipase activity assay, under the same conditions, an increase in the triglyceride content was seen in the sample of ZF-EVs **(Figure 51D)**.

To further validate these results, Bopidy staining of intact EVs was performed and analyzed by flow cytometry **(Figure 52).** The population of EVs was selected based on their forward and side scatter properties, not considering the background of PBS, in which the EVs are resuspended **(Figure 52A)**. The selected gate (P1) was specific to the population of ZL- **(Figure 52B)** and ZF-EVs **(Figure 52C)**. Four independent pairs of EVs were assayed. **Figure 52D** shows the histograms of the FITC-A intensity peaks in ZL- and ZF-stained EVs in matched preparations. Quantification of the median FITC-A fluorescent intensity, although not significant, it showed an increase in Bodipy-stained lipids in ZF-EVs, in agreement with previous results of lipase activity assay in intact EVs **(Figure 52B)**.

5.4.2.8 Testing the Presence of Active Compounds in Zucker Hepatocyte-derived EVs

Hepatic triacylglycerol lipase (LIPC) was identified by proteomic analysis to be present in EVs, and although not significant, a trend to be higher in ZF-EVs was observed. This was a trigger to investigate whether the enzyme was active and could catalyze the hydrolysis of TG. We modified the lipase assay and used our EVs as a possible external source of lipase. Briefly, for this experiment, 20 µg of ZL- and ZF-EVs were lysed and each sample assayed in duplicate (10 µg each). VLDLs were selected as a substrate for the assay and used in a concentration of 1µg per sample. Intact EV samples were also included in the assay. Results are represented in **Figure 53A**.

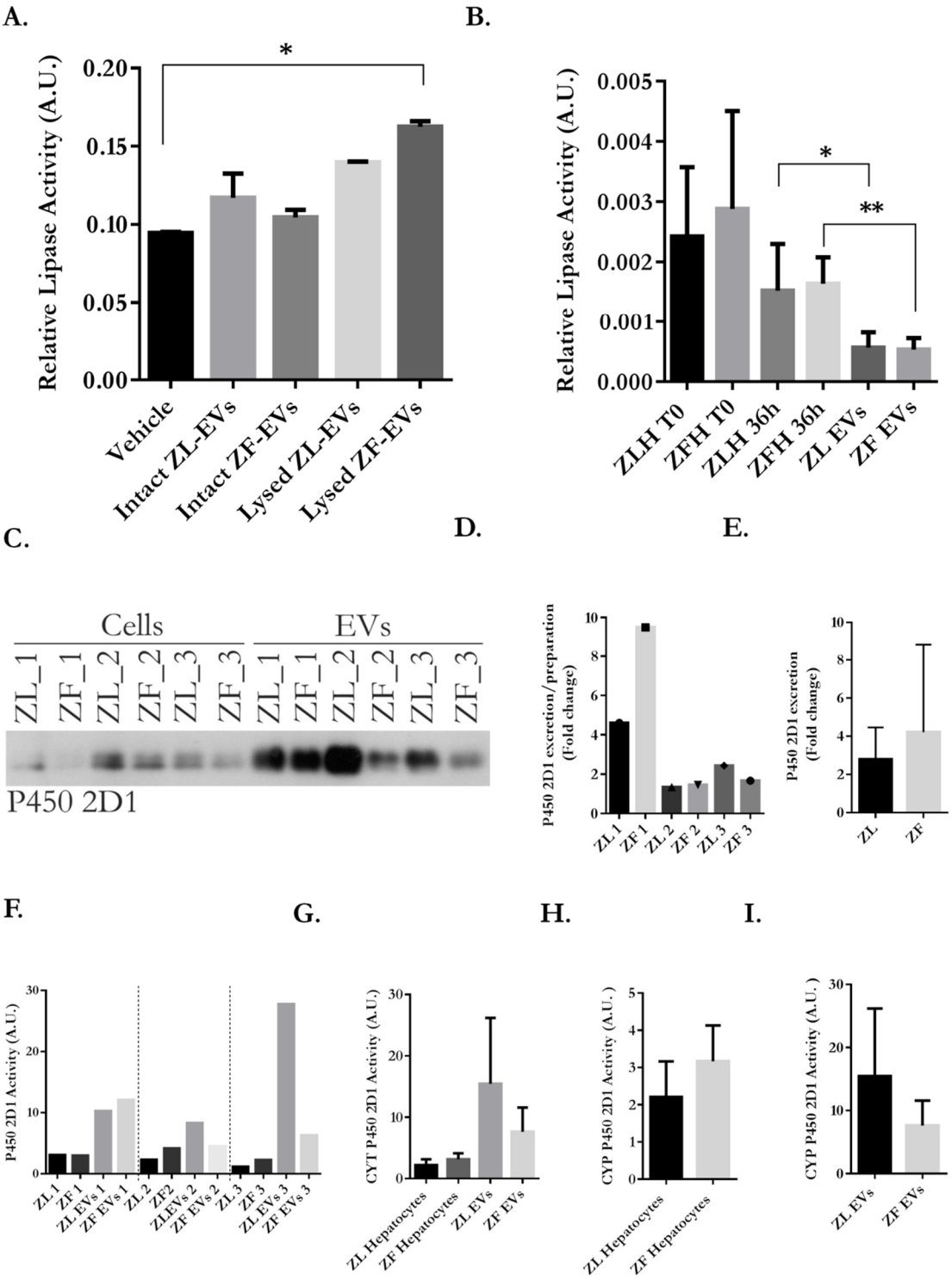
A.
B.
Relative Lipase Activity (A.U.)
0.20
0.15
0.10
0.05
0.00
*
Vehicle
Intact ZL-EVs
Intact ZF-EVs
Lysed ZL-EVs
Lysed ZF-EVs
Relative Lipase Activity (A.U.)
0.005
0.004
0.003
0.002
0.001
0.000
*
**
ZLH T0
ZFH T0
ZLH 36h
ZFH 36h
ZL EVs
ZF EVs
C.
D.
E.
Cells
EVs
ZL_1
ZF_1
ZL_2
ZF_2
ZL_3
ZF_3
ZL_1
ZF_1
ZL_2
ZF_2
ZL_3
ZF_3
P450 2D1
P450 2D1 excretion/preparation (Fold change)
ZL 1
ZF 1
ZL 2
ZF 2
ZL 3
ZF 3
P450 2D1 excretion (Fold change)
ZL
ZF
F.
G.
H.
I.
P450 2D1 Activity (A.U.)
ZL 1
ZF 1
ZL EVs 1
ZF EVs 1
ZL 2
ZF2
ZLEVs 2
ZF EVs 2
ZL 3
ZF 3
ZL EVs 3
ZF EVs 3
CYT P450 2D1 Activity (A.U.)
ZL Hepatocytes
ZF Hepatocytes
ZL EVs
ZF EVs
CYP P450 2D1 Activity (A.U.)
ZL Hepatocytes
ZF Hepatocytes
CYP P450 2D1 Activity (A.U.)
ZL EVs
ZF EVs

Figure 53 Active molecules in Zucker rat hepatocyte-derived EVs. (A) Lipase activity assay in Zucker rat hepatocyte secreted-EVs, using VLDL as a substrate; n=4 **(B)** Lipase activity assay in Zucker rat hepatocyte secreted EVs, using Triglyceride Mix as a substrate; n=4. **(C)** Representative WB figure immunoblotted for Cyp2d1 in Zucker rat hepatocytes and their corresponding EVs; n=3 **(D)** Quantification of the fold change in the Cyp2d1 protein secreted in ZL- and ZF-EVs. **(E)** Average fold change Cyp2d1 of the three independent preparations. **(F)** Activity assay in Zucker rat hepatocyte secreted EVs in three independent preparations; n=3 **(G)** The average activity of Cyp2d1; n=3. **(H)** The activity in Zucker rat hepatocyte alone. **(I)** The activity in Zucker rat hepatocyte-derived EVs alone. Error bars=SD. The *p* values were denoted as follows: 0.01-0.05=*, 0.01-0.001=**, 0.001-0.0001=***. Unpaired student t-test was performed to determine significant differences.

Lipase activity was detected in all samples; however, it was higher in lysed-EVs as compared to intact ones, which indicates that the lipase was not only associated to the surface of the EV, and some enzymatic activity was enclosed in EVs. In agreement with the proteomics data, a statistically significant increase in activity was seen in lysed ZF-EVs compared to ZL-EVs **(Figure 51C)**.

In addition, we also compared the activity in lysates from Zucker rat hepatocyte at T0 and 36h **(Figure 53B)**. 10 µl of each sample was assayed and the resultant OD values were normalized by predetermined protein concentration. Using a triglyceride mix as a substrate, lipase activity was detected in hepatocyte extracts, both at T0 and at 36h, although significant reduction in activity was observed in that time frame. Moreover, the level of activity detected in EVs was significantly lower as compared to their parent cells **(Figure 53B)**. Compared with the previous experiment, very low activity was seen in EVs with no differences between the sample of ZL- and ZF-EVs **(Figure 53B)**. This could be due to the different substrates used in both assays.

In our proteomic analysis of EVs, coming from Zucker rat hepatocytes, we also observed the presence of various subfamilies, C, D, and B of the P450 enzymes. In particular, cytochrome P450 2D1, an enzyme found in liver microsomes, involved in the NADPH-dependant electron transport and a oxidizes variety of compounds, fatty acids, steroids, and xenobiotics, was found to be significantly

down-regulated in ZF-EVs as compared to the control. This result was validated by WB, not only in EVs but also in parent cell whole lysates, which as missing in our proteomic analysis, and was associated with very interesting finding **(Figure 53C)**. First, significantly more Cyp2d1 was associated with hepatic-EVs as compared to their secreting cells. The densitometry of the Cyp2d1 excreted in EVs into the extracellular space as compared to the remaining in the secreting cell, although highly variable between the three independant preparations **(Figure 53D)**, revealed that more Cyp2d1 was associated to ZF-EVs **(Figure 53E)**. To study in more detail, the presence of Cyp2d1 in Zucker rat hepatocyte-derived EVs, we decided to explore the possibility that the enzyme contained within EVs, could, in fact, be in an active form. A luminescent assay, specific for the measurement of P450 2D1 was used. The activity of P450 2d1 was measured in 20 µl of EVs purified from primary Zucker rat hepatocytes after 36 h of *in vitro* culture and their corresponding hepatocyte lysates, from three independent sets of samples **(Figure 53F)**. The activity of Cyp2d1 was readily detectable in EVs, confirming that the enzyme, which is carried in Zucker-EVs was active. Moreover, the activity of P450 2d1 in EVs was significantly higher than in parent cell lysates **(Figure 53G)**. In addition, as mentioned above, we observed a significant variability in the level of activity, between independent preparations **(Figure 53F)**. The average of three sample sets is presented in **Figure 53G**. In terms of the difference in activity between the ZL- and ZF-hepatocytes and their corresponding EVs, our results indicate that slightly more active Cyp2d1 was associated to ZF-hepatocytes and the opposite trend was seen in EVs.

In summary, we have detected the lipase activity as well as Cyp2d1 activity in our ZL- and ZF-EVs. More active lipase was associated to ZF-EVs when the VLDLs were used as a substrate. When using the triglyceride MIX as substrate, we detected higher level of lipase activity in cells than their secreted EVs, with more lipase being present in ZF-hepatocytes. The levels of activity have dropped between T0 and 36 h. On the other hand, we showed that the Cyp2d1 enzyme associated with hepatic-EVs was active. In terms of the protein expression we

confirmed that less Cyp2d1 protein was found in ZF-EVs as compared to the control EVs. Interestingly, however, when the difference the expression in cells and in secreted EVs was compared, which was missing in our proteomic analysis, we found that more Cyp2d1 was associated to ZF-EVs.

5.5 Summary

In summary, we conclude that our model of hepatocellular steatosis is valid and reflects the state of lipid overload in hepatocytes during simple steatosis. Moreover, with the experimental approach taken for the isolation of EVs, our preparations were free of contamination and exhibit significant enrichment in proteins related with EVs.

The conditions of steatosis did affect the secretion and protein markers associated to EVs, isolated from all three hepatocyte-like cells. The result was confirmed in our primary hepatocyte model, which represents genetically induced obesity-related steatosis. Overall, the secretion of EVs increased in these steatotic conditions. The majority of exosomal proteins were significantly downregulated with an increase in heat shock proteins.

We discovered that Zucker rat hepatocytes, lean and fatty show significant metabolic differences. It seems that during steatosis, mitochondrial functions are affected and accompanied by an increase in glycolysis. Interestingly, these conditions were reflected their secreted-EVs. The proteomic analysis of ZL- and ZF-EVs has revealed that the differentially expressed proteins up-regulated in ZF-EVs are related with PPP, pyruvate and fat metabolism, in contrary mitochondrial proteins were significantly down-regulated as well as proteins related to hepatic functions such as xenobiotic metabolism. We showed that the lipase enzyme and Cyp2d1 enzyme were active in hepatic-EVs.

In addition, we identified that the abundance of adiponectin in ZF-EVs reflected the state of obesity, as judged by the reduction in adiponectin in ZF-EVs. Finally,

we identified nucleic acids in Zucker hepatocyte-derived EVs and slightly more contained in ZF-EVs. Graphically represented on **Figure 54**.

5.6 Discussion

Many studies have shown that hepatocytes can uptake the long-chain fatty acids, with C12-C18, and esterify them into neutral fat droplets that are then stored in their cytoplasm (Yan et al. 2015). The first case of an *in vitro* hepatic steatosis model was induced by the addition of 50% rat serum in a co-culture of adult and neonatal rat hepatocytes (Vajta et al. 1986). The use of FFAs was first established in HepG2 hepatoma cell line (Cui et al. 2010). In this study, researchers have induced the triglyceride accumulation with OA (1 mM), which resulted in lipid accumulation into the cytoplasm accompanied by the increase in ApoB protein. In addition, the Glut2 gene expression was upregulated in steatotic cells, which has been previously correlated with an increased glucose output from the liver and gluconeogenesis (Okamoto et al. 2002; Cui et al. 2010). Moreover, an OA-induced steatosis in HepG2 cells was associated with increased production and secretion of TNF and decreased expression of PPARα (Cui et al. 2010). It cannot be ignored however, that HepG2 is a cancer cell line that can exhibit abnormal function and altered metabolism. Chang liver cells were also used to induce lipid accumulation with OA and characterized as being viable model (Yan et al. 2015). A very elegant *in vitro* model was developed to study hepatic steatosis in the Reuber H35 rat hepatoma carrying the GFP reporter cells cultured in oleic or linoleic acid (Amol et al. 2009). The cells have been shown to recapitulate the main features of the actual disease such as increased fatty acid intake, intracellular triglyceride accumulation, increased reactive oxygen species accumulation, and decreased mitochondrial membrane potential. Moreover, it allows the study of the role of transcriptional regulation of nuclear factor κB (NFκB), heat shock response elements (HSE), and glucocorticoid response element (GRE) (Amol et al. 2009). While steatosis

represents a reversible state of excess intra-hepatic lipids, it is known to lead to generation of intracellular reactive oxygen species (ROS), via the oxidation of FAs, that in turn reduces the induction of oxidative stress and a reduction in the mitochondrial membrane potential. Moreover it has been shown that steatosis partially attenuated the NFκB reporter response to TNF in a dose dependant manner of free fatty acids (Amol et al. 2009).

Fatty acid metabolism can be cell type specific and the different doses of FFAs and exposure time might be required, therefore, for our study, we selected three different hepatocyte-like cell lines, AML12, MLP29 and hepatoma HepG2 cells. We chose them to determine whether these differences would influence the amount of secreted EVs and in their marker composition. In order to achieve maximal lipid accumulation with minimal cytotoxic effect for subsequent isolation of EVs, we used oleic and palmitic acids, in a ratio of 2:1 at a final concentration of 1mM (Gómez-Lechón et al. 2007).

One of the first reports on hepatic-EVs was by Conde-Vancells and co-workers where they successfully isolated EVs from the conditioned medium of the MLP29 cells as well as primary rat hepatocytes, and pinpointed specific hepatic protein associated to EVs, asialoglycoprotein receptor (Asgr) (Conde-Vancells et al. 2008). In this thesis for the first time we demonstrate the characterization of EVs secreted by hepatocytes in conditions of simple steatosis. Surprisingly, most the research conducted on liver-EVs, related with metabolic diseases, is related with non-alcoholic fatty liver disease (NAFLD) or non-alcoholic steatohepatitis (NASH) (Povero et al. 2008; Povero et al. 2015; Povero et al. 2014; Hirsova et al. 2016; Kakazu et al. 2015; Ban et al. 2016). It is unexpected, because simple steatosis is asymptomatic and reversible, with appropriate measures, therefore, we considered studying EVs at this stage of liver disease as vital for discovery of diagnostic measures.

In our cellular models of steatosis, induced in the AML12 and MLP29 cells, we observed that the overall concentration of EVs was increased, which was not the case HepG2 cells, which could be due to its origin and better handling of cellular

stress or already increased rate of metabolism. As already mentioned, it is well described that cells under pathological conditions release higher concentration of EVs. Depending on the nature of EVs, it could be either a mechanism of disposal as a defence measure to cellular stress or release of mediators of protective immune response or signalling a proinflammatory response.

In addition to increase in the amount of secreting EVs, we found significant difference in the abundance of EV-related proteins in steatotic conditions. Furthermore, we discovered variability in the expression of EV-related proteins between our three models, which could arise from their different origin, as the conditions of the purification process were kept constant throughout. It has been described that exosomal content vary depending on the source and the pathological conditions of the cell and can provide insight into how cells cope with the pathology (McDonald et al. 2014). Lipid overloaded-AML12 cells secreted EVs with downregulated markers of exosomes, such as Cd81, Aip1/Alix and Tsg101. Our results are in agreement with a recent research on EVs isolated from palmitic acid induced lipotoxicity in hepatoma cell line, Huh7 (Hirsova et al. 2016). EVs in these conditions were shown to exhibit decreased expression of Alix, Tsg101 and Cd63 proteins, and were, as in accordance with our study, small vesicles of a maximum size of 200 nm. More importantly, they have shown, by targeting ROCK1, a kinase required for membrane blebbing, as well as Rab27b important for exosome biogenesis, that the main site of origin of this population of EVs was the plasma membrane (Hirsova et al. 2016). This could suggest, that the population, at least in part, of EVs secreted by our steatotic AML12 cells is composed by microvesicles, originating from the plasma membrane.

On the other hand, MLP29 cells, responded completely different to the lipid overload. Their secreted-EVs did carry exosomal marker proteins with an enrichment of Rab8, Hsp70 and Flotillin-1 in steatotic-EVs. Interestingly, there was a significant amount of lysosomal marker LimpII in these EVs and lysosome function has been implicated in the regulation of EV content and secretion (Eitan

et al. 2016). The increase in Hsp70 could indicate a stress response, which might be induced due to accumulation of misfolded or aggregated protein in the cells, because of oxidative stress, and EVs reflect metabolic state of the cell and serve as a cargo disposal. Enhanced expression of Flotillin-1 in steatotic MLP29-EVs, could indicate an involvement of lipid-rafts in EVs secretion as it has been described as one of the ESCRT-independent secretory pathways. In this system the Cd81 protein was detected in cells and affected by steatosis, however this result is not reflected in their secreted EVs. To sum up, these data suggest that these cells secrete more than one population of EVs, and depending on the condition the amount of each of them is altered.

Despite the still limited knowledge on liver-EVs, as compared to other origins, initial observations suggest that these vesicles are important in liver physiology and pathophysiology (Masyuk et al. 2013). It has been shown that EVs isolated from an *in vitro* cell culture model of saturated fatty acid-induced lipotoxicity exhibit proangiogenic effect mediated by the protein vanin-1 associated to EVs (Povero et al. 2013). Utilizing the choline-deficient L-amino acid (CDAA) dietary murine NASH model, the same group have demonstrated the increased secretion of EVs in NASH (Povero et al. 2014). In addition, an involvement of hepatocyte-derived EVs on liver repair and regeneration via increasing the synthesis of sphingosine-1-phosphate (S1P) has recently been discovered (Nojima et al. 2016)

Our research contributes to the knowledge on hepatocyte-EVs in physiology and pathology of hepatic steatosis. We have shown that steatotic hepatocytes secrete higher amount of EVs and that their content is significantly affected by these conditions, as seen by the change in protein marker expression, which could be further explored for disease biomarker discovery. Further experiments would be needed to confirm whether serum-EVs reflect the nature of EVs from steatotic hepatocytes.

Although cell lines are suitable *in vitro* models to study EVs secreted by hepatocytes, primary hepatocytes are meant to provide more relevant data since

it is the *in vitro* model that more closely mimics the *in vivo* state of these cells. In this study, we use hepatocytes from the livers of Zucker rats (Lean and Fatty), and for the isolation of EVs we culture them in standard cell culture conditions with EV-depleted medium for the period of 36h. The animals used for the study were all males, age-matched between 12-14 weeks that already have the manifestations of MetS, including the obesity accompanied by hyperinsulinemia, hyperlipidemia, adipose hypertrophy, insulin resistance, and hepatic steatosis. Livers were dispersed using a collagenase and cell suspension subjected to a Percoll density centrifugation to eliminate contamination from other cells of the liver. As observed during the hepatic perfusion, the livers of ZF animals were larger and were paler due to a very high fat content. Although only a few studies have been conducted on primary Zucker hepatocytes, it has been concluded that the Zucker fa/fa rat's obesity is expressed at the organismal as well as cellular levels (Kava et al. 1990). In addition to that, another study demonstrated that hepatocytes derived from Zucker rats can be successfully grown in primary culture and can be used to study the effects of the *Fa* gene (Goldstein & Johnson 1980) which makes it suitable in vitro model for short time culture.

Study on mitochondria from ZF rats showed that due to hepatic accumulation of fat, there was an impairment of mitochondrial function, reflecting the loss of oxidative phosphorylation capacity (Teodoro et al. 2006). The excessive build up of FFAs most probably causes a shift in metabolism of hepatocytes. To get more insights into the energy metabolism of our primary hepatocytes, we used an extracellular flux analyzer to measure their mitochondrial and glycolytic functions at 4 hours and following 24 hours in culture. ZF-hepatocytes exhibit a significant loss in all mitochondrial functions, which are slightly recovered after the 24 hours, and enhanced glycolytic parameters. Under normal conditions, the liver has a tremendous capacity for regeneration after injury, however this compensatory proliferation is compromised in steatotic livers (Vetelainen et al. 2007). Furthermore, as already mentioned, steatosis is a reversible process. Therefore, one possible explanation for the slightly recovery which we observe at 24h, could be the fact that the cells are trying to improve their metabolic phenotype which is

reflected as an increase in maximal respiration in ZF-hepatocytes. This improvement could also be attributed to the lack of stimulus from the expanding adipose tissue, which feeds FFAs to the liver due to uninhibited lipolysis (Qureshi & Abrams 2007). Moreover, it could also be associated with the increase in expression of genes encoding for hepatic functions.

In terms of lipid accumulation assessment by Bodipy staining we discovered that hepatocytes isolated from the Lean (*Fa/?*) rat liver, accumulated some intracellular lipid droplets. It could be due to the high glucose media, as the animals heterozygous for the fa allele are prone to diet induced metabolic disturbances (Morris et al. 2003). For future studies, we could used a Sprague Dawley rat, which is a match genetic background control to ZL rat (*fa/+*) to exclude any effects of the heterozygosity of the *fa* allele.

A theory has been put forward, that following the necessary change of media, after the cell attachment, some essential factors important for their own maintenance and conditioning are removed with arginine being proposed as an important conditioning factor (Goldstein & Johnson 1980). Moreover, lack of other cells of the liver also contribute to the effect of cell culture conditions.

Interestingly, we found that the expression of Rab10 upon stimulation with insulin was significantly reduced in ZF-hepatocytes. Rab proteins are important regulators of insulin-stimulated Glut4 translocation to the plasma membrane (Chen et al. 2012), which has been described in cultured 3T3-L1 adipocytes (Vazirani et al. 2016). Moreover, it has been shown that the adipose-specific Rab10 knockout mice exhibit significantly reduced insulin-stimulated glucose uptake and Glut4 translocation and severely inhibited glucose production (Vazirani et al. 2016). As it is a partial inhibition, full effect of insulin on adipose tissue is the combined effect of Rab10-dependant and Rab10-independant pathways, which as indicated by our results may also cause the hepatic insulin resistance.

The first study on the nature and composition of EVs isolated from the conditioned medium of Zucker rat hepatocytes (Lean and Fatty) is presented in this thesis. We have performed a comprehensive analysis of their biochemical nature, protein cargo and showed that they carry active molecules.

ZF-EV samples were significantly more concentrated when compared to their control ZL-EVs, both by protein amount (determined by Bradford and BCA assays) and by particle number (determined by NTA). In agreement with this result, increased number of circulating vesicles has been linked with obesity, inflammation and insulin resistance (M.-J. Lee et al. 2016). However, we observed that this alteration in amount accompanied by important differences in the presence of EV-related protein between ZL and ZF-EVs. Initially, we suspected that the abundance of lipids (expected to be hgher in ZF-EVs) could be interfering with the determination and then our interpretation that steatosis affects exosomal secretion in hepatocytes could be wrong. As we are working with primary culture of hepatocytes, we considered the possibility of lipoprotein co-isolation with our EVs, which would also influence the final quantification of the preparaions. Some ApoB signal was detected in EVs, indicating some extent of lipoprotein presence in EV preparations, however no significant differences were observed between ZL- and ZF-EVs, discarding that the observed differences in EV secretion were due to a higher lipoprotein contamination in ZF-EV preparations. We also loaded a SDS-PAGE gel with equal amount of protein, according to the estimation done by Bradford, and again based on Comassie and Ponceu, no difference was found between ZL- and ZF-EVs. Together, these data indicate that different population of EVs were secreted by steatotic hepatocytes. This was also supported by the change in the size distribution and in the idioxanol density gradient that showed the presence of vesicles with different densities when comparing ZL- and ZF-EV preparations.

There was one main population of vesicles associated with fraction 8 at density of 1.16g/ml, as seen by the distribution of Cd63, Rab8 and Apoe markers. However, in the sample of ZF-EVs, additionally the markers were also enriched

in fraction 9 at density of 1.19g/mL, corresponding to heavier vesicles. Interestingly, in ZF-EVs ApoE was solely present in vesicles of higher-density Moreover, the protein very highly enriched in the fraction 9 was Rab8 -a member of the Rab family of small GTPases- which plays an important role in membrane trafficking from the *trans*-Golgi network and recycling endosomes to the plasma membrane (Wang et al. 2015). The possibility that different routes, such as regulated by specific Rab GTPases, might be implicated in the production and secretion of EVs, with different biological functions has been proposed (Blanc & Vidal 2017). Each transport step requires that the activated Rab proteins bind to soluble factors that act as 'effectors' to transduce the signal of the Rab GTPase in the transport mechanism (Zerial & McBride 2001). Interestingly, the effector function of Rab8 is the stress activated protein kinase, which would be the second evidence that vesicles isolated from conditioned medium of ZF-hepatocytes reflect the state of the cell and carry cell-specific markers. This would suggest a mechanism of specific cargo sorting or a specialized way that cell uses for the management of cellular stress.

In connection with that, the composition of EVs is not a mere copy of cytosolic content; rather, specific molecules are selectively sorted into EVs to be secreted and amount and content of EVs can change in response to different stimuli (Villarroya-Beltri et al. 2016). In the case of ZF-EVs, their production must be governed by different mechanisms when compared with ZL-EVs, as seen by changes in all markers assessed, the Rab8, Cd81, Cd63, Tsg101, Aip1/Alix, Flotillin-1 and LimpII, and the overall increase in the secretion of EVs as measured by Bradford and NTA. We are possibly dealing with the enrichment in cell type-specific population of EVs. It must be considered that vesicular trafficking in the cells is a very complex process and involved endosomes, lysosomes, TGN and even the mitochondria. Therefore, more targeted experiments would be needed to unravel the exact origin of steatotic-EVs.

Along these lines, increased levels of microvesicles have been observed in plasma, urine and other body fluids in patients suffering from a wide range of

complex diseases, which has been directly related with cell activation and pathogenesis (Müller 2012). Their release is often modulated by specific extracellular signals, which in the case of ZF-EVs could be caused by lipotoxicity, increased fatty acid synthesis or the ROS production in steatosis, supported by the controlled and regulated secretion of Hsp's in ZF-EVs, accompanied by a clear reduction in the secreting cell.

To gain further insight into the nature of Zucker hepatocyte derived-EVs we performed their proteomic, LC-MS/MS analysis. The obtained results have confirmed a very clear functional distinction between down- and up-regulated proteins enriched in ZF-EVs. In agreement with our results on mitochondrial and glycolytic functions in Zucker hepatocytes, which revealed that mitochondrial functions in ZF-hepatocytes were significantly downregulated when compared to the control with a respective increase in glycolytic capacity. The proteomic analysis of EVs secreted by these cells has shown that they seem to reflect the metabolic state of the cell. Most of proteins identified were down-regulated (>75%) in ZF-EVs and interestingly most of the down-regulated proteins were mitochondrial proteins. Furthermore, as shown by LC-MS/MS analysis, ZF-EVs concentrate proteins involved in glycolysis, *de novo* lipogenesis and PPP, which again goes in agreement with our previous results showing augmented glycolytic functions in ZF-hepatocytes. Our results indicate that cellular stress conditions are reflected in the content of cell derived-EVs. According to the proteomic analysis of EVs secreted by hypoxic 3T3-L1 adipocytes there was an enrichment in enzymes related to *de novo* lipogenesis such as acetyl-CoA carboxylase, glucose-6-phosphate dehydrogenase, and fatty acid synthase, which was confirmed in serum exosomes from *ob/ob* mice (Sano et al. 2014). We could hypothesize that the phenotype could be related with excessive lipid accumulation in tissues such as adipose hypertrophy, which in fact results in hypoxia and could also be related with hepatic steatosis, as reflected in our results. It is reasonable to hypothesize that steatotic-EVs could mediate phenotypic transfer in healthy cells, propagating the pathology.

Hepatocytes are the main functional constituents of the liver (<80%) which is involved in many vital functions of an organism, such as glycogen storage, hormone production, plasma protein synthesis, detoxification and production of bile necessary for digestion. In relation with the liver functions, it was previously shown by Conde-Vancells *et al.* that exosomes secreted by primary rat hepatocytes contain proteins involved in the detoxification processes as well as proteins synthesized in the liver (Conde-Vancells et al. 2008). The detoxifying enzymes are sorted in two different classes: those that induce chemical changes in the compound such as P450s (phase I metabolism), and those that are capable of forming adducts with the metabolite to facilitate its clearance from circulation such as UGTs and GSTs (Phase II metabolism) (Iyanagi 2007). In accordance with previously published results, we have identified members of P450 superfamily of enzymes, mainly of the class 2D, as well as uridine 5'-diphospho-glucuronosyltransferase's (UGTs) and Glutathione *S*-transferases (GSTs). Interestingly, most of these proteins primarily residue in the ER near each other and their extracellular existence is not a common phenomenon, neither their association with EVs. Moreover, it seems to be specific to certain members of the distinct families of drug metabolizing enzymes. The reason for this segregation is still unknown.

Interestingly, LC-MS/MS analysis has revealed a consistent decrease in the abundance of all proteins necessary for drug metabolism in ZF-EVs as validated by WB and activity assay of Cyp2d1. In addition, as to the protein abundance, it was also consistently decreased in ZF-hepatocytes and interestingly the Cyp2d1 activity was associated to EVs and in lesser extent to hepatocytes. The decrease in the number of drug-metabolizing enzymes may lead to inappropriate drug metabolism or have adverse effects on the liver. Significant alterations in the activity of drug-metabolizing enzymes may affect the clearance of therapeutic drugs, with the potential to result in harmful drug reactions. These results would indicate that steatotic liver could be more susceptible to liver damage due to lower expression of enzymes responsible for detoxification. Our results in EVs, are in agreement with previous findings that decreased P450 activities and

protein levels were observed with steatosis, and moreover, significant correlation between P450 activities and liver fat content have been found (Donato et al. 2006).

Interestingly, the proteomic analysis has also revealed the presence of the Catechol-*O*-methyltransferase (COMT) in Zucker hepatocyte-derived EVs. COMT is an enzyme predominantly expressed in the liver and is found in soluble (S-COMT) or membrane bound (MB-COMT) form (Doyle et al. 2004). Its main function includes degrading catecholamines such as dopamine, epinephrine, and norepinephrine and various other drugs and substances having catechol structure. It is involved in the inactivation of the catecholamine neurotransmitters by introducing a methyl group to the catecholamine donated by S-adenosyl methionine (SAM) (Raxworthy et al. 1982; Doyle et al. 2004; Casal et al. 2016). The association of COMT protein and activity with hepatic-EVs has been shown before (Conde-Vancells et al. 2008; Casal et al. 2016). However, in this doctoral thesis we show for the first time the significantly enhanced secretion of the soluble, short form Comt (S-Comt) of 24kDa, associated to steatotic-EVs, when compared to the control. COMT is predominantly expressed in the liver and a study has found elevated level of the protein in both liver tissue and plasma during liver injury to be a blood-marker of acetaminophen (APAP)-induced hepatotoxicity (Hu et al. 2014). Furthermore, our findings would also support the involvement of COMT in the response to liver injury. Methylation of catechols by COMT limits their oxidation and conjugation to glutathione therefore if this process is downregulated due to increased secretion of Comt, extracellularly, it would ultimately give rise to increased accumulation of toxic metabolites.

There are some evidence of abnormalities in catecholamine metabolism in obesity (Levin et al. 1981). The *ob/ob* mice were shown to have less COMT activity in their liver than a normal mice (Feldman & Henderson 1978), which is in complete agreement with our results. According to the proteomic analysis and WB validation, we detected less Comt protein in hepatocyte lysates, however the phenotype of increase in secretion of Comt in EVs was evident. This would

support the hypothesis that decreased activity in the liver of the *ob/ob* mice could mean that more Comt protein is being secreted in association with EVs. Our results support that elevated levels of Comt in EVs could permit early detection of simple steatosis which will avoid that metabolic syndrome evolve to a more advanced state.

In relation with MetS conditions, our proteomic analysis has also identified the presence of two lipases, the 60kDa lysophospholipase (LPP60) and the hepatic triacylglycerol lipase (LIPC). Both were increased in ZF-EVs, 1.68 and 2.6 folds respectively. The first studies on the function of hepatic lipase, performed in whole animals revealed that the enzyme was involved in the metabolism of remnant lipoproteins (Galan et al. 2000). Hepatic triacylglycerol lipase (H-TGL) is a lipolytic enzyme synthesized by hepatocytes and present in liver sinusoid capillaries bound to heparin sulphate proteoglycans (Miksztowicz et al. 2012). Its catalytic activity contributes to the hepatic uptake of HDL cholesterol by reducing particle size (Marques-Vidal et al. 1994). The activity of hepatic lipase was detected in plasma of both fed and fasted rats and was correlated with that in the liver (Galan et al. 2000). Our preliminary results show that the lipase associated to ZF-EVs could be active as we showed that they might be able to catalyze the hydrolysis of VLDL.

The early studies on secretion of hepatic lipase were conducted on isolated rat liver parenchymal cells and in primary cultures of rat hepatocytes, and concluded that the continuous secretion requires protein syntheses (Galan et al. 2000). In that regard, results of our proteomic analysis indicate that one of the groups of up-regulated proteins in ZF-EVs, were related with protein synthesis and post-translational modifications such as 40S ribosomal protein S4, elongation factor 1-alpha, 60S ribosomal protein L9, and elongation factor 1-delta.

The increase in hepatic lipase activity affects the remodelling of remnants lipoproteins and of HDL and subsequently increases the formation of small, dense LDL and smaller HDL particles (Carr et al. 2002). Its action leads to increase in FFA pool, which is available for uptake into hepatocytes (Miksztowicz

et al. 2012). Hepatic lipase activity is increased in insulin resistance states. In addition, patients with hepatic steatosis had higher lipase activity, which positively correlated with the severity of hepatic steatosis, even after controlling the insulin resistance (Miksztowicz et al. 2012). Interestingly it has correlated with the reduction in circulating adiponectin, which agrees with our results. Adiponectin has a hepato-protective role suppressing the *in situ* pro-inflammatory adipokines expression (Lucero et al. 2011).

Our results indicate that the cargo of EVs released by steatotic hepatocytes do reflect the molecular state of the parent cell. Moreover, the fact that the lipase carried in ZF-EVs was active could negatively contribute to the atherogenic profile seen in MetS.

We performed detailed proteomic analysis of EVs secreted by steatotic hepatocytes. Moreover, we gained some insight into their lipidic nature and lastly, we have shown that Zucker hepatocyte-derived EVs also contain nucleic acids. The Bioanalyzer RNA analysis has revealed, that no ribosomal RNA was detected and according to the nt count, that the predominant population of nucleic acids were of small size. ExoRNA was isolated using commercial columns from 250 µg of starting material, and samples were analysed before and following the DNaseI treatment. In the untreated experimental group, a predominant peak was identified at low nt count, which disappeared following the DNaseI treatment. These results indicate that along with the RNA we co-purifying small DNA species. Taking that into account, the RNA quantification of the DNase treated samples were indicative that the overall overall amount of RNA isolated was limited. We also observed that, ZF-EVs contained higher amout of RNA that their lean counterpart. The open question remains whether the RNA isolated is functional and how could it influence the physiology of a target cell. Our results are in agreement with the previous report of the existence of mRNA in EVs isolated from the conditioned medium of hepatic cell lines as well as primary hepatocytes, which was incorporated by recipient hepatic stellate cells (Royo et al. 2013). In addition, they identified that a significant subset of RNAs

was associated with hepatic functions, which points towards an existence of a regulated sorting mechanism and that the RNA content greatly depended on the cellular model (Royo et al. 2013). As to the potential DNA contamination, the possibility of apoptotic DNA contribution cannot be discarded, however our WB results did not indicate significant enrichement in cleaved Parp, neither the trypan blue viability assessment. Moreover, the intensity of the peak, in the DNase untreated samples, in both ZL- and ZF-EV samples was comparable. These results argue against the DNA present in EVs mostly come from undergoing apoptosis, and open the question about the possible role of the DNA associated to Zucker-EVs. The presence of single-stranded exosomal DNA (exoDNA) was found in microvesicles from tumour cells (Balaj et al. 2011). Genomic DNA fragments were discovered in prostate cancer secreted EVs. Moreover, the p53 and PTEN genes in the EV subpopulations had the same mutation as the parental tumour cells (Lazaro-Ibanez et al. 2014).

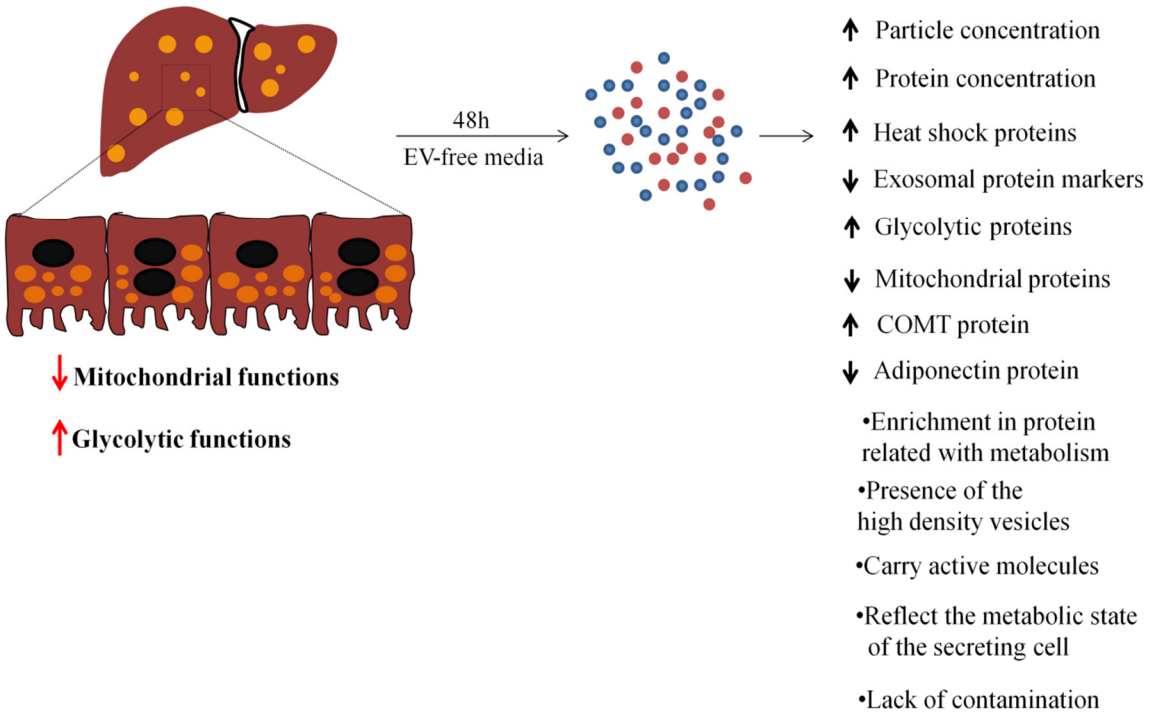

Figure 54 Summary diagram of results describen in chapter 3. Graphical representation of results regarding the characterization of EVs isolated from steatotic hepatocytes.

RESULTS CHAPTER 4

6. The effect of Zucker rat hepatocyte-derived EVs on 3T3-L1 adipocytes

6.1 Chapter 4 Aims:

- Study the possible influence of hepatic-EVs on 3T3-L1 adipogenesis.
- Investigate the changes in adipokine secretion by 3T3-L1 adipocytes upon exposure to hepatic-EVs.
- Study whether Zucker-EVs can transfer their glycolytic phenotype on recipient 3T3-L1 adipocytes.
- Investigate insulin sensitivity in 3T3-L1 adipocytes following the treatment with hepatic-EVs.

6.2 Introduction

As it has been emphasized along this thesis that the adipose tissue in the context of obesity is highly affected in terms of physiology and metabolism. In addition, adipose tissue greatly influences the physiology of peripheral tissues involved in the development of MetS. Besides, it has been shown that, at least in part, these effects are mediated by adipose-derived EVs. They have been shown to cause activation in peripheral blood monocytes and acquisition of the proinflammatory phenotype with increased secretion of TNF and IL-6 (Deng et al. 2009). Moreover, human AT-EVs are able to modulate insulin signalling in hepatocytes and thereby contribute to systemic insulin resistance (Mariëtte E G Kranendonk et al. 2014). More recently it was concluded that AT is a very

important source of circulating exosomal miRNAs, which can regulate gene expression in target tissues such as liver and muscle (Thomou et al. 2017). These are just few examples, but overall, most of research on the involvement of EVs in the development of MetS addresses the effect produced by adipose-derived EVs. Conversely, based on data presented in this thesis, other cell types metabolically affected, such as hepatic steatosis not only secrete EVs, but of a significantly distinct phenotype, which in physiological conditions contribute to the pool of circulating EVs.

Having that in mind, in the last part of this thesis, we focused on the possible effects that EVs, isolated from steatotic hepatocytes, may have on adipocytes. Our preliminary analysis covers processes such as adipogenesis progression, gene expression, adipokine secretion, energy metabolism and finally insulin sensitivity.

6.3 Results

6.3.1 Effect of Zucker Rat Hepatocyte-derived EVs on 3T3-L1 Adipocyte Differentiation

The 3T3-L1 cell line is derived from 17-19-day-old Swiss 3T3 mouse embryos (Sarjeant & Stephens 2012) and can be propagated indefinitely in culture. For differentiation into adipocytes, once the confluent monolayer is reached, the 3T3 cells stop growing and remain viable in resting state for a long period of time when the accumulation of lipid droplets is observed (Green & Kehinde 1974) which has been shown to be significantly enhanced by insulin (Green & Kehinde 1975; Efthimios 1978). Furthermore, apart from insulin other hormones are involved in the differentiation process of the 3T3-L1 pre-adipocyte cell line such as prostaglandins, which increase cyclic AMP levels in fibroblasts and lower them in adipocytes. Indomethacin, an inhibitor of prostaglandin biosynthesis, has

been found to shorten the differentiation time significantly in the presence of insulin and increase the expression of lipogenic enzyme activity (Williams & Polakis 1977).

In the presence of an adipogenic cocktail, confluent 3T3-L1 cells differentiate to mature adipocytes. The basic adipogenic cocktail contains insulin, DEX, and IBMX and in some studies, rosiglitazone. The usage of rosiglitazone additive was based on the earlier observation that human liposarcoma cells can be induced to undergo adipose differentiation in the presence of thiazolidinedione (Zebisch et al. 2012). In recent years several microarray studies on the gene expression in the 3T3-L1 cell differentiation have been published, which came with the discovery of several differentiation markers.

AT in obesity is characterized by dysfunctional hypertrophic adipocytes, an increase in proportion of adipose progenitors and infiltration of immune cells. The limitation in AT expansion, in part due to inhibition of adipocyte progenitor differentiation in an inflammatory microenvironment, which in turn leads to ectopic accumulation of lipids in peripheral tissues (Dani 2013).

Having all that in mind, we first sought to study the effect of Zucker rat hepatocyte secreted EVs on the progression of the 3T3-L1 cells differentiation. The workflow of the experimental design is shown in **Figure 55**. Briefly, standard protocol for the differentiation of 3T3-L1 cells was followed with the minor modification of EV-depleted medium being used throughout the differentiation process instead of the ordinary DMEM, to avoid confusing results produced by FBS-EVs. Once the 3T3-L1 fibroblasts reached confluence, cells were replenished with the fresh growth medium for 48 h before commencing the differentiation. At that point the first sample was collected. Subsequently, together with the adipogenic cocktail, all six experimental groups, one for each time point, were treated with 30 μg of ZL-, ZF-EVs or left untreated, as indicated in **Figure 55**. After 48 h, the first ´Differentiation ´experimental group was collected and stored at -80^{0}C, following the next round of treatment for the remaining groups. Once all experimental groups were collected, total RNA was

isolated and processed for the qPCR analysis of adipogenesis-related gene expression. Each sample was run in duplicate. Validation and normalization was done using various housekeeping genes, depending on the differentiation stage of the 3T3-L1 cells.

The issue of housekeeping genes used at different stages of 3T3-L1 cell differentiation has been studied already and the research paper validating reference genes for qPCR gene expression analysis was published (Arsenijevic et al. 2012). Here, the recommended, most stable housekeeping genes were used, moreover the analysis was performed with each individual housekeeping gene to assure accuracy. The ATP synthase subunit beta, mitochondrial (ATP-5b) and hypoxanthine-guanine phosphoribosyltransferase (HPRT) were used to normalize the clonal expansion phase sample group and the large ribosomal protein L13a (RPL), Non-POU-domain containing octamer binding protein (NoNo) and ß-actin (ACTB) the terminal differentiation phase experimental groups. Clonal expansion corresponds to the differentiation experimental groups and the remaining to the terminal differentiation.

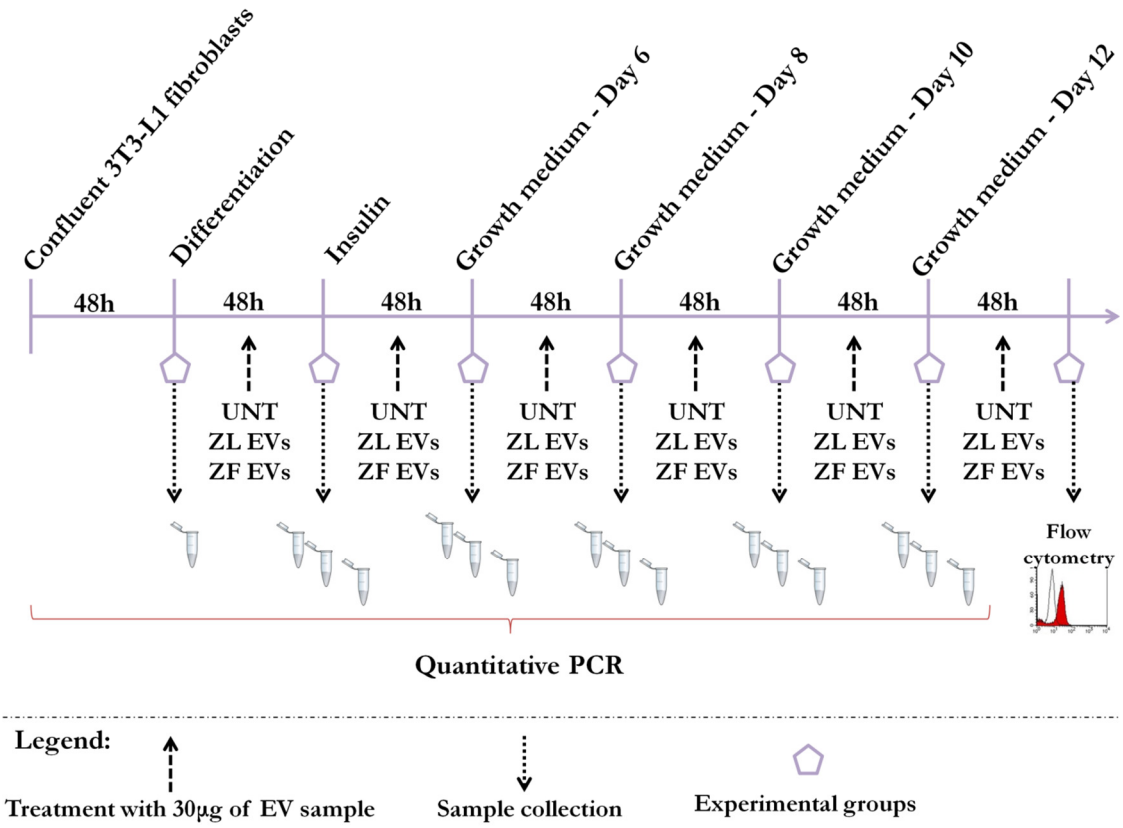

Figure 55 Experimental design of the study of the effect of Zucker rat hepatocyte secreted EVs on differentiation of 3T3-L1 cells. Diagram representing the experimental designed to study the influence of Zucker rat hepatocyte secreted EVs on the progression of differentiation of 3T3-L1 cells into adipocytes. 3T3-L1 cells were differentiated following the standard protocol with minor modifications of the EV depleted medium being used. As indicated by upward dotted arrow, at each time point, cells were differentiated as usual or in the presence of 30 µg of ZL- or ZF-EVs. The protocol follows 12-day differentiation timeline with media change every 48h. At each time point samples were collected for subsequent qPCR analysis. The final samples were analyzed by flow cytometry for lipid accumulation by staining the cells with Bodipy.

Following the induction of differentiation, at the clonal expansion stage, gene expression analysis was performed and compared to the expression in 3T3-L1 fibroblasts, which were used as a control **(Figure 56)**. Then, the same panel of genes was analyzed at the terminal differentiation stage that begins after insulin addition and ends at day 12 **(Figure 56)**. In this case, the level of gene expression in pre-adipocytes was used as control **(Figure 57)**. We analysed the expressions of several representative genes of various classes such as differentiation related *Pparg,* adipocyte fatty acid binding protein (*Ap2)* and CCAAT/enhancer binding protein alpha (*Cebpa)* **(Figure 56A).** PPARγ is a master regulator of adipogenesis and has been shown to be crucial and sufficient for adipocyte development *in vitro* and *in vivo* (Sarjeant & Stephens 2012). AP2 is a key mediator of intracellular transport and metabolism of fatty acids. Its expression during adipocyte differentiation is regulated through the actions of PPARγ and C/EBPalpha (Sun et al. 2003). Another set of genes was related with lipid metabolism such as fatty acid synthase (*Fasn*), adipose differentiation-related protein (*Plin2*), perilipin-3 (*Plin3*), involved in lipid droplet formation (Nose et al. 2013). Furthermore, adiponectin gene (*Adipoq)*, which promotes adipocyte differentiation, insulin sensitivity, and lipid accumulation was also induced in our panel. Moreover, the ability of adipocytes to respond to insulin and to express fatty acid binding protein genes, lipoprotein lipase and Glut4 is required during their differentiation into mature adipocytes (Yamamoto et al. 2002). Knowing that, the expression of *Slc2a4* gene, encoding for Glut4 was also assessed in our study. Finally, the expression of known adipose-produced chemokine, CCL5 (RANTES), which promotes the recruitment of macrophages to adipose tissue (Keophiphath et al. 2010) was also measured.

The results indicate that no major changes were seen in the level of expression of *Pparg* and *Ap2* in cells differentiated in the presence of EVs, as compared to the untreated sample at the clonal expansion stage. Upon differentiation, the expression of the *Cebpa* increased 8-fold, however, cells differentiated in the presence of EVs did not reach that level of expression. Nearly, a 2-fold decrease was observed in cells treated with ZL-EVs and 1.5 times in ZF treated cells. More

pronounced changes were seen in the expression of lipid-related genes **(Figure 56B).** The expression of *Fasn* was increased in cells differentiated with ZF-EVs and in turn slightly decreased in cells treated with ZL-EVs. Moreover, the increase in the expression of *Plin3* in ZF-EV treated adipocytes was observed with the same trend for the *Slc2a4* gene, nearly 5-fold increase in ZF-EV treated cells. Differentiation strongly induced the expression of adiponectin, however treated cells, did not reach the same level of abundance of adiponectin mRNA as the untreated cells. The association of chronic, low grade inflammation and the secretion of inflammatory cytokines and chemokines with the adipose tissue in obesity has been well described with TNF and IL-6 being the first ones to be identified as a possible link (Matter & Handschin 2007). Since then many more have been identified, among them, CCL5 also known as RANTES, a T-cell expressed and secreted chemokine (Matter & Handschin 2007), which seems to be very strongly induced by ZL-EVs **(Figure 56C and 56C)**.

The same panel of genes, as in **Figure 57**, was assessed during the terminal differentiation stage of adipogenesis at four different time points. First, after the addition of insulin and later at day 6, day 8, and day 10 of differentiation with the addition of complete medium **(Figure 55)** The data was analyzed using pre-adipocytes, just after the induction of differentiation as a control.

With regards to genes involved in the differentiation process, we found that cells treated with ZF-EVs did not respond to insulin as the ZL-control or the untreated **(Figure 57)**. The same trend was seen for *Ap2* and *Cebpa* gene expression. At a subsequent stage with the first addition of complete medium (day 6), the response was recovered, with a notable increase in expression of all three genes, *Pparg*, *Ap2*. ZL-EV treated cells caused slightly higher induction of *Ap2* and *Cebpa* and ZF-EVs in *Pparg*. The increasing trend was also maintained in the following stage, at day 8, the elevated expression in EV-treated samples in the expression of all three genes, more in ZF-EVs treated cells.

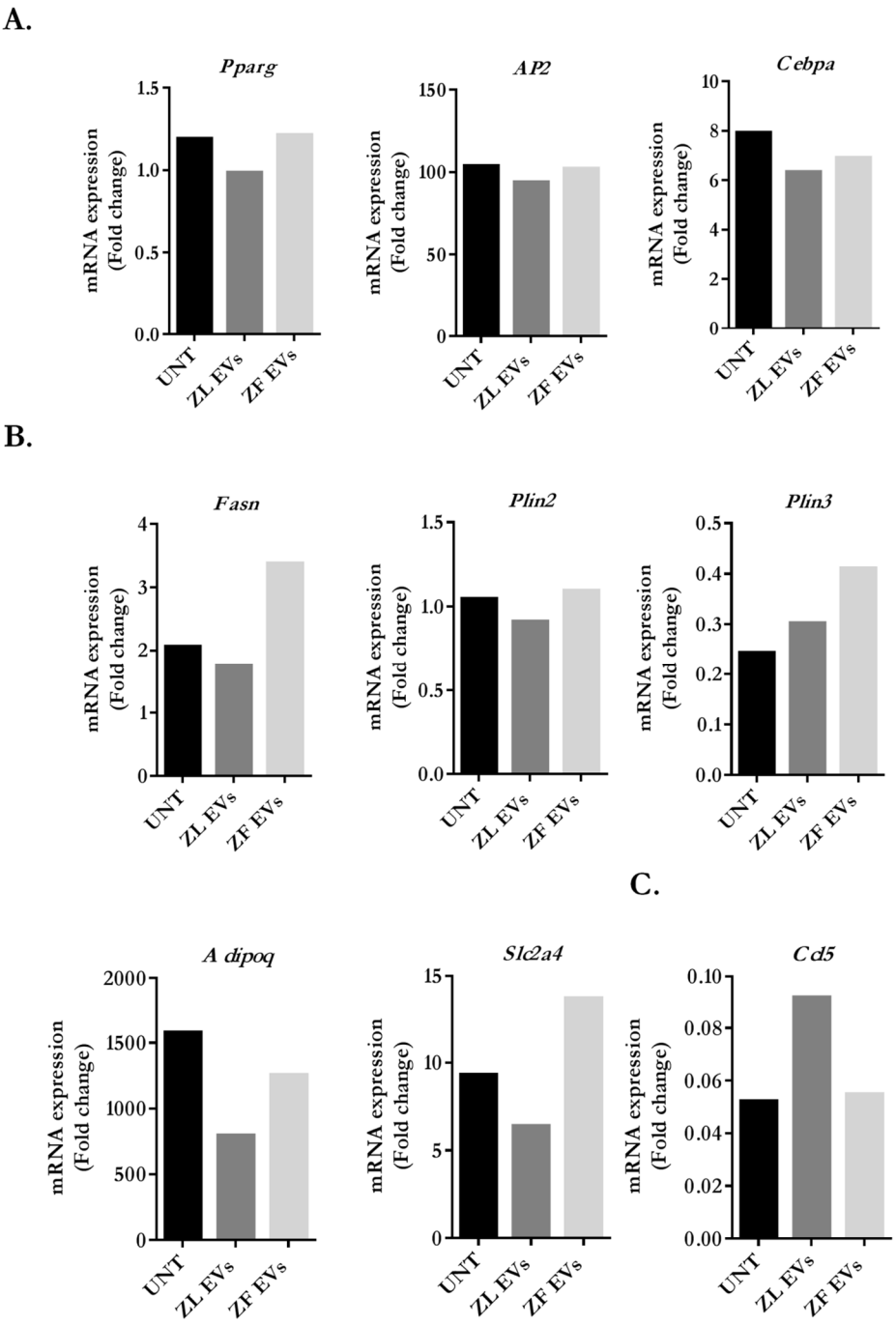

Figure 56 Gene expression analysis in differentiating 3T3-L1 cells in the presence of Zucker rat hepatocyte secreted EVs. mRNA levels of genes encoding for **(A)** Peroxisome proliferator-activated receptor gamma, Fatty acid binding protein, CCAAT/enhancer-binding protein alpha, respectively **(B)** Fatty acid synthase, Perilipin2, Perilipin3, Adiponectin, Glut4, respectively **(C)** RANTES, at the clonal expansion stage of the differentiation. Biological replicates = 1, technical replicate = 3.

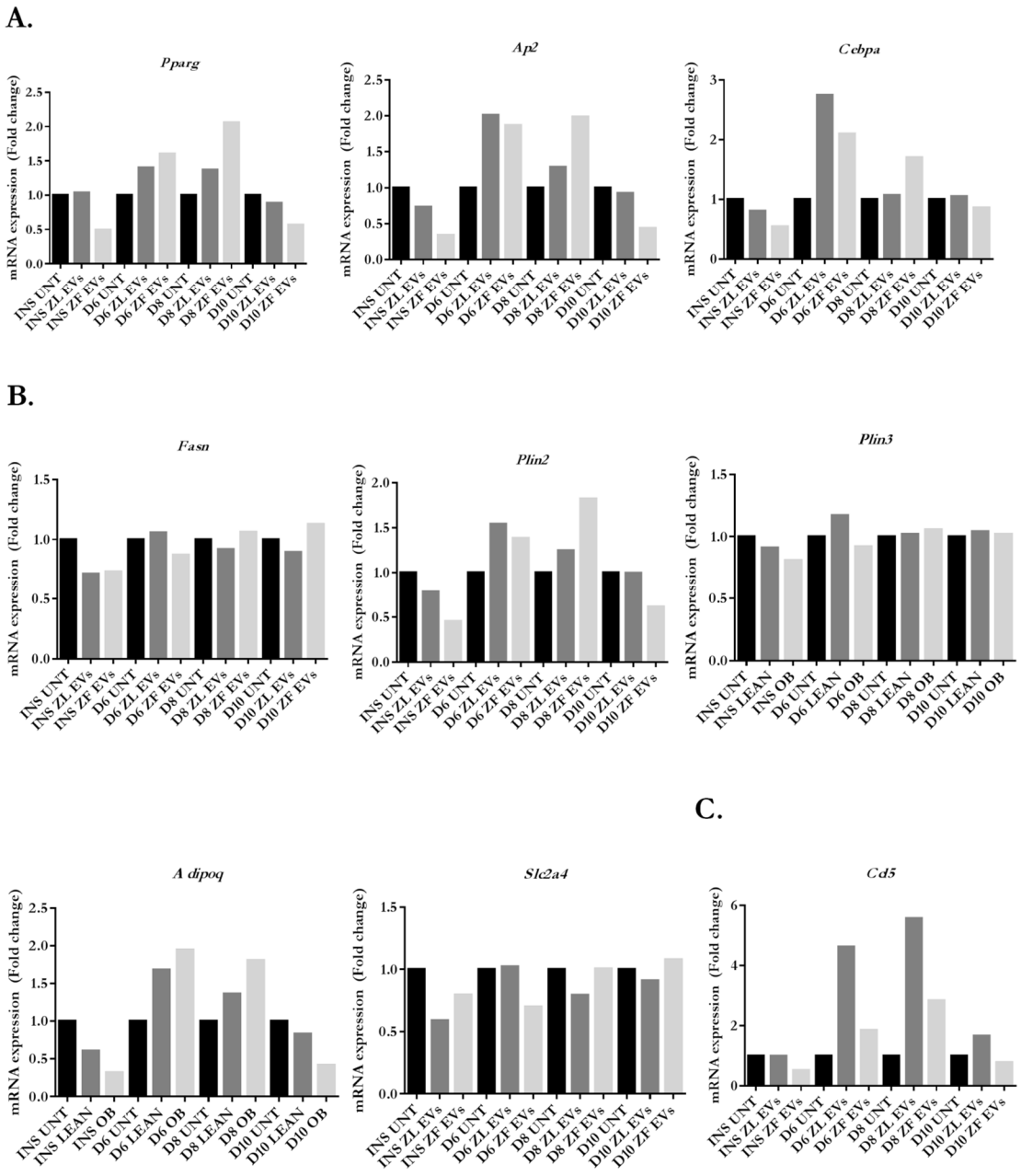

Figure 57 Gene expression analysis in differentiating 3T3-L1 cells in the presence of Zucker rat hepatocyte secreted EVs. mRNA levels of genes encoding for **(A)** Peroxisome proliferator-activated receptor gamma, Fatty acid binding protein, CCAAT/enhancer-binding protein alpha, respectively **(B)** Fatty acid synthase, Perilipin2, Perilipin3, Adiponectin, Glut4, respectively **(C)** RANTES, at the terminal stage of differentiation. Biological replicates = 1, technical replicate = 3.

At later stages of differentiation, when cells mostly accumulate lipids, the trend was reversed, as seen by the decline in expression of adipogenesis-related genes in cells differentiated with ZF-EVs. In the lipid-related gene group we found decreasing tendency in treated cells, upon the stimulation with insulin, for all genes analyzed. Remarkably, *Adipoq* and *Plin2* expression was specifically reduced in ZF-EV treated cells. At day 6, the first day when growth medium without other factors was added to cells, the response in EV-treated cells was recovered with cells exposed to ZF-EVs exhibit lowered capacity to recover as compared to cells treated with ZL-EVs. Higher expression was only seen in *Adipoq* following exposure to ZF-EVs. Interestingly, between day 8 and day 10 of differentiation, the expression profiles reversed. *Plin2* and *Adipoq* expression switches from being markedly increased at day 8 to being reduced at day 10, when compared to untreated as well as ZL-treated cells. The expression pattern of both genes followed the same trend throughout the remaining of the differentiation process. In the last two stages, *Plin3* expression remained unchanged across all sample groups.

The expression of *Ccl5* was very specific and mainly associated with ZL-EV treated cells. The five-fold increase seen at day 8 recovered significantly during the final stage (day 10). A very slight increase was also associated to ZF-EV treated cells, again more visible at day 8, as with cells treated with ZL-EVs **(Figure 57C)**.

At day 12 of differentiation, when adipocytes were fully differentiated, cells were collected for lipid accumulation analysis by staining with Bodipy and subsequent quantification by flow cytometry. The analysis revealed that the presence of both, ZL and ZF-EV negatively influenced lipid accumulation in 3T3-L1 adipocytes (**Figure 58A**). Although not statistically significant, there was a decrease in lipid accumulation in adipocytes differentiated with ZL-EVs and even further when exposed to ZF-EVs (**Figure 58B**).

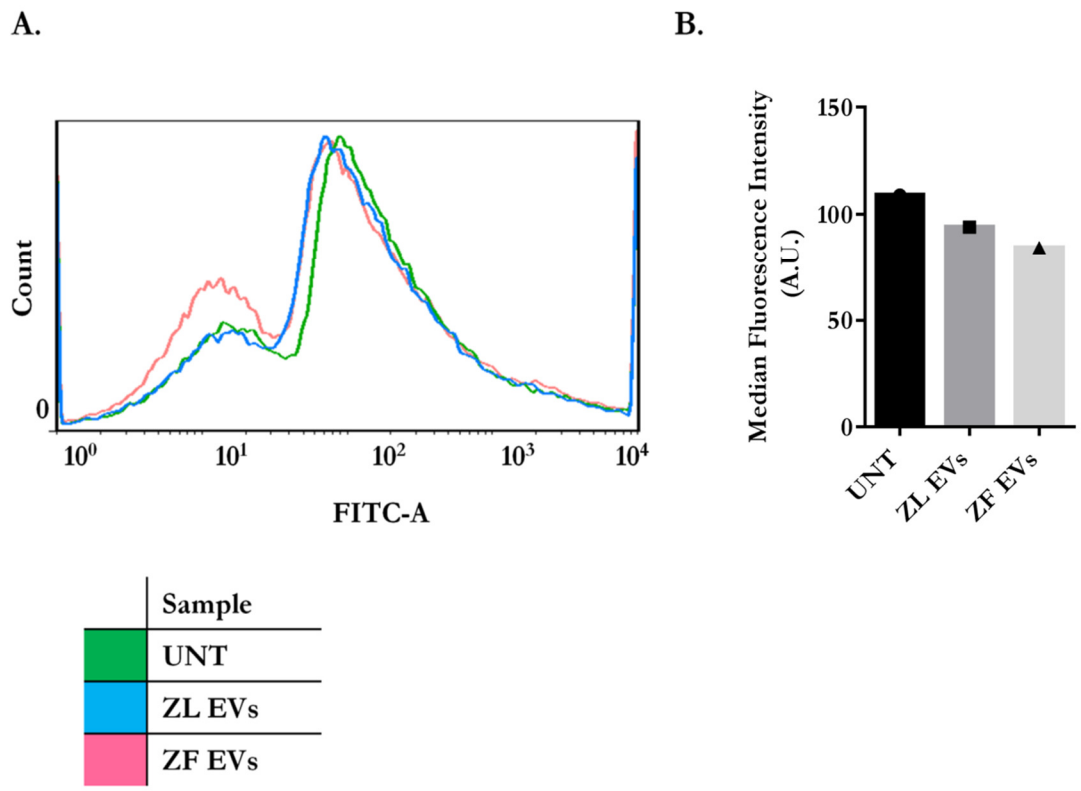

Figure 58 Decreased lipid accumulation following differentiation of the 3T3-L1 cells in the presence of Zucker rat hepatocyte EVs. 3T3-L1 cells were differentiated in the presence of EVs. On day 12, cells were collected and stained with Bodipy (10 µg/ml) and analyzed by flow cytometry. **(A)** Flow cytometry histograms. **(B)** Quantification of the median FITC-A fluorescence; n=1.

In conclusion of this part, EVs seem to affect the differentiation of 3T3-L1 cells and depending on the differentiation stage, a response of different genes varies. At the clonal expansion stage, ZF-EVs specifically increased the expression in the *Fasn* and *Slc2a4* genes. Moreover, ZF-EVs specifically decreased the expression of *Adipoq*, which could indicate a transfer of phenotype as we have previously shown that ZF-EVs carried decreased adiponectin. Finally, the induction of *Ccl5* expression by ZL-EVs was very specific and was also seen at later stages.

6.3.2 The influence of acute and chronic exposure of hepatic-EVs on the gene expression profile of the 3T3-L1 adipocytes

We next sought to investigate the acute and chronic effects of hepatocyte-derived EVs on gene expression in recipient 3T3-L1 adipocytes. The experimental design is shown on **Figure 59**. Briefly, 3T3-L1 adipocytes were grown and differentiated in 12-multiwell plate. Mature adipocytes were either left untreated or treated with ZL and ZF-EVs (30 µg) for 24 h in EV-depleted medium. At that point a set of samples (acute) was collected and cell pellets kept at -80^{0}C, until needed. Then, another set of cells were given three subsequent treatments with Zucker rat hepatocyte-derived EVs, 10 µg, each time for the 24 h period. Three days later, the second set of samples was collected, and RNA isolated for subsequent qPCR analysis.

Gene expression analysis of several selected genes of various classes was performed on acute **(Figure 60)** and chronically **(Figure 61)** treated adipocytes. The untreated cells were used as a control in the analysis.

We determined the expression of *Pparg, Rent, Fasn, Plin3, Tnf, COXIII* and *Adipoq* **(Figure 60)**. The results indicate that the genes mostly affected by acute treatment with ZF-EVs were those encoding for Pparg and Resistin proteins. As already mentioned, PPARγ is an essential regulator of adipogenesis, as no single factor has been identified that can drive adipogenesis in its absence. It is also important for the maintenance of the fully differentiated state both *in vivo* and *in vitro* (Lee & Ge 2014). Resistin, on the other hand, is a signalling molecule that is induced during adipogenesis and nearly exclusively secreted by white adipose tissue. With its discovery in 2002, many studies followed, which associated the elevated expression of Resistin with diet-induced obesity, confirmed in genetic models of obesity such as *ob*/*ob* and *db*/*db* mice. Moreover, purified Resistin was able to induce reduction in insulin stimulated glucose uptake in 3T3-L1 adipocytes (Steppan et al. 2002).

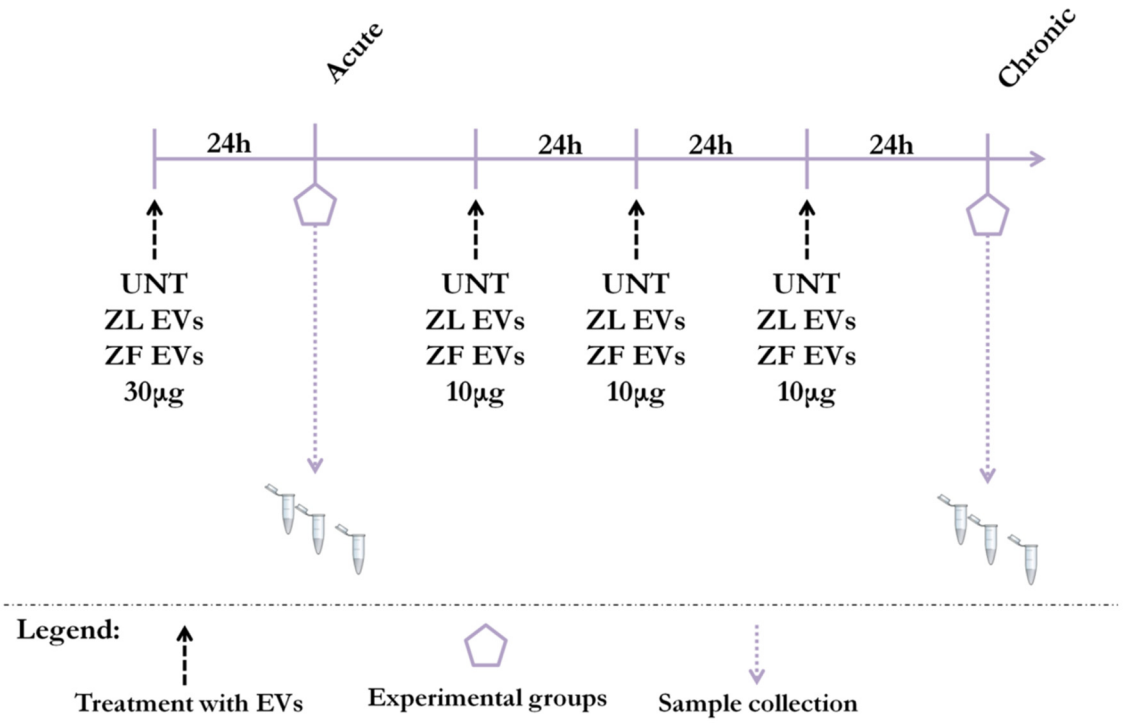

Figure 59 Experimental design of the study of the effect of Zucker rat hepatocyte secreted EVs on the gene expression in 3T3-L1 adipocytes. Diagram representing the experimental design to study the influence of Zucker rat hepatocyte secreted EVs on gene expression in 3T3-L1 adipocytes. 3T3-L1 cells were differentiated following standard protocol. On day 13, 3T3-L1 adipocytes were acutely treated with 30 µg of ZL- and ZF-EVs and in the chronic experimental group, cells were treated three times with 10 µg of ZL and ZF-EVs for 24 h each.

Moreover, the expression of *Fasn* and *Plin3*, lipid-related genes were unaffected by exposure to Zucker-EVs. A very small increase was seen in the expression of genes encoding for Adiponectin and for the Cytochrome *c* oxidase subunit III (COXIII), following acute exposure to ZF-EVs. A more extensive panel of genes was screened in the chronic experimental group **(Figure 61)**. First, when comparing the expression of the same genes in both experimental groups, acute and chronic.

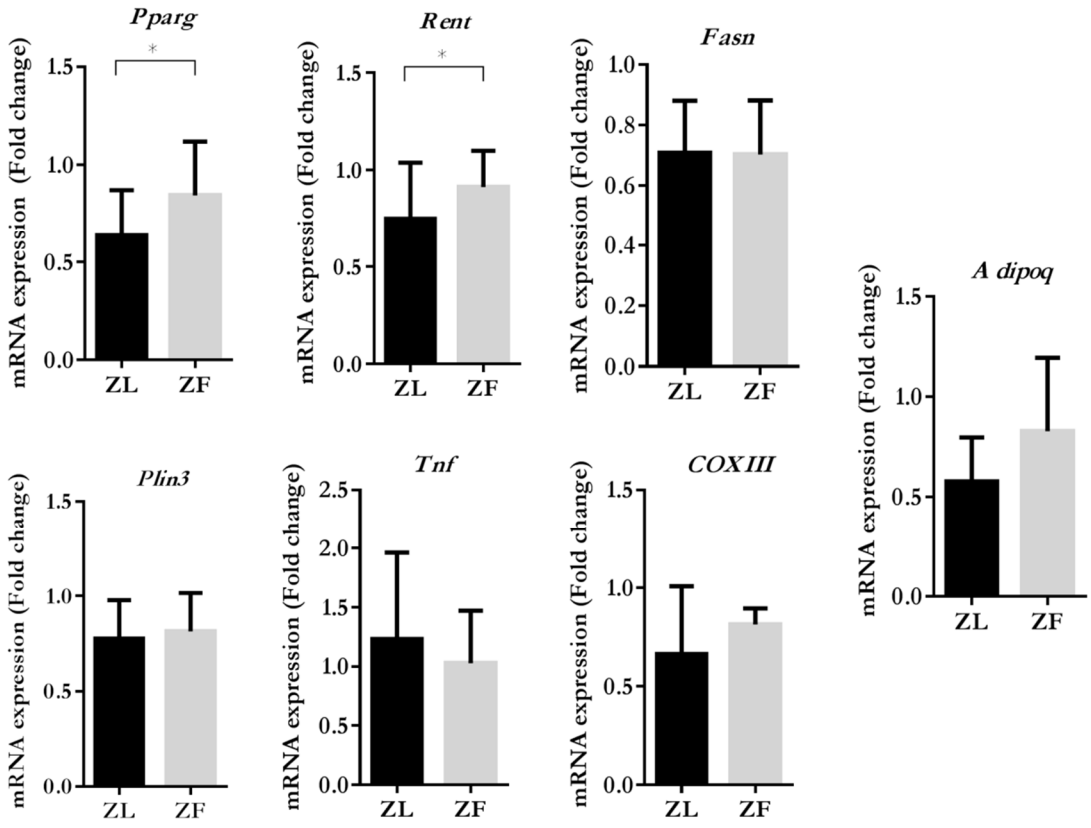

Figure 60 Changes in the gene expression in 3T3-L1 adipocytes upon acute exposure on Zucker rat hepatocyte secreted EVs. qPCR analysis of gene expression in 3T3-L1 adipocytes following acute exposure to ZL-and ZF-EVs, biological replicates n=3, technical replicates n=2; housekeeping gene used for normalization was ß-actin. Error bars = SD. Unpaired student t-test was performed to determine significant differences.

The fold induction of expression increased in samples following the chronic treatment. Importantly, in both experimental settings, there was an increase in *Pparg* and *Rent* gene expression, following the treatment with ZF-EVs. Moreover, an increase in *COXIII* transcription following the acute treatment with ZF-EVs becomes significant after chronic exposure to those EVs.

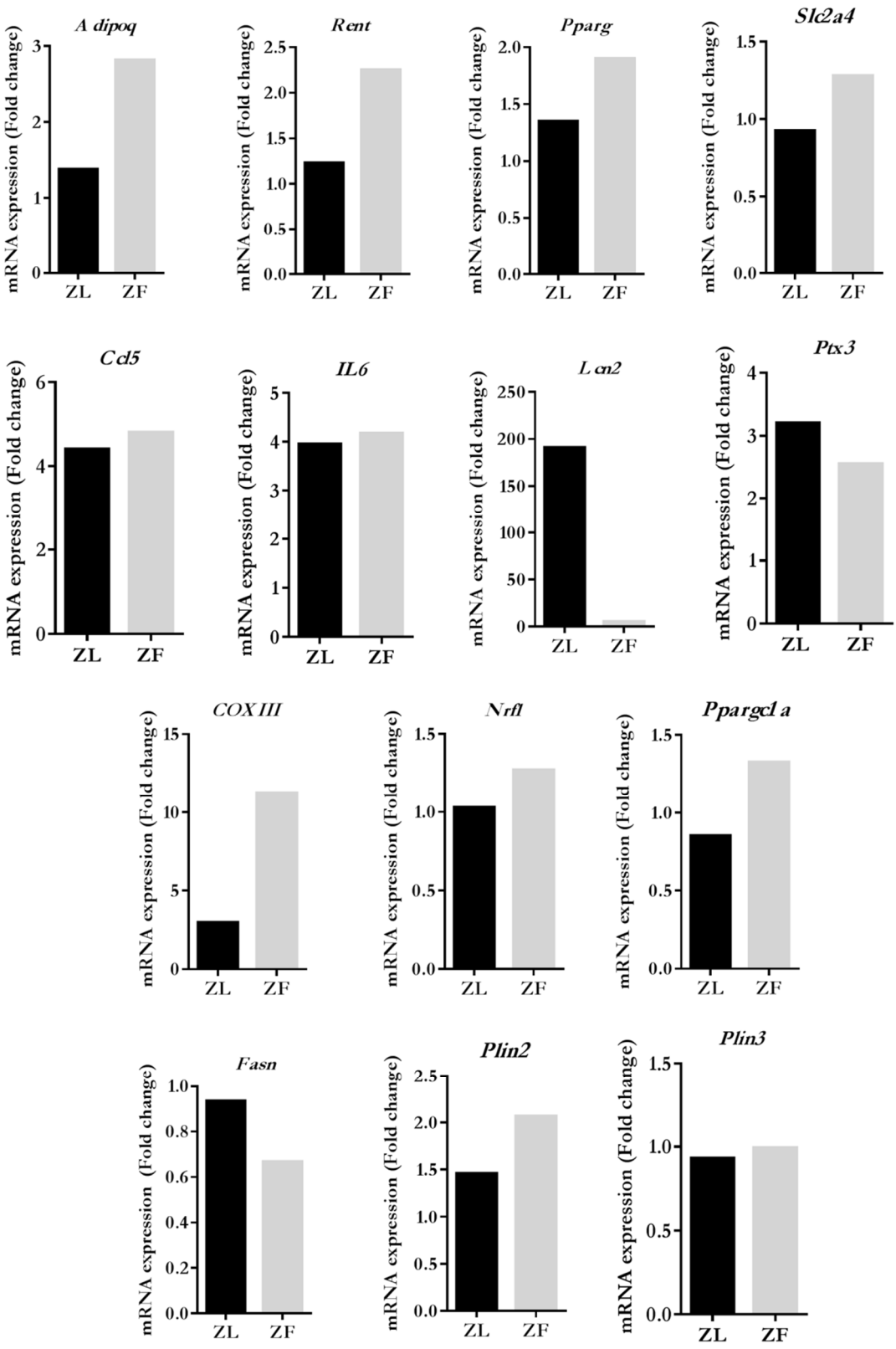
A dipoq
Rent
Pparg
Slc2a4
Ccl5
IL6
Lcn2
Ptx3
COXIII
Nrf1
Ppargc1a
Fasn
Plin2
Plin3
mRNA expression (Fold change)
ZL
ZF

Figure 61 Changes in the gene expression in 3T3-L1 adipocytes upon chronic exposure on Zucker rat hepatocyte secreted EVs qPCR analysis of gene expression in 3T3-L1 adipocytes following chronic exposure to ZL-and ZF-EVs, biological replicates n=1, technical replicates n=2; housekeeping gene used for normalization was ß-actin.

Interestingly, in terms of the respiratory functions there seem to be a ligth increase in the transcription of the *Nrf1* gene encoding for the nuclear respiratory factor 1, which could indicate a transient enhancement in mitochondrial respiratory capacity in 3T3-L1 adipocytes. Interestingly, genes related with lipid metabolism such as *Fasn* was downregulated as opposed to *Plin2* which was highly upregulated in 3T3-L1 adipocytes exposed to ZF-EVs.

Overall, we observed that, EVs secreted by Zucker rat hepatocytes could modify gene expression in recipient 3T3-L1 adipocytes and, through that, to influence a broad spectrum of biological processes involved in their physiology.

6.3.3 The influence of hepatic-EVs on the adipokine secretion of the 3T3-L1 adipocytes

Based on our findings, described in the previous sections on modulation of gene expression by hepatic-EVs in 3T3-L1 adipocytes, we wanted to determine whether, treatment with EVs secreted by Zucker rat hepatocytes, in ZL and ZF models provoked changes in adipokine secretion in 3T3-L1 adipocytes by using the Proteome Profiler Mouse Adipokine Array Kit **(Section.2.16.)**. **Figure 62** shows the design of the adipokine experiment. The array was used to screen supernatants from 3T3-L1 adipocytes previously exposed to Zucker hepatocyte-derived EVs. Results of densitometry were normalized to the untreated sample and presented as a fold increase in a heatmap diagram with the gradient of colours ranging from downregulated red to upregulated green **(Figure 62)**. Moreover, a percentage of standard deviation between duplicates in both groups was also calculated. A total of 28 out of 38 adipokines were detected in our supernatants and overall, the expression of several adipokines was found altered upon the treatment with EVs and interestingly, most of the changes were mediated by ZL-EVs **(Figure 62)**.

Exposure to ZL-EVs caused a very important increase in the secretion of several adipokines by 3T3-L1 adipocytes including RANTES (Ccl5), Il-6, Lipocalin2 and FetuinA. The up-regulation of RANTES by ZL-EVs in differentiating 3T3-L1 cells was previously shown by qPCR **(Figure 55C** and **Figure 56C)**. The circulating levels of RANTES were shown to be increased in subjects with impaired glucose tolerance and type 2 diabetes (Nomura et al. 2000). Moreover, the release of RANTES is adipocyte size dependant, with larger fat cells releasing significantly more (Skurk et al. 2009). Over 8-fold increase in RANTES secretion was seen upon treatment with Zucker rat hepatocyte-derived EVs **(Figure 63)**.

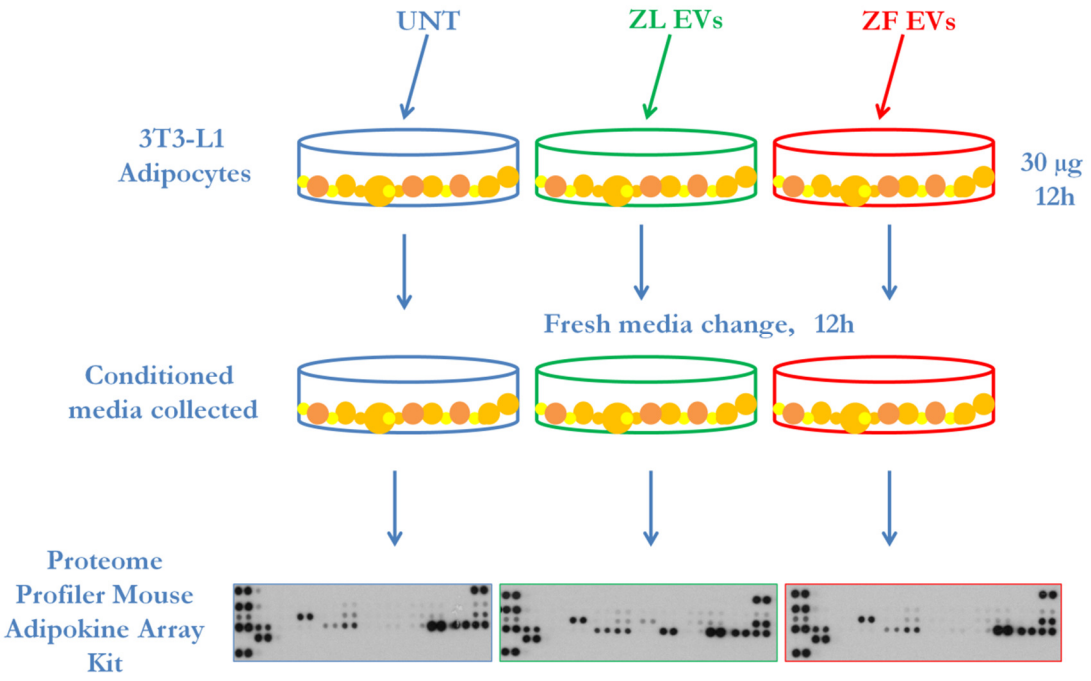

Figure 62 Experimental design of the adipokine array experiment. 3T3-L1 adipocytes were grown and differentiated in 12-well plate format. At day 13, cells were treated with 30 µg of ZL- and ZF-EVs or left untreated for 12 h, in EV depleted medium. The treatment was then removed and replaced with fresh medium for another 12 h. The conditioned medium of adipocytes was assayed for the presence of 38 adipokines.

The second most highly up-regulated adipokine by ZL-EVs, was IL-6, which increased concentration positively correlate with obesity and insulin resistance (Rotter et al. 2003). Moreover, FetuinA was also found highly up-regulated upon exposure to ZL EVs **(Figure 63)**. This multifunctional protein, modulates a number of signalling pathways such as TGF-ß and insulin (Nangami et al. 2014).

			StDev (%)	
Adipokines	**ZL EVs**	**ZF EVs**	**ZL EVs**	**ZF EVs**
Resistin	0.88	0.95	1.343503	1.979899
Lipocalin2	5.81	4.51	0.282843	0.636396
M-CSF	1.20	1.05	0.777817	0.565685
Pentraxin3	1.51	1.01	0.919239	0.494975
IGFII	1.24	1.39	1.06066	0.636396
IL-6	7.30	1.30	0.282843	0
RANTES (CCL5)	8.29	1.10	0.141421	0.424264
IGFBP-6	0.81	0.78	0	0.494975
Serpin E1	0.80	0.88	0.636396	1.414214
TIMP1	0.83	0.98	0.424264	0.282843
Endocan	1.16	1.07	0.212132	0.212132
IGF-I	0.84	0.99	0.636396	0.424264
Adiponectin	0.94	1.00	0.494975	0.353553
MCP-1	0.85	0.95	0.777817	0.777817
DPPIV (CD26/DPP4)	2.47	1.22	0.282843	0.212132
Fetuin A	5.71	1.41	0.141421	0.282843
FGF acidic	1.06	0.88	0.141421	0.212132
HGF	1.57	1.28	0.636396	0.141421
ICAM-1	1.30	1.57	0.070711	0.070711
IGFBP-2	0.86	0.78	0.636396	0.141421
IGFBP-3	1.25	1.21	0.636396	0.707107
IGFBP-5	1.22	1.00	0.353553	0.212132
IL-10	1.37	0.66	0.565685	0.424264
Leptin	1.18	1.18	3.394113	2.12132
Pentraxin2 (PTX2/SAP)	1.05	0.98	0.353553	0.070711
Pref-1	1.01	0.99	1.202082	0.212132
TNFα	0.77	1.12	0	0.919239
VEGF	1.10	1.12	0.707107	0.636396

Figure 63 Adipokine Array Heatmap. Changes observed in the secretion of a adipokines by 3T3-L1 adipocytes upon exposure to ZL- and ZF-EVs (30 μg/12h). SD (%) is shown/adipokine; biological replicate = 1, technical replicate = 2.

It has been shown to be involved in cell adhesion, one mechanism proposed being, a shuttle of histones in exosomes by FetuinA which then by interacting with cell surface heparin sulfate proteoglycans mediate cell adhesion. On the other hand, in adipose tissue FetuinA acts as chemoattractant for macrophage migration and polarizes adipose tissue M2 macrophages to the proinflammatory M1 subtype (Chatterjee et al. 2013).

We found that the majority of adipokines tested were either unchanged or downregulated upon treatment with ZF-EVs. A marked decrease in the expression of anti-inflammatory cytokine IL-10 was observed. One of its anti-inflammatory effects is antagonizing the action of TNF (Lumeng, Bodzin, et al. 2007). Here, no change in TNF was observed. The decrease in circulating IL-10 in serum of obese subjects has been associated with obesity (Esposito et al. 2003). Moreover, the increased secretion of Lipocalin2 by 3T3-L1 adipocytes was caused by both ZL as well as ZF-EVs, the effect that seems to be associated to hepatic-EVs. None of those differences reached statistical significance, most likely due to the limited sample number.

6.3.4 The Influence of Zucker Rat hepatocyte-derived EVs on lipid metabolism of 3T3-L1 adipocytes

Our previous results indicate that there was a slight increase in lipid content in the sample of ZF-EVs as compared to ZL-EVs. However, detailed lipidomic analysis would be needed to identify specific types of lipids and their proportion in ZL- and ZF-EVs. Lipid transport can be mediated by EVs, which carry bioactive lipids such as sphingomyelin, cholesterol, lysophosphatidylcholine, arachidonic acid and other fatty acids, prostaglandins, and leukotrienes among others, either in their membrane or in their lumen (Record et al. 2014).

With that in mind, we wanted to investigate whether EVs, secreted by steatotic hepatocytes from Zucker fatty rat hepatocytes could modulate the lipid content in recipient 3T3-L1 adipocytes. The approach taken was to measure the amount of free glycerol **(Section 2.13)** released by 3T3-L1 adipocytes following the treatment with ZL and ZF-EVs **(Figure 64A),** as well as, upon the exposure to the conditioned medium coming from the previously EV-treated adipocytes **(Figure 64B)** and finally the number of triglycerides was measured directly in treated cells **(Figure 64C)**.

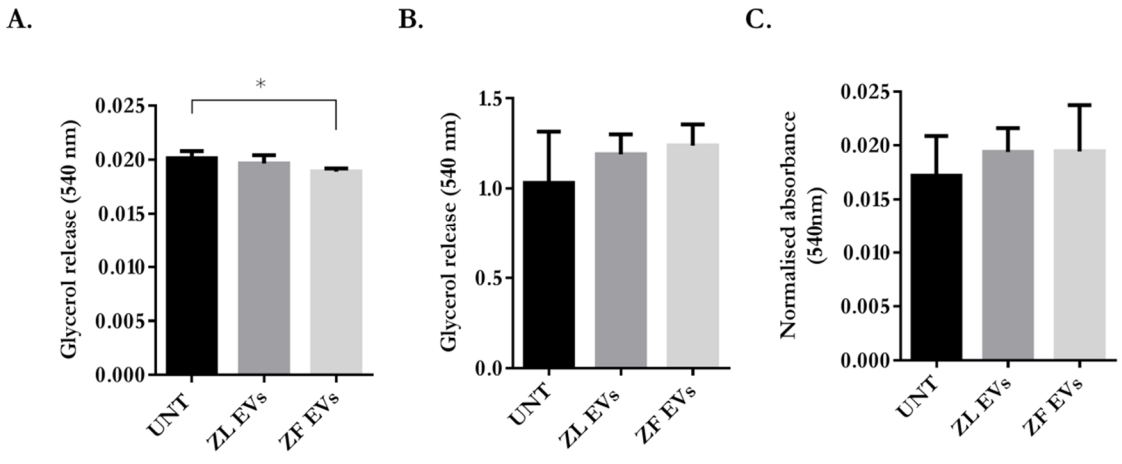

Figure 64 Changes in the lipid content in 3T3-L1 adipocytes upon treatment with Zucker rat hepatocyte secreted EVs. **(A)** The amount of free glycerol was determined in supernatant of the 3T3-L1 adipocytes following the 24h treatment with 10 μg of ZL and ZF EVs; n = 3. **(B)** Conditioned medium of 3T3-L1 adipocytes treated with ZL and ZF-EVs from the previous experimental group; n= 3. **(C)** The lipase assay was used to measure the triglyceride content in lysates from 3T3-L1 adipocytes previously treated with ZL- and ZF-EVs; n= 3. Error bars = SD. Unpaired student t-test was performed to determine significant differences

Our results indicate that ZF-EVs could influence lipid metabolism of 3T3-L1 adipocytes. On one hand, there was a significant decrease in free glycerol released by cells treated with ZF-EVs **(Figure 64A)**. Interestingly, when 3T3-L1 adipocytes were cultured in the presence of the conditioned medium of 3T3-L1 adipocytes previously exposed to ZL- and ZF-EVs, an increasing tendency can be seen in treated cells **(Figure 64B)**. The increase in absorbance at 540nm was directly proportional to the glycerol concentration in the sample and therefore to the triglyceride content. Moreover, when the triglyceride concentration was assessed in cells previously treated with EVs, an elevated concentration of free glycerol released was found **(Figure 64C)**.

6.3.5 The influence of hepatic-EVs on the glycolytic function of the 3T3-L1 adipocytes

The proteomic analysis revealed that most represented proteins in ZF-EVs were those related with glycolysis and a pentose phosphate pathway **(Table 10)**. We therefore wanted to find out whether they were able to modulate the bioenergetics of the 3T3-L1 adipocytes, and transfer their glycolytic phenotype onto the recipient cells. The experimental design, aimed to study the glycolytic functions in 3T3-L1 adipocytes exposed to ZL- or ZF-EVs **(Figure 65)**. Briefly, 3T3-L1 fibroblasts were grown and differentiated on a Seahorse XF24 V7 microplates. At day 12 of differentiation, mature adipocytes were either left untreated or treated with 10 µg of ZL- or ZF-EVs for 24 h. The 24h-conditioned medium of EV-treated adipocytes was given to other adipocytes, and originally treated adipocytes received another dose of ZL- and ZF-EVs (**Figure 65)**. Glycolytic function of the 3T3-L1 adipocytes in both settings was assessed using a Seahorse XF glycolysis stress test with various parameters being represented, such as the non-glycolytic acidification rate, glycolysis, glycolytic capacity and glycolytic reserve for the EVs treated cells **(Figure 66A)** and the conditioned medium treated cells **(Figure 66B)**. Our results indicate that ZF-EVs may have an influence on metabolic responses in 3T3-L1 adipocytes as seen by a significantly increased rate of glycolysis in 3T3-L1 adipocytes treated with ZF-EVs **(Figure 66A)**.

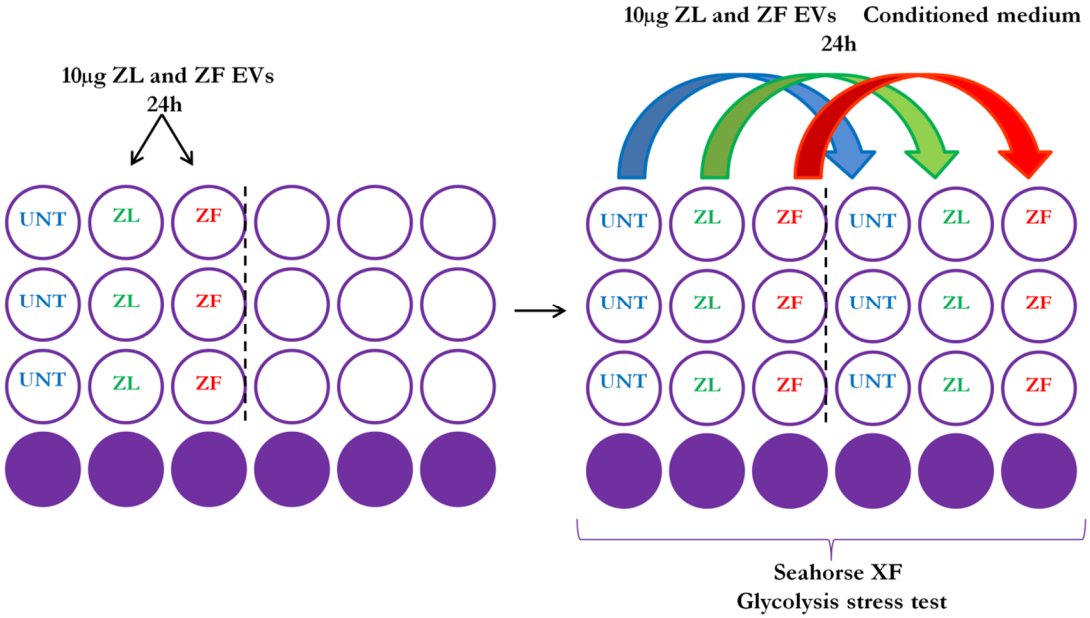

Figure 65 Experimental design to study the influence of Zucker rat hepatocyte-EVs on glycolytic functions of the 3T3-L1 adipocytes. Seahorse XF metabolic flux analyzer was used to perform glycolysis stress test on adipocytes previously treated with two doses of ZL- and ZF-EVs (10 µg) and cells cultured with the conditioned medium of adipocytes previously treated with ZL- and ZF-EVs; n=3/condition.

In the remaining glycolytic parameters, no changes were observed. Moreover, culturing 3T3-L1 adipocytes in the presence of conditioned medium of adipocytes previously treated with ZL- and ZF-EVs did not have a significant influence on glycolytic function of recipient cells **(Figure 66B)** which could indicate that the effect is specifically mediated by EVs.

A.

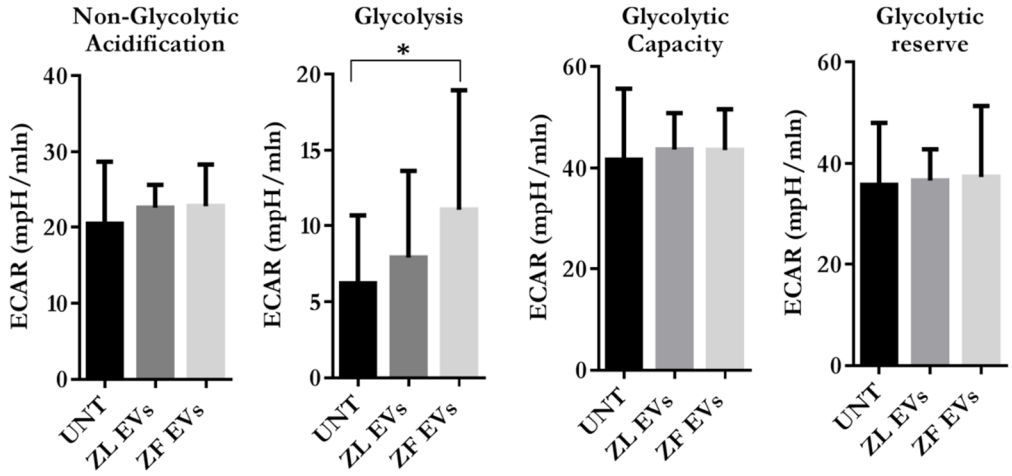

B.

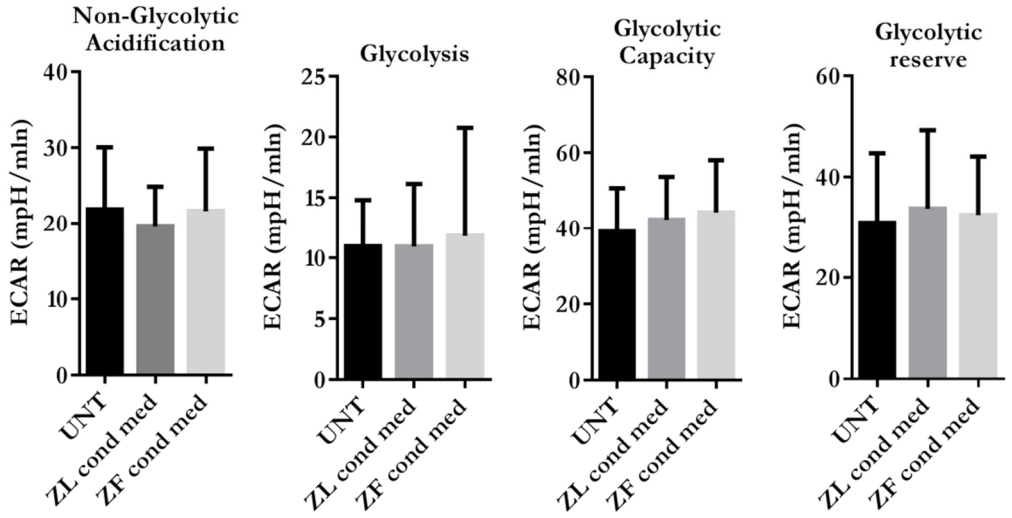

<u>Figure 66</u> Glycolytic changes in 3T3-L1 adipocytes upon treatment with Zucker rat hepatocyte-secreted EVs. (A) The effect of Zucker rat hepatocyte EVs; n=3 and **(B)** conditioned medium of adipocytes previously exposed to Zucker rat hepatocyte EVs on glycolytic functions of 3T3-L1 adipocytes, n=3. Glycolytic parameters such as non-glycolytic acidification, glycolysis, glycolytic capacity and glycolytic reserve was measured using Seahorse XF analyzer; error bars=SD *p* value=0.01- 0.05=*. Unpaired student t-test was performed to determine significant differences.

6.3.6 The influence of hepatic-EVs on insulin sensitivity of the 3T3-L1 adipocytes

Insulin resistance is one of the principal causes of metabolic perturbations associated with MetS. Therefore, we next decided to investigate the possible effect of Zucker rat hepatocyte-EVs on insulin sensitivity in 3T3-L1 adipocytes. For that, 3T3-L1 adipocytes were treated with ZL- and ZF-EVs, and WB analysis was carried out for insulin activated Akt(Ser473) and Erk1/2 protein phosphorylation **(Figure 67A)**.

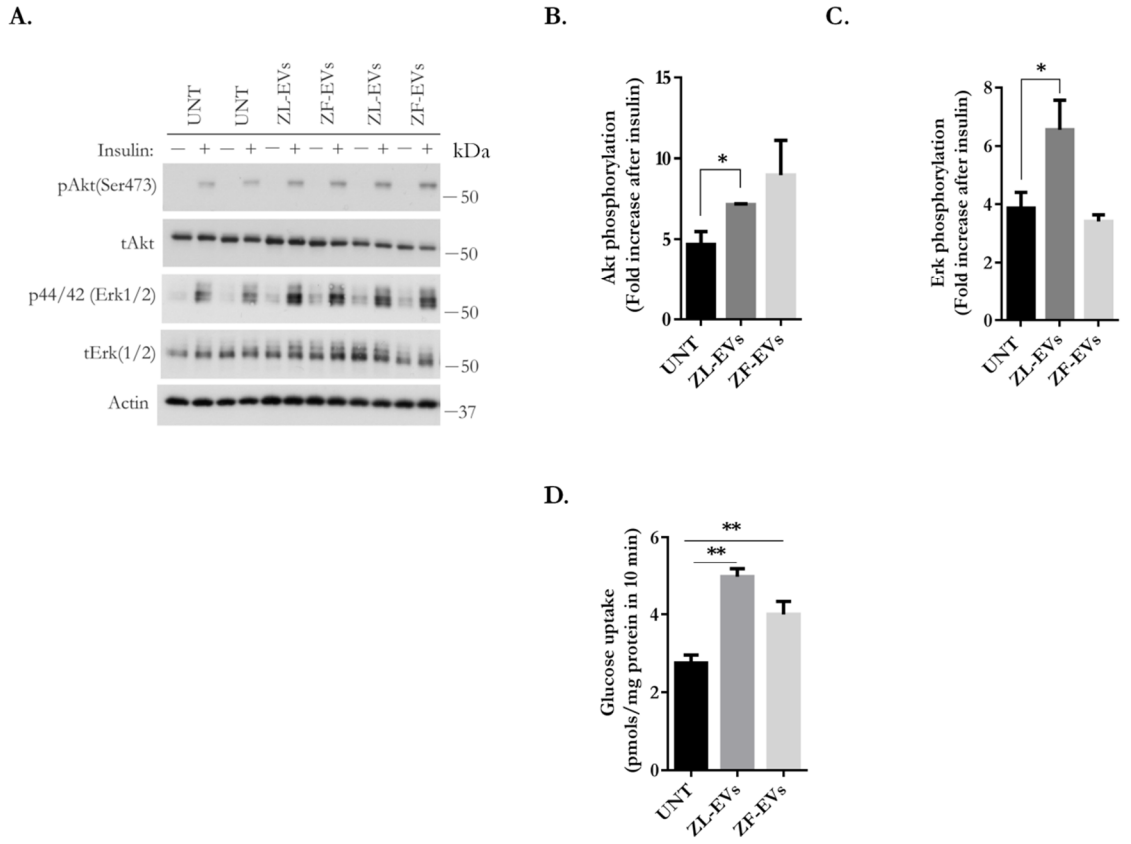

Figure 67 Insulin sensitivity studies in 3T3-L1 adipocytes upon acute exposure to Zucker rat hepatocyte-derived EVs. **(A)** Representative WB for of 3T3-L1 adipocytes acutely exposed to Zucker rat hepatocyte derived-EVs (30 μg) for 24 h **(B)** Fold increase in Akt(Ser473) phosphorylation upon insulin stimulation **(C)** Fold increase in Erk1/2 phosphorylation upon insulin stimulation; n=2/condition **(D)** Insulin stimulated glucose uptake in 3T3-L1 adipocytes upon treatment with ZL- and ZF-EVs; biological replicate=1,

technical replica=6; error bars=SD *p* values were denoted as follows: 0.01- 0.05=*, 0.01-0.001=**. Unpaired student t-test was performed to determine significant differences.

Results of densitometry were presented as a fold increase in phosphorylation upon induction with insulin. The quantification revealed that upon acute treatment with ZL-EVs, there was a significant increase in insulin stimulated phosphorylation of Akt(Ser473) and even further with ZF-EVs. Interestingly, the same result was obtained when insulin stimulated glucose uptake was performed in the 3T3-L1 adipocytes pre-treated with ZL and ZF-EVs **(Figure 67D)**. Moreover, ZL-EVs caused enhanced phosphorylation of Erk1/2 protein whereas in ZF-EV treated cells, a decreasing trend was detected **(Figure 67C)**.

The increase in Akt(Ser473) phosphorylation upon acute treatment with EVs could be a transient response or a step before the resistance develops. We therefore repeated the experiment with three subsequent doses of EVs. Two independent experiments were carried out (4 biological samples/condition) and the representative WB is shown in **Figure 68A**. The quantifications of activated Akt(Ser473) is shown in **Figure 68B** and **Figure 68C** and are represented as a percentage of phosphorylated protein at basal state and upon insulin stimulation. Then, the fold change increase in phosphorylation upon insulin stimulation was calculated, and the average of the 4 samples plotted **(Figure 68D)**. Although, not significant, results indicate that ZF-EVs cause a reduction in Akt(Ser473) phosphorylation in the recipient 3T3-L1 adipocytes. ZL-EVs on the other hand cause an increase in phosphorylation. The same trend was seen in the phosphorylation of Erk1/2 protein **(Figure 68G)**.

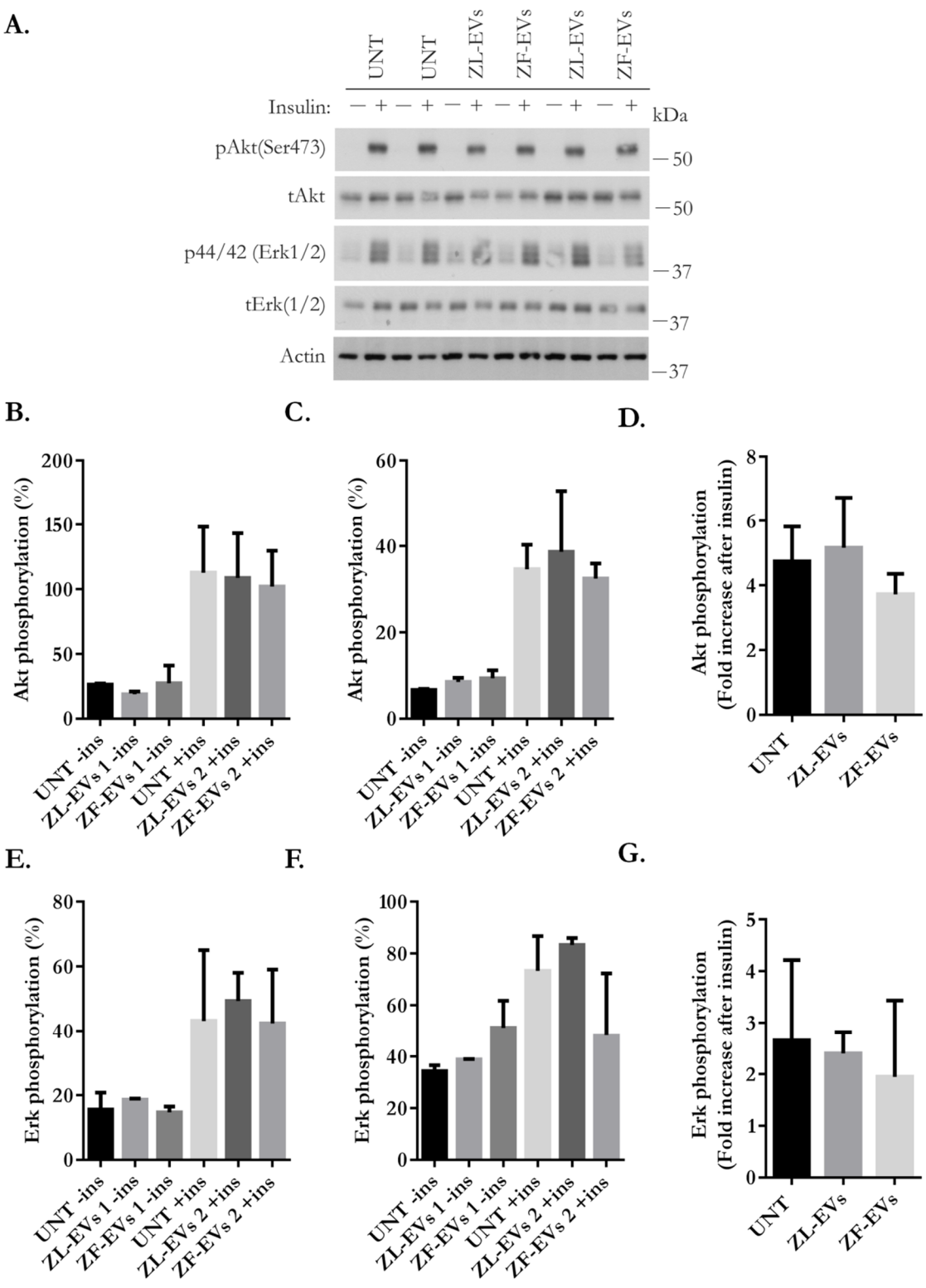
A.
UNT
UNT
ZL-EVs
ZF-EVs
ZL-EVs
ZF-EVs
Insulin: − + − + − + − + − + − +
kDa
pAkt(Ser473)
50
tAkt
50
p44/42 (Erk1/2)
37
tErk(1/2)
37
Actin
37
B.
Akt phosphorylation (%)
200
150
100
50
0
UNT -ins
ZL-EVs 1 -ins
ZF-EVs 1 -ins
UNT +ins
ZL-EVs 2 +ins
ZF-EVs 2 +ins
C.
Akt phosphorylation (%)
60
40
20
0
UNT -ins
ZL-EVs 1 -ins
ZF-EVs 1 -ins
UNT +ins
ZL-EVs 2 +ins
ZF-EVs 2 +ins
D.
Akt phosphorylation (Fold increase after insulin)
8
6
4
2
0
UNT
ZL-EVs
ZF-EVs
E.
Erk phosphorylation (%)
80
60
40
20
0
UNT -ins
ZL-EVs 1 -ins
ZF-EVs 1 -ins
UNT +ins
ZL-EVs 2 +ins
ZF-EVs 2 +ins
F.
Erk phosphorylation (%)
100
80
60
40
20
0
UNT -ins
ZL-EVs 1 -ins
ZF-EVs 1 -ins
UNT +ins
ZL-EVs 2 +ins
ZF-EVs 2 +ins
G.
Erk phosphorylation (Fold increase after insulin)
5
4
3
2
1
0
UNT
ZL-EVs
ZF-EVs

Figure 68 Insulin sensitivity studies in 3T3-L1 adipocytes upon chronic exposure to Zucker rat hepatocyte-derived EVs. **(A)** Representative WB of 3T3-L1 adipocytes chronically exposed to Zucker rat hepatocyte derived-EVs (3X10 μg) for 24 h each time **(B)** Quantification of the Akt(Ser473) phosphorylation (%), experiment 1 **(C)** Quantification of the Akt(Ser473) phosphorylation (%), experiment 2 **(D)** Fold increase in Akt(Ser473) phosphorylation upon insulin stimulation (100 nm insulin; 5 min) **(E)** Quantification of the Erk1/2 phosphorylation (%), experiment 1 **(F)** Quantification of the Erk1/2 phosphorylation (%), experiment 2 **(G)** Fold increase in Erk1/2 phosphorylation upon insulin stimulation; n=4; error bars=SD; ImageJ software was used for densitometry.

To complement the study, we decided to examine the phosphorylation of the mechanistic target of rapamycin (mTOR) via its targets, the 4E-BP1 and ribosomal protein S6, in response to insulin, following the same study design as of acute and chronic exposure. Phosphorylation of the ribosomal protein S6 (rpS6) was the first discovered to be post-translationally modified (Gressner & Wool 1974).

RpS6 phosphorylation is commonly used as a readout of mechanistic target of rapamycin complex 1 (mTORC1) activity (Biever et al. 2015) and the abnormal induction of mTORC1 signalling has been observed in response to insulin resistance and associated with diabetes progression (Tsai et al. 2016). In addition, mTOR serves a central role in controlling and regulating vital processes such as metabolism, proliferation, growth and survival (Laplante & Sabatini 2013).

The representative WB figure is shown in **Figure 69A**. Bands were quantified, and the results represented as a fold increase in phosphorylation of 4E-BP1 and rpS6 proteins upon insulin stimulation (**Figure 69B** and **Figure 69**, respectively). Our results show that when the 3T3-L1 adipocytes were acutely exposed to ZL-EVs, an increase in 4E-BP1 was observed, only a very small increase was seen in cells treated with ZF-EVs. However, the phosphorylation of the ribosomal protein S6 was significantly reduced when EVs were applied **(Figure 69C)**.

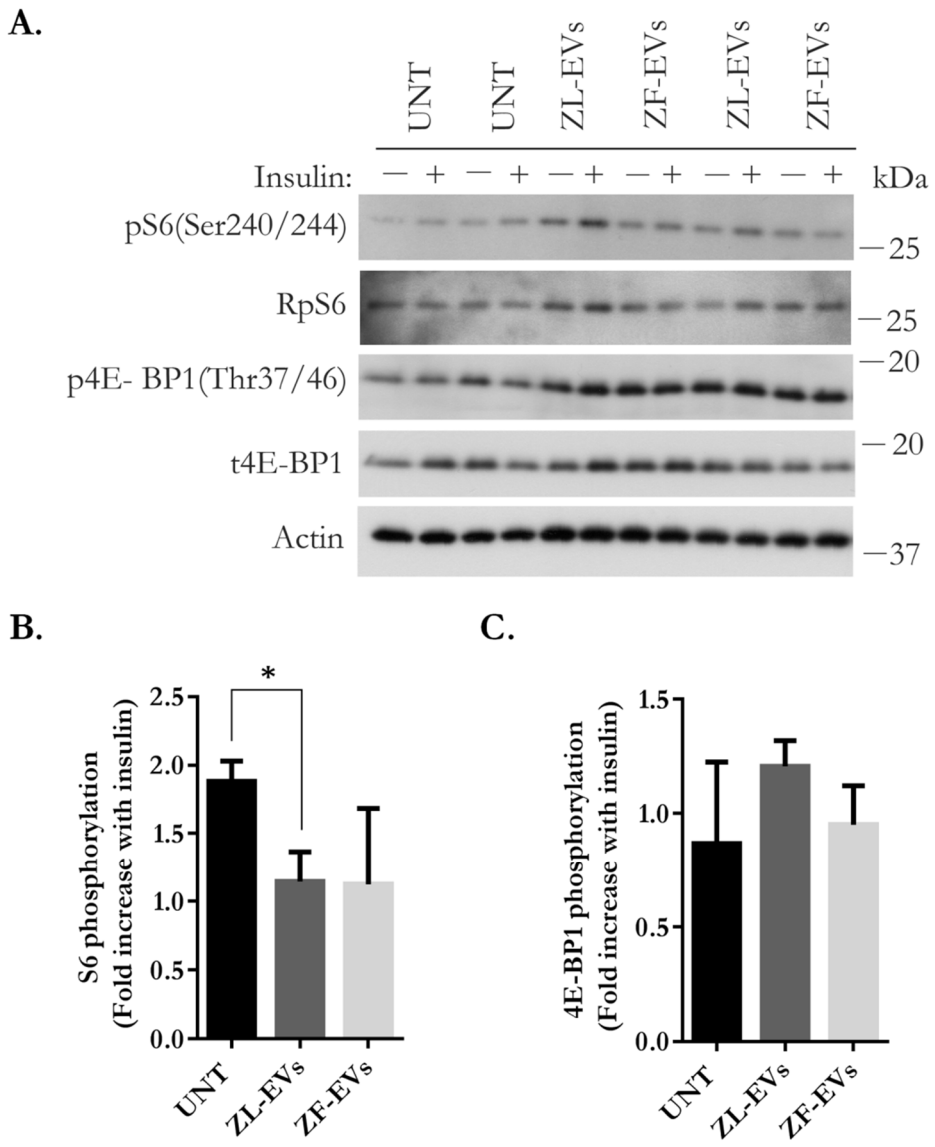

Figure 69 Insulin sensitivity studies in 3T3-L1 adipocytes upon acute exposure to Zucker rat hepatocyte-derived EVs. Representative WB of 3T3-L1 adipocytes acutely exposed to Zucker rat hepatocyte derived-EVs (30 μg) for 24h (B) Fold increase in rpS6 phosphorylation upon insulin stimulation (100nm insulin; 5min) (C) Fold increase in 4E-BP1 phosphorylation upon insulin stimulation; n=2/condition; error bars=SD; ImageJ software was used for densitometry. Unpaired student t-test was performed to determine significant differences.

The experiment was repeated, this time culturing cells in the presence of three subsequent doses of Zucker rat hepatocyte-derived EVs, over a 72-h period, as previously. The representative WB figure is shown in **Figure 70A** with the quantification of two independent experiments, carrying 4 biological replicates, meaning 4 independent preparation of ZL- and ZF-EVs, was done for 4E-BP1 and rpS6 proteins at basal and insulin induced states **(Figure 70B** and **Figure 70C)** When the fold change was calculated, it was shown that cells exposed to EVs had reduced 4E-BP1 phosphorylation, with no difference between ZL- and ZF-treated cells **(Figure 70D)**. More importantly, it was found that ZF-EV-treated adipocytes had significantly reduced phosphorylation of rpS6 **(Figure 70G)**.

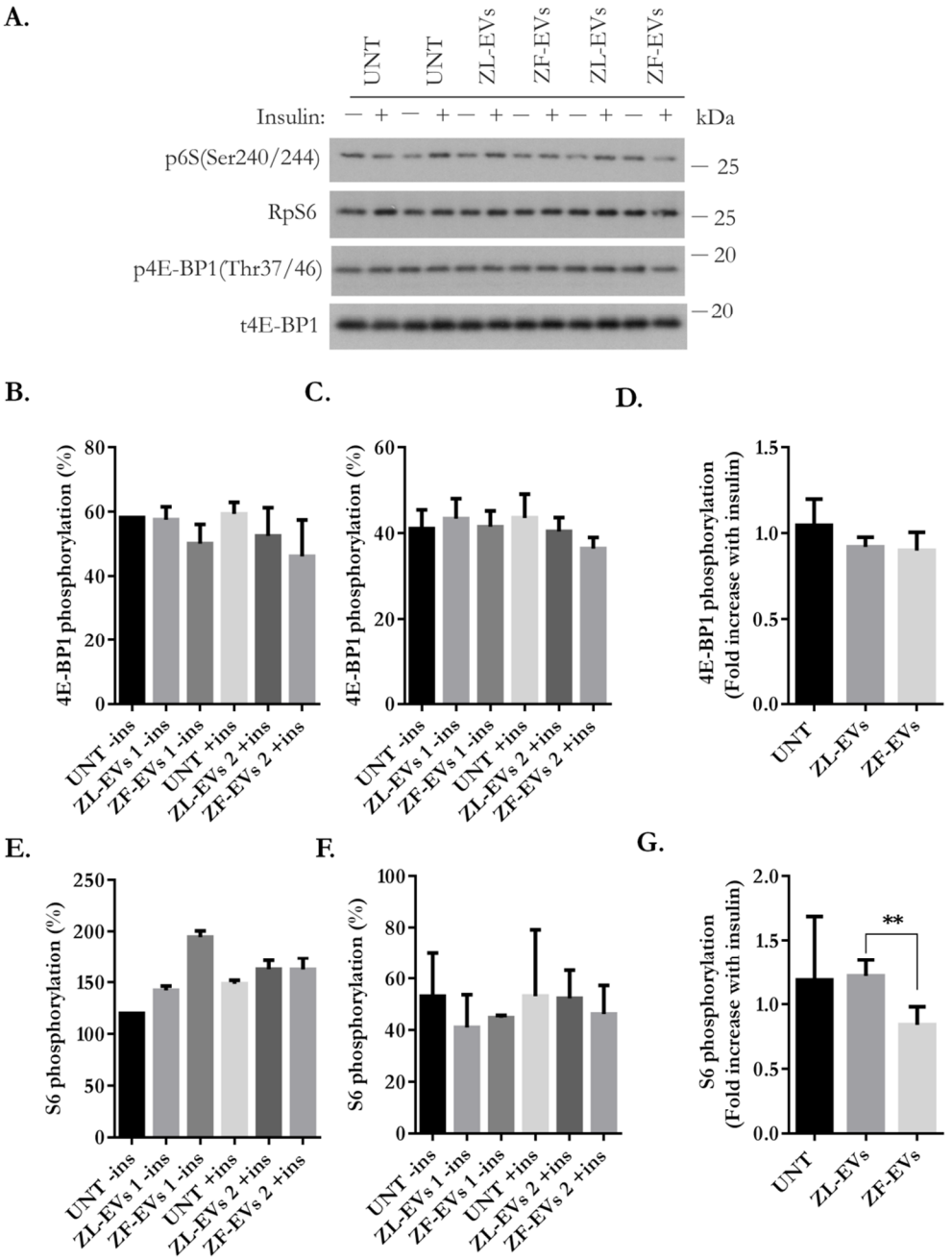

Figure 70 Insulin sensitivity studies in 3T3-L1 adipocytes upon chronic exposure to Zucker rat hepatocyte-derived EVs. (A) Representative WB of 3T3-L1 adipocytes chronically exposed to Zucker rat hepatocyte derived-EVs (3X10 μg) for 24h each time **(B)** Quantification of the 4E-BP1 phosphorylation (%), experiment 1 **(C)** Quantification of the 4E-BP1 phosphorylation (%), experiment 2 **(D)** Fold increase in rpS6 phosphorylation upon insulin stimulation (100nm insulin; 5min) **(E)** Quantification of the Erk1/2 phosphorylation (%), experiment 1 **(F)** Quantification of the rpS6 phosphorylation (%), experiment 2 **(G)** Fold increase in Erk1/2 phosphorylation upon insulin stimulation; n=4; error bars=SD; *p*

values were denoted as follows: 0.01- 0.05=*, 0.01-0.001=**, ImageJ software was used for densitometry. Unpaired student t-test was performed to determine significant differences.

6.4 Summary

We conclude that hepatocyte-derived EVs can influence physiology and metabolism of the 3T3-L1 adipocytes on different levels.

First, during the differentiation of 3T3-L1 cells into adipocytes, they influenced the expression of an array of genes, including master regulators of adipogenesis, PPARγ and C/EBPα. In terms of lipid metabolism, ZF-EVs, specifically increased the expression of genes encoding for the Fatty acid synthase, Perilipin3 and Glut4, upon induction of differentiation. Moreover, hepatic-EVs were able to decrease the expression of adiponectin gene, at the clonal expansion stage and interestingly, exclusively ZL-EVs induced RANTES expression.

During the terminal differentiation stage of the 3T3-L1, cells differentiation in the presence of ZF-EVs did not respond to the addition of insulin media in the case of all assayed genes. Although the response was later recovered, at the final time point, it seems that ZF-EVs can negatively regulate the expression of all analysed genes and negatively influence the accumulation of lipids in 3T3-L1 adipocytes. Hepatic-EVs also regulated gene expression in already mature 3T3-L1 adipocytes, differentially upon acute and chronic exposure.

In addition, hepatic-EVs modulated the secretion of adipokines in recipient 3T3-L1 adipocytes. We observed that upon exposure to EVs, they show evidence of inflammatory phenotype with increased secretion of pro-inflammatory cytokines and decreased anti-inflammatory IL-10.

Along these lines, ZF-EVs were able to transfer the glycolytic phenotype showed by the parental hepatocytes onto the 3T3-L1 adipocytes, as judged by the increased rate of glycolysis after treatment with EVs.

Lastly, hepatic-EVs modified the insulin sensitivity in 3T3-L1 adipocytes, differentially, depending on the length of the treatment. Our results indicate that upon acute treatment, hepatic-EVs caused the increase in insulin-stimulated Akt(Ser473) phosphorylation and glucose uptake, however significant reduction in the ribosomal S6 protein phosphorylation. Interestingly, while ZL-EVs caused a significant increase in Erk1/2 phosphorylation, on a contrary in a group treated with ZF-EVs there was a decreasing trend. In the chronic experimental group, ZF-EVs caused the reduction in Akt(Ser473) and Erk1/2 phosphorylation as well as significantly decreased the ribosomal S6 phosphorylation. Graphically represented on **Figure 71**.

6.5 Discussion

The study on Zucker rats has showed that while the substrate necessary to create and to sustain the enlarged adipose mass of the obese animal has more than a single site of origin, several lines of evidence suggest that the liver is the major site of synthesis for the substrate (Goldstein & Johnson 1980). Moreover, it has been reported that 80-90% of the substrate for adipose tissue in the obese Zucker rat is supplied by the liver (Godbole & York 1978). Elevated rates of hepatic lipogenesis have been found in Zucker obese rats when compared to their lean littermates as early as 44 days of age (Goldstein & Johnson 1980).

Therefore, the last part of this doctoral thesis was dedicated to study the possible effects that EVs secreted by steatotic hepatocytes may exhibit on adipocytes.

Decrease in abdominal subcutaneous preadipocyte differentiation capacity is associated with visceral obesity, adipocyte hypertrophy, and a dysmetabolic state (Lessard et al. 2014). Moreover, reduced generation of new adipocytes in the state of hypertrophy was correlated with insulin resistance (Arner et al. 2010). With that in mind, we hypothesized whether hepatic EVs were implicated in the

pathology of reduced adipogenic capacity. We used the multi-stepdifferentiation of 3T3-L1 cells into adipocytes, that can be tightly controlled by the presence of hormonal cocktail consisting of insulin, DEX and IBMX. The addition of these compounds allows controlling fundamental steps in the adipocytes differentiation process including the expression of adipocyte-specific genes and the accumulating triacylglycerol lipid droplets (Gregoire et al. 1998). The adipogenic differentiation involved a series of media replenishment every 48-h starting with the differentiation cocktail, then insulin containing media and three rounds or complete media replenishments. Therefore, the experimental design employed here was that at every point of replenishment, the media was supplemented with 10 µg of ZL- or ZF-EVs or left untreated. At the molecular level, adipogenesis is regulated by a complex transcriptional cascade. In one study, which explored the effects of macrophage-conditioned medium on adipocytes, the researchers found that the critical time point for the inhibition was the first 2 days of the 8-day differentiation period, the period associated with the mitotic clonal expansion phase (Constant et al. 2008).

We showed that during the clonal expansion stage, the presence of EVs did affect the expression of adipogenesis regulators, the *Pparg, Ap2 and Cebpa.* However, ZF-EVs specifically caused an increase in expression of the lipogenic enzyme, the fatty acid synthase, which was accompanied by the increase in the expression of adipocyte-related perilipin 3 protein. Elevated lipogenesis is a key determinant of excessive fat deposition in adipose tissue (Boizard et al. 1998). We have already shown that the pro-lipogenic profile of ZF-EVs may be transferable and the increase in lipogenic gene expression could be the step towards the induction of hypertrophic phenotype in 3T3-L1 adipocytes. We have also shown that by exposing adipocytes to ZF-EVs, we shifted the metabolic profile of these cells by causing the augment in the rate of glycolysis **(Figure 62A)**. Thus, the promotion of lipid synthesis at the early stages of adipogenesis elevated lipogenesis that is a characteristic of the obese state. Later, when solely insulin containing media was applied, ZF-EVs impaired the response of adipogenesis regulators *Pparg, Ap2* and *Cebpa*, as well as, genes related with

lipid metabolism. This could indicate that cells in the presence of hepatic EVs were not able to respond to adipogenic effects of insulin. Alternatively, a lower population of differentiated adipocytes could be present in the culture. It could also be that the first increase in gene expression response was priming effect, which could also be related with a transient increase in DNA synthesis, which occurs after the addition of the differentiation cocktail (Reichert & Eick 1999). During the serum-based stage of 3T3-L1 differentiation, at day 6 and 8, the presence of EVs caused an increase in transcription of most genes tested. Importantly, when considering the last time point of the differentiation steps, ZF-EVs exerted negative effects on the expression of adipogenesis regulators, lipid droplet associated perilipin 2, and adiponectin. Generally, adiponectin is present in plasma at very high concentration and is inversely associated with visceral fat accumulation. Overexpressing adiponectin in *ob/ob* mice has been shown to dramatically improve the metabolic and inflammatory phenotype of these mice with the restoration of insulin sensitivity, mediated by increased PPARγ and redistribution of lipids from ectopic deposits in peripheral organs to the subcutaneous adipose depots (Kim et al. 2007). Our results show that the reduced levels of adiponectin associated to ZF-EVs could resemble the state of reduced adiponectin in obesity, which would again indicate the transfer of specific aspects of cellular phenotype by ZF-EVs onto recipient cells. Additional experiment would be needed to reveal the exact mechanism, but it could be related with downregulation of specific signalling pathways, which we observed in 3T3-L1 adipocytes upon exposure to ZF-EVs. All together, these results show that at each stage of the differentiation process there are specific responses to the stimulus of hepatic-EVs. Our data suggest that the main process affected by hepatic-EVs during adipocyte differentiation was lipid accumulation. This could also be associated with less cells being differentiated in the presence of hepatic-EVs. Furthermore, our preliminary results indicate that in already mature 3T3-L1 adipocytes, ZF-EVs may promote lipolysis, which is also one of the characteristics of obese state.

According to current knowledge, in normal conditions adipocytes release biologically active molecules known as 'adipokines' and anti-inflammatory cytokines such as IL-10, IL-1R to maintain homeostasis and protect from development of obesity associated IR and inflammation (Caruso et al. 2010). The state of obesity causes significant deregulation in adipokine secretion and a shift towards the pro-inflammatory state. Our adipokine array experiment showed that hepatic-EVs were able to significantly modulate the secretion of adipokines in 3T3-L1 adipocytes. Treatment with ZF-EVs decreased the expression of anti-inflammatory IL-10 secretions, which is a change associated with obesity. Unexpectedly, ZL-EVs caused very significant induction in pro-inflammatory, IL-6 and RANTES adipokine secretion in 3T3-L1 adipocytes, which was not the case for the ZF-EVs. Moreover, ZL-EVs specifically induced nearly 6-fold increase in FetuinA secretion by 3T3-L1 adipocytes. Moreover, we showed that the secretion of lipocalin2 by 3T3-L1 adipocytes was highly elevated by the exposure to hepatic-EVs, which has been shown to be strongly associated with obesity and was found elevated in 3T3-L1 adipocytes by IR promoting agents (Yan et al. 2007). Overall, there were changes in secretion of nearly 30 adipokines, which indicate that hepatic-EVs may cause a shift in an overall metabolic phenotype of 3T3-L1 cells seen in obese-adipose tissue.

Lastly, we focused our efforts on studying the effects of hepatic-EVs on insulin sensitivity in 3T3-L1 adipocytes by assessment of Akt, Erk1/2, and components of mTOR pathway, rpS6, and 4E-BP1 phosphorylation, at basal state and upon insulin stimulation following exposure to ZL- and ZF-EVs. In addition, our experimental design included two-time points, the acute and chronic treatment with hepatic-EVs. We observed significant differences in response of 3T3-L1 adipocytes between the two treatment groups. Our results indicate that acute (24 h) exposure to hepatic-EVs cause transient increase in phosphorylation of Akt(Ser473) and Erk1/2 as well as in insulin-stimulated glucose uptake, which following chronic exposure (3x24 h) was attenuated by ZF-EVs. Furthermore, the phosphorylation of rpS6 was significantly reduced already at acute exposure by hepatic-EVs and specifically by ZF-EVs at a chronic time point. Dysregulation of

the mTORC1 pathway has been implicated in the obesity and its related metabolic complications (Catania et al. 2011). Overnutrition leads to persistent hyperactive mTORC1/S6K1 signalling which phosphorylates IRS1 at serine residues leading to reduction in insulin signalling (mTORC2/Akt). This decrease in insulin sensitivity results in metabolic imbalance (Yang & Ming 2012). Elevated levels of insulin, pro-inflammatory cytokines and nutrients most probably feed mTORC1 activity in obesity (Laplante & Sabatini 2013). In that regard, it has been postulated that the action of mTORC1 on insulin resistance in adipose tissue is via the S6K1-mediated inhibition of insulin signalling and may aggravate systemic insulin resistance by promoting FFA release by adipocytes, ectopic fat deposition, and lipotoxicity (Laplante & Sabatini 2013).

In contrary, another study has shown that mTORC1 activation by insulin was attenuated in adipocytes from patient in obese, insulin-resistant state (Öst et al. 2010). In addition, treatment with rapamycin was linked to inhibition of IRS1 and induction of insulin resistance phenotype (Paolo et al. 2006). Steatotic EVs seem to contribute to the induction of insulin resistance phenotype related with the development of MetS, however to reveal mechanism behind this effect, more experiments would have to be conducted. mTORC1 has been shown to play a key role in lipid storage by stimulating the synthesis of triglycerides in WAT and differentiation of preadipocytes into adipocytes through up-regulation of PPARγ (Yang & Ming 2012). In agreement with our results, ZF-EVs cause a decrease in phosphorylation of rpS6 in 3T3-L1 adipocytes, and during adipogenesis, they affect lipid accumulation in differentiating 3T3-L1 cells. These data together could indicate that this effect on lipid accumulation in differentiating adipocytes is mediated by reduction in rpS6. However, further experiments are needed to confirm this aspect. Although our results on functional effects of hepatic-EVs on the physiology of the 3T3-L1 adipocytes are still preliminary, they indicate that EVs secreted by hepatocytes may have a profound effect on the physiology of adipocytes in the context of MetS. We show that they may be contributing factor towards the development of insulin resistance in adipocytes.

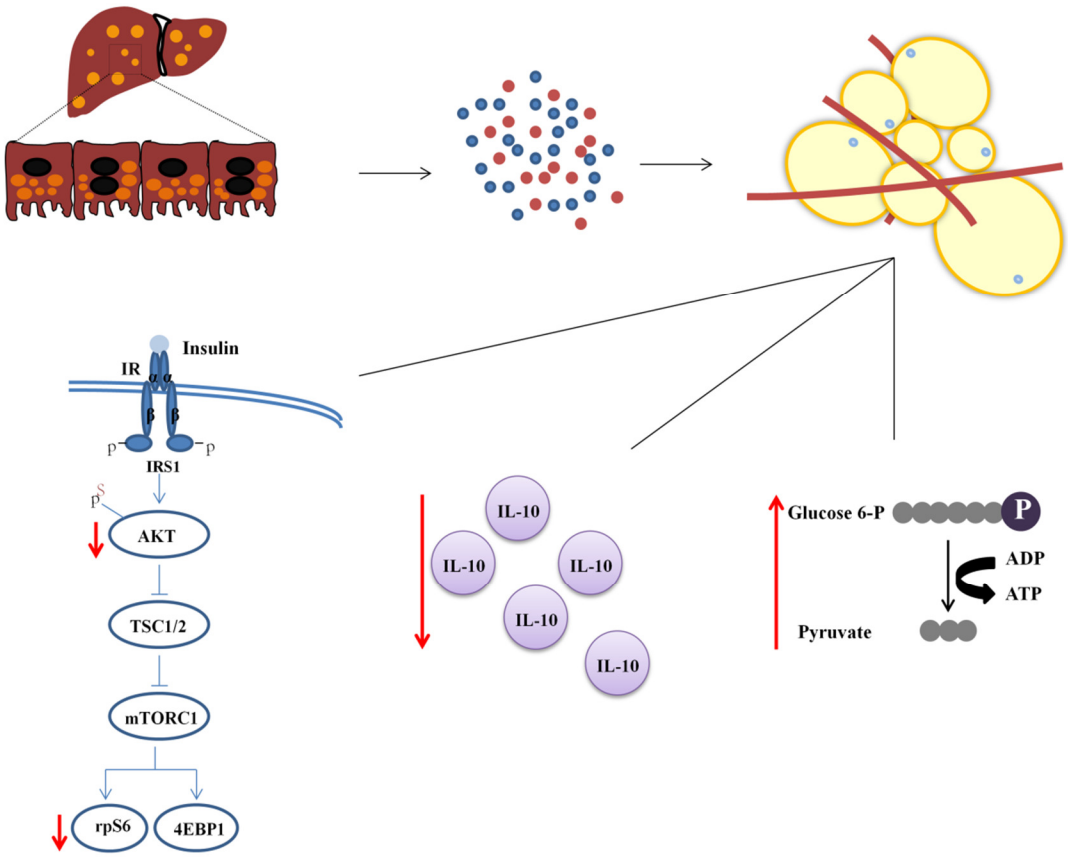

Figure 71 Summary diagram of results described in chapter 4. Graphical representation of results regarding the effects of steatotic-EVs on insulin sensitivity, adipokine secretion and metabolism of the 3T3-L1 adipocytes.

CONCLUDING DISCUSSION

7. Concluding discussion

EVs have emerged as very important mediators in cell-to-cell communication, maintaining homeostasis but also propagating the development of different pathologies. They are under intense research in a wide range of areas from cancer to immunology, degenerative and infectious diseases, metabolic and inflammatory conditions among many others. They already serve as non-invasive biomarkers and have proven useful in regenerative therapies. It is therefore crucial to understand the mechanisms that govern their production and release, their selective packaging of different molecules and their interaction with the extracellular environment, under homeostatic conditions and during pathology.

In this study **we hypothesized, that the secretion and the content of extracellular vesicles, are affected by different manifestations of metabolic syndrome and that they influence adipocytes biology**. To address these issues, we established and characterized *in vitro* cellular models resembling the metabolic syndrome conditions in different tissues. The 3T3-L1 adipocytes were exposed to three independent pathological states, namely hypoxia (1%), the macrophage-conditioned medium and the FFA mix to induce the conversion into lipid-overloaded enlarged adipocytes. Additionally, the Raw264.7 macrophages were activated with LPS to induce the M1 proinflammatory phenotype. Moreover, the hepatocellular steatosis was induced in three different hepatic cell lines, AML12, MLP29 and HepG2 with the mix of FFAs. Finally, primary steatotic hepatocytes were isolated from the Zucker fatty rat that constitutes a well-known genetic model of obesity. The culture conditions of all cellular models were carefully chosen for the subsequent isolation of EVs from the conditioned medium. In the last part, we focused on studying the possible influence of the proinflammatory macrophage derived-EVs and steatotic derived-EVs on adipocytes.

The three most important tissues involved in fatty acid metabolism are the adipose tissue, skeletal muscle and liver, each of which has a triglyceride store,

which can be mobilized by hydrolysis when needed. Fatty acids from adipose tissue can be released into the circulation for delivery to other tissues and in liver they serve as a substrate for re-esterification within the endoplasmic reticulum (ER) to make triglycerides that will be secreted as VLDL. These processes are controlled by the action of insulin (Frayn et al. 2006). It is clear, that there is cooperation amongst the tissues, which is deregulated in MetS, and the notion that this cooperation is mediated by EVs has already been shown. Most of studies regarding the involvement of EVs in MetS, focused on the adipose tissue derived–EVs, and the effect on peripheral organs. However, hepatocytes are also known to release EVs, therefore the possibility that hepatocyte secreted-EVs are taken up by adipocytes and modulate their physiology cannot be discarded.

This study demonstrates that the profile of small EVs secreted by all our cellular models of MetS is highly affected in terms of the profile of proteins and the concentration of secreted-EVs. There is an overall enhanced secretion of EVs with very minor changes in the mean particle size. The lipid overload in 3T3-L1 adipocytes caused increased secretion of vesicles containing exosomal markers such as Cd81, Aip1/Alix and Flotillin1 and the lysosomal-LIMPII. It is an interesting result considering that in all remaining models used, under the pathological conditions the expression of these protein markers is highly decreased. Moreover, we found Glut4 to be associated to adipocyte secreted-EVs and importantly to be increased in hypoxic-EVs and those from adipocytes cultured in the presence of the macrophage-conditioned medium. Unexpectedly, we found very significant decrease in the secretion of EVs by LPS-activated macrophages, with all protein markers being downregulated. Interestingly, those expressed in basal macrophage-derived EVs are modified, showing at different molecular weights when compared to lysate controls. Furthermore, EVs isolated from our models of hepatocellular steatosis showed some striking differences. In steatotic AML12 derived-EVs there was a clear decrease in exosomal protein markers in treated cells, and the opposite effect was observed for the MLP29 derived-EVs. Moreover, the MLP-EVs expressed overall more protein markers

Overall, we have seen increase in the secretion of EVs in those conditions. Our main model of hepatocyte-derived EVs to address the effect on adipocytes was the one isolated from ZL and ZF primary hepatocytes. Metabolic profiling of ZL and ZF primary hepatocytes has revealed a very significant decrease in all mitochondrial functions and increase in glycolytic capacity of steatotic hepatocytes. In terms of EVs, the differences were observed in all analyses that were carried out. ZF-EV preparations exhibit significantly higher protein content, and significantly increased concentration of particles. There is a decreasing tendency in most of EV-related protein markers except for HSPs and unexpectedly a COMT protein in ZF-EVs. Density gradient reveals the existence of different populations of EVs and proteomic analysis of these EVs has strengthen the findings as to the metabolic differences seen in cells. Most upregulated proteins in ZF-EVs were associated with glycolysis, pentose phosphate pathway and the fat metabolism. On the other hand, those downregulated were mostly mitochondrial. Thus, EV-observed changes reflected cellular metabolism. Related to that, we found adiponectin associated to hepatocytes-secreted EVs, and being highly downregulated in ZF-EVs, in agreement with the circulating low adiponectin reported in obese samples.

Moreover, we isolated nucleic acids from Zucker EVs and found higher content of RNA in those EVs derived from ZF-hepatocytes. Active P450 2D1 was detected in Zucker hepatocytes-EVs, with lower activity in ZF-EVs. These results suggest that these EVs have the potential to significantly influence the extracellular environment. Then, we have progressed onto studying the possible effect of those EVs on adipocyte biology. We have seen that at the early stages of adipogenesis ZF-EVs were able to increase the expression of genes encoding for the fatty acid synthase, perilipin3 and glut4. In addition, at later stages they were able to modulate genes, which regulate the transcriptional cascade of adipogenesis, such as the *Pparg, Ap2, Cebpa* and *Adipoq.* This result was also observed when we analyzed the gene expression in adipocytes following chronic exposure ZF-EVs. Adipokine array on adipocytes treated with ZF-EVs revealed a drop in anti-inflammatory cytokine IL-10 secretion. Finally, they, very specifically,

influenced the phosphorylation of S6, the target of S6 kinase of the mTOR pathway.

The formation of EVs and their secretion has received great attention in last decades, however, the mechanisms that govern specific packaging in normal and pathological conditions are still not well understood. In that regard, when we consider our cellular models of MetS consistently exhibit a significant decrease in the expression of exosomal markers, which means that pathological conditions, not only affect the number of EVs secreted but also their protein content. Our result also points towards the existence of different EV subtypes secreted by steatotic hepatocytes with nonclassical protein cargo. The alteration of environmental parameters results in changes in the EVs' molecular signature (Giebel 2017). It could be a regulated stress response with HSPs strongly associated to EVs secreted by affected cells. More commonly proposed roles of EVs include the transport of signalling/regulatory molecules for intracellular communication and modulation of functions in recipient cells (H. Lee et al. 2016). Considering this, as already emphasized, here for the first time we have shown that hepatic-EVs may greatly influence the many aspects of adipocyte biology in the context of MetS. Our preliminary results indicate that EVs can transfer their phenotype onto a recipient cell.

Importantly, we discovered that these EVs faithfully reflect the cell of origin, not only carrying cell-specific protein markers but also reflect the metabolic state of the parent cell. We have shown that EVs secreted by pro-inflammatory Raw264.7 macrophages activated with LPS carry Tnf associated, which could be mediating the effect that they exert over mitochondrial functions of the 3T3-L1 adipocytes. Tnf caused mitochondrial dysfunction, decreased mitochondrial membrane potential and decreased reduction of ATP in 3T3-L1 adipocytes (Chen et al. 2010). We have shown that EVs released by steatotic hepatocytes reflect glycolytic phenotype of the parent cell with the reduction in mitochondrial proteins, which was the feature of our steatotic hepatocytes. It could be that under steatotic conditions, mitochondrial-mediated ROS formation or lipotoxicity

caused accumulation of toxic material that can then be secreted via EVs. Concerning this, it cannot be discarded that in these conditions, EVs could serve as an alternative disposal of unwanted or damaged cellular material.

We have characterized our EVs in terms of the expression of classical EV markers, therefore in the future studies we would aim for the identification of specific marker associated to or differentially expressed in steatotic-EVs. Furthermore, our results would have to be validated *in vivo*, although it is not an easy task as serum contains a pool of circulating EVs released from more than one site of origin. Furthermore, to date, no single marker was identified which would allow clear discrimination between different subtypes of EVs as different vesicle types are enriched in parallel fractions (Giebel 2017).

Our work on characterization of EVs secreted by steatotic hepatocytes is first of this kind and contributes to the basic knowledge on the nature of these EVs. Moreover, here for the first time, we show that hepatic-EVs may deeply affect the physiology of adipocytes. Our results validate, at least to some extent, the hypothesis that in fact, EVs are one of the means of cell-cell cross talk in tissues involved in the development and propagation of pathology of MetS.

Future studies should consider (***i***) further characterization of miRNA content of EVs isolated from different models of metabolic syndrome to identify their possible dysregulation in pathology. Another vital issue would be (***ii***) performing lipidomic studies on EVs isolated from our models to determine whether the lipid overload phenotype of cells in obesity has got an impact on a lipid content of their secreted EVs. Moreover, essential would be to (***iii***) characterize the contribution of different subpopulations of EVs by inhibition of their release would be important to understand whether during pathological conditions any of the secretory pathways is affected or whether there exists a compensatory switch. In addition to that, in terms of functional studies, it would be important to identify the population which mostly contribute to the effects of 3T3-L1 adipocytes. Following on that idea, next step would be to (***iv***) identify the biological components of steatotic EVs which are responsible for effect on different aspects of the 3T3-L1

adipocyte biology Finally, (***v***) for further studies on the effect of EVs on the recipient cells, it would be important to do the dose-response curve to establish the working range of EVs necessary to produce maximal effect.

Limitations and considerations

Given the EV isolation procedure used in this study, this thesis is focused in the study of small EVs. Techniques normally used to purify EVs mainly involve differential ultracentrifugation, and hence, are not selective for any specific type of vesicles, thus our EV preparations can contain exosomes, small microvesicles and small apoptotic blebs. In addition, some non-vesicular material including lipoproteins and protein aggregates may also be isolated in the EV preparations. To control the amount of these non-vesicular material we have routinately performed WB for markers of intracellular organelles, and in the case of primary hepatocytes of lipoproteins. As judged by the WB analysis, the level of contamination by intracellular organelles and lipoproteins were low in our EV preparations.

Primary hepatocytes are the gold-standard *in vitro* system to study hepatocyte biology, however it has several limitations. When hepatocyte are cultured in standard cell culture medium in a plastic container, the cells lose their gap junctions within 12-24 h and adapt to flattened shape (Na et al. 2014). It has been widely recognized that cultured hepatocytes are subject to a gradual loss of liver-specific functions, especially a decreased in some CYP expression. For example, CYP 2E1 and CYP 3A4 are diminished in few days in culture however the CYP 1A2 and CYP 2C9 are unaffected by isolation and culture (George et al. 1997). Various culturing methods have been explored to maintain the liver-specific characteristics of hepatocytes during prolonged culture. The addition of specific nutrients, hormones, and inducers to the culture medium (Block et al., 1996; ’t Hoen et al., 2000; Sewer and Morgan, 1997; Vernia et al., 2001); and, the co-culturing of hepatocytes with other cell types (e.g., the hepatic Kupffer

cells) may be necessary for cofactor supply (Milosevic et al., 1999). In many studies they have used insulin as an additive to the culture media as it enhances initial cell attachment, especially important for cells seeded onto tissue culture plastic. Moreover, the common use of corticosteroids, such as, DEX are equally important as contributes to the preservation of hepatocyte morphology, survival and tissue-specific functions (e.g. albumin synthesis). Once isolated, hepatocytes can be maintained in monolayer culture for a maximum of 4 weeks (Brandon et al. 2003). To study cells keeping most of the hepatocyte functions, in our experiments we did not exceed 36 h in culture for primary rat hepatocytes.

In vivo physiological conditions represent a complex, multi-organ interaction and therefore reproducing these settings *in vitro* can be challenging. Setting up the co-culture systems would be one possibility for improvement, such that in our experimental design, the culture of primary hepatocytes with conditioned medium of adipocytes could have been an option. We chose to use Zucker rat hepatocytes as a model of hepatic steatosis for further isolation of EVs having in mind the yield necessary for further experiments. The *ob/ob* or *db/db* mice models would be more suitable in terms of species mach, however the yield would probably be significantly less and would limit the possibility of performing all functional studies.

The issue with normalization and loading control for WB when working with EVs is still unresolved. There is no marker yet known to be ubiquitously in all EVs, regardless the origin. In addition, the expression of EV-related markers in pathological conditions may be largely affected. Also, the choice of normalization technique depends a lot on downstream purpose. The number of EVs seems like a reasonable approach however, there is no consensus yet as to the physiological and pathological concentration of circulating EVs.

CONCLUSSIONS

8. Conclusions

- Successful establishment of *in vitro* cellular models reflecting the conditions of MetS such as adipocyte hypertrophy, adipocytes in hypoxia, adipocytes exposed to the proinflammatory cytokines, hepatocellular steatosis and inflammation.

- Our cell culture models were valid for isolation of EVs from the conditioned-medium by removal of the treatment containing medium, for subsequent production of EVs.

- MetS-resembling conditions alter the expression of EV-related proteins.

- Hypertrophy and hypoxia induce higher secretion of EVs in adipocytes.

- Hypertrophic adipocytes secrete EVs with increased expression of Cd81, LimpII, and Flotillin1 proteins.

- Adipocytes under hypoxic conditions secrete EVs that are able to inhibit insulin stimulated Akt(Ser473) phosphotylation and glucose uptake in 3T3-L1 adipocytes.

- Macrophages after initial activation of LPS secrete fewer small EVs than unactivated macrophages.

- EVs secreted by LPS-activated macrophages carry Tnf and has lower amount of EVs-related proteins.

- EVs secreted by LPS-activated macrophages decrease mitochondrial function and alter insulin sensitivity on adipocytes.

- EVs secreted by steatotic MLP29 cells exhibit significantly different EV-phenotype than AML12-derived EVs, with a decrease in Cd81 and an increase in Aip1, Rab8, Hsp70, and Flotillin1.

- EVs secreted by steatotic hepatocytes secrete significantly more EVs than their lean counterpart, and carry a distint protein cargo with a severe reduction in exosomal markers.

- EVs derived from hepatocytes carry adiponectin, and the abundance are lower in in ZF-EVs.

- EVs derived from hepatocytes affect adipocytes differentiation, adipokines secretion and insulin sensitivity in adipocytes.

General Conclusion:

- The results presented in this thesis show that the composition of EVs is significantly altered in conditions of MetS and that they could play a very important role in the development and propagation of MetS associated pathologies.

BIBLIOGRAPHY

9. Bibliography

Abel, E.D. et al., 2001. Adipose-selective targeting of the GLUT4 gene impairs insulin action in muscle and liver. *Nature*, 409(6821), pp.729–733.

Abels, E.R. & Breakefield, X.O., 2016. Introduction to Extracellular Vesicles: Biogenesis, RNA Cargo Selection, Content, Release, and Uptake. *Cellular and Molecular Neurobiology*, 36(3), pp.301–312.

Ailhaud, G., 2006. Adipose tissue as a secretory organ: from adipogenesis to the metabolic syndrome. *Comptes Rendus - Biologies*, 329(8), pp.570–577.

Aiston, S., Peak, M. & Agius, L., 2000. Impaired glycogen synthesis in hepatocytes from Zucker fatty fa/fa rats: The role of increased phosphorylase activity. *Diabetologia*, 43(5), pp.589–597.

Akers, J.C. et al., 2013. Biogenesis of extracellular vesicles (EV): Exosomes, microvesicles, retrovirus-like vesicles, and apoptotic bodies. *Journal of Neuro-Oncology*, 113(1), pp.1–11.

Al-Dwairi, A. et al., 2014. Enhanced gastrointestinal expression of cytosolic malic enzyme (ME1) induces intestinal and liver lipogenic gene expression and intestinal cell proliferation in mice. *PLoS ONE*, 9(11), pp.1–15.

Alberti, K.G.M.M. et al., 2009. Harmonizing the Metabolic Syndrome: A Joint Interim Statement of the International Diabetes Federation Task Force on Epidemiology and Prevention; National Heart, Lung, and Blood Institute; American Heart Association; World Heart Federation; International . *Circulation*, 120(16), pp.1640–1645.

Ali, A.T. et al., 2013. Adipocyte and adipogenesis. *European Journal of Cell Biology*, 92(6–7), pp.229–236.

Amol, J. et al., 2009. Development of an in Vitro Cell Culture Model of Hepatic Steatosis Using Hepatocyte-Derived. , 102(5), pp.1466–1474.

Apweiler, R. & Freund, P., 1993. Development of glucose intolerance in obese (fa/fa) Zucker rats. *Horm Metab Res*, 25(10), pp.521–524. Available at:

http://www.ncbi.nlm.nih.gov/pubmed/8262460.

Araya, J. et al., 2004. Increase in long-chain polyunsaturated fatty acid n - 6/n - 3 ratio in relation to hepatic steatosis in patients with non-alcoholic fatty liver disease. *Clinical science (London, England : 1979)*, 106(6), pp.635–643.

Arner, E. et al., 2010. Adipocyte Turnover : Relevance to Human Adipose Tissue. *Diabetes*, 59(January), pp.105–109.

Arsenijevic, T. et al., 2012. Murine 3T3-L1 Adipocyte cell differentiation model: Validated reference genes for qPCR gene expression analysis. *PLoS ONE*, 7(5), pp.1–8.

Augstein, P. & Salzsieder, E., 2009. Morphology of Pancreatic Islets: A Time Course of Pre-diabetes in Zucker Fatty Rats. *Methods Molecular Biology*, 560, pp.159–189. Available at: http://www.springerlink.com/index/10.1007/978-1-59745-448-3.

Baietti, M.F. et al., 2012. Syndecan–syntenin–ALIX regulates the biogenesis of exosomes. *Nature Cell Biology*, 14(7), pp.677–685. Available at: http://dx.doi.org/10.1038/ncb2502.

Balaj, L. et al., 2011. Tumour microvesicles contain retrotransposon elements and amplified oncogene sequences. *Nat Communications*, 2(180), pp.1–19. Available at: http://www.pubmedcentral.nih.gov/articlerender.fcgi?artid=3040683&tool=pmcentrez&rendertype=abstract%5Cnhttp://www.nature.com/ncomms/journal/v2/n2/abs/ncomms1180.html.

Ban, L.A., Shackel, N.A. & McLennan, S. V., 2016. Extracellular vesicles: A new frontier in biomarker discovery for non-alcoholic fatty liver disease. *International Journal of Molecular Sciences*, 17(3), pp.1–14.

Bechmann, L.P. et al., 2012. The interaction of hepatic lipid and glucose metabolism in liver diseases. *Journal of Hepatology*, 56(4), pp.952–964. Available at: http://dx.doi.org/10.1016/j.jhep.2011.08.025.

Bellingham, S.A., Coleman, B.M. & Hill, A.F., 2012. Small RNA deep sequencing reveals a distinct miRNA signature released in exosomes from prion-infected neuronal cells. *Nucleic Acids Research*, 40(21), pp.10937–10949.

Bellingham, S.A., Guo, B. & Hill, A.F., 2015. The secret life of extracellular vesicles in metal homeostasis and neurodegeneration. *Biology of the Cell*, 107(11), pp.389–418.

Belting, M. & Christianson, H.C., 2015. Role of exosomes and microvesicles in hypoxia-associated tumour development and cardiovascular disease. *Journal of Internal Medicine*, 278(3), pp.251–263.

Biddinger, B.S. et al., 2005. Hepatic Insulin Resistance is Sufficient to Produce Dyslipidemia and Susceptibility to Atherosclerosis. *Biophysical Chemistry*, 257(5), pp.2432–2437.

Biever, A., Valjent, E. & Puighermanal, E., 2015. Ribosomal Protein S6 Phosphorylation in the Nervous System□ : From Regulation to Function. *Frontiers in Molecular Neuroscience*, 8(12), pp.1–14.

Blanc, L. & Vidal, M., 2017. New insights into the function of Rab GTPases in the context of exosomal secretion. *Small GTPases*, 0(0), pp.1–12. Available at: https://www.tandfonline.com/doi/full/10.1080/21541248.2016.1264352.

Blüher, M. et al., 2002. Adipose tissue selective insulin receptor knockout protects against obesity and obesity-related glucose intolerance. *Developmental Cell*, 3(1), pp.25–38.

Boing, A.N. et al., 2014. Single-step isolation of extracellular vesicles by size-exclusion chromatography. *Journal of extracellular vesicles*, 3(23430), pp.1–11.

Boizard, M. et al., 1998. Obesity-related Overexpression of Fatty-acid Synthase Gene in Adipose Tissue Involves Sterol Regulatory Element-binding Protein Transcription Factors*. , 273(44), pp.29164–29171. Available at: http://www.jbc.org/content/273/44/29164.full.pdf.

Borges, F.T. et al., 2013. TGF- 1-Containing Exosomes from Injured Epithelial Cells Activate Fibroblasts to Initiate Tissue Regenerative Responses and Fibrosis. *Journal of the American Society of Nephrology*, 24(3), pp.385–392. Available at: http://www.jasn.org/cgi/doi/10.1681/ASN.2012101031.

Boucher, J., Kleinridders, A. & Kahn, C.R., 2014. Insulin Receptor Signaling in Normal and Insulin-Resistant States. *Cold Spring Harb Perspect Biol 2014*, 6, pp.1–15.

Brandon, E.F.A. et al., 2003. An update on in vitro test methods in human hepatic drug biotransformation research: Pros and cons. *Toxicology and Applied Pharmacology*, 189(3), pp.233–246.

Bronner, D.N. et al., 2015. Endoplasmic Reticulum Stress Activates the Inflammasome via NLRP3- and Caspase-2-Driven Mitochondrial Damage. *Immunity*, 43(3), pp.451–462.

Brown, C.E. et al., 2016. Transient hypoxia reprograms differentiating adipocytes for enhanced insulin sensitivity and triglyceride accumulation. , 21(18), pp.4062–4072.

Browning, J.D. & Horton, J.D., 2004. JCI - Molecular mediators of hepatic steatosis and liver injury. , 114(2). Available at: http://www.jci.org/articles/view/22422.

Brüning, J.C. et al., 1998. A muscle-specific insulin receptor knockout exhibits features of the metabolic syndrome of NIDDM without altering glucose tolerance. *Molecular cell*, 2(5), pp.559–569.

Bruno, S. et al., 2009. Mesenchymal Stem Cell-Derived Microvesicles Protect Against Acute Tubular Injury. *J Am Soc Nephrol*, 20(5), pp.1053–1067.

Camussi, G. et al., 2010. Exosomes/microvesicles as a mechanism of cell-to-cell communication. *Kidney International*, 78(9), pp.838–848. Available at: http://dx.doi.org/10.1038/ki.2010.278.

Carbó, N., López-Soriano, F.J. & Argilés, J.M., 1991. Glucose handling by hepatocytes from obese Zucker rats. *Bioscience Reports*, 11(5), pp.285–292.

Carr, M.C. et al., 2002. Contribution of hepatic lipase, lipoprotein lipase, and cholesteryl ester transfer protein to LDL and HDL heterogeneity in healthy women. *Arteriosclerosis, Thrombosis, and Vascular Biology*, 22(4), pp.667–673.

Caruso, C., Balistreri, C.R. & Candore, G., 2010. The role of adipose tissue and adipokines in obesity-related inflammatory diseases. *Mediators of Inflammation*, 2010, pp.1–19.

Casal, E. et al., 2016. A novel sensitive method to measure catechol-o-methyltransferase activity unravels the presence of this activity in extracellular vesicles released by rat hepatocytes. *Frontiers in Pharmacology*, 7(12), pp.1–13.

Catania, C., Binder, E. & Cota, D., 2011. mTORC1 signaling in energy balance and metabolic disease. *International Journal of Obesity*, 35(6), pp.751–761. Available at: http://www.nature.com/doifinder/10.1038/ijo.2010.208.

Chan, Pei-chi and Hsieh, P.-S., 2017. The Role of Adipocyte Adipocyte Hypertrophy Hypertrophy and Hypoxia in the in the Development of Obesity-Associated Adipose Development of Obesity-Associated Adipose Resistance. In *InTech*.

Chatterjee, P. et al., 2013. Adipocyte fetuin-a contributes to macrophage migration into adipose tissue and polarization of macrophages. *Journal of Biological Chemistry*, 288(39), pp.28324–28330.

Cheatham, B. & Kahn, C.R., 1995. Insulin action and the insulin signaling network. *Endocrine Reviews*, 16(2), pp.117–142.

Chen, X.-H. et al., 2010. TNF-α induces mitochondrial dysfunction in 3T3-L1 adipocytes. *Molecular and Cellular Endocrinology*, 328(1–2), pp.63–69.

Chen, Y. et al., 2012. Rab10 and myosin-va mediate insulin-stimulated GLUT4 storage vesicle translocation in adipocytes. *Journal of Cell Biology*, 198(4), pp.545–560.

Cho, J.A. et al., 2005. Exosomes: A new delivery system for tumor antigens in cancer immunotherapy. *International Journal of Cancer*, 114(4), pp.613–622.

Colombo, M. et al., 2013. Analysis of ESCRT functions in exosome biogenesis, composition and secretion highlights the heterogeneity of extracellular vesicles. *Journal of cell science*, 126(Pt 24), pp.5553–65. Available at: http://www.ncbi.nlm.nih.gov/pubmed/24105262.

Combs, P.T. & Marliss, B.E.B., 2014. Adiponectin signaling in the liver. *Reviews in Endocrine and Metabolic Disorders*, 15(2), pp.137–147.

Conde-Vancells, J. et al., 2008. Characterization and comprehensive proteome profiling of exosomes secreted by hepatocytes. *Journal of Proteome Research*, 7(12), pp.5157–5166.

Conde-Vancells, J. et al., 2010. Overview of Extracellular Microvesicles in Drug Metabolism. *Expert Opin Drug Metab Toxicol*, 6(5), pp.543–554.

Connolly, K.D. et al., 2015. Characterisation of adipocyte-derived extracellular vesicles released pre- and post-adipogenesis. *Journal of extracellular vesicles*, 4(11), pp.1–9. Available at: http://www.ncbi.nlm.nih.gov/pubmed/26609807.

Constant, V.A. et al., 2006. Macrophage-conditioned medium inhibits the differentiation of 3T3-L1 and human abdominal preadipocytes. *Diabetologia*, 49(6), pp.1402–1411.

Constant, V.A. et al., 2008. The antiadipogenic effect of macrophage-conditioned medium depends on ERK1/2 activation. *Metabolism: Clinical and Experimental*, 57(4), pp.465–472.

Cornelius, P., Macdougald, O. a & Lane, M.D., 1994. Regulation of adipocyte development. *Annual Review of Nutrition*, 14(7), pp.99–129.

Cornely, R. et al., 2011. Annexin A6 is an organizer of membrane microdomains to regulate receptor localization and signalling. *IUBMB Life*, 63(11), pp.1009–1017.

Costantini, S. et al., 2013. Gene expression signature of human HepG2 cell line. *Gene*, 518(2), pp.335–345. Available at: http://dx.doi.org/10.1016/j.gene.2012.12.106.

Crossno, T.J. et al., 2006. Rosiglitazone promotes development of a novel adipocyte population from bone marrow–derived circulating progenitor cells. *Journal of Clinical Investigation*, 116(12), pp.3220–3228.

Cui, W., Chen, S.L. & Hu, K.Q., 2010. Quantification and mechanisms of oleic acid-induced steatosis in HepG2 cells. *American Journal of Translational Research*, 2(1), pp.95–104.

Dani, C., 2013. Activins in adipogenesis and obesity. *International Journal of Obesity*, 37(2), pp.163–166. Available at: http://www.nature.com/doifinder/10.1038/ijo.2012.28.

Daniel, M.J., 2011. Lipid management in patients with type 2 diabetes. *American health & drug benefits*, 4(5), pp.312–22. Available at: http://www.pubmedcentral.nih.gov/articlerender.fcgi?artid=4105726&tool=pmcentrez&rendertype=abstract.

Demel, R.A. & Jackson, R.L., 1985. Lipoprotein Lipase Hydrolysis of Trioleoylglycerol in a Phospholipid Interface. *The Journal of biological chemistry*, 260(17), pp.9589–9592.

Deng, Z. -b. et al., 2009. Adipose Tissue Exosome-Like Vesicles Mediate Activation of

Macrophage-Induced Insulin Resistance. *Diabetes*, 58(11), pp.2498–2505. Available at: http://diabetes.diabetesjournals.org/cgi/doi/10.2337/db09-0216.

Van Deun, J. et al., 2014. The impact of disparate isolation methods for extracellular vesicles on downstream RNA profiling. *Journal of extracellular vesicles*, 3(9), pp.1–14.

Donato, M.T.M. et al., 2006. Potential impact of steatosis on cytochrome P450 enzymes of human hepatocytes isolated from fatty liver grafts. *Drug metabolism and disposition*, 34(9), pp.1556–1562. Available at: http://dmd.aspetjournals.org/content/34/9/1556.short.

Doyle, A.E.S. et al., 2004. Catechol-O-methyltransferase low activity genotype (COMTLL) is associated with low levels of COMT protein in human hepatocytes. *Cancer Letters*, 214(2), pp.189–195.

Dragsbæk, K. et al., 2016. Metabolic syndrome and subsequent risk of type 2 diabetes and cardiovascular disease in elderly women. *Medicine (Baltimore)*, 95(36), pp.1–8.

Durcin, M. et al., 2017a. Characterisation of adipocyte-derived extracellular vesicle subtypes identifies distinct protein and lipid signatures for large and small extracellular vesicles. *Journal of Extracellular Vesicles*, 6(1), p.1305677. Available at: https://www.tandfonline.com/doi/full/10.1080/20013078.2017.1305677.

Durcin, M. et al., 2017b. Characterisation of adipocyte-derived extracellular vesicle subtypes identifies distinct protein and lipid signatures for large and small extracellular vesicles. *Journal of Extracellular Vesicles*, 6(1), pp.1–14. Available at: https://www.tandfonline.com/doi/full/10.1080/20013078.2017.1305677.

Düvel, K. et al., 2010. Activation of a metabolic gene regulatory network downstream of mTOR complex 1. *Molecular Cell*, 39(2), pp.171–183.

Efthimios, S., 1978. to Adipocytes. *Differentiation*, 253(13), pp.4693–4696.

Eitan, E. et al., 2016. Impact of Lysosome Status on Extracellular Vesicle Content and Release. *Ageing Res Rev.*, 32(2), pp.65–74.

Emanuela, F. et al., 2012. Inflammation as a link between obesity and metabolic syndrome. *Journal of Nutrition and Metabolism*, 2012(11), pp.1–7.

Engering, A. et al., 2003. Differential post-translational modification of CD63 molecules during maturation of human dendritic cells. *European Journal of Biochemistry*, 270(11), pp.2412–2420.

Ervin, R.B., 2009. Prevalence of metabolic syndrome among adults 20 years of age and over, by sex, age, race and ethnicity, and body mass index: United States, 2003-2006. *National health statistics reports*, 5(13), pp.1–7.

Escribano, O. et al., 2009. Role of a Liver-Pancreas Endocrine Axis Through Insulin Receptor A Isoform. *Diabetes*, 58(4), pp.820–828.

Esposito, K. et al., 2003. Association of low interleukin-10 levels with the metabolic syndrome in obese women. *Journal of Clinical Endocrinology and Metabolism*, 88(3), pp.1055–1058.

Falcón-Pérez, J.M., Lu, S.C. & Mato, J.M., 2010. Sub-proteome approach to the knowledge of liver. *Proteomics. Clinical applications*, 4(4), pp.407–415.

Fan, J.Y. et al., 1983. Morphological changes of the 3T3-L1 fibroblast plasma membrane upon differentiation to the adipocyte form. *Journal of cell science*, 61(1), pp.219–30. Available at: http://www.ncbi.nlm.nih.gov/pubmed/6885939.

Farah, R., Khamisy-Farrah, R. & Shurtz-Swirski, R., 2013. Calcium channel blockers effect on insulin resistance and inflammaion markers in essential hypertension patients. *Int Angiol*, 32(1), pp.85–93.

Feldman, J.M. & Henderson, J.H., 1978. Monoamine Oxidase , Norepinephrine Levels in Mice with the Hereditary Obese-hyperglycemic Syndrome. *Diabetes*, pp.389–395.

Ferrante, C.S. et al., 2015. Adipocyte-derived Exosomal miRNAs: A Novel Mechanism for Obesity-Related Disease. *Pediatr Res.*, 77(3), pp.447–54.

Finucane, O.M. et al., 2014. Macrophage migration inhibitory factor deficiency ameliorates high-fat diet induced insulin resistance in mice with reduced adipose inflammation and hepatic steatosis. *PLoS ONE*, 9(11), pp.1–14.

Fonsato, V. et al., 2012. Human liver stem cell-derived microvesicles inhibit hepatoma

growth in SCID mice by delivering antitumor microRNAs. *Stem Cells*, 30(9), pp.1985–1998.

Frayn, K.N., Arner, P. & Yki-Jarvinen, H., 2006. Fatty acid metabolism in adipose tissue, muscle and liver in health and disease. *Essays in Biochemistry*, 42(4), pp.89–103.

Fujihara, M. et al., 2003. Molecular mechanisms of macrophage activation and deactivation by lipopolysaccharide: Roles of the receptor complex. *Pharmacology and Therapeutics*, 100(2), pp.171–194.

Fujioka, K., 2006. Metabolic syndrome treatment strategies. *Pharmacotherapy*, 26(12 Pt 2), p.222S–226S.

Furtado, L.M. et al., 2002. Activation of the glucose transporter GLUT4 by insulin. *Biochemistry and cell biology = Biochimie et biologie cellulaire*, 80(5), pp.569–78. Available at: http://www.ncbi.nlm.nih.gov/pubmed/12440698.

Galan, X. et al., 2000. Secretion of Hepatic Lipase by Perfused Liver and Isolated Hepatocytes. *Lipids*, 35(9), pp.1017–1026.

Gao, W. et al., 2016. Exosomes derived from mature dendritic cells increase endothelial inflammation and atherosclerosis via membrane TNF-?? mediated NF-??B pathway. *Journal of Cellular and Molecular Medicine*, 20(12), pp.2318–2327.

Gardiner, C. et al., 2016. Techniques used for the isolation and characterization of extracellular vesicles: results of a worldwide survey. *Journal of Extracellular Vesicles*, 1(10), pp.1–6.

Gavrilova, O. et al., 2003. Liver Peroxisome Proliferator-activated Receptor Contributes to Hepatic Steatosis , Triglyceride Clearance , and Regulation of Body Fat Mass *. *The Journal of biological chemistry*, 278(36), pp.34268–34276.

George, J. et al., 1997. Time-dependent expression of cytochrome P450 genes in primary cultures of well-differentiated human hepatocytes. *The Journal of laboratory and clinical medicine*, 129(6), pp.638–48. Available at: http://www.ncbi.nlm.nih.gov/pubmed/9178731.

Gerets, H.H.J. et al., 2012. Characterization of primary human hepatocytes , HepG2 cells , and HepaRG cells at the mRNA level and CYP activity in response to inducers and their predictivity for the detection of human hepatotoxins. *Cell Biol Toxicol*, 28, pp.69–87.

Getz, G.S. & Reardon, C.A., 2009. Apoprotein E as a lipid transport and signaling protein in the blood, liver, and artery wall. *J. Lipid Res*, 50(4), pp.156–161.

Giebel, B., 2017. On the function and heterogeneity of extracellular vesicles. *Annals of Translational Medicine*, 5(6), pp.150–150. Available at: http://atm.amegroups.com/article/view/13943/14373.

Glebov, O.O., Bright, N. a & Nichols, B.J., 2006. Flotillin-1 defines a clathrin-independent endocytic pathway in mammalian cells. *Nature Cell Biology*, 8(1), pp.46–54. Available at: http://www.nature.com/doifinder/10.1038/ncb1342.

Gocze, P.M. & Freeman, D.A., 1994. Factors Underlying the Variability of Lipid Droplet Fluorescence in MA-10 Leydig Tumor Cells. *Cytometry*, 17(2), pp.151–158.

Godbole, V. & York, D.A., 1978. Lipogenesis in situ in the Genetically Obese Zucker Fatty Rat (fa/fa): Role of Hyperphagia and Hyperinsulinaemia. *Diabetologia*, 14(3), pp.191–197.

Goldstein, A.L. & Johnson, P.R., 1980. Primary cultures of fetal hepatocytes from the genetically obese Zucker rat: characterization and total lipogenesis. *In Vitro Cellular and Developmental Biology*, 16(4), pp.288–296.

Gómez-Lechón, M.J. et al., 2007. A human hepatocellular in vitro model to investigate steatosis. *Chemico-Biological Interactions*, 165(2), pp.106–116.

Gonzalez, E. & Falcon-Perez, J.M., 2015. Cell-derived extracellular vesicles as a platform to identify low-invasive disease biomarkers Cell-derived extracellular vesicles as a platform to identify low-invasive disease biomarkers. *Expert Rev. Mol. Diagn.*, 15(7), pp.907–923.

Goossens, G.H., 2008. The role of adipose tissue dysfunction in the pathogenesis of obesity-related insulin resistance. *Physiology and Behavior*, 94(2), pp.206–218.

Gornicka, A. et al., 2012. Adipocyte hypertrophy is associated with lysosomal permeability both in vivo and in vitro: role in adipose tissue inflammation. *American journal of physiology. Endocrinology and metabolism*, 303(5), pp.E597-606.

Green, H. & Kehinde, O., 1975. An established preadipose cell line and its differentiation in culture II. Factors affecting the adipose conversion. *Cell*, 5(1), pp.19–27.

Green, H. & Kehinde, O., 1974. Sublines of mouse 3T3 cells that accumulate lipid. *Cell*, 1(3), pp.113–116.

Gregoire, F.M., Smas, C.M. & Sul, H.S., 1998. Understanding adipocyte differentiation. *Physiological reviews*, 78(3), pp.783–809. Available at: http://www.ncbi.nlm.nih.gov/pubmed/9674695.

Gressner, M.A. & Wool, G.I., 1974. The Phosphorylation of Liver Ribosomal Proteins in Vito: Evidence that only a single subunit protein (S6) is phosphorylated. *The Journal of biological chemistry*, 249(21), pp.6917–6926.

Gross, J.C. et al., 2012. Active Wnt proteins are secreted on exosomes. *Nature Cell Biology*, 14(10), pp.1036–1045. Available at: http://dx.doi.org/10.1038/ncb2574.

Grundy, S.M., 2015. Adipose tissue and metabolic syndrome: Too much, too little or neither. *European Journal of Clinical Investigation*, 45(11), pp.1209–1217.

Grundy, S.M. et al., 2005. Diagnosis and management of the metabolic syndrome: An American Heart Association/National Heart, Lung, and Blood Institute scientific statement. *Circulation*, 112(17), pp.2735–2752.

Grundy, S.M., 2016. Metabolic syndrome update. *Trends in Cardiovascular Medicine*, 26(4), pp.364–373. Available at: http://dx.doi.org/10.1016/j.tcm.2015.10.004.

Guo, L. & Guo, N., 2015. Exosomes: Potent regulators of tumor malignancy and potential bio-tools in clinical application. *Critical reviews in oncology/hematology*, 95(3), pp.346–358. Available at: http://eutils.ncbi.nlm.nih.gov/entrez/eutils/elink.fcgi?dbfrom=pubmed&id=25982702&retmode=ref&cmd=prlinks%0Afile:///Users/Nakazawa-lab/Documents/Papers-shere/Articles/2015/Guo/Crit. Rev. Oncol. Hematol. 2015

Guo.pdf%0Apapers2://publication/doi/10.1016/j.c.

György, B. et al., 2011. Membrane vesicles, current state-of-the-art: Emerging role of extracellular vesicles. *Cellular and Molecular Life Sciences*, 68(16), pp.2667–2688.

H.-G. Zhang (ed.), *Emerging Concepts of Tumor Exosome-Mediated Cell-Cell Communication*,

Ha, D., Yang, N. & Nadithe, V., 2016. Exosomes as therapeutic drug carriers and delivery vehicles across biological membranes : current perspectives and future challenges. *Acta Pharmaceutica Sinica B*, 6(4), pp.287–296. Available at: http://dx.doi.org/10.1016/j.apsb.2016.02.001.

Hall, J.E., 2000. Pathophysiology and treatment of obesity hypertension. *Current Hypertension Reports*, 2(2), pp.139–147.

Haney, M.J. et al., 2015. Exosomes as Drug Delivery Vehicles for Parkinson's Disease Therapy. *Journal of Controlled Release*, 207(6), pp.18–30. Available at: http://dx.doi.org/10.1016/j.jconrel.2015.03.033.

Hanna, M.G. et al., 2016. Sar1 GTPase activity is regulated by membrane curvature. *Journal of Biological Chemistry*, 291(3), pp.1014–1027.

Hashiramoto, M. & James, D.E., 2000. Characterization of insulin-responsive GLUT4 storage vesicles isolated from 3T3-L1 adipocytes. *Molecular and cellular biology*, 20(1), pp.416–27. Available at: http://www.pubmedcentral.nih.gov/articlerender.fcgi?artid=85096&tool=pmcentrez&rendertype=abstract.

Heid, E.M. et al., 2013. Mitochondrial ROS induces NLRP3-dependent lysosomal damage and inflammasome activation. *Computer*, 191(10), pp.724–732.

Hemmings, B.A. & Restuccia, D.F., 2012. PI3K-PKB / Akt Pathway. *Cold Spring Harbor perspectives in biology*, 4(1), pp.1–4.

Hirsova, P. et al., 2016. Lipid-Induced Signaling Causes Release of Inflammatory Extracellular Vesicles from Hepatocytes. *Gastroenterology*, 150(4), pp.956–967. Available at: http://dx.doi.org/10.1053/j.gastro.2015.12.037.

Hosogai, N. et al., 2007. Adipose tissue hypoxia in obesity and its impact on adipocytokine dysregulation. *Diabetes*, 56(4), pp.901–911.

Hu, E., Liang, P. & Spiegelman, B.M., 1996. AdipoQ is a novel adipose-specific gene dysregulated in obesity. *Journal of Biological Chemistry*, 271(18), pp.10697–10703.

Hu, Z. et al., 2014. Quantitative liver-specific protein fingerprint in blood: A signature for hepatotoxicity. *Theranostics*, 4(2), pp.215–228.

Huang, D.W., Lempicki, R. a & Sherman, B.T., 2009. Systematic and integrative analysis of large gene lists using DAVID bioinformatics resources. *Nature Protocols*, 4(1), pp.44–57.

Huang, S. & Czech, M.P., 2007. Review The GLUT4 Glucose Transporter. *Cell Metabolism*, 5(4), pp.237–252.

Hüttemann, M. et al., 2007. Regulation of mitochondrial oxidative phosphorylation through cell signaling. *Biochimica et Biophysica Acta (BBA) - Molecular Cell Research*, 1773(12), pp.1701–1720. Available at: http://www.sciencedirect.com/science/article/pii/S0167488907002364.

Ide, J. et al., 2011. Macrophage-conditioned medium inhibits the activation of cyclin-dependent kinase 2 by adipogenic inducers in 3T3-L1 preadipocytes. *Journal of Cellular Physiology*, 226(9), pp.2297–2306.

Ikramuddin, S. & Buchwald, H., 2011. How bariatric and metabolic operations control metabolic syndrome. *British Journal of Surgery*, 98(10), pp.1339–1341.

Imani Fooladi, A.A. & Hosseini, H.M., 2014. Biological functions of exosomes in the liver in health and disease. *Hepatitis Monthly*, 14(5), pp.5–7.

Iraci, N. et al., 2016. Focus on extracellular vesicles: Physiological role and signalling properties of extracellular membrane vesicles. *International Journal of Molecular Sciences*, 17(171), pp.1–7.

Iyanagi, T., 2007. Molecular Mechanism of Phase I and Phase II Drug-Metabolizing Enzymes: Implications for Detoxification. *International Review of Cytology*, 260(6), pp.35–112.

Jaishy, B. & Abel, E.D., 2016. Lipids, lysosomes, and autophagy. *Journal of lipid research*, 57(9), pp.1619–35. Available at: http://www.ncbi.nlm.nih.gov/pubmed/27330054 [Accessed May 7, 2017].

Jayachandran, M. et al., 2011. Alterations in platelet function and cell-derived microvesicles in recently menopausal women: Relationship to metabolic syndrome and atherogenic risk. *Journal of Cardiovascular Translational Research*, 4(6), pp.811–822.

Jo, J. et al., 2009. Hypertrophy and/or hyperplasia: Dynamics of adipose tissue growth. *PLoS Computational Biology*, 5(3), pp.1–13.

Johnson, A.R., Milner, J.J. & Makowski, L., 2012. The inflammation highway: metabolism accelerates inflammatory traffic in obesity. *Immunol Rev*, 249(1), pp.218–238.

Johnstone, R.M. et al., 1991. Exosome formation during maturation of mammalian and avian reticulocytes: Evidence that exosome release is a major route for externalization of obsolete membrane proteins. *Journal of Cellular Physiology*, 147(1), pp.27–36.

Johnstone, R.M. et al., 1987. Vesicle formation during reticulocyte maturation. Association of plasma membrane activities with released vesicles (exosomes). *Journal of Biological Chemistry*, 262(19), pp.9412–9420.

Jovic, M. et al., 2010. The early endosome: a busy sorting station for proteins at the crossroads. *Histol Histolopathol.*, 25(1), pp.99–112.

Ju, R. et al., 2014. Angiopoietin-2 secretion by endothelial cell exosomes: Regulation by the phosphatidylinositol 3-kinase (PI3K)/Akt/endothelial nitric oxide synthase (eNOS) and syndecan-4/syntenin pathways. *Journal of Biological Chemistry*, 289(1), pp.510–519.

Kakazu, E. et al., 2015. Hepatocytes Release Ceramide-enriched Proinflammatory Extracellular Vesicles in an IRE1alpha-dependent Manner. *Journal of lipid research*, 57(2), pp.233–245. Available at: http://www.jlr.org/content/early/2015/11/30/jlr.M063412.long.

Kallen, C.B. & Lazar, M.A., 1996. Antidiabetic thiazolidinediones inhibit leptin (ob) gene expression in 3T3-L1 adipocytes (obesity/nuclear receptor/peroxisome proliferator-activated receptor y). *Cell Biology*, 93(June), pp.5793–5796.

Kalra, H. et al., 2012. Vesiclepedia: A Compendium for Extracellular Vesicles with Continuous Community Annotation. *PLoS Biology*, 10(12), pp.8–12.

Kalra, H., Drummen, G.P.C. & Mathivanan, S., 2016. Focus on extracellular vesicles: Introducing the next small big thing. *International Journal of Molecular Sciences*, 17(2).

Kanuri, G. & Bergheim, I., 2013. In vitro and in vivo models of non-alcoholic fatty liver disease (NAFLD). *International journal of molecular sciences*, 14(6), pp.11963–11980.

Karunanithi, S. et al., 2014. A Rab10:RalA G protein cascade regulates insulin-stimulated glucose uptake in adipocytes. *Mol Biol Cell*, 25(19), pp.3059–3069. Available at: http://www.ncbi.nlm.nih.gov/pubmed/25103239%5Cnhttp://www.ncbi.nlm.nih.gov/pmc/articles/PMC4230594/pdf/3059.pdf.

Kasuga, Masato, Karlsson F. Anders, Kahn, C.R., 1982. Insulin Stimulates the Phosphorylation of the 95,000 Dalton Subunit of Its Own Receptor. *Science (New York, N.Y.)*, 215(4529), pp.185–7.

Katsuda, T. et al., 2013. Human adipose tissue-derived mesenchymal stem cells secrete functional neprilysin-bound exosomes. *Scientific reports*, 3(1197), pp.1–11. Available at: http://www.pubmedcentral.nih.gov/articlerender.fcgi?artid=3561625&tool=pmcentrez&rendertype=abstract.

Kaur, J., 2014. A comprehensive review on metabolic syndrome. *Cardiology Research and Practice*, 2014(94362), pp.1–21.

Kava, R., Greenwood, M.R.C. & Johnson, P.R., 1990. Zucker (fa / fa) Rat. *ILAR Journal*, 32(3), pp.4–8.

Keophiphath, M. et al., 2010. CCL5 promotes macrophage recruitment and survival in human adipose tissue. *Arteriosclerosis, Thrombosis, and Vascular Biology*, 30(1), pp.39–45.

Keuper, M. et al., 2014. Spare mitochondrial respiratory capacity permits human adipocytes to maintain ATP homeostasis under hypoglycemic conditions. *FASEB Journal*, 28(2), pp.761–770.

Kiefer, F.W. et al., 2012. Retinaldehyde dehydrogenase 1 coordinates hepatic

gluconeogenesis and lipid metabolism. *Endocrinology*, 153(7), pp.3089–3099.

Kim, D.K. et al., 2015. EVpedia: A community web portal for extracellular vesicles research. *Bioinformatics*, 31(6), pp.933–939.

Kim, J. et al., 2007. Obesity-associated improvements in metabolic profile through expansion of adipose tissue. *Journal of Clinical Investigation*, 117(9), pp.2621–2637.

Kim, J.I. et al., 2015. Lipid-overloaded enlarged adipocytes provoke insulin resistance independent of inflammation. *Molecular and cellular biology*, 35(10), pp.1686–99. Available at: http://mcb.asm.org/content/35/10/1686.short.

Klover, P.J. & Mooney, R.A., 2004. Hepatocytes: Critical for glucose homeostasis. *International Journal of Biochemistry and Cell Biology*, 36(5), pp.753–758.

Knutson, V.P. & Balba, Y., 2012. 3T3-L1 Adipocytes as a Cell Culture Model of Insulin Resistance. , 33(2), pp.77–81.

Koeck, E.S. et al., 2014. Adipocyte exosomes induce transforming growth factor beta pathway dysregulation in hepatocytes: A novel paradigm for obesity-related liver disease. *Journal of Surgical Research*, 192(2), pp.268–275. Available at: http://dx.doi.org/10.1016/j.jss.2014.06.050.

Kohli, R. et al., 2007. Mitochondrial reactive oxygen species signal hepatocyte steatosis by regulating the phosphatidylinositol 3-kinase cell survival pathway. *Journal of Biological Chemistry*, 282(29), pp.21327–21336.

Koo, S.H., Dutcher, A.K. & Towle, H.C., 2001. Glucose and Insulin Function through Two Distinct Transcription Factors to Stimulate Expression of Lipogenic Enzyme Genes in Liver. *Journal of Biological Chemistry*, 276(12), pp.9437–9445.

Kowal, J. et al., 2016. Proteomic comparison defines novel markers to characterize heterogeneous populations of extracellular vesicle subtypes. *Proceedings of the National Academy of Sciences of the United States of America*, 113(8), pp.E968-77. Available at: http://www.ncbi.nlm.nih.gov/pubmed/26858453%5Cnhttp://www.pubmedcentral.nih.gov/articlerender.fcgi?artid=PMC4776515%5Cnhttp://www.ncbi.nlm.nih.gov/pubmed/26858453%5Cnhttp://www.pubmedcentral.nih.gov/articlerender.fcgi?artid=PM

C4776515.

Kranendonk, M.E.G. et al., 2014. Effect of extracellular vesicles of human adipose tissue on insulin signaling in liver and muscle cells. *Obesity (Silver Spring, Md.)*, 22(10), pp.2216–23. Available at: http://www.ncbi.nlm.nih.gov/pubmed/25045057.

Kranendonk, M.E.G. et al., 2014. Human adipocyte extracellular vesicles in reciprocal signaling between adipocytes and macrophages. *Obesity*, 22(5), pp.1296–1308.

Kulkarni, R.N. et al., 1999. Tissue-specific knockout of the insulin receptor in pancreatic β cells creates an insulin secretory defect similar to that in type 2 diabetes. *Cell*, 96(3), pp.329–339.

Kusminski, C.M. & Scherer, P.E., 2012. Mitochondrial dysfunction in white adipose tissue. *Trends in Endocrinology and Metabolism*, 23(9), pp.435–443. Available at: http://dx.doi.org/10.1016/j.tem.2012.06.004.

Kylin, E., 1923. Studien ueber das Hypertonie-Hyperglyca "mie-Hyperurika" miesyndrom. *Zentralblatt fuer Innere Medizin*, 44(1), pp.105–127.

Lakhter, A.J. & Sims, E.K., 2015. Minireview: Emerging Roles for Extracellular Vesicles in Diabetes and Related Metabolic Disorders. *Molecular Endocrinology (Baltimore, Md.)*, 29(11), pp.1535–1548. Available at: http://press.endocrine.org/doi/pdf/10.1210/me.2015-1206%5Cnhttp://www.ncbi.nlm.nih.gov/pubmed/26393296.

Lancaster, G.I. & Febbraio, M.A., 2005. Exosome-dependent trafficking of HSP70: A novel secretory pathway for cellular stress proteins. *Journal of Biological Chemistry*, 280(24), pp.23349–23355.

Laplante, M. & Sabatini, D.M., 2013. mTOR signaling in growth control and disease. *Cell*, 149(2), pp.274–293. Available at: http://dx.doi.org/10.1016/j.cell.2012.03.017.

Lawson, C. et al., 2016. Microvesicles and exosomes: New players in metabolic and cardiovascular disease. *Journal of Endocrinology*, 228(2), pp.R57–R71.

Lazaro-Ibanez, E. et al., 2014. Different gDNA content in the subpopulations of prostate

cancer extracellular vesicles: apoptotic bodies, microvesicles, and exosomes. *TheProstate*, 74(14), pp.1379–1390.

Lebiedzinska, M. et al., 2009. Interactions between the endoplasmic reticulum, mitochondria, plasma membrane and other subcellular organelles. *International Journal of Biochemistry and Cell Biology*, 41(10), pp.1805–1816.

Lee, C. et al., 2014. Exosomes Mediate the Cytoprotective Action of Mesenchymal Stromal Cells on Hypoxia-Induced Pulmonary Hypertension Changjin. *Circulation*, 126(22), pp.2601–2611.

Lee, H. et al., 2016. Extracellular Vesicles Facilitate the Intercellular Communications in the Pathogenesis of Lung Injury. *Cell & Developmental Biology*, 5(2), pp.2–5. Available at: http://www.omicsgroup.org/journals/extracellular-vesicles-facilitate-the-intercellular-communications-in-thepathogenesis-of-lung-injury-2168-9296-1000175.php?aid=76702.

Lee, J.-E. & Ge, K., 2014. Transcriptional and epigenetic regulation of PPARγ expression during adipogenesis. *Cell & bioscience*, 4(29), pp.1–11. Available at: http://www.pubmedcentral.nih.gov/articlerender.fcgi?artid=4046494&tool=pmcentrez&rendertype=abstract.

Lee, L. & Sanders, R.A., 2002. Metabolic Syndrome. *AAOHN Journal*, 33(10), pp.459–468.

Lee, M.-J., Park, D.-H. & Kang, J.-H., 2016. Exosomes as the source of biomarkers of metabolic diseases. *Ann Pediatr Endocrinol Metab*, 21(1), pp.119–125. Available at: http://dx.doi.org/10.6065/apem.

Lessard, J. et al., 2014. Low abdominal subcutaneous preadipocyte adipogenesis is associated with visceral obesity, visceral adipocyte hypertrophy, and a dysmetabolic state. *Adipocyte*, 3(3), pp.197–205. Available at: http://www.tandfonline.com/doi/abs/10.4161/adip.29385.

Levental, I., Grzybek, M. & Simons, K., 2010. Greasing their way: Lipid modifications determine protein association with membrane rafts. *Biochemistry*, 49(30), pp.6305–6316.

Levin, B.E., Triscari, J. & Sullivan, A.N.N.C., 1981. Defective catecholamine metabolism in

peripheral organs of genetically obese zucker rats. *Brain Research*, 224, pp.353–366.

Li, L. et al., 2016. Exosomes derived from hypoxic oral squamous cell carcinoma cells deliver miR-21 to normoxic cells to elicit a prometastatic phenotype. *Cancer Research*, 76(7), pp.1770–1780.

Li, T. et al., 2012. Exosomes derived from human umbilical cord mesenchymal stem cells alleviate liver fibrosis. *Stem Cells and Development*, 22(6), pp.845–54.

Li, X. et al., 2016. Mitochondria-Translocated PGK1 Functions as a Protein Kinase to Coordinate Glycolysis and the TCA Cycle in Tumorigenesis. *Molecular Cell*, 61(5), pp.705–719. Available at: http://dx.doi.org/10.1016/j.molcel.2016.02.009.

Lirk, P., Hoffmann, G. & Rieder, J., 2002. Inducible nitric oxide synthase--time for reappraisal. *Current drug targets. Inflammation and allergy*, 1(1), pp.89–108.

Liu, J. et al., 2005. The stomatin/prohibitin/flotillin/HflK/C domain of flotillin-1 contains distinct sequences that direct plasma membrane localization and protein interactions in 3T3-L1 adipocytes. *Journal of Biological Chemistry*, 280(16), pp.16125–16134.

Lo, K.A. et al., 2014. Analysis of in vitro insulin resistance models and their physiological relevance to in vivo diet-induced adipose insulin resistance. *Cell Reports*, 5(1), pp.1–20.

Lucero, D. et al., 2011. Pro-inflammatory and atherogenic circulating factors in non-alcoholic fatty liver disease associated to metabolic syndrome. *Clinica chimica acta; international journal of clinical chemistry*, 412(1–2), pp.143–7. Available at: http://www.ncbi.nlm.nih.gov/pubmed/20887718.

Lumeng, C.N., Bodzin, J.L. & Saltiel, A.R., 2007. Obesity induces a phenotipic switch in adipose tissue macrophage polarization. *J Clin Invest*, 117(1), pp.175–184.

Lumeng, C.N., Deyoung, S.M. & Saltiel, A.R., 2007. Macrophages block insulin action in adipocytes by altering expression of signaling and glucose transport proteins. *Am J Physiol Endocrinol Metab*, 292(1), pp.1–23.

Lumeng, C.N. & Saltiel, A.R., 2011. Review series Inflammatory links between obesity and metabolic disease. *Life Sciences*, 121(6), pp.2111–2117.

Maas, S.L.N., Breakefield, X.O. & Weaver, A.M., 2017. Extracellular Vesicles: Unique Intercellular Delivery Vehicles. *Trends in Cell Biology*, 27(3), pp.172–188. Available at: http://linkinghub.elsevier.com/retrieve/pii/S0962892416301799.

Mallea-Gil, M. et al., 2012. IGF-1 levels in different stages of liver steatosis and its association with metabolic syndrome. *Acta Gastroenterol Latinoam.*, 42(4), pp.6–20.

Marques-Vidal, P. et al., 1994. Hepatic lipase promotes the uptake of HDL esterified cholesterol by the perfused rat liver: a study using reconstituted HDL particles of defined phospholipid composition. *Journal of lipid research*, 35(3), pp.373–84. Available at: http://www.ncbi.nlm.nih.gov/pubmed/8014574.

Masyuk, A.I., Masyuk, T. V. & Larusso, N.F., 2013. Exosomes in the pathogenesis, diagnostics and therapeutics of liver diseases. *Journal of Hepatology*, 59(3), pp.621–625. Available at: http://dx.doi.org/10.1016/j.jhep.2013.03.028.

Matter, C.M. & Handschin, C., 2007. RANTES (regulated on activation, normal T cell expressed and secreted), inflammation, obesity, and the metabolic syndrome. *Circulation*, 115(8), pp.946–948.

Maurya, M.R. et al., 2013. Analysis of inflammatory and lipid metabolic networks across RAW264.7 and thioglycolate-elicited macrophages. *Journal of lipid research*, 54(9), pp.2525–42. Available at: http://www.ncbi.nlm.nih.gov/pubmed/23776196.

Mcardle, M.A. et al., 2013. Mechanisms of obesity-induced inflammation and insulin resistance : insights into the emerging role of nutritional strategies. *Frontiers in Endocrinology*, 4(5), pp.1–23.

McDonald, M.K. et al., 2014. Functional significance of macrophage-derived exosomes in inflammation and pain. *Pain*, 155(8), pp.1527–1539.

Medina-Santillán, R. et al., 2013. Hepatic manifestations of metabolic syndrome. *Diabetes/metabolism research and reviews*, 7(1), pp.1–36. Available at: http://www.ncbi.nlm.nih.gov/pubmed/23471889.

Meex, R.C. et al., 2015. Fetuin B Is a Secreted Hepatocyte Factor Linking Steatosis to

Impaired Glucose Metabolism. *Cell Metabolism*, 22(6), pp.1078–1089. Available at: http://dx.doi.org/10.1016/j.cmet.2015.09.023.

Mehra, A., Macdonald, I. & Pillay, T.S., 2007. Variability in 3T3-L1 adipocyte differentiation depending on cell culture dish. *Analytical Biochemistry*, 362(2), pp.281–283.

Meister, M. & Tikkanen, R., 2014. Endocytic trafficking of membrane-bound cargo: A flotillin point of view. *Membranes*, 4(3), pp.356–371.

De Meyts, P., 2016. The Insulin Receptor and Its Signal Transduction Network. In L. De Groot, G. Chrousos, & K. Dungan, eds. *EndoText*. South Dartmouth (MA): Endotext internet, p. 2000-. Available at: https://www.ncbi.nlm.nih.gov/books/NBK378978/.

Miksztowicz, V. et al., 2012. Hepatic lipase activity is increased in non-alcoholic fatty liver disease beyond insulin resistance. *Diabetes/Metabolism Research and Reviews*, 28, pp.535–541. Available at: http://libweb.anglia.ac.uk/.

Mittelbrunn, M. & Sánchez-Madrid, F., 2012. Intercellular communication: diverse structures for exchange of genetic information. *Nature Reviews Molecular Cell Biology*, 13(5), pp.328–335. Available at: http://dx.doi.org/10.1038/nrm3335.

Momen-Heravi, F. et al., 2015. Exosomes derived from alcohol-treated hepatocytes horizontally transfer liver specific miRNA-122 and sensitize monocytes to LPS. *Scientific Reports*, 5(1), p.9991. Available at: http://www.nature.com/articles/srep09991.

Montecalvo, A. et al., 2012. Mechanism of transfer of functional microRNAs between mouse dendritic cells via exosomes. *Blood*, 119(3), pp.756–766.

Montgomery, M.K. & Turner, N., 2014. Mitochondrial dysfunction and insulin resistance: an update. *Endocrine Connections*, 4(1), pp.R1–R15. Available at: http://www.endocrineconnections.com/cgi/doi/10.1530/EC-14-0092.

Moreira, R.K., 2007. Hepatic Stellate Cells and Liver Fibrosis. *Arch Pathol Lab Med*, 131(11), pp.1728–1734.

Moreno-Gonzalo, O., Villarroya-Beltri, C. & Sánchez-Madrid, F., 2014. Post-translational modifications of exosomal proteins. *Frontiers in immunology*, 5(383), pp.1–7. Available at:

http://www.pubmedcentral.nih.gov/articlerender.fcgi?artid=4128227&tool=pmcentrez&rendertype=abstract.

Moreno-Navarrete, Jose Maria and Fernandez-Real, J.M., 2012. Adipose tissue biology. In *Adipose Diferentiation*. pp. 17–38.

Morioka, H., Tennyson, G.E. & Nikodem, V.M., 1988. Structural and functional analysis of the rat malic enzyme gene promoter. *Mol Cell Biol*, 8(8), pp.3542–3545. Available at: http://www.ncbi.nlm.nih.gov/entrez/query.fcgi?cmd=Retrieve&db=PubMed&dopt=Citation&list_uids=3211151.

Morris, K.L., Namey, T.C. & Zemel, M.B., 2003. Effects of dietary carbohydrate on the development of obesity in heterozygous Zucker rats. *The Journal of Nutritional Biochemistry*, 14(1), pp.32–39. Available at: http://www.sciencedirect.com/science/article/pii/S0955286302002498.

Morrison, M.C. & Kleemann, R., 2015. Role of Macrophage Migration Inhibitory Factor in Obesity, Insulin Resistance, Type 2 Diabetes, and Associated Hepatic Co-Morbidities: A Comprehensive Review of Human and Rodent Studies. *Frontiers in immunology*, 6(308), pp.1–13. Available at: http://www.pubmedcentral.nih.gov/articlerender.fcgi?artid=4467247&tool=pmcentrez&rendertype=abstract.

Mulcahy, L.A., Pink, R.C. & Carter, D.R.F., 2014. Routes and mechanisms of extracellular vesicle uptake. *Journal of extracellular vesicles*, 3(8), pp.1–14. Available at: http://www.pubmedcentral.nih.gov/articlerender.fcgi?artid=4122821&tool=pmcentrez&rendertype=abstract%5Cnhttp://www.ncbi.nlm.nih.gov/pubmed/25143819%5Cnhttp://www.pubmedcentral.nih.gov/articlerender.fcgi?artid=PMC4122821.

Müller, G., 2012. Novel tools for the study of cell type-specific exosomes and microvesicles. *Journal of Bioanalysis and Biomedicine*, 4(4), pp.46–60.

Munich, S. et al., 2012. Dendritic cell exosomes directly kill tumor cells and activate natural killer cells via TNF superfamily ligands. *OncoImmunology*, 1(7), pp.1074–1083. Available at: http://www.tandfonline.com/doi/abs/10.4161/onci.20897.

Myers, M.G. et al., 1992. IRS-1 activates phosphatidylinositol 3'-kinase by associating with src homology 2 domains of p85. *Proceedings of the National Academy of Sciences of the United States of America*, 89(21), pp.10350–10354.

Na, G.H. et al., 2014. Effects of glucose concentration in the medium on rat hepatocyte culture. *Ann Surg Treat Res*, 87(2), pp.53–60. Available at: http://www.pubmedcentral.nih.gov/articlerender.fcgi?artid=4127907&tool=pmcentrez&rendertype=abstract.

Nabi, I.R. & Le, P.U., 2003. Caveolae/raft-dependent endocytosis. *Journal of Cell Biology*, 161(4), pp.673–677.

Nangami, G. et al., 2014. Fetuin-A associates with histones intracellularly and shuttles them to exosomes to promote focal adhesion assembly resulting in rapid adhesion and spreading in breast carcinoma cells. *Experimental Cell Research*, 328(2), pp.388–400.

Nicholls, D.G. et al., 2010. Bioenergetic profile experiment using C2C12 myoblast cells. *Journal of visualized experiments*, 6(46), pp.3–7. Available at: http://www.pubmedcentral.nih.gov/articlerender.fcgi?artid=3159644&tool=pmcentrez&rendertype=abstract.

van Niel, G. et al., 2015. Apolipoprotein E Regulates Amyloid Formation within Endosomes of Pigment Cells. *Cell Reports*, 13(1), pp.43–51.

Nojima, H. et al., 2016. Hepatocyte exosomes mediate liver repair and regeneration via sphingosine-1-phosphate. *Journal of Hepatology*, 64(1), pp.60–68. Available at: http://dx.doi.org/10.1016/j.jhep.2015.07.030.

Nomura, S. et al., 2000. Significance of chemokines and activated platelets in patients with diabetes. *Clin Exp Immunol*, 121(3), pp.437–443. Available at: http://www.ncbi.nlm.nih.gov/pubmed/10971508.

Nose, F. et al., 2013. Crucial Role of Perilipin-3 (TIP47) in Formation of Lipid Droplets and PGE 2 Production in HL-60-Derived Neutrophils. *PLoS ONE*, 8(8), pp.1–6.

Ntambi, M.J. & Kim, Y.-C., 2000. Adipocyte Differentiation and Gene Expression. *J. Nutr*, 130(12), p.3122S–3126S.

O'Hara, A. et al., 2009. Microarray analysis identifies matrix metalloproteinases (MMPs) as key genes whose expression is up-regulated in human adipocytes by macrophage-conditioned medium. *Pflugers Archiv European Journal of Physiology*, 458(6), pp.1103–1114.

O'Neill, S. et al., 2016. Blood-Based Biomarkers for Metabolic Syndrome. *Trends in Endocrinology and Metabolism*, 27(6), pp.363–374. Available at: http://dx.doi.org/10.1016/j.tem.2016.03.012.

O'Neill, S. & O'Driscoll, L., 2015. Metabolic syndrome: A closer look at the growing epidemic and its associated pathologies. *Obesity Reviews*, 16(1), pp.1–12.

Okamoto, Y., Tanaka, S. & Haga, Y., 2002. Enhanced GLUT2 gene expression in an oleic acid-induced in vitro fatty liver model. *Hepatology Research*, 23(2), pp.138–144.

Oshino, N., Imai, Y. & Sato, R., 1971. A function of cytochrome b5 in fatty acid desaturation by rat liver microsomes. *Journal of biochemistry*, 69(1), pp.155–167. Available at: http://www.ncbi.nlm.nih.gov/pubmed/5543646.

Öst, A. et al., 2010. Attenuated mTOR Signaling and Enhanced Autophagy in Adipocytes from Obese Patients with Type 2 Diabetes Anita. *Molecular Medicine*, 16(7–8), p.1. Available at: http://www.molmed.org/content/pdfstore/10_23_Ost.pdf.

Pan, B.-T. et al., 1985. Electron Microscopic Evidence for Externalization of the Transferrin Receptor in Vesicular Form in Sheep Reticulocytes. *The Journal of Cell Biology*, 101(1), pp.942–948.

Pan, B.T. & Johnstone, R.M., 1983. Fate of the transferrin receptor during maturation of sheep reticulocytes in vitro: Selective externalization of the receptor. *Cell*, 33(3), pp.967–978.

Paolo, S. Di et al., 2006. Chronic Inhibition of Mammalian Target of Rapamycin Signaling Downregulates Insulin Receptor Substrates 1 and 2 and AKT Activation: A Crossroad between Cancer and Diabetes? *Journal of the American Society of Nephrology*, 17(8), pp.2236–2244. Available at: http://www.jasn.org/cgi/doi/10.1681/ASN.2006030196.

Parolini, I. et al., 2009. Microenvironmental pH is a key factor for exosome traffic in tumor cells. *Journal of Biological Chemistry*, 284(49), pp.34211–34222.

Peinado, H. et al., 2012. Melanoma exosomes educate bone marrow progenitor cells toward a pro-metastatic phenotype through MET. *Nature medicine*, 18(6), pp.883–91. Available at: http://www.nature.com.sire.ub.edu/nm/journal/v18/n6/full/nm.2753.html.

Pelletier, M. et al., 2014. Extracellular flux analysis to monitor glycolytic rates and mitochondrial oxygen consumption. *Methods in Enzymology*, 542(1), pp.125–149. Available at: http://dx.doi.org/10.1016/B978-0-12-416618-9.00007-8.

Phillips, M.S. et al., 1996. Leptin receptor missense mutation in the fatty Zucker rat. *Nature Genetics*, 13(1), pp.18–19. Available at: http://www.ncbi.nlm.nih.gov/pubmed/8673096.

van der Pol, E. et al., 2016. Recent developments in the nomenclature, presence, isolation, detection and clinical impact of extracellular vesicles. *Journal of Thrombosis and Haemostasis*, 14(1), pp.48–56.

Polyzos, S. a et al., 2010. The role of adiponectin in the pathogenesis and treatment of non-alcoholic fatty liver disease. *Diabetes, obesity & metabolism*, 12(5), pp.365–383.

Porquet, D. et al., 1984. LIPOGENESIS FROM U;4C LACTATE IN OBESE ZUCKER RAT HEPATOCYTES. EFFECT OF ALBUMIN-BOUND OLEATE. *Life Sciences*, 35(7), pp.1213–1219.

Postic, C. & Girard, J., 2008. Contribution of de novo fatty acid synthesis to hepatic steatosis and insulin resistance: Lessons from genetically engineered mice. *Journal of Clinical Investigation*, 118(3), pp.829–838.

Povero, D. et al., 2014. Circulating extracellular vesicles with specific proteome and liver microRNAs are potential biomarkers for liver injury in experimental fatty liver disease. *PLoS ONE*, 9(12), pp.1–28.

Povero, D. et al., 2015. Lipid-Induced Hepatocyte-Derived Extracellular Vesicles Regulate Hepatic Stellate Cells via MicroRNA Targeting Peroxisome Proliferator-Activated Receptor-gamma. *CMGH Cellular and Molecular Gastroenterology and Hepatology*, 1(6), pp.646–663. Available at: http://dx.doi.org/10.1016/j.jcmgh.2015.07.007.

Povero, D. et al., 2013. Lipid-induced toxicity stimulates hepatocytes to release angiogenic

microparticles that require vanin-1 for uptake by endothelial cells. *Science Signaling*, 6(296), pp.1–15.

Povero, D. et al., 2008. Lipid-induced toxicity stimulates hepatocytes to release angiogenic microparticles that require Vanin-1 for uptake by endothelial cells. *Computer*, 144(5), pp.724–732.

Prasad, M. et al., 2017. Mitochondrial metabolic regulation by GRP78. *Science Advances*, 3(2), pp.1–11.

Putz, U. et al., 2012. The Tumor Suppressor PTEN Is Exported in Exosomes and Has Phosphatase Activity in Recipient Cells. *Cell Biology*, 5(243), pp.1–11.

Quesenberry, P.J. et al., 2015. Potential functional applications of extracellular vesicles: a report by the NIH Common Fund Extracellular RNA Communication Consortium. *Journal of extracellular vesicles*, 4(27575), pp.1–11. Available at: http://www.ncbi.nlm.nih.gov/pubmed/26320942%5Cnhttp://www.pubmedcentral.nih.gov/articlerender.fcgi?artid=PMC4553260.

Qureshi, K. & Abrams, G., 2007. Metabolic liver disease of obesity and role of adipose tissue in the pathogenesis of nonalcoholic fatty liver disease. *World Journal of Gastroenterology*, 13(26), pp.3540–53.

Raiborg, C. & Stenmark, H., 2009. The ESCRT machinery in endosomal sorting of ubiquitylated membrane proteins. *Nature*, 458(7237), pp.445–52. Available at: http://www.ncbi.nlm.nih.gov/pubmed/19325624.

Ramzan, R. et al., 2013. GAPDH: the missing link between glycolysis and mitochondrial oxidative phosphorylation? *Biochemical Society transactions*, 41(5), pp.1294–7. Available at: http://www.ncbi.nlm.nih.gov/pubmed/24059522.

Raposo, G. et al., 1996. B lymphocytes secrete antigen-presenting vesicles. *The Journal of experimental medicine*, 183(3), pp.1161–72. Available at: http://www.pubmedcentral.nih.gov/articlerender.fcgi?artid=2192324&tool=pmcentrez&rendertype=abstract.

Raposo, G. & Stoorvogel, W., 2013. Extracellular vesicles: Exosomes, microvesicles, and

friends. *Journal of Cell Biology*, 200(4), pp.373–383.

Raschke, W.C. et al., 1978. Functional Macrophage Cell Lines Transformed by Abelson Leukemia Virus. *Cell*, (September).

Rask-Madsen, C. & Kahn, C.R., 2012. Tissue-specific insulin signaling, metabolic syndrome, and cardiovascular disease. *Arteriosclerosis, Thrombosis, and Vascular Biology*, 32(9), pp.2052–2059.

Ratajczak, J. et al., 2006. Membrane-derived microvesicles: important and underappreciated mediators of cell-to-cell communication. *Leukemia : official journal of the Leukemia Society of America, Leukemia Research Fund, U.K*, 20(9), pp.1487–95. Available at: http://www.ncbi.nlm.nih.gov/pubmed/16791265.

Raxworthy, M.J., Gulliver, P.A. & Hughes, P.J., 1982. The cellular location of catechol-O-methyltransferase in rat liver. *Naunyn-Schmiedeberg's Archives of Pharmacology*, 320(2), pp.182–188.

Reaven, G.M., 1991. Relationship between insulin resistance and hypertension. *Diabetes care*, 14(4), pp.33–38.

Reaven, G.M., 1988. Role of Insulin Resistance in Human Disease Is Insulin Resistance Becoming a Global Epidemic ? *Diabetes*, 37(1595), pp.64–66.

Record, M. et al., 2014. Exosomes as new vesicular lipid transporters involved in cell-cell communication and various pathophysiologies. *Biochimica et Biophysica Acta - Molecular and Cell Biology of Lipids*, 1841(1), pp.108–120. Available at: http://dx.doi.org/10.1016/j.bbalip.2013.10.004.

Regazzetti, C. et al., 2009. Hypoxia Decreases Insulin Signaling Pathways in. *Diabetes*, 58(1), pp.95–103.

Reichert, M. & Eick, D., 1999. Analysis of cell cycle arrest in adipocyte differentiation. *Oncogene*, 18(2), pp.459–466.

Reis, J. et al., 2011. LPS-induced formation of immunoproteasomes: TNF-α and nitric oxide production are regulated by altered composition of proteasome-active sites. *Cell*

biochemistry and biophysics, 60(1–2), pp.77–88. Available at: http://www.ncbi.nlm.nih.gov/pubmed/21455682 [Accessed February 4, 2017].

Di Rocco, G., Baldari, S. & Toietta, G., 2016. Towards Therapeutic Delivery of Extracellular Vesicles: Strategies for In Vivo Tracking and Biodistribution Analysis. *Stem Cells International*, 2016(5029619), pp.1–12. Available at: https://www.hindawi.com/journals/sci/2016/5029619/.

Rong, L. et al., 2016. Immunosuppression of breast cancer cells mediated by transforming growth factor-B in exosomes from cancer cells. *Oncology Letters*, 11(1), pp.500–504.

Rosen, E.D. et al., 2000. Transcriptional regulation of adipogenesis Transcriptional regulation of adipogenesis. *Genes & Development*, 14(11), pp.1293–1307.

Rotter, V., Nagaev, I. & Smith, U., 2003. Interleukin-6 (IL-6) Induces Insulin Resistance in 3T3-L1 Adipocytes and Is, Like IL-8 and Tumor Necrosis Factor-α, Overexpressed in Human Fat Cells from Insulin-resistant Subjects. *Journal of Biological Chemistry*, 278(46), pp.45777–45784.

Royo, F. et al., 2016. Metabolically active extracellular vesicles released from hepatocytes under drug-induced liver-damaging conditions modify serum metabolome and might affect different pathophysiological processes.

Royo, F. et al., 2013. Transcriptome of Extracellular Vesicles Released by Hepatocytes. *PLoS ONE*, 8(7), pp.1–11.

Royo, F. & Falcon-Perez, J.M., 2012. Liver extracellular vesicles in health and disease. *Journal of extracellular vesicles*, 1(September), pp.1–7. Available at: http://www.ncbi.nlm.nih.gov/pubmed/24009882%5Cnhttp://www.pubmedcentral.nih.gov/articlerender.fcgi?artid=PMC3760641.

Rutkowski, J.M., Stern, J.H. & Scherer, P.E., 2015. The cell biology of fat expansion. *Journal of Cell Biology*, 208(5), pp.501–512.

Rutledge, H.R. et al., 2012. Gene expression profiles of RAW264.7 macrophages stimulated with preparations of LPS differing in isolation and purity. *Innate immunity*, 18(1), pp.80–8. Available at: http://www.ncbi.nlm.nih.gov/pubmed/21239457.

Sacks, F. et al., 2001. DASH - Sodium Collaborative Research Group. Effects on blood pressure of reduced dietary sodium and the Dietary approaches to stop Hypertension (DASH)diet. *N Engl J Med*, 344(1), pp.3–10.

Sagar, G. et al., 2015. Pathogenesis of pancreatic cancer exosome-induced lipolysis in adipose tissue. *Gut*, 65(7), pp.1–10. Available at: http://gut.bmj.com/cgi/doi/10.1136/gutjnl-2014-308350.

Salans, L.B., Cushman, S.W. & Weismann, R.E., 1973. Studies of human adipose tissue. Adipose cell size and number in nonobese and obese patients. *The Journal of clinical investigation*, 52(4), pp.929–941.

Sano, S. et al., 2014. Lipid synthesis is promoted by hypoxic adipocyte-derived exosomes in 3T3-L1 cells. *Biochemical and Biophysical Research Communications*, 445(2), pp.327–333. Available at: http://dx.doi.org/10.1016/j.bbrc.2014.01.183.

Sarbassov, D.D. et al., 2005. Phosphorylation and regulation of Akt/PKB by the rictor-mTOR complex. *Science (New York, N.Y.)*, 307(5712), pp.1098–1101.

Sarjeant, K. & Stephens, J.M., 2012. Adipogenesis. *Cold Spring Harbor perspectives in biology*, 4(9), pp.1–20.

Sarkar, A. et al., 2009. Monocyte derived microvesicles deliver a cell death message via encapsulated caspase-1. *PLoS ONE*, 4(9), pp.1–9.

Schinner, S. et al., 2005. Molecular mechanisms of insulin resistance. *Diabetic medicine : a journal of the British Diabetic Association*, 22(6), pp.674–682.

Schmidt, A., Forne, I. & Imhof, A., 2014. Bioinformatic analysis of proteomics data. *BMC systems biology*, 8(Suppl 2), pp.1–7. Available at: http://www.biomedcentral.com/1752-0509/8/S2/S3.

Schöttl, T. et al., 2015. Limited OXPHOS capacity in white adipocytes is a hallmark of obesity in laboratory mice irrespective of the glucose tolerance status. *Molecular Metabolism*, 4(9), pp.631–642. Available at: http://dx.doi.org/10.1016/j.molmet.2015.07.001.

Shen, J. et al., 2016. The role of exosomes in hepatitis, liver cirrhosis and hepatocellular carcinoma. *Journal of Cellular and Molecular Medicine*, 21(5), pp.986–992. Available at: http://doi.wiley.com/10.1111/jcmm.12950.

Sheng, X. et al., 2014. Adipocyte differentiation is affected by media height above the cell layer. *International Journal of Obesity*, 38(2), pp.315–320. Available at: http://www.nature.com/doifinder/10.1038/ijo.2013.96.

Simons, M. & Raposo, G., 2009. Exosomes--vesicular carriers for intercellular communication. *Current opinion in cell biology*, 21, pp.575–581.

Simpson, R.J. et al., 2009. Exosomes: proteomic insights and diagnostic potential. *Expert review of proteomics*, 6(3), pp.267–283.

Simpson, R.J., Jensen, S.S. & Lim, J.W.E., 2008. Proteomic profiling of exosomes: Current perspectives. *Proteomics*, 8(19), pp.4083–4099.

Skolnik, E.Y. et al., 1993. The SH2/SH3 domain-containing protein GRB2 interacts with tyrosine-phosphorylated IRS1 and Shc: implications for insulin control of ras signalling. *The EMBO journal*, 12(5), pp.1929–36. Available at: http://www.pubmedcentral.nih.gov/articlerender.fcgi?artid=413414&tool=pmcentrez&rendertype=abstract.

Skurk, T. et al., 2009. Expression and secretion of RANTES (CCL5) in human adipocytes in response to immunological stimuli and hypoxia. *Horm Metab Res.*, 41(3), pp.183–189.

Soromou, L.W. et al., 2012. Regulation of inflammatory cytokines in lipopolysaccharide-stimulated RAW 264.7 murine macrophage by 7-O-methyl-naringenin. *Molecules*, 17(3), pp.3574–3585.

Steppan, C.M., Lazar, M.A. & Lazar, M.A., 2002. Resistin and obesity-associated insulin resistance. *Trends in Endocrinology & Metabolism*, 13(1), pp.18–23.

Stöckli, J., Fazakerley, D.J. & James, D.E., 2011. GLUT4 exocytosis. *Journal of cell science*, 124(24), pp.4147–4159. Available at: http://jcs.biologists.org/content/124/24/4147.abstract.

Sun, D. et al., 2009. A Novel Nanoparticle Drug Delivery System : The Anti-inflammatory Activity of Curcumin Is Enhanced When Encapsulated in Exosomes. *Molecular Therapy*, 18(9), pp.1606–1614. Available at: http://dx.doi.org/10.1038/mt.2010.105.

Sun, F.-C. et al., 2006. Localization of GRP78 to mitochondria under the unfolded protein response. *The Biochemical journal*, 396(1), pp.31–39.

Sun, L. et al., 2003. Adipogenic differentiating agents regulate expression of fatty acid binding protein and CD36 in the J744 macrophage cell line. *ASBMB*, 44(10), pp.1877–1886.

Symonds, M.E., 2012. Adipose tissue biology. *Adipose Tissue Biology*, pp.1–413.

Syn, N. et al., 2016. Exosome-Mediated Metastasis: From Epithelial-Mesenchymal Transition to Escape from Immunosurveillance. *Trends in Pharmacological Sciences*, 37(7), pp.606–617. Available at: http://dx.doi.org/10.1016/j.tips.2016.04.006.

Tang, Q.-Q., Otto, T.C. & Lane, M.D., 2003. CCAAT/enhancer-binding protein beta is required for mitotic clonal expansion during adipogenesis. *Proceedings of the National Academy of Sciences of the United States of America*, 100(3), pp.850–855.

Taylor, D.D. & Shah, S., 2015. Methods of isolating extracellular vesicles impact down-stream analyses of their cargoes. *Methods*, 87(3), pp.3–10. Available at: http://dx.doi.org/10.1016/j.ymeth.2015.02.019.

Teodoro, J. et al., 2006. Decreased ANT content in Zucker fatty rats: Relevance for altered hepatic mitochondrial bioenergetics in steatosis. *FEBS Letters*, 580(8), pp.2153–2157.

Teslaa, T. & Teitell, M.A., 2014. Techniques to monitor glycolysis. *Methods in Enzymology*, 542(12), pp.91–114.

Tetta, C. et al., 2013. Extracellular vesicles as an emerging mechanism of cell-to-cell communication. *Endocrine*, 44(1), pp.11–19.

Thery, C. et al., 2001. Proteomic analysis of dendritic cell-derived exosomes: A secreted subcellular compartment distinct from apoptotic vesicles. *The Journal of Immunology*, 166(12), pp.7309–7318.

Théry, C., Duban, L., et al., 2002. Indirect activation of naïve CD4+ T cells by dendritic cell-derived exosomes. *Nature immunology*, 3(12), pp.1156–1162.

Théry, C. et al., 2006. Isolation and Characterization of Exosomes from Cell Culture Supernatants. *Current protocols in cell biology*, Chapter 3, pp.1–29. Available at: http://www.ncbi.nlm.nih.gov/pubmed/18228490.

Théry, C., Zitvogel, L. & Amigorena, S., 2002. Exosomes: composition, biogenesis and function. *Nature reviews. Immunology*, 2(8), pp.569–579.

Thomou, T. et al., 2017. Adipose-derived circulating miRNAs regulate gene expression in other tissues. *Nature*, 542(7642), pp.450–455. Available at: http://www.nature.com/doifinder/10.1038/nature21365.

Tong, Q. et al., 2005. Interaction between GATA and the C / EBP Family of Transcription Factors Is Critical in GATA-Mediated Suppression of Adipocyte Differentiation Interaction between GATA and the C / EBP Family of Transcription Factors Is Critical in GATA-Mediated Suppressio. *Molecular and cellular biology*, 25(2), pp.706–715.

Trajkovic, K. et al., 2008. Ceramide triggers budding of exosome vesicles into multivesicular endosomes. *Science (New York, N.Y.)*, 319(5867), pp.1244–1247.

Trams, E.G. et al., 1981. Exfoliation of membrane ecto-enzymes in the form of micro-vesicles. *BBA - Biomembranes*, 645(1), pp.63–70.

Trayhurn, P., Wang, B. & Wood, I.S., 2008. Hypoxia in adipose tissue: a basis for the dysregulation of tissue function in obesity? *The British journal of nutrition*, 100(2), pp.227–235.

Tsai, S. et al., 2016. Increased 4E-BP1 expression protects against diet-induced obesity and insulin resistance in male mice. *Cell Reports*, 16(7), pp.1903–1914.

Tutar, L. & Tutar, Y., 2010. Heat Shock Proteins: An Overview. *Current Pharmaceutical Biotechnology*, 11(2), pp.216–222. Available at: http://www.eurekaselect.com/openurl/content.php?genre=article&issn=1389-2010&volume=11&issue=2&spage=216.

Vadas, O. et al., 2011. Structural basis for activation and inhibition of class I phosphoinositide 3-kinases. *Sci Signal*, 4(195), pp.1–13. Available at: http://stke.sciencemag.org/content/4/195/re2.long.

Vajta, G. et al., 1986. Fatty degeneration in cultured hepatocytes - A new experimental model. *Virchows Archiv B Cell Pathology Including Molecular Pathology*, 52(1), pp.177–184.

Valadi, H. Ekstrom, K. Bossios, A. et al., 2007. Exosome-mediated transfer of mRNAs and microRNAs is a novel mechanism of genetic exchange between cells. *Nature cell biology*, 9(6), pp.654–659.

Vazirani, P.R. et al., 2016. Disruption of Adipose Rab10-Dependent Insulin Signaling Causes Hepatic Insulin Resistance. *Diabetes*, 65(6), pp.1–35.

Verma, M. et al., 2015. Extracellular vesicles: potential applications in cancer diagnosis, prognosis, and epidemiology. *BMC clinical pathology*, 15(6), pp.1–9. Available at: http://www.scopus.com/inward/record.url?eid=2-s2.0-84927943823&partnerID=tZOtx3y1.

Vetelainen, R., van Vliet, A.K. & van Gulik, T.M., 2007. Severe Steatosis Increases Hepatocellular Injury and Impairs Liver Regeneration in a Rat Model of Partial Hepatectomy. *Annals of Surgery*, 245(1), pp.44–50.

Viaud, S. et al., 2010. Dendritic cell-derived exosomes for cancer immunotherapy: What's next? *Cancer Research*, 70(4), pp.1281–1285.

Villarroya-Beltri, C. et al., 2016. ISGylation controls exosome secretion by promoting lysosomal degradation of MVB proteins. *Nature Communications*, 7(13588), pp.1–5. Available at: http://www.nature.com/doifinder/10.1038/ncomms13588.

Wang, G. et al., 2006. Cyclin D3 maintains growth-inhibitory activity of C/EBPalpha by stabilizing C/EBPalpha-cdk2 and C/EBPalpha-Brm complexes. *Molecular and cellular biology*, 26(7), pp.2570–2582.

Wang, J. et al., 2015. Activation of Rab8 guanine nucleotide exchange factor Rabin8 by ERK1/2 in response to EGF signaling. *Proceedings of the National Academy of Sciences*, 112(1), pp.148–153. Available at:

http://www.pnas.org/lookup/doi/10.1073/pnas.1412089112.

Watson, R.T., Kanzaki, M. & Pessin, J.E., 2004. Regulated membrane trafficking of the insulin-responsive glucose transporter 4 in adipocytes. *Endocrine Reviews*, 25(2), pp.177–204.

Weir, G.C. et al., 2001. ??-Cell Adaptation and Decompensation During the Progression of Diabetes. *Diabetes*, 50(SUPPL. 1).

Weisberg, S.P. et al., 2003. Obesity is associated with macrophage accumulation in adipose tissue. *Journal of Clinical Investigation*, 112(12), pp.1796–1808.

Williams, I.H. & Polakis, S.E., 1977. Biochamical and Biophysical Research Communications. *BBRC*, 77(1), pp.175–186.

Willms, E. et al., 2016. Cells release subpopulations of exosomes with distinct molecular and biological properties. *Scientific reports*, 6(22519), pp.1–12. Available at: http://www.pubmedcentral.nih.gov/articlerender.fcgi?artid=4773763&tool=pmcentrez&rendertype=abstract.

Wilson, P.W.F. & Grundy, S.M., 2003. The Metabolic Syndrome: Practical Guide to Origins and Treatment: Part I. *Circulation*, 108(12), pp.1422–1424. Available at: http://circ.ahajournals.org/cgi/doi/10.1161/01.CIR.0000089505.34741.E5.

Wisniewski, J.R. et al., 2009. Universal sample preparation method for proteome analysis. *Nature Meth.*, 6(5), pp.359–362. Available at: http://www.ncbi.nlm.nih.gov/pubmed/19377485.

Witek, R.P. et al., 2009. Liver Cell-Derived Microparticles Activate Hedgehog Signaling and Alter Gene Expression in Hepatic Endothelial Cells. *Gastroenterology*, 136(1), p.320–330.e2. Available at: http://dx.doi.org/10.1053/j.gastro.2008.09.066.

Witwer, K.W. et al., 2013. Standardization of sample collection, isolation and analysis methods in extracellular vesicle research. *Journal of extracellular vesicles*, 2(20360), pp.1–25.

Wolf, P., 1967. The nature and significance of platelet products in human plasma. *British journal of haematology*, 13(3), pp.269–288.

Wu, J.C., Merlino, G. & Fausto, N., 1994. Establishment and characterization of differentiated, nontransformed hepatocyte cell lines derived from mice transgenic for transforming growth factor alpha. *Proceedings of the National Academy of Sciences of the United States of America*, 91(2), pp.674–678.

Xinxu, Y. et al., 2016. Generating Hypertrophic Adiocytes deom 3t3 L1 cell Line and Characterizing the Phenotypic Transition. *The FASEB Journal*, 30(1 Supplement), pp.1–6.

Xu, X. et al., 2013. Obesity activates a program of lysosomal-dependent lipid metabolism in adipose tissue macrophages independently of classic activation. *Cell Metabolism*, 18(6), pp.816–830. Available at: http://dx.doi.org/10.1016/j.cmet.2013.11.001.

Yahagi, N. et al., 2002. Absence of sterol regulatory element-binding protein-1 (SREBP-1) ameliorates fatty livers but not obesity or insulin resistance in Lepob/Lepob mice. *Journal of Biological Chemistry*, 277(22), pp.19353–19357.

Yamamoto, H. et al., 2002. Reduced IRS-2 and GLUT4 expression in PPAR γ 2- induced adipocytes derived from C / EBP β and C / EBP δ - deficient mouse embryonic fibroblasts. *Journal of cell science*, 115(18), pp.3601–3607.

Yan, D. et al., 2015. Establishment of a hepatocyte steatosis model using Chang liver cells. *Genetics and Molecular Research*, 14(4), pp.15224–15232.

Yan, Q. et al., 2007. The Adipokine Lipocalin 2 Is Regulated by Obesity and Promotes Insulin Resistance. *Diabetes*, 56(October), pp.2533–40.

Yáñez-Mó, M. et al., 2015. Biological properties of extracellular vesicles and their physiological functions. *Journal of extracellular vesicles*, 4(27066), pp.1–60.

Yang, Z. & Ming, X.F., 2012. mTOR signalling: The molecular interface connecting metabolic stress, aging and cardiovascular diseases. *Obesity Reviews*, 13(SUPPL.2), pp.58–68.

Ye, J. et al., 2012. Primer-BLAST : A tool to design target-specific primers for polymerase chain reaction. *BMC Bioinformatics*, 13(134), pp.2–11.

Yeung, Y.-G. & Stanley, E.R., 2010. Rapid detergent Removal From Peptide Samples With Ethyl Acetate from MassSpectrometry Analysis. *Curr Protoc Protein Sci.*, 16(12), pp.1–6.

Yoon, S.-O., Shin, S. & Mercurio, A.M., 2005. Hypoxia Stimulates Carcinoma Invasion by Stabilizing Microtubules and Promoting the Rab11 Trafficking of the A6B4 Integrin. *Cancer Res*, 65(7), pp.2761–9.

Zebisch, K. et al., 2012. Protocol for effective differentiation of 3T3-L1 cells to adipocytes. *Analytical Biochemistry*, 425(1), pp.88–90. Available at: http://dx.doi.org/10.1016/j.ab.2012.03.005.

Zerial, M. & McBride, H., 2001. Rab proteins as membrane organizers. *Nature reviews. Molecular cell biology*, 2(2), pp.107–117.

Zhang, H.-G. et al., 2006. A Membrane Form of TNF- Presented by Exosomes Delays T Cell Activation-Induced Cell Death. *The Journal of Immunology*, 176(12), pp.7385–7393.

Zhang, Y. et al., 2015. Inflamed macrophage microvesicles induce insulin resistance in human adipocytes. *Nutrition & metabolism*, 12, p.21.

Zhang, Y. et al., 2011. Insulin-regulated Srebp-1c and Pck1 mRNA expression in primary hepatocytes from zucker fatty but not lean rats is affected by feeding conditions. *PLoS ONE*, 6(6), pp.1–8.

Zhang, Y. et al., 1994. Positional cloning of the mouse obese gene and its human homologue. *Nature*, 372(12), pp.425–432.

Zhang, Y., Yu, M. & Tian, W., 2016. Physiological and pathological impact of exosomes of adipose tissue. *Cell Proliferation*, 49(1), pp.3–13.

Zheng, J., 2012. Energy metabolism of cancer: Glycolysis versus oxidative phosphorylation (review). *Oncology Letters*, 4(6), pp.1151–1157.

Zitvogel, L. et al., 1998. Eradication of established murine tumors using a novel cell-free vaccine: dendritic cell-derived exosomes. *Nature Medicine*, 4(5), pp.594–600.

Zucker, L.M. & Zucker, T.F., 1961. Fatty, a new mutation in the rat. *Journal of Heredity*, 52(6), pp.275–278.

10. Supplementary information

Table 16 Down-regulated DEPs in ZF-EVs.

Description	Mapped ID	Peptide count	Unique peptide	ANOVA (pvalue)	Fold change
Lysosome-associated membrane glycoprotein 1	LAMP1_RAT	2	2	0.00216	**21.1**
4F2 cell-surface antigen heavy chain	4F2_RAT	2	2	0.000332	**8.2**
Solute carrier organic anion transporter family member 1A4	SO1A4_RAT	6	5	0.000751	**7.8**
Serum albumin	ALBU_RAT	10	9	0.004688	**6.7**
Glutamate dehydrogenase 1, mitochondrial	DHE3_RAT	17	16	0.000455	**6.1**
Membrane-associated progesterone receptor component 1	PGRC1_RAT	7	7	0.000282	**5.9**
Integrin beta-1	ITB1_RAT	2	2	0.009592	**5.8**
CD81 antigen	CD81_RAT	4	4	0.010499	**5.8**
Cytochrome P450 2C11	CP2CB_RAT	9	7	0.000135	**5.7**
Mannose-binding protein C	MBL2_RAT	3	3	0.001403	**4.6**
Basigin	BASI_RAT	4	4	0.000395	**4.5**
Propionyl-CoA carboxylase beta chain, mitochondrial	PCCB_RAT	3	3	0.010487	**4.5**
UDP-glucuronosyltransferase 2B15	UDB15_RAT	2	1	0.003722	**4.5**
Retinol dehydrogenase 7	RDH7_RAT	14	7	0.000666	**4.4**
Alpha-1-macroglobulin	A1M_RAT	13	13	0.011078	**4.2**
Aldehyde dehydrogenase, mitochondrial	ALDH2_RAT	12	10	0.00631	**4.1**
Cytochrome P450 2D4	CP2D4_RAT	7	1	0.000996	**4.0**
Cytochrome b5	CYB5_RAT	4	4	0.003195	**3.9**
Monocarboxylate transporter 1	MOT1_RAT	2	2	0.000853	**3.9**
UDP-	UDB17_RAT	5	4	0.000309	**3.7**

glucuronosyltransferase 2B17					
Isocitrate dehydrogenase [NADP], mitochondrial	IDHP_RAT	5	4	0.009461	**3.7**
Epoxide hydrolase 1	HYEP_RAT	15	14	0.005863	**3.7**
Peroxisomal acyl-coenzyme A oxidase 2	ACOX2_RAT	6	4	0.032224	**3.6**
Retinol dehydrogenase 2	RDH2_RAT	10	3	0.000416	**3.6**
Ubiquitin-40S ribosomal protein S27a	RS27A_RAT	2	2	0.000894	**3.6**
Pyruvate carboxylase, mitochondrial	PYC_RAT	10	10	0.001833	**3.5**
Cytochrome P450 2D26	CP2DQ_RAT	21	14	0.001033	**3.5**
Syndecan-4	SDC4_RAT	3	3	0.000117	**3.4**
Hydroxymethylglutaryl-CoA lyase, mitochondrial	HMGCL_RAT	4	4	0.001007	**3.4**
Angiopoietin-related protein 4	ANGL4_RAT	6	6	0.003935	**3.4**
Propionyl-CoA carboxylase alpha chain, mitochondrial	PCCA_RAT	6	6	0.001953	**3.4**
Protein disulfide-isomerase A3	PDIA3_RAT	19	19	5.38E-05	**3.4**
Cytochrome P450 2C23	CP2CN_RAT	2	1	0.00802	**3.4**
Sodium/potassium-transporting ATPase subunit alpha-1	AT1A1_RAT	7	7	0.000241	**3.4**
Cytochrome P450 2D1	CP2D1_RAT	14	2	0.000934	**3.3**
Methylcrotonoyl-CoA carboxylase subunit alpha, mitochondrial	MCCA_RAT	3	3	0.012852	**3.3**
Galectin-3-binding protein	LG3BP_RAT	3	3	0.031651	**3.2**
Coronin-1A	COR1A_RAT	3	3	0.024358	**3.2**
Cytochrome P450 2D10	CP2DA_RAT	15	2	0.001969	**3.2**
Selenium-binding protein 1	SBP1_RAT	7	7	0.04765	**3.2**
Eukaryotic translation initiation factor 3 subunit E	EIF3E_RAT	3	3	0.009031	**3.1**
17-beta-hydroxysteroid dehydrogenase type 6	H17B6_RAT	2	1	0.001532	**3.1**
Medium-chain specific acyl-CoA dehydrogenase, mitochondrial	ACADM_RAT	4	4	0.013927	**3.0**
Phenazine biosynthesis-	PBLD_RAT	5	5	0.038428	**2.9**

like domain-containing protein					
Major vault protein	MVP_RAT	18	18	0.002022	**2.9**
Alanine--glyoxylate aminotransferase 2, mitochondrial	AGT2_RAT	2	2	0.009529	**2.9**
Plasminogen	PLMN_RAT	2	2	0.010958	**2.9**
Isovaleryl-CoA dehydrogenase, mitochondrial	IVD_RAT	2	1	0.002316	**2.9**
Solute carrier family 2, facilitated glucose transporter member 2	GTR2_RAT	3	3	0.000316	**2.9**
Aconitate hydratase, mitochondrial	ACON_RAT	10	10	0.036747	**2.8**
Delta-1-pyrroline-5-carboxylate dehydrogenase, mitochondrial	AL4A1_RAT	3	3	0.030486	**2.8**
Catalase	CATA_RAT	19	18	0.000515	**2.7**
Carbamoyl-phosphate synthase [ammonia], mitochondrial	CPSM_RAT	58	56	0.022821	**2.7**
Phosphatidylinositide phosphatase SAC1	SAC1_RAT	2	2	0.002129	**2.7**
Sarcosine dehydrogenase, mitochondrial	SARDH_RAT	11	10	0.029758	**2.65**
3-ketoacyl-CoA thiolase, mitochondrial	THIM_RAT	13	13	0.02138	**2.61**
40S ribosomal protein S25	RS25_RAT	2	2	0.032298	**2.60**
60S ribosomal protein L27a	RL27A_RAT	2	2	0.001893	**2.57**
Sulfotransferase 1C1	ST1C1_RAT	4	4	0.016644	**2.56**
Solute carrier family 22 member 7	S22A7_RAT	2	2	0.012442	**2.55**
Choline dehydrogenase, mitochondrial	CHDH_RAT	8	8	0.038216	**2.55**
D-beta-hydroxybutyrate dehydrogenase, mitochondrial	BDH_RAT	5	4	0.029277	**2.54**
Protein disulfide-isomerase A4	PDIA4_RAT	4	4	0.001487	**2.53**
Microsomal glutathione S-transferase 1	MGST1_RAT	2	2	0.003286	**2.52**

Fibrinogen gamma chain	FIBG_RAT	13	13	0.047215	**2.50**
Clusterin	CLUS_RAT	15	14	0.023728	**2.33**
Succinate dehydrogenase [ubiquinone] flavoprotein subunit, mitochondrial	SDHA_RAT	4	4	0.017234	**2.32**
Hydroxymethylglutaryl-CoA synthase, mitochondrial	HMCS2_RAT	15	13	0.026934	**2.26**
Cytochrome P450 2C7	CP2C7_RAT	5	5	0.034547	**2.26**
Programmed cell death 6-interacting protein	PDC6I_RAT	15	15	0.002796	**2.26**
Secreted phosphoprotein 24	SPP24_RAT	3	3	0.044347	**2.24**
Glycogen [starch] synthase, liver	GYS2_RAT	5	5	0.000323	**2.23**
Electron transfer flavoprotein-ubiquinone oxidoreductase, mitochondrial	ETFD_RAT	6	6	0.020697	**2.22**
NADH dehydrogenase [ubiquinone] 1 alpha subcomplex subunit 10, mitochondrial1	NDUAA_RAT	3	3	0.045338	**2.22**
Serum paraoxonase/arylesterase 1	PON1_RAT	4	4	0.00649	**2.21**
Malate dehydrogenase, mitochondrial	MDHM_RAT	7	7	0.012193	**2.19**
Estrogen sulfotransferase, isoform 1	ST1E1_RAT	11	10	0.007945	**2.19**
Peroxisomal trans-2-enoyl-CoA reductase	PECR_RAT	5	5	0.011374	**2.13**
Methylmalonate-semialdehyde dehydrogenase [acylating], mitochondrial	MMSA_RAT	10	9	0.021764	**2.12**
Tripeptidyl-peptidase 2	TPP2_RAT	10	8	0.000676	**2.12**
60S ribosomal protein L15	RL15_RAT	3	3	0.004057	**2.08**
Transforming protein RhoA	RHOA_RAT	2	2	0.000621	**2.06**
40S ribosomal protein S8	RS8_RAT	5	5	0.006537	**2.06**
26S protease regulatory	PRS7_RAT	9	9	0.018345	**2.06**

subunit 7					
UDP-glucuronosyltransferase 2B21	UD2B2_RAT	3	3	0.016515	**2.04**
Serine/threonine-protein phosphatase PP1-alpha catalytic subunit	PP1A_RAT	2	2	0.003579	**2.03**
Serotransferrin	TRFE_RAT	4	4	0.007944	**2.03**
Guanine nucleotide-binding protein subunit beta-2-like 1	GBLP_RAT	9	8	0.019976	**2.03**
78 kDa glucose-regulated protein	GRP78_RAT	5	3	0.007385	**2.03**
2-hydroxyacyl-CoA lyase 1	HACL1_RAT	2	2	0.006172	**1.99**
Guanine nucleotide-binding protein G(i) subunit alpha-2	GNAI2_RAT	4	4	0.013582	**1.94**
Fatty aldehyde dehydrogenase	AL3A2_RAT	6	5	0.018048	**1.91**
Calreticulin	CALR_RAT	3	3	0.019479	**1.90**
60S ribosomal protein L32	RL32_RAT	2	1	0.034898	**1.88**
60 kDa heat shock protein, mitochondrial	CH60_RAT	6	6	0.005119	**1.88**
Peroxisomal acyl-coenzyme A oxidase 3	ACOX3_RAT	2	2	0.002165	**1.86**
60S ribosomal protein L18	RL18_RAT	4	4	0.018596	**1.85**
Ras-related protein Rap-1b	RAP1B_RAT	3	3	0.00527	**1.78**
Annexin A6	ANXA6_RAT	9	9	0.037249	**1.77**
Pituitary tumor-transforming gene 1 protein-interacting protein	PTTG_RAT	2	2	0.012884	**1.77**
Adenylyl cyclase-associated protein 1	CAP1_RAT	2	2	0.002424	**1.7**
NAD kinase 2, mitochondrial	NAKD2_RAT	5	4	0.040639	**1.7**
Xaa-Pro aminopeptidase 1	XPP1_RAT	4	4	0.023784	**1.7**
Endoplasmin	ENPL_RAT	12	11	0.027676	**1.7**
UDP-glucose 6-dehydrogenase	UGDH_RAT	7	7	0.024328	**1.7**
Cytoplasmic dynein 1	DYHC1_RAT	18	18	0.040524	**1.6**

heavy chain 1					
Methyltransferase-like protein 7B	MET7B_RAT	2	2	0.010377	**1.6**
Heat shock 70 kDa protein 1A	HS71A_RAT	7	5	0.033711	**1.6**
Ras-related protein Rab-1A	RAB1A_RAT	4	2	0.014829	**1.6**
Peroxisomal multifunctional enzyme type 2	DHB4_RAT	8	8	0.020389	**1.6**

Table 17 Up-regulated DEPs in ZF-EVs.

Description	Mapped ID	Peptide count	Unique peptide	ANOVA (pvalue)	Fold change
Glucose-6-phosphate 1-dehydrogenase	G6PD_RAT	6	5	0.000605	7.2
NADP-dependent malic enzyme	MAOX_RAT	3	3	2.09E-05	6.6
60S ribosomal protein L23	RL23_RAT	2	2	0.005227	5.1
Alcohol sulfotransferase A	ST2A2_RAT	7	5	0.003782	3.9
ATP-citrate synthase	ACLY_RAT	42	42	0.000618	3.6
Retinal dehydrogenase 1	AL1A1_RAT	10	4	0.001163	3.5
6-phosphogluconate dehydrogenase, decarboxylating	6PGD_RAT	16	16	3.56E-07	3.4
Aldehyde dehydrogenase, cytosolic 1	AL1A7_RAT	10	4	0.018937	3.1
Microtubule-associated protein RP/EB family member 2	MARE2_RAT	2	2	0.018809	3.0
Glutathione S-transferase kappa 1	GSTK1_RAT	3	3	0.012802	2.8
Glutathione S-transferase theta-1	GSTT1_RAT	4	4	0.038933	2.5
Fatty acid synthase	FAS_RAT	83	82	0.002199	2.5
Long-chain-fatty-acid--CoA ligase 5	ACSL5_RAT	3	2	0.00896	2.5
Cytochrome P450 2A1	CP2A1_RAT	4	4	0.013636	2.4
Carboxymethylenebutenolidase homolog	CMBL_RAT	3	3	0.011306	2.4
Destrin	DEST_RAT	2	2	0.012824	2.3

Tubulin alpha-1C chain	TBA1C_RAT	17	3	0.009453	2.3
Synaptic vesicle membrane protein VAT-1 homolog	VAT1_RAT	5	5	0.008198	2.1
60S ribosomal protein L9	RL9_RAT	2	2	0.037221	2.0
Bifunctional purine biosynthesis protein PURH	PUR9_RAT	2	2	0.011392	1.9
Macrophage migration inhibitory factor	MIF_RAT	2	2	0.000123	1.9
Dihydropteridine reductase	DHPR_RAT	7	7	0.040027	1.9
Polyadenylate-binding protein 1	PABP1_RAT	2	2	0.000186	1.86
Transitional endoplasmic reticulum ATPase	TERA_RAT	10	10	0.019298	1.81
Aspartate--tRNA ligase, cytoplasmic	SYDC_RAT	7	7	0.013114	1.7
Elongation factor 1-alpha 1	EF1A1_RAT	7	7	0.006062	1.7
GTP-binding protein SAR1b	SAR1B_RAT	3	3	0.011995	1.7
Phosphoglycerate kinase 1	PGK1_RAT	17	15	0.009191	1.7
60 kDa lysophospholipase	LPP60_RAT	3	3	0.045716	1.7
Elongation factor 1-delta	EF1D_RAT	4	4	0.040249	1.6
Cytosolic 10-formyltetrahydrofolate dehydrogenase	AL1L1_RAT	39	37	0.006914	1.6
Glucokinase regulatory protein	GCKR_RAT	4	4	0.010341	1.6
Acetyl-CoA carboxylase 1	ACACA_RAT	54	54	0.021909	1.5
Phenylalanine-4-hydroxylase	PH4H_RAT	7	7	0.049157	1.5
40S ribosomal protein S4, X isoform	RS4X_RAT	6	6	0.003988	15.5
Glucose-6-phosphate 1-dehydrogenase	G6PD_RAT	6	5	0.000605	7.2
NADP-dependent malic enzyme	MAOX_RAT	3	3	2.09E-05	6.6
60S ribosomal protein L23	RL23_RAT	2	2	0.005227	5.1
Alcohol sulfotransferase A	ST2A2_RAT	7	5	0.003782	3.9
ATP-citrate synthase	ACLY_RAT	42	42	0.000618	3.6
Retinal dehydrogenase 1	AL1A1_RAT	10	4	0.001163	3.5
6-phosphogluconate dehydrogenase, decarboxylating	6PGD_RAT	16	16	3.56E-07	3.4
Aldehyde dehydrogenase, cytosolic 1	AL1A7_RAT	10	4	0.018937	3.1
Microtubule-associated protein RP/EB family member 2	MARE2_RAT	2	2	0.018809	3.0

Glutathione S-transferase kappa 1	GSTK1_RAT	3	3	0.012802	2.8
Glutathione S-transferase theta-1	GSTT1_RAT	4	4	0.038933	2.5
Fatty acid synthase	FAS_RAT	83	82	0.002199	2.5
Long-chain-fatty-acid--CoA ligase 5	ACSL5_RAT	3	2	0.00896	2.5
Cytochrome P450 2A1	CP2A1_RAT	4	4	0.013636	2.4
Carboxymethylenebutenolidase homolog	CMBL_RAT	3	3	0.011306	2.4
Destrin	DEST_RAT	2	2	0.012824	2.3
Tubulin alpha-1C chain	TBA1C_RAT	17	3	0.009453	2.3
Synaptic vesicle membrane protein VAT-1 homolog	VAT1_RAT	5	5	0.008198	2.1
60S ribosomal protein L9	RL9_RAT	2	2	0.037221	2.0
Bifunctional purine biosynthesis protein PURH	PUR9_RAT	2	2	0.011392	1.9
Macrophage migration inhibitory factor	MIF_RAT	2	2	0.000123	7.2